MICROMECHANICAL MODELLING OF HYBRID UNIDIRECTIONAL COMPOSITE MATERIALS UNDER FIBRE TENSILE LOADING

José Manuel Guerrero Garcia

Universitat de Girona

Doctoral Thesis

Micromechanical modelling of hybrid unidirectional composite materials under fibre tensile loading

José Manuel Guerrero Garcia

2019

Universitat de Girona

Doctoral Thesis

Micromechanical modelling of hybrid unidirectional composite materials under fibre tensile loading

José Manuel Guerrero Garcia

2019

Doctoral Program in Technology

Advisor:

Dr. Joan Andreu Mayugo Majo
Universitat de Girona

Thesis submitted to the Universitat de Girona for the degree of Doctor of Philosophy

José Manuel Guerrero Garcia

Micromechanical modelling of hybrid unidirectional composite materials under fibre tensile loading

Doctoral Thesis, 2019
Doctoral Program in Technology
Advisor: Dr. Joan Andreu Mayugo Majo

Universitat de Girona
AMADE Research Group
Escola Politècnica Superior
Dept. d'Enginyeria Mecànica i de la Construcció Industrial
Carrer Universitat de Girona, 4. Campus de Montilivi
17003 Girona

To my family, my friends and my girlfriend.

If I have seen further than others, it is by standing upon the shoulders of giants.

— Isaac Newton
(mathematician, astronomer and physicist)

Everybody is a genius. But if you judge a fish by its ability to climb a tree, it will live its whole life believing that it is stupid.

— Albert Einstein
(Physicist)

Science isn't about why – it's about why not.

— Cave Johnson
(Portal 2)

The more you know, the more you know you don't know.

— Aristotle
(Philosopher)

Struggle is nature's way of strengthening it.

— John Locke
(The Lost TV series)

The moment money becomes your motivation, you are immediately not as good as someone who is stimulated by passion and internal will.

— Sebastian Vettel
(Formula 1 driver)

Preface

The work contained in this Ph.D. thesis was conducted in the AMADE Research Group (Escola Politècnica Superior, Dept. d'Enginyeria Mecànica i de la Construcció Industrial, Universitat de Girona, Spain). The thesis was carried out with predoctoral Grant BES-2016-078270 from the 'Subprograma Estatal de Formación del MICINN' co-financed by the European Social Fund. The author also acknowledges the financial support from the Spanish Ministerio de Economía, Industria y Competitividad (MINECO) under the projects MAT2015-69491-C3-1-R and TRA2015-71491-R co-financed by the European Regional Development Fund (ERDF). In addition, the author thanks the financial support of the grant RTI2018-097880-B-I00 from the Spanish Ministerio de Ciencia, Innovación y Universidades.

Girona, December 2019

José Manuel Guerrero Garcia

Acknowledgements

Firstly, I would like to thank my main advisor Joan Andreu Mayugo for his endless support. Despite of his full agenda, Joan Andreu always found a moment to meet me and lead the thesis into the right direction. This work would not have been the same without him.

Secondly, I would like to acknowledge Josep Costa and Albert Turon for all meetings we performed together with Joan Andreu. These reunions were really helpful to always point out the next steps to take in the thesis.

I would also like to thank Rodrigo P. Tavares, Pedro P. Camanho and Fermin Otero from the University of Porto. The collaboration performed with them was very fruitful for improving the contributions derived from this work.

Moreover, I would also like to express my gratitude to all the organisers of the *II international benchmarking exercise for longitudinal strength models of unidirectional composites* for the invitation to participate in the event. Engaging in the benchmark was an enriching task. Not only it aided to point-point the pros and cons of the work proposed in this thesis, but also allowed to collaborate with outstanding experts on this field.

També m'agradaria molt agrair a tots els membres del grup de recerca AMADE, tant els meus companys estudiants com els professors, el seu continuat recolzament. L'ambient de treball durant tots aquests anys ha sigut immillorable.

Finalment, vull donar les gràcies a totes aquelles persones properes que m'han ajudat de forma directe o indirecte durant aquests últims anys. Especialment, la meva família, els meus amics, els meus sogres i sobretot, la meva xicota.

List of Publications

The present Ph.D. thesis has been prepared as a compendium of peer-reviewed journal papers, according to the regulations of the Universitat de Girona.

Publications in refereed journals

The main body of this thesis is comprised of the following papers:

A) **J. M. Guerrero**, J. A. Mayugo, J. Costa, A. Turon. A 3D Progressive Failure Model for predicting pseudo-ductility in hybrid unidirectional composite materials under fibre tensile loading. *Composites Part A: Applied Science and Manufacturing* 107 (2018) 579-591. doi: https://doi.org/10.1016/j.compositesa.2018.02.005.
ISSN: 1359-835X, Impact Factor: 6.282, ranked 3/49 in the category of *Engineering, Manufacturing* and ranked 3/25 in the category of *Materials Science, Composites* (1st quartile)[1].

B) **J. M. Guerrero**, R. P. Tavares, F. Otero, J. A. Mayugo, J. Costa, A. Turon, P. P. Camanho. An analytical model to predict stress fields around broken fibres and their effect on the longitudinal failure of hybrid composites. *Composite Structures* 211 (2019) 564–576. doi: https://doi.org/10.1016/j.compstruct.2018.12.044.
ISSN: 0263-8223, Impact Factor: 4.829, ranked 6/25 in the category of *Materials Science, Composites* (1st quartile)[1].

C) **J. M. Guerrero**, J. A. Mayugo, J. Costa, A. Turon. Failure of hybrid composites under longitudinal tension: Influence of dynamic effects and thermal residual stresses. *Composite Structures.* In Press, journal pre-proof (2019). doi: https://doi.org/10.1016/j.compstruct.2019.111732.
ISSN: 0263-8223, Impact Factor: 4.829, ranked 6/25 in the category of *Materials Science, Composites* (1st quartile)[1].

D) **J. M. Guerrero**, J. A. Mayugo, J. Costa, A. Turon. Size effects in hybrid unidirectional polymer composites under longitudinal tension: a

[1] According to the 2018 Journal Citation Reports

micromechanical investigation. *Submitted to Composites Part A: Applied Science and Manufacturing* (October 2019).
ISSN: 1359-835X, Impact Factor: 6.282, ranked 3/49 in the category of *Engineering, Manufacturing* and ranked 3/25 in the category of *Materials Science, Composites* (1st quartile)[1].

E) **J. M. Guerrero**, J. A. Mayugo, J. Costa, A. Turon. The influence the hybrid configuration has on damage development in hybrid polymer composites under fibre tensile loading. *In preparation for submission.*

Other publications that have been derived from this thesis but do not belong to this thesis, and are not included in this document, are listed below:

– R. P. Tavares, **J. M. Guerrero**, F. Otero, A. Turon, J. A. Mayugo, J. Costa, P. P. Camanho. Effects of local stress fields around broken fibres on the longitudinal failure of composite materials. *International Journal of Solids and Structures* 156–157 (2019) 294-305. doi: https://doi.org/10.1016/j.ijsolstr.2018.08.027.
ISSN: 0020-7683, Impact Factor: 2.787, ranked 34/134 in the category of *Mechanics* (2nd quartile)[1].

Conference proceedings

Finally conference papers and presentations are listed below:

– **J. M. Guerrero**, J. A. Mayugo, J. Costa, A. Turon. A comparison of algorithms for determining the cluster development in unidirectional composite materials under fibre tensile loading. *7th ECCOMAS Thematic Conference on the Mechanical Response of Composites (COMPOSITES 2019)*. Girona (Spain), 18-20th September 2019.
International Conference. Oral presentation and conference paper.

– **J. M. Guerrero**, J. A. Mayugo, J. Costa, A. Turon. A micromechanical progressive failure model for predicting the tensile failure and damage development in hybrid unidirectional composite materials. *FiBreMoD Conference*. KU Leuven (Belgium), 11-12th December 2019.
International Conference. Accepted oral presentation.

Declaration

Universitat de Girona

Dr. Joan Andreu Mayugo Majo, Professor of AMADE Research Group, Dept. d'Enginyeria Mecànica i de la Construcció Industrial at Universitat de Girona,

hereby CERTIFIES that

The work entitled *Micromechanical modelling of hybrid unidirectional composite materials under fibre tensile loading*, submitted for the doctoral degree by José Manuel Guerrero Garcia, has been conducted under his supervision.

Girona, December 2019.

Joan Andreu Mayugo Majo
Universitat de Girona

List of Symbols

Acronyms

FRP	Fibre Reinforced Polymer
RVE	Representative Volume Element
SCF	Stress Concentration Factor
HVF	Hybrid Volume Fraction
UD	Unidirectional
LE	Low Elongation
HE	High Elongation
PLAW	Power Law Accelerated Weibull distribution
WOW	Weibull of Weibull
GLS	Global Load Sharing
LLS	Local Load Sharing
SFF	Simultaneous Fibre-Failure
HLS	Hierarchical Scaling Law
SEM	Spring Element Model
PFM	Progressive Failure Model
PMCs	Polymer-matrix Composites
FEM	Finite Element Model
FBM	Fibre Bundle Model
HM	High Modulus
LM	Low Modulus

Mechanical and statistical symbols

E	Longitudinal Young's modulus (with different sub-indices)
G	Shear modulus (with different sub-indices)
ν	Poisson's ratio (with different sub-indices)
A	Cross-sectional area (with different sub-indices)
$s\prime$	Cross-sectional area factor (with different sub-indices)
d_{f}	Fibre diameter
R	Radius (with different sub-indices)
R_{t}	RVE equivalent radius
R_{b}	Planar cluster equivalent radius

R_e	Experimentally determined fibre-fibre interaction radius
R_ε	Hybrid effect
N_q	Number of fibres in the RVE
N_b	Number of broken fibres in the RVE or number of bundles
n	Number of broken fibres in a cluster (with different sub-indices)
n^{ult}	Critical number of fibre breaks in the SFF model
N_p	Number of planes or layers or bundles
N_1, N_2	Number of fibres of population 1 and 2 respectively
N_s	Number of fibres connected to a certain fibre in SEM
N_L	Number of longitudinal elements in SEM
N_T	Number of transverse elements in SEM
N_l	Number of layers in interlayer hybrid composite
N_{gue}	Number of guesses in fibre generator
N_{max}	Maximum number of iterations in fibre generator
N_c	Number of iterations to change criterion in fibre generator
s	Average fibre spacing of the RVE
S	Average fibre spacing of a cluster (with different sub-indices)
S_0	Initial square size in fibre generator
Δ_S	Square size increment in fibre generator
V	Volume fraction (with different sub-indices)
L	Total length of the fibres or the RVE
l	Element length or length of a bundle
a, b	RVE width and height, respectively
h_m	Matrix thickness
P	Failure probability (with different sub-indices)
α_w	Length correction factor in PLAW distribution
m	Weibull modulus
L_0	Weibull reference gauge length
σ_0	Weibull reference strength
m'	WOW modulus for the strength distribution along a fibre
ρ_w	WOW modulus for the characteristic strength of the fibre
σ_{01}, σ_{02}	Bimodal Weibull strength for population flaw 1 and 2, respectively
m_1, m_2	Bimodal Weibull modulus for population flaw 1 and 2,

	respectively
SD	Fibre strength standard deviation with a normal distribution
μ_{n}	Mean fibre failure strain with a normal distribution
ε^{u}	Failure strain of a fibre or element (with different sub-indices)
$\varepsilon^{\mathrm{ult}}$	Failure strain of the composite
ε^{0}	Applied strain
ε	Fibre or element strain (with different sub-indices)
ε^{r}	Thermal residual strain (with different sub-indices)
$\varepsilon_{\mathrm{y}}^{\mathrm{ult}}$	Matrix shear yield strain
εCF	Strain concentration factor (with different sub-indices)
σ^{ult}	Composite failure stress
σ^{0}	Composite stress
σ^{u}	Failure strength of a fibre or element (with different sub-indices)
$\bar{\sigma}$	Average stress
σ_{R}	Reference strength in GLS models
σ	Fibre or element longitudinal stress (with different sub-indices)
σ^{∞}	Applied stress or far-field stress (with different sub-indices)
$\tilde{\sigma}$	Effective stress (with different sub-indices)
σ^{r}	Thermal residual stress (with different sub-indices)
σ^{y}	Yield stress
σ_{ν}	Poisson stress
σ_{s}	Fibre stress at the end of the debonded region in Ivens model
$\Delta\sigma$	Increase of stress for a fibre due to broken surrounding fibres (with different sub-indices)
Ω	Stress ratio (with different sub-indices)
B_{f}	Longitudinal strain-displacement transformation matrix
τ	Shear stress
τ_{y}	Matrix shear yield stress
τ_{s}	Debonded or frictional shear stress
$\tau_{\mathrm{s}}^{\mathrm{ult}}$	Interfacial shear strength
SCF	Stress concentration factor (with different sub-indices)
δ	Radial distance function related to SCF (with different sub-indices)

λ	Plane distance function related to *SCF* (with different sub-indices)
α	Stress concentration factor exponent or coefficient of thermal expansion (with different sub-indices)
I	Constant to calculate the *SCF* (with different sub-indices)
r	Distance between cluster and intact fibre (with different sub-indices)
P_1, P_2	Constants from a micro-mechanic finite element model
M_d	Dynamic magnification factor for the *SCF*
k	Stiffness of a fibre, matrix or plane (with different sub-indices)
K	Global stiffness
D	Damage (with different sub-indices)
L^in	Ineffective length of a broken fibre (with different sub-indices)
ζ	Percentage of stress recovery
L_s^in	Length of the debonded or slipping region
L_e^in	Length of the elastic region
ς	Debonding coefficient in Lacroix's shear-lag model
H	Ineffective length scaling factor (with different sub-indices)
C	Shear-lag profile (with different sub-indices)
β^c, β^I, β^L, β^N	Shear-lag parameter of Cox, Ivens, Lacroix and Nayfeh, respectively (with different sub-indices)
$P\left(x, E_\mathrm{f}\varepsilon^0\right)$	Fragment length distribution
x	Fragment length
z	Longitudinal distance from a fibre break
F	Force (with different sub-indices)
u, $\ddot{u}$, $\dot{u}$	Displacement, acceleration and velocity respectively (with different sub-indices)
Δu	Displacement increment
t	Step number
y	Iteration number
ρ	Density (with different sub-indices)
ρ_b	Fibre break density
$\rho_\mathrm{b}^\mathrm{ult}$	Fibre break density at failure
ε^d	Pseudo-ductile strain (also referred as ductile strain)
M	Mass (with different sub-indices)

C	Rayleigh damping
α^{r}	Mass proportional damping coefficient
β^{r}	Stiffness proportional damping coefficient
d^{c}	Distance between two fibre centres (with different sub-indices)
d_{r}	Radial distance between two broken elements
d_{l}	Axial distance between two broken elements
k_{ε}	Stiffness ratio
μ	Fibre-matrix interphase frictional coefficient
HVF_{HE}	HE hybrid volume fraction
$S_{U,c}^{[i_{\mathrm{b}}+1]}$	Survival probability of the generic level-$[i_{\mathrm{b}}+1]$ bundle
$S_{U,e}^{[i_{\mathrm{b}}]}(\sigma^{\infty})$	Survival probability of a level-$[i_{\mathrm{b}}]$ bundle
$S_{K,e}^{[i_{\mathrm{b}}]}(\sigma^{\infty})$	Survival probability of a level-$[i_{\mathrm{b}}]$ bundle under stress concentration
α_{s}, β_{s}, γ_{s}	Parameters in Ivens model
χ	Material constant in Ivens model
Υ	Experimental function depending on the material properties
κ, η	Constants in Ohno model
T	Test temperature or thickness (with different sub-indices)
T_{r}	Stress-free reference temperature
Hyb_{t}	Type of hybrid configuration in fibre generator
$D_{\min}$	Minimum distance between fibre centres

Subscripts and superscripts

m	Matrix
f	Fibre
H	Hybrid
LE	Low Elongation fibre
HE	High Elongation fibre
LE,H	Low Elongation fibre inside the hybrid composite
q or j	Fibre index
p or i	Plane index
e	Element index
f1, f2 or 1, 2	Fibre populations 1 and 2 respectively
c	Cluster index
b	bundle

List of Figures

List of Tables

List of Algorithms

Contents

Abstract

Fibre Reinforced Polymers (FRP) are widely employed in lightweight applications mainly thanks to their excellent specific strength and stiffness. Nonetheless, FRP suffer from a lack of ductility and toughness which leads to fibre tensile failure with nearly any damage symptom. Consequently, composite materials are often overdesigned, which potentially limits the costs and weight savings. This also makes them unsuitable for applications where ductility is mandatory.

Fibre hybridisation is a promising strategy which can overcome the quasi-brittle behaviour and low toughness of FRP. When a Low Elongation (LE) fibre is combined with a High Elongation (HE) fibre in a single matrix, a hybrid material is obtained. Within a proper hybridisation design, the failure of the LE fibre in the hybrid can be delayed compared to that of the baseline non-hybrid composite, something known as the hybrid effect. Moreover, an increase of ductility can occur, getting rid of the catastrophic brittle failure of composite materials. Currently, there are three main reasons to explain this phenomenon: dynamic effects, thermal residual stresses and changes in the failure development.

Despite the great benefits of hybrid composites, their fibre tensile failure process is not yet entirely understood. Moreover, derived from this insufficient understanding, there is a lack of efficient tools to predict such failure. Currently, different models exist in the literature that attempt to simulate the failure and damage development of hybrid composite materials. Nonetheless, most models omit dynamic effects and assume simplistic elastic matrix behaviours. In addition, models usually consider the fibres to be placed within a square or hexagonal packing, instead of being randomly distributed. Such a simplification does not allow to properly simulate hybrid composites with fibres of different radius and does not permit to accurately capture the stress redistribution around broken fibres. Last but not least, some models cannot compute the entire stress-strain curve of the material, which does not allow to explicitly predict ductile effects. Thus, the development of new models, able to characterise the tensile failure process of hybrid composites more accurately, is necessary.

Departing from the literature need of developing more accurate models, as well as the requirement of designing and further understanding composite materials

exhibiting a ductile behaviour, the main purpose of this thesis is to develop an efficient tool for predicting the tensile failure process in hybrid unidirectional FRP under fibre tensile loading. The model proposed must consider the main mechanisms involved in the tensile failure of hybrid composites, and should also be capable of studying non-hybrid materials. Derived from this, the second main purpose of this work is to establish the influence that different parameters have on the tensile response and failure development in hybrid composites.

On the first contribution originated from this work, a micromechanical progressive failure model which can simulate the fibre tensile failure and damage development in hybrid unidirectional FRP is formulated. The model is validated by comparing with literature results exhibiting a good agreement.

On the second article derived from this thesis, the model is further improved by including a more realistic stress redistribution around broken fibres. The influence the matrix behaviour (plastic or elastic) has on the modelling results is investigated. Results suggest that an elastic matrix cannot realistically capture either the formation of clusters or the damage development in hybrid composites.

On the third article of this work, dynamic effects and thermal residual stresses are added into the model. The influence these features have on the failure of hybrid composites is studied. Results show that, while the dynamic effects have a large influence on the formation of clusters, the thermal residual stresses do not. Their effect in final failure is very reduced for both. Moreover, hybrid composites exhibiting large ductile response are shown.

On the fourth contribution derived from this work, the influence that the specimen size has on the failure and damage development in hybrid composites is investigated. Results prove that scaling up the composite length causes an earlier failure, marginally decreases the ductility of the material, but considerably increases the hybrid effect. Contrary to this, scaling up the composite cross-section decreases the hybrid effect, may delay final failure and may increase ductility. Moreover, the maximum cluster size always increases by increasing the composite volume and the presence of ductility does not alter the size effects.

On the final contribution of this thesis, the influence the hybrid configuration has on the tensile response and damage development in hybrid composites is explored. Furthermore, the model is validated by comparing it against experimental

results of hybrid composites. Results show that the intrayarn hybridisation leads to higher hybrid effects, yield stress and strength than the interlayer and intralayer configurations. However, the interlayer and intralayer lead to greater failure and ductile strains than the intrayarn. The dispersion of the fibres is seen to be a key parameter. Finally, the micromechanical model shows qualitatively a good agreement compared with experimental data.

Resum

Els polímers reforçats amb fibres (FRP) són àmpliament utilitzats en aplicacions de baix pes principalment gràcies a la seva excel·lent resistència específica i rigidesa. Tot i així, els FRP pateixen d'una manca de ductilitat i tenacitat que condueix a la ruptura de fibres a tracció sense pràcticament cap símptoma de dany. Conseqüentment, els materials compòsits generalment es sobredimensionen, cosa que limita el potencial estalvi de cost i pes. Això també els fa inadequats per aplicacions on la ductilitat és necessària.

La hibridació de fibres és una prometedora estratègia que pot eradicar el comportament quasi-fràgil i la baixa tenacitat dels FRP. Quan una fibra de Baixa Elongació (LE) es combina amb una d'Alta Elongació (HE) en una sola matriu, s'obté un material híbrid. Mitjançant un disseny apropiat, la ruptura de la fibra LE en l'híbrid pot ser retardada comparada amb la del material no-híbrid de base, fenomen conegut com a efecte híbrid. D'altra banda, es pot produir un augment de la ductilitat, aconseguint desfer-se de la ruptura fràgil i catastròfica dels materials compòsits. Actualment, existeixen tres principals raons per explicar aquest fenomen: efectes dinàmics, tensions tèrmiques residuals i canvis en el procés de trencament.

Malgrat els grans beneficis dels compòsits híbrids, el seu procés de ruptura a tracció en la direcció de les fibres encara no està totalment comprès. A més a més, derivat d'aquest insuficient coneixement, no hi ha eines eficients per predir aquest trencament. Actualment, existeixen diferents models en la literatura que permeten simular la ruptura i el desenvolupament de dany en materials compòsits híbrids. No obstant això, la majoria de models ometen els efectes dinàmics i assumeixen matrius amb un simple comportament elàstic. A més, els models usualment consideren que les fibres estan col·locades en un paquet quadrat o hexagonal, en lloc d'estar distribuïdes aleatòriament. Tal simplificació no permet simular adequadament compòsits híbrids amb fibres de diferent radi i no possibilita capturar amb precisió la redistribució de tensió al voltant de fibres trencades. Per últim, alguns models no poden capturar la corba tensió-deformació en la seva totalitat, cosa que no permet predir efectes dúctils de forma explícita. Per tant, el desenvolupament de nous models, capaços de

caracteritzar el procés de ruptura a tracció de compòsits híbrids amb major fiabilitat, és necessari.

Partint de la necessitat en la literatura de desenvolupar models més precisos, així com també el requeriment de dissenyar i comprendre amb major exactitud materials compòsits que presentin un comportament dúctil, el propòsit principal d'aquesta tesis és desenvolupar una eina eficient per predir el procés de ruptura a tracció de materials unidireccionals híbrids FRP sotmesos a càrregues longitudinals. El model proposat ha de considerar els principals mecanismes involucrats en la ruptura a tracció de compòsits híbrids i també hauria de ser capaç d'estudiar materials no-híbrids. Derivat d'això, el segon propòsit principal d'aquest treball consisteix en establir la influència que diferents paràmetres tenen sobre la resposta a tracció i el desenvolupament de dany en materials híbrids.

En la primera contribució originada d'aquest treball, es formula un model micromecànic de ruptura progressiu capaç de simular el trencament de fibres a tracció i el desenvolupament de dany en materials unidireccionals híbrids FRP. El model és validat comparant-lo amb resultats de la literatura mostrant una gran conformitat.

En el segon article derivat d'aquesta tesis, el model es millora encara més mitjançant una redistribució de tensions més realista al voltant de les fibres trencades. La influència que el comportament de la matriu (plàstica o elàstica) té en els resultats modelats és investigada. Els resultats suggereixen que una matriu elàstica no pot capturar de forma realista ni la formació de clústers, ni el desenvolupament de dany en compòsits híbrids.

En el tercer article d'aquest treball, s'inclouen efectes dinàmics i tensions tèrmiques residuals en el model. La influència que aquests fenòmens tenen en la ruptura de compòsits híbrids és estudiada. Els resultats mostren que, mentre que els efectes dinàmics tenen una gran influència en la formació de clústers, les tensions residuals no. El seu efecte en la ruptura final és molt reduït per tots dos. A més, es mostren materials compòsits amb una gran ductilitat.

En la quarta contribució obtinguda d'aquest treball, s'investiga la influència que la mida de la proveta té en el trencament i el desenvolupament de dany en compòsits híbrids. Els resultats demostren que augmentar la longitud del

compost provoca un trencament prematur, disminueix lleugerament la ductilitat del material, però augmenta considerablement l'efecte híbrid. Contràriament, augmentar la secció transversal del compòsit disminueix l'efecte híbrid, pot endarrerir el trencament i pot amplificar la ductilitat. A més, la mida màxima del clúster sempre creix quan s'augmenta el volum del compost i la presència de ductilitat no altera els efectes de mida.

En la contribució final d'aquesta tesi, s'explora la influència que la configuració híbrida té en la resposta a tracció i el desenvolupament de dany en compòsits híbrids. A més a més, el model es valida comparant-lo amb resultats experimentals de compostos híbrids. Els resultats mostren que la hibridació intrayarn produeix efectes híbrids, tensió de fluència i resistència més elevats que la configuració interlayer i intralayer. Tot i això, les configuracions interlayer i intralayer presenten una deformació última i una ductilitat major que l'intrayarn. La dispersió de les fibres és un paràmetre clau. Finalment, el model micromecànic mostra qualitativament un bon acord comparat amb les dades experimentals.

Resumen

Los polímeros reforzados con fibras (FRP) son ampliamente utilizados en aplicaciones de bajo peso principalmente gracias a su excelente resistencia específica y rigidez. Sin embargo, los FRP sufren de una ausencia de ductilidad y tenacidad que conlleva a la rotura de fibras a tracción sin apenas ningún síntoma de daño. Consecuentemente, los materiales compuestos generalmente se sobredimensionan, lo cual limita el potencial ahorro de coste y peso. Esto también los hace inadecuados para aplicaciones donde la ductilidad es necesaria.

La hibridación de fibras es una prometedora estrategia que puede erradicar el comportamiento casi-frágil y la baja tenacidad de los FRP. Cuando una fibra de Baja Elongación (LE) se combina con una de Alta Elongación (HE) en una sola matriz, se obtiene un material híbrido. Mediante un diseño apropiado, la rotura de la fibra LE en el híbrido puede ser retardada comparada con la del material no-híbrido de base, fenómeno conocido como efecto híbrido. Además, se puede producir un incremento de ductilidad, consiguiendo así deshacerse de la rotura frágil y catastrófica de los materiales compuestos. Actualmente, existen tres principales razones para explicar este fenómeno: efectos dinámicos, tensiones térmicas residuales y cambios en el proceso de rotura.

A pesar de los grandes beneficios de los compuestos híbridos, su proceso de rotura a tracción en la dirección de las fibras aún no está enteramente comprendido. A más a más, derivado de este insuficiente entendimiento, no hay herramientas eficientes para predecir tal ruptura. Actualmente, existen distintos modelos en la literatura que tratan de simular la rotura y el desarrollo de daño en materiales compuestos híbridos. No obstante, la mayoría de modelos omiten los efectos dinámicos y asumen matrices con un simple comportamiento elástico. Asimismo, los modelos usualmente consideran que las fibras están colocadas en un paquete cuadrado o hexagonal, en vez de estar distribuidas aleatoriamente. Tal simplificación no permite simular adecuadamente compuestos híbridos con fibras de diferente radio y no posibilita capturar con precisión la redistribución de tensión alrededor de fibras rotas. Por último, algunos modelos no pueden capturar la curva tensión-deformación en su totalidad, lo cual no permite predecir efectos dúctiles de forma explícita. Por tanto, el desarrollo de nuevos modelos,

capaces de caracterizar el proceso de rotura a tracción de compuestos híbridos con mayor fiabilidad, es necesario.

Partiendo de la necesidad en la literatura de desarrollar modelos más precisos, así como también el requerimiento de diseñar y entender con mayor exactitud materiales compuestos que presenten un comportamiento dúctil, el propósito principal de esta tesis es desarrollar una herramienta eficiente para predecir el proceso de rotura a tracción de materiales unidireccionales híbridos FRP sometidos a cargas longitudinales. El modelo propuesto debe considerar los principales mecanismos involucrados en la rotura a tracción de compuestos híbridos y también debería ser capaz de estudiar materiales no-híbridos. Derivado de esto, el segundo propósito principal de este trabajo consiste en establecer la influencia que distintos parámetros tienen en la respuesta a tracción y el desarrollo de daño en materiales híbridos.

En la primera contribución originada de este trabajo, se formula un modelo micromecánico de rotura progresivo capaz de simular la rotura de fibras a tracción y el desarrollo de daño en materiales unidireccionales híbridos FRP. El modelo es validado comparándolo con resultados de la literatura mostrando una gran conformidad.

En el segundo artículo derivado de esta tesis, el modelo se mejora aún más añadiendo una redistribución de tensión más realista alrededor de las fibras rotas. La influencia que el comportamiento de la matriz (plástica o elástica) tiene en los resultados modelados es investigada. Los resultados sugieren que una matriz elástica no puede capturar de forma realista ni la formación de clústeres, ni el desarrollo de daño en compuestos híbridos.

En el tercer artículo de este trabajo se incluyen efectos dinámicos y tensiones térmicas residuales en el modelo. La influencia que estos fenómenos tienen en la rotura de compuestos híbridos es estudiada. Los resultados muestran que, mientras que los efectos dinámicos tienen una gran influencia en la formación de clústeres, las tensiones residuales no. Su efecto en la rotura final es muy reducido para ambos. Además, se muestran materiales compuestos con una gran ductilidad.

En la cuarta contribución derivada de este trabajo, se investiga la influencia que el tamaño de la probeta tiene en la rotura y el desarrollo de daño en los

compuestos híbridos. Los resultados demuestran que aumentar la longitud del compuesto causa una ruptura prematura, disminuye ligeramente la ductilidad del material, pero aumenta considerablemente el efecto híbrido. Contrariamente, aumentar la sección transversal del compuesto disminuye el efecto híbrido, puede retrasar la rotura y puede incrementar la ductilidad. Además, el tamaño máximo del clúster siempre crece al aumentar el volumen del compuesto y la presencia de ductilidad no altera los efectos de tamaño.

En la contribución final de esta tesis, se explora la influencia que la configuración híbrida tiene en la respuesta a tracción y el desarrollo de daño en compuestos híbridos. Además, el modelo se valida comparándolo con resultados experimentales de compuestos híbridos. Los resultados muestran que la hibridación intrayarn conduce a efectos híbridos, tensión de fluencia y resistencia mayores que las configuraciones interlayer y intralayer. Sin embargo, las configuraciones interlayer y intralayer presentan una deformación última y una ductilidad mayor que la intrayarn. La dispersión de las fibras es un parámetro clave. Finalmente, el modelo micromecánico muestra cualitativamente un buen acuerdo comparado con los datos experimentales.

Part I

Introduction and literature review

Introduction

1

1.1 Contextual background

Composite materials consist of mixing two or more components during the manufacturing process, with the aim of marrying together the best qualities of each constituent. Unlike metallic alloys, each material retains its separate physical, chemical and mechanical properties. One constituent works principally as a matrix while the other works as a reinforcement. The fibres, acting as reinforcements, are stiff high-strength fibres that are the main loading constituent. Usually, the length of the fibres is much greater than their radius. This is known as the aspect ratio. Continuous fibres have long aspect ratios, whereas discontinuous fibres have short aspect ratios. The matrix, on the other hand, has a low stiffness and strength compared to the fibres and, above all, transmits the loads between fibres and gives the geometrical shape to the structure, see Fig. 1.1. The matrix can be a polymer, metal or a ceramic. Polymers have low stiffness and strength, metals have intermediate strength and stiffness and high ductility, while ceramics have high stiffness and strength but are brittle.

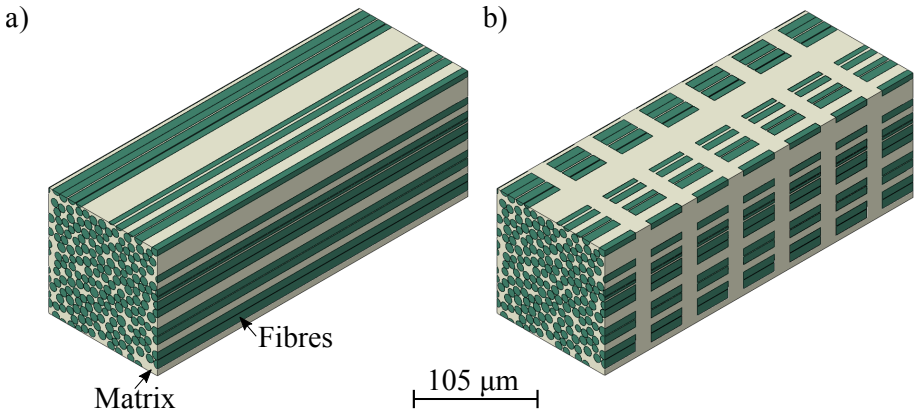

Figure 1.1: Microscopic representation of a composite material, showing the fibres and the matrix. Notice that only a small volume is here represented, since the real material would contain millions of fibres. a) continuous composite and b) discontinuous composite.

Fibre Reinforced Polymer composites (FRP) appeared in the early 1960s. These FRP composites combine carbon or glass fibres, which have a high specific stiffness (high stiffness by mass unit) and high specific strength (high strength by

mass unit), with polymer matrices. Thus, FRPs have the advantage of exhibiting a considerable strength comparable to traditional metals like steel, but with a greatly reduced weight, which makes them highly attractive. Nowadays, the use of FRP is firmly established in the aircraft industry, wind turbine components, spacecraft, motorsports and high specification sporting equipment, mainly thanks to their low weight and excellent stiffness and strength. Moreover, FRP are being used more and more in other applications such as the automotive industry.

Continuous FRPs are stacked into thin layers which, in the case of carbon FRP, typically range from between $0.05 - 0.2$ mm thick. Layers must be stacked one on top of the other to obtain a laminate. A laminate may have all its fibres oriented in the same direction, leading to a Unidirectional (UD) composite material, or it may have layers where the fibres are oriented in different directions, thus leading to a multidirectional composite laminate, see Fig. 1.2. Such design freedom allows designers to maximise and optimise the material by aligning the fibres in the direction of the most critical loads, although this, admittedly, makes the material more difficult to analyse.

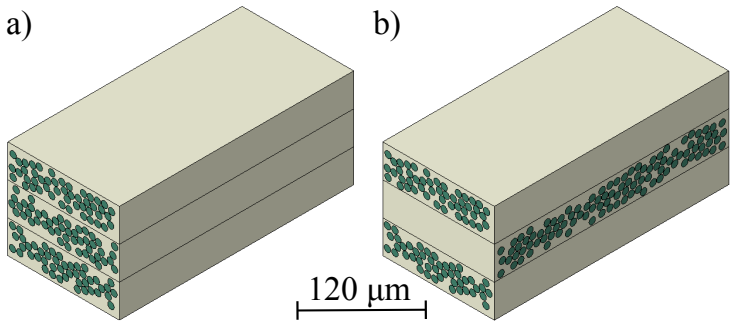

Figure 1.2: Microscopic representation of a composite material laminate comprised of 3 layers, a) a unidirectional composite with all fibres oriented in the same direction and b) a multidirectional composite with layers oriented in different directions.

Despite all the benefits and advantages composite materials offer compared to those of traditional metals, they are not trouble-free. Like many other materials, composite materials suffer from a lack of toughness and, consequently, exhibit a quasi-brittle failure behaviour, which leads to fibre tensile failure with barely any damage symptoms [1–3]. Moreover, their failure process is very complex, involving different failure mechanisms such as damage (loss of stiffness and strength), fatigue (loss of strength under cyclic loading), debonding (loss of

adherence between fibre and matrix), delamination (loss of adherence between layers), matrix cracking, matrix yielding and fibre breakage. Nowadays, these complex phenomena are not yet entirely understood and are under continuous study. As a consequence, there is a lack of efficient predictive tools able to accurately predict all these failure mechanisms [4, 5]. These facts, together with the composites lack of toughness, lead to designers employing large safety factors when designing structures. This in turn, does not allow the benefits of the composites to be fully exploited. Moreover, it also limits their applicability to other industries like the automotive or the construction industries, where the lack of toughness is a major concern and a serious stumbling block.

1.2 Motivation

Fibre hybridisation is a potential solution to the quasi-brittle failure behaviour dilemma of composite materials. In a fibre hybrid composite, two fibres with different failure strains are mixed. Within a proper hybridisation design, the failure process of the material can be altered, leading to hybrid effects and a larger ductility than that of non-hybrid composites [3, 6–21]. The development of such materials exhibiting a ductile failure with a wide margin between damage initiation and final failure is therefore greatly attractive.

Despite their potential to increase the low toughness of composite materials, the state of the art in hybrid composites is not yet sufficiently advanced enough. Currently, there are still several unknowns concerning the failure of hybrid composites. In addition, there is a lack of models able to accurately capture the tensile failure of hybrid composites. Overall, the current state of the art models present significant discrepancies compared with experiments. Therefore, the development of more advanced models that can close this gap and move the state of the art of hybrid composites forward is necessary.

1.3 Objectives

This thesis presents two main research objectives. The first is to develop a micromechanical numerical model able to simulate the tensile failure and damage development in hybrid unidirectional polymer composite materials under fibre tensile loading. Following on from this, the second main objective consists of

establishing the influence that different parameters have on the tensile response and failure development of hybrid composites.

In order to achieve these goals, different specific objectives have been derived. These, given below, have been addressed systematically.

A) Develop a micromechanical Fibre Bundle Model (FBM) which can simulate hybrid composites containing a random distribution of fibres with different elastic and geometrical properties. The model must capture the entire failure process of these materials, so as to assess their ductility. The model formulation should be flexible in order to allow new effects to be added without having to reformulate the entire model. Furthermore, it must also be computationally efficient for solving materials with a large volume.

B) Formulate an analytical model for predicting the stress redistribution around a cluster of broken fibres in hybrid composites taking into account the material properties of each fibre, the volume fractions, the specimen size as well as the matrix behaviour involved (i.e. plastic or elastic). Reveal the influence that the fibre properties, as well as matrix yielding, have on the stress redistribution around fibre breaks, the formation of clusters and damage progression with different hybrid composites. Establish whether the common assumption of modelling the matrix as elastic, is acceptable or not.

C) Include dynamic effects, due to the failure of broken fibres and thermal residual stresses as a result of the manufacturing process, in the FBM developed. Expose the impact that the dynamic effects and thermal residual stresses have on the tensile behaviour of hybrid composites as well as on the formation and development of clusters.

D) Investigate the influence that specimen size has on the hybrid effect, formation of clusters and damage development in hybrid composites (i.e. the so-called size effect).

E) Propose an algorithm able to generate realistic fibre packings of hybrid composites containing a random distribution of fibres with their own radius, and with the fibres being hybridised within an interlayer, intralayer

or an intrayarn configuration. Reveal whether the hybrid configuration has any significant impact on the hybrid effect and damage development using the realistic fibre packing developed.

1.4 Thesis structure

The present thesis has been developed as a compendium of five peer-reviewed publications, each of which addresses the specific objectives A)-E) of the thesis, respectively. With this in mind, the document has been divided into several chapters, grouped into different parts according to their context.

In Chapter 2, a literature review into hybrid composite materials is thoroughly outlined. This review first gives an introductory overview to hybrid composites as a whole, explaining the synergistic effects that occur in these materials. Afterwards, the most relevant micromechanical models available in the literature to predict the failure of hybrid and non-hybrid composites under longitudinal loading are analysed. It is worth mentioning that this review, and the greater part of this thesis, will deal with continuous FRP composites, made of carbon and/or glass fibres, since these materials are more attractive thanks to their high performance. Together with Chapter 1, this constitutes Part I of this thesis.

The core of this work is presented in Part II, which is composed of Chapters 3, 4, 5, 6 and 7. In these chapters, the whole text of each publication derived from this thesis is presented, respectively, each one addressing objectives A)-E) accordingly. To give the present thesis coherence, an introductory overview to the contribution each paper makes is given at the beginning of each chapter.

The culmination of this thesis is presented in Part III, with Chapter 8 providing a general discussion of the results obtained from all the papers, and Chapter 9 drawing the general conclusions and outlining future work.

Finally, a reproduction of the papers published at the time of the submission of the thesis, in their journal form, is included in Appendix A. A conference paper derived from the thesis is also enclosed in the Appendix.

Literature review

2

2.1 Fibre hybridisation in polymer composites

Fibre hybridisation is a promising strategy which can overcome the inherent quasi-brittle behaviour and low toughness of composite materials [3, 6–18, 22–28]. In a hybrid composite, two fibres with different mechanical properties are embedded into a single matrix. It is important to remark that both fibres simply need to have different mechanical properties, but can be of the same nature, e.g. a hybrid can be made of two different carbon fibres. The fibre with lower failure strain is called a Low Elongation (LE) fibre, while its counterpart is known as a High Elongation (HE) fibre. Thanks to this combination, the failure strain of the LE fibre can be enhanced compared to that of the baseline non-hybrid composite. This remarkable fact is known as the 'hybrid effect'. In addition, an increase in ductility and a more gradual failure can be obtained by removing the catastrophic brittle failure of composite materials [3, 6–21]. This is usually called 'pseudo-ductility' since it emulates the behaviour of ductile metals by means of a controlled damage failure progress, see Fig. 2.1. It should be noted that the failure strain of the HE fibre does not necessarily need to be 'large', but it must be larger than that of the LE fibre. It is also worth mentioning that, currently, there is no evidence that fibre hybridisation increases the toughness of non-hybrid composites. Nonetheless, owing to the larger ductility of hybrid materials, an increase of toughness is theoretically expected.

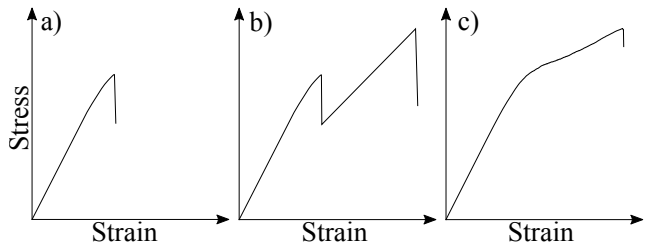

Figure 2.1: Typical failure response of different composite materials: a) a common non-hybrid composite with a brittle failure, b) a hybrid composite within the LE and HE fibre population failing at different strains without progressive failure and c) a ductile hybrid composite with a progressive failure.

Fibre hybridisation may take place at three levels or configurations which can also be combined [3, 19]: interlayer or layer-by-layer, where the layers of two

fibre types are stacked onto each other, intralayer or yarn-by-yarn, where the two fibre types are mixed within the layers but in separate yarns, and intrayarn or fibre-by-fibre or intermingled, where the fibres are mixed at the fibre level, see Fig. 2.2.

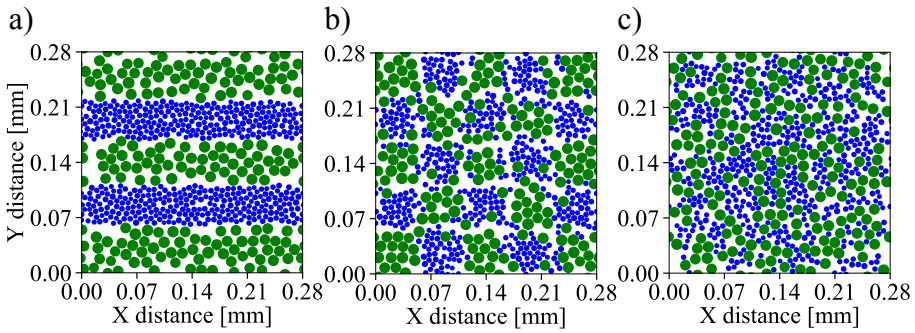

Figure 2.2: Main hybrid configurations: a) interlayer hybrid, with the different fibres placed in alternating layers, b) intralayer hybrid, with the fibres placed in different bundles and c) intrayarn hybrid, with the fibres completely mixed at the fibre level. The LE fibre is shown in blue, and the HE fibre in green.

The so-called 'hybrid effect' was first described by Hayashi [23], who observed a 40% failure strain enhancement on carbon fibre layers in a carbon-glass interlayer hybrid composite compared with the baseline carbon non-hybrid material. To determine the hybrid effect, different definitions are available. The most basic of which is also the most widely accepted: 'the apparent failure strain enhancement of the LE fibre in a hybrid composite compared to the failure strain of the LE fibre-reinforced non-hybrid composite' [3, 6]. Consequently, it is given by

$$R_\varepsilon = \frac{\varepsilon^{\text{ult}}_{\text{LE,H}} - \varepsilon^{\text{ult}}_{\text{LE}}}{\varepsilon^{\text{ult}}_{\text{LE}}} \tag{2.1}$$

where $\varepsilon^{\text{ult}}_{\text{LE,H}}$ is the failure strain of the LE fibre population inside the hybrid composite, whilst $\varepsilon^{\text{ult}}_{\text{LE}}$ is the failure strain of the LE non-hybrid composite, see Fig. 2.3a. It should be noted that, applying this definition is not always straightforward, since determining the failure of the LE fibre inside the hybrid composite is not always a trivial task. For instance, within a ductile failure like the one shown in Fig. 2.1c, such a failure point cannot be easily determined. Moreover, it is important to accurately compute the failure strain of the LE non-hybrid composite. If this failure strain is wrongly underpredicted, then the hybrid effect may be overestimated [3, 15, 29]. Overall, the typical range

of failure strain enhancement reported in the literature is between 10-50% [3]. Values larger than 50% or even negative hybrid effects have also been (albeit rarely) reported, but these are probably due to a wrong determination of ε_{LE}^{ult}, or due to an incorrect definition of the hybrid effect [3].

Since fibre hybridisation also modifies the mechanical properties, the hybrid effect may also be defined as a deviation from the linear rule of mixtures. This is well illustrated in Fig. 2.3b. The advantage of this last definition is that it can also be applied to mechanical properties rather than just the failure strain. However, applying this definition is not straightforward because of the following reasons [3]:

- The rule of mixtures is not necessarily linear for all properties.
- Each rule of mixtures needs a certain composition parameter.
- It does not apply for all mechanical properties (for example in bending).

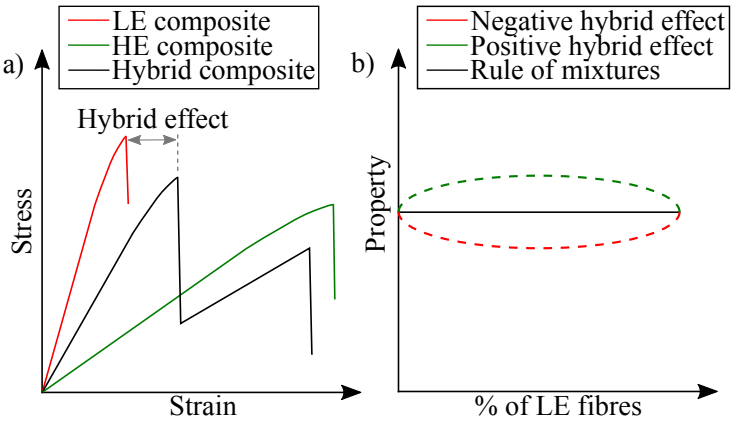

Figure 2.3: Hybrid effect definitions: a) as an apparent failure strain enhancement of the LE fibres and b) as a deviation from the rule of mixtures.

Since the discovery of the hybrid effect, different work has demonstrated that a low content of LE fibres, high fibre strength scatters, larger ratio between the LE fibre Young's modulus over the HE fibre Young's modulus and a larger failure strain ratio between the HE fibres over the LE fibres, among others, all lead to higher hybrid effects [30–35]. This will be discussed in detail in Section 2.1.2.

Currently there are three main reasons to explain the presence of the hybrid effect [3, 6–8, 22, 26]:

- Changes in the failure propagation compared to non-hybrid composites.

– The influence of thermal residual stresses.
– The presence of dynamic effects.

The failure development is considered to be the most important, while the influence of thermal residual stresses has been proved to be secondary. Finally, the dynamic effects have barely been studied and thus, their possible significance is unknown. In the following, these are reviewed.

2.1.1 Hypothesis for the hybrid effect

2.1.1.1 Failure development

The most important hypothesis regarding the hybrid effect is that failure develops differently in hybrid composites compared to non-hybrids. To explain this more in depth, first the strength of brittle fibres, such as glass or carbon, is not deterministic due to the presence of flaws, and follows a statistical distribution. When a composite is loaded in the fibre direction, the weakest fibre fails whenever its stress reaches its strength. The broken fibre then loses its load carrying capability over a distance known as ineffective length. Along this length, the matrix surrounding the broken fibre is loaded in shear and transmits the load back onto the broken fibre, thus, allowing the load in the fibre to be recovered. Furthermore, throughout this region, the neighbouring intact fibres take the load loss of the broken fibre, thus being subjected to a stress concentration that increases their probability of failure (Fig. 2.4a).

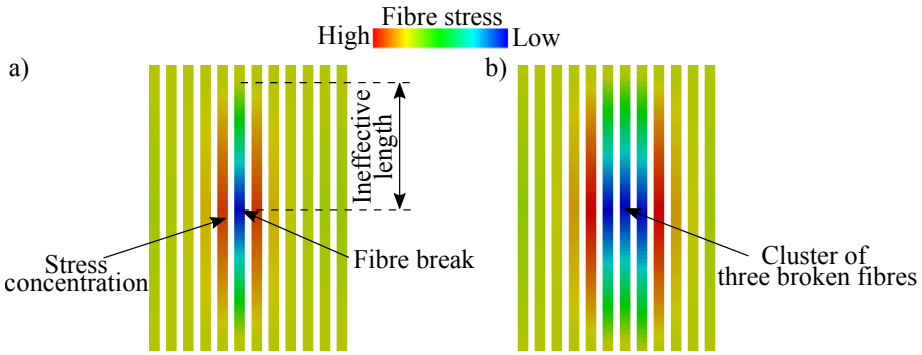

Figure 2.4: Key events in the fibre tensile failure process of composite materials: a) failure of a fibre and consequent stress redistribution around the broken fibre and b) formation of a cluster of broken fibres.

This stress redistribution can be different according to the matrix behaviour. If

the matrix behaves as an elastic solid, the ineffective length is small, while the stress concentration is very localised, being relatively large for fibres nearby the broken fibre, but low for fibres further away [5, 36–38]. Therefore, few neighbouring fibres carry a significant stress concentration. Nonetheless, if the matrix yields, the matrix shear yield stress limits the stress transfer. This generates smaller stress concentration factors than when it behaves as an elastic solid, but more fibres are affected by the stress concentration and the ineffective length becomes longer [5, 37–39]. The latter is usually the case in FRP since the shear yield stress of polymer matrices is relatively small, with typical values ranging between $50 - 100$ MPa [37]. In addition, debonding (fibre-matrix separation) may occur which may lead to fibre pull-out and longer ineffective lengths. Matrix cracking can also appear, causing slightly larger stress concentrations [40], see Fig. 2.5. To make things even more complex, this process is transitory, that is, dynamic effects occur which change the stress redistribution around the broken fibres along time. This will be explained in Section 2.1.1.2.

At low fragmentation stages, fibre breaks occur at random places depending on the fibre strength scatter. However, as the load is incremented, clusters of neighbouring broken fibres start to form due to the presence of the stress concentration (Fig. 2.4b). Eventually, final failure is reached either due to the accumulation of damage or the unstable propagation of a large critical cluster [4, 41, 42].

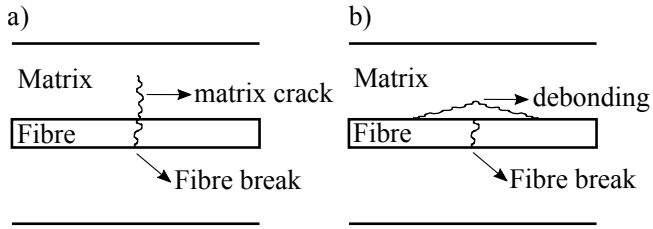

Figure 2.5: a) mode I matrix cracks may appear around a fibre break increasing the stress concentration carried by the surrounding fibres and b) a weak bonding between the fibre-matrix interphase may cause debonding and fibre pull-out. Additionally, all scenarios may appear altogether and also include matrix yielding, creating a very complex stress state.

In a non-hybrid composite, this process leads to a quasi-brittle, catastrophic failure. Nonetheless, in a hybrid composite, the failure development is altered leading to a delay of the failure strain of the LE fibre [3, 8, 10, 18, 22, 24, 27, 31–

33, 35, 39, 43, 44]. This alteration is because of the following reasons. Firstly, the presence of two fibres with different stiffness and diameter (LE and HE) fibres, changes the magnitude of the Stress Concentration Factors (*SCFs*) around the broken fibres compared to the baseline non-hybrid composites [45, 46]. Since the HE fibre usually has a smaller Young's modulus, the HE fibre carries larger *SCF* than the LE fibre [45, 46]. This in turn, delays the formation of clusters in the LE fibre population. Secondly, given that the HE fibres have a larger failure strain, the presence of HE fibres surrounding a cluster of broken LE fibres can act as a crack arrester, delaying the propagation of the cluster [31]. A final fact is the presence of size effects [3]. It is well known that composite materials exhibit a size effect, that is, the strength of the material decreases by increasing the volume of the material [47–55]. Given that a hybrid composite of the same volume as that of a non-hybrid composite contains fewer LE fibres, the failure strain of the LE fibre in the hybrid should already be larger than that of the baseline non-hybrid composite due to the associated size effects.

Although the failure development in hybrid composites has been widely studied and is relatively well understood, there are still some unknowns. Currently, the importance of size effects, matrix cracking and yielding as well as debonding has not been investigated. Some of these gaps will be discussed further in Section 2.1.2.

2.1.1.2 Dynamic effects

Another important hypothesis for the hybrid effect is the presence of dynamic effects. When a fibre breaks, the elastic energy that was sustained by the fibre is released in the form of a stress wave which dampens after some time. During this period, dynamic stress concentrations which exceed the static condition appear, see Fig. 2.6. Such a temporal increase of stress concentration could lead to more fibre failures.

Hedgepeth [56] was the first author to study the dynamic *SCF* around broken fibres in non-hybrid composites considering an elastic matrix. The maximum dynamic *SCF* was 60% higher than the static when a single fibre failed. Later Xing *et al.* [26] studied, for the first time, the dynamic effects in hybrid composites using a simplified model consisting of one row of LE fibres and another row of HE fibres in an elastic matrix. The authors found smaller dynamic *SCFs* in

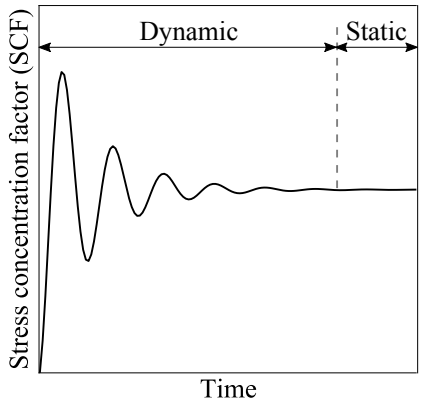

Figure 2.6: Schematic representation of the dynamic stress concentration carried by an intact fibre caused by a fibre failure.

the hybrid than in the LE non-hybrid composite. Accordingly, this was caused because of two independent and out-of-phase stress waves, one for each fibre population, that developed and propagated through the hybrid composite. This phenomenon by itself should lead to hybrid effects. Further improvements were performed in Ji *et al.* [57], who observed that the dynamic effect decreased by increasing the distance from the fibre break plane. That should lead to the formation of more co-planar clusters [5]. Sakharova and Ovchinskii [58, 59] found even larger *SCFs* in non-hybrid composites than Hedgepeth [56], with dynamic *SCFs* that were 200% higher than the static. The authors also obtained larger dynamic *SCFs* when the fibre volume fraction was around 60–70%. Recently, Ganesh *et al.* [60, 61] obtained similar results to those of Hedgepeth and Xing *et al.* [56, 57] using a more advanced 2D finite element model.

Bullegas [62] was the first author to incorporate dynamic effects into a model for simulating the tensile strength and damage development of non-hybrid composites under longitudinal tension. The dynamic effects decreased the strength by 10% compared to the static. Moreover, the formation of clusters was clearly altered, as the average distance between consecutive breaks decreased when using the dynamic model. More recently, Tavares *et al.* [63], presented an advanced spring element model considering dynamic effects. The dynamic *SCF* with a plastic matrix in a non-hybrid composite was, on average, 43.2% higher, whereas it was 83.2% higher with an elastic matrix compared to the static. While the formation of clusters was seen to be closer to the experimental data using the dynamic model, nevertheless the predictions of final failure did

not significantly change, especially when using a plastic matrix. Be that as it may, they did not study the influence the dynamic effects have on the failure of hybrid composites.

Despite the increasing number of studies concerning dynamic effects, this area is still poorly investigated in hybrid composites. At present, all the work regarding dynamic effects has been numerical, which limits the veracity of the models. Currently, the influence that the dynamic effects have on the tensile failure and damage development in hybrid composites has not been explored. Their impact on the hybrid effect has also yet to be clarified. Consequently, this topic merits further research due to its possible importance.

2.1.1.3 Thermal residual stresses

The final hypothesis for explaining the hybrid effect is related to the thermal residual stresses derived from the manufacturing process due to the different coefficients of thermal expansion of the fibres and the matrix. This phenomenon occurs as follows. Once the temperature is raised to cure the thermoset matrix, the LE and HE fibres attempt to change their length according to their respective coefficients of thermal expansion. After the resin is cured and the composite is cooled down, a force equilibrium is satisfied, inducing different residual stresses into the LE and HE fibres [3]. In the classic hybrid composite consisting of carbon and glass fibres, this leads to compressive residual stresses in the LE fibres, and tensile in the HE fibres. Therefore, the failure strain of the LE fibre is delayed, leading to hybrid effects.

In any case, it has been proved that the thermal residual stresses can only account for 10% of the hybrid effect [7, 8, 22]. Because hybrid effects up to 50% have been reported, it is clear that the thermal residual stresses only play a secondary role. Nonetheless, the influence they have on the formation of clusters has not been explored.

2.1.2 Influencing parameters on the hybrid effect

There are different parameters that have an impact on the hybrid effect. The most important ones correspond to the hybrid volume fraction, the fibre elastic properties, the failure strain ratio, the fibre strength scatter, the degree of disper-

sion of the fibres and the matrix properties. In the following, these parameters and their respective implications are highlighted.

2.1.2.1 Hybrid volume fraction

The Hybrid Volume Fraction (*HVF*) is one of the most important parameters influencing the hybrid effect. Here, the *HVF* is referred to as the fibre volume fraction of LE fibres, V_{LE}, over the total, V_{f}, so that $HVF = V_{\mathrm{LE}}/V_{\mathrm{f}}$. Different studies have demonstrated that a lower number of LE fibres, i.e. a lower *HVF*, leads to larger hybrid effects [9, 27, 31, 34, 35, 64, 65]. This can easily be understood. When the *HVF* is low, there are few LE fibres in the composite. This hinders the creation of clusters of LE fibres since the LE fibres are mainly surrounded by HE fibres, resulting in higher hybrid effects [66]. The failure of the material is therefore dominated by the HE fibre population. Nonetheless, given that the failure strength of the LE fibres is usually larger than that of the HE fibres, the failure strength may be lower. On the contrary, when more LE fibres are added, the failure of the composite is dominated by the LE fibre since clusters are easily formed. In general, this leads to greater strength but smaller hybrid effects. Thus, the aim should be to attempt to reach larger hybrid effects with larger *HVF* to also maximise the strength of the material [3]. This may be possible with a certain combination of fibres, e.g. by hybridising an HE fibre with a failure strength larger or similar to that of the LE fibre.

It has also been demonstrated that the *HVF* significantly affects neither the *SCF* nor the ineffective length on the LE fibres when an LE fibre is broken [45]. This means that, the increase in the hybrid effect due to a smaller *HVF*, occurs only because of the HE fibres surrounding LE fibres and delaying the formation of clusters.

2.1.2.2 Elastic properties

The elastic properties of each fibre are of great importance because they modify both the *SCF* around intact fibres and the ineffective length of broken fibres [22, 25, 37, 45, 67–70]. In a hybrid composite, the presence of fibres with different elastic properties alters the *SCF* around breaks compared to non-hybrids. This may cause a reduction of the *SCF* carried by LE fibres compared to the all LE non-hybrid composite, resulting in a delay in the formation of

LE clusters and the development of damage [33, 45, 46, 71]. According to Swolfs *et al.* [45] a stiffer HE fibre reduces the *SCF* on the HE fibres when the LE fibre is broken, while this influence on the *SCF* carried by the LE fibres is negligible. Conversely, increasing the ratio between the Young's modulus of the LE fibre over the HE fibre, decreases the *SCF* on the LE fibres compared to the non-hybrid material when the HE fibre is broken [31], while the influence on the *SCF* carried by HE fibres should be small. Thus, on the one hand, a stiffer HE fibre may help to delay the formation of HE clusters when the LE fibre is broken but, on the other hand, a softer HE fibre may help to reduce the *SCF* on LE fibres when the HE fibre is broken. To maximise the hybrid effect, a lower HE stiffness may be better, but this will undoubtedly depend on each material system.

2.1.2.3 Failure strain ratio

Another important parameter is the failure strain ratio. If the HE fibre failure strain is similar to that of the LE, some HE fibres will break before all the LE fibres have failed due to the strength scatter, reducing the hybrid effect. Otherwise, if the HE failure strain is much larger than the LE failure strain, both fibres will act independently and a higher hybrid effect will be produced. Notwithstanding, a ductile failure process may not be achieved because the failure of both fibres will not be continuous [3, 35]. As a result, maximising the failure strain ratio between the LE and HE fibres while maintaining a progressive failure should be the best scenario. According to some work, the failure strain ratio increases the hybrid effect up to a plateau where no more gain is observed [33, 72]. This plateau is reached within a ratio equal to 2.

2.1.2.4 Fibre strength scatter

The fibre strength scatter of both LE and HE fibres also plays a significant role. It is well accepted that a higher strength scatter leads to a more progressive formation of clusters and higher hybrid effects [25, 33–35, 64]. This occurs because a wider strength scatter allows fibres to progressively fail in a wider strain margin. Conversely, if the scatter is very narrow, a progressive failure cannot be achieved because all fibres simply break at once. As Fukunaga *et al.* [64] pointed out, 'had the LE strength scatter been zero, the hybrid effect

would not have existed'. Or a similar quote from Manders [73], 'the hybrid effect arises from a failure to realise the full potential strength of the fibres in all-carbon fibre composites, rather than from an enhancement of their strength in the hybrids'.

2.1.2.5 Degree of dispersion

Another important aspect of hybrid composites, which is very closely related to the hybridisation level, is the degree of dispersion of the fibres [3]. This is defined as how well the two fibres are mixed. For example, the hybrid composite illustrated previously in Fig. 2.2a, presents a very low dispersion. A higher dispersion can be accomplished by increasing the number of layers or decreasing the thickness of the layers [3]. A better dispersion is obtained within the intralayer hybrid shown in Fig. 2.2b. By decreasing the bundle thickness or increasing the number of bundles as such, dispersion can be further enhanced [3]. Nonetheless, the best dispersion is theoretically obtained within the randomly allocated fibres, leading to an intrayarn hybrid, see Fig. 2.2c.

Many authors have found greater hybrid effects with higher dispersions [8, 30–32, 64]. Considering that an intrayarn hybrid leads to the greatest dispersion, hybridisation at that level should be the most effective. Nevertheless, Swolfs *et al.* [31] studied the effect of the dispersion of fibres on the hybrid effect and the highest was found for interlayer instead of intrayarn hybrids. Despite these findings, Swolfs *et al.* used a simplified geometry of fibres, with all fibres having the same radius, to model the hybrid composites. This could have affected the results. Moreover, the authors focused their study on $HVF = 50\%$ in a carbon-glass hybrid. Since the failure development is very dependent on the HVF and the fibre properties, the conclusions found in their work may not apply to different hybrid composites or other HVF. Despite the importance of the fibre dispersion, this term has generally not been rigorously calculated. To overcome this issue, Swolfs *et al.* [74] defined the dispersion as the ratio of the LE fibre radius, R_{LE}, over the average centre-to-centre distance, d_i^{c}, from a LE fibre to the six nearest HE fibres averaged over all LE fibres. Consequently, dispersion is given by

$$Dis = \left\langle \frac{R_{\mathrm{LE}}}{\sum_{i=1}^{6} d_i^{\mathrm{c}} \left(LE_j \rightarrow HE_i\right)/6} \right\rangle \text{all j} \tag{2.2}$$

This definition allows a more rigorous description of which is the degree of dispersion of a certain hybrid composite, thus facilitating the comparison between different hybridisations. The downside, is that choosing the six nearest neighbours to calculate the average distance is somewhat arbitrary.

To date, the effect that the hybrid configuration (interlayer, intralayer or intrayarn) has on the ductile response of the hybrid is unexplored. Since the hybrid configuration changes the dispersion of the fibres, it may not only influence the hybrid effect, but it may also change the ductile behaviour of the hybrid. Moreover, its influence on the hybrid effect for different *HVF* than that studied by Swolfs *et al.* [31] should also be investigated.

2.1.2.6 Matrix properties

The matrix also plays an important role because it transmits the load between fibres. As a consequence, it has a considerable influence on both the ineffective length and the *SCF*. The presence of matrix cracking, debonding and matrix yielding can further affect stress redistribution around fibre breaks, which may alter the hybrid effect and the failure of the material. Unfortunately, little work has been done on this area in hybrid composites.

The importance matrix yielding has on stress redistribution around fibre breaks in non-hybrid composites has been pointed out by many authors [4, 36–39, 75–78]. Accordingly, adding matrix plasticity reduces the *SCF*, but spreads the load loss over more fibres and increases the ineffective length. This occurs because the shear stress transfer is limited by the matrix shear yield stress. Adding matrix plasticity to models also leads to a more realistic formation of clusters compared to experimental data [37]. So far, the effect matrix yielding has on the *SCF* around broken fibres in hybrid composites has not yet been investigated. Pan and Postle [79] demonstrated that increasing the matrix shear yield strength increases the hybrid effect if the *HVF* is large. However, they did not check the influence that including matrix yielding has on the *SCF* nor on the damage development.

The influence of matrix cracking in non-hybrid composites was investigated by Swolfs *et al.* [40]. Although matrix cracking led to larger *SCFs* around fibre breaks, nonetheless it did not significantly affect either the development of

clusters or the failure strain [40]. In any case, the authors recognised that more experimental work is needed to determine exactly when these matrix cracks occur. Currently, no studies have explored or incorporated matrix cracks in hybrid composites, and hence their impact is yet to be revealed.

Fibre-matrix debonding is generally omitted in many studies. Currently, research dealing with debonding in non-hybrid composites remains scarce [80–86]. In general, debonding has a similar effect to that of matrix yielding, with the difference being that it leads to larger ineffective lengths and smaller *SCFs*. This is because the shear stress transfer in a debonded matrix is (in theory) smaller than in a yielded matrix. The magnitude of the *SCF* and that of the ineffective length greatly depends on the friction in the fibre-matrix interphase [82, 83]. A smaller friction, will produce smaller shear stresses, hence reducing the *SCF* and increasing the ineffective length. To the author's best knowledge, debonding has not been studied in hybrid composites. This makes it difficult to establish its importance as well as the effect associated parameters, such as the fibre-matrix interphase strength, have. Another problem is the difficulty in observing debonding in composites with millions of fibres [5]. Common techniques such as micro-Raman spectroscopy or synchrotron radiation computed tomography do not have enough resolution to see debonding [41, 42, 87].

The viscoelastic behaviour of polymer and metal matrix composites may also be somewhat implicated. When the matrix is maintained under constant load, it creeps, decreasing the stress carried by the matrix, and thus increasing the stress in the fibres [5, 88, 89]. Moreover, over time the matrix becomes 'more ductile'. Basically, this causes the *SCF* around broken fibres to be reduced, but more fibres are subjected into *SCF*, and the ineffective length increases [5, 88, 90–95]. Therefore, if the viscoelastic effects are important, the formation of clusters may be altered, affecting the damage development and failure of the material. To the author's best knowledge, the implication that the viscoelastic matrix behaviour has in the failure of hybrid composites has not yet been explored. Thus, it is difficult to judge the importance of this topic.

Given that the matrix plays an important role on the load redistribution around fibre breaks, this area merits further study with hybrid composites. The effect of matrix yielding, cracking, debonding as well as that of the viscoelastic behaviour should be further investigated and incorporated into models.

2.1.2.7 Other parameters

There are other properties such as the interlaminar strength and fracture toughness, which may also have some influence on the hybrid effect [3]. The importance that the mode II interlaminar fracture toughness has on the failure of interlayer hybrid composites has been highlighted [18]. If the strain energy released by the LE fibre after failure is larger than the mode 2 interlaminar fracture toughness, delamination occurs. This may lead to final failure depending on the layer thickness of each ply, the ply allocation and the relative thickness between the layers (which also governs the *HVF*). By reducing the LE layer thickness, the strain energy is reduced, avoiding catastrophic delamination and allowing a progressive fragmentation of the LE fibre leading to a ductile failure. According to Jalalvand *et al.* [11, 96], four failure scenarios, which are mainly governed by the thickness of the layers, arise: a) premature failure of the HE fibre, b) catastrophic delamination followed by HE failure, c) progressive fragmentation of the LE fibres and then HE fibre failure and d) progressive fragmentation of the LE fibre material followed by dispersed delamination and then HE fibre failure.

2.1.3 Tensile behaviour of hybrid composites

The longitudinal Young's modulus of hybrid composite materials follows a linear rule of mixtures [7] with $E_H = E_{LE}V_{LE} + E_{HE}V_{HE} + E_mV_m$, where E_{LE}, E_{HE} and E_m are the longitudinal Young's modulus whilst V_{LE}, V_{HE} and V_m are the volume fractions ($V_{LE} + V_{HE} + V_m = 1$), where subindices LE, HE and m stand for the LE fibre, HE fibre and matrix, respectively. According to Swolfs *et al.* [3], deviations from the linear rule of mixtures might be explained because of variations in the fibre volume fractions and fibre orientation.

The tensile strength of hybrid composites may follow a bi-linear rule of mixtures [3, 97]. During the tensile failure of hybrid composites, the LE fibre population fails first. After that, different possibilities may happen. If the volume fraction of HE fibres is very large, the stress usually reaches higher stresses than the stress at the failure strain of the LE fibres. Therefore, the strength is dominated by the stress of HE fibres at their failure strain. Otherwise, at low volume fractions of HE fibres, the stress of the LE fibres may exceed that of the HE fibres, see Fig. 2.7. However, these behaviours may differ depending on the

hybrid configuration, the distinct parameters affecting the hybrid effect and the presence of pseudo-ductility. Hence, the bi-linear response may only occur when the LE and HE fibres fail separately.

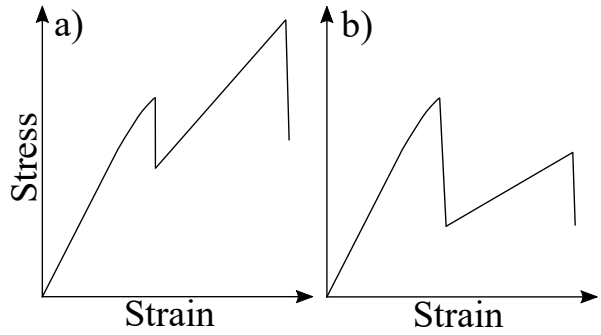

Figure 2.7: Bi-linear behaviour of some hybrid composites. a) the strength is dominated by the HE fibre population and b) the strength is dominated by the LE fibres.

As previously discussed in Section 2.1, fibre hybridisation can lead to a ductile failure process. If the failure between the LE and HE fibres in the hybrid is gradual, a ductile response similar to those of ductile metals like steel, can be achieved (Fig. 2.1b). This is usually called pseudo-ductility [3, 6–18, 35, 39]. Notice that in non-hybrid composite materials, it is also possible to obtain pseudo-ductility by controlling the damage mechanisms [98]. Nonetheless, in this thesis the focus is solely on hybrid composites. Nowadays, many authors have obtained a ductile response in hybrid composites both numerically and experimentally.

In terms of the experimental work, most authors have focused on testing interlayer hybrid composites, as these are easier to manufacture. Generally, it seems that pseudo-ductility can only be achieved if the *HVF* is low, and the thickness of the LE fibre plies is thin [3, 15, 18]. In the 1970s, Bunsell and Harris [7], and Manders and Bader [8], achieved pseudo-ductility in carbon-glass hybrids with high *HVF* thanks to the fact that at that time carbon fibres were weaker than they are nowadays. With stronger carbon fibres, reducing the *HVF* may be the only way to achieve a ductile behaviour [3]. However, the actual focus should be on achieving pseudo-ductility at high *HVF*, as then the composite may be stronger. A minimal bonding strength between layers is also necessary to achieve pseudo-ductility in interlayer hybrid composites [7]. Not only can the failure strain be enhanced, but so too the failure strength. Jones

and Dibenedetto [9] hybridised carbon fibres with either glass or aramid fibres. A 92% improvement in the strength of the carbon fibres was obtained when the carbon fibre content was lower than 6%, thus allowing all carbon fibres to act independently. More recently, Czél and Wisnom [18] manufactured and tested in tension interlayer unidirectional hybrid composites by sandwiching various numbers of thin carbon prepreg plies between standard thickness glass prepreg plies. The specimens containing one and two plies of thin carbon failed in a desired pseudo-ductile manner, whereas the specimens with three and four plies failed with unstable delamination. Thus, the LE layer thickness played a crucial role in the material failure. Reducing the LE layer thickness reduced the strain energy after the LE failure, avoiding catastrophic delamination and allowing progressive fragmentation of the fibres. Similar findings were obtained in Wisnom *et al.* [15], with failure strains up to 20% for the ductile hybrids.

Further work was performed by Yu *et al.* [17], who intermingled hybrid composites comprising high-modulus carbon with E-glass using aligned discontinuous fibres. As a result of the progressive carbon fibre fragmentation, good pseudo-ductile responses were obtained. Albeit employing discontinuous fibres, this is currently the only experimental work that has achieved pseudo-ductility using an intrayarn hybrid configuration. Diao *et al.* [99] were able to manufacture and test intrayarn hybrid composites of continuous carbon-carbon epoxy, but the tensile behaviour obtained did not present a safe and large pseudo-ductility. In addition, Jalalvand *et al.* [11, 96] tested hybrid specimens comprising thin-ply carbon fibres with standard thick-plies of glass fibres leading to large pseudo-ductile responses. Similar pseudo-ductile responses were later obtained by Czél *et al.* [16], this time by hybridising thin-ply UD all carbon-epoxy composites of high modulus and strength. Finally, Fotouhi *et al.* [12] also obtained large pseudo-ductile responses in all fibre orientations under fibre tensile loading with quasi-isotropic high performance thin-ply carbon-glass hybrid laminates.

In the numerical work, most authors that modelled pseudo-ductility employed intrayarn hybrid composites, unlike the experimental work, although there were some exceptions [15, 31, 100]. In general, the modelling work has confirmed the influence that the different parameters involving the hybrid effect (discussed in Section 2.1.2) have on pseudo-ductility [15, 31, 33–35, 39, 96]. To achieve pseudo-ductility, a wide strength scatter, low LE fibre content, a large failure

strain ratio and a continuity between the failure of the fibres is necessary. The different models available in the literature for predicting failure will be discussed in Section 2.3.

Another possibility to achieve a higher failure strain is to hybridise a brittle fibre such as glass or carbon with a ductile fibre such as steel, polyamide, polyethylene, or to use natural fibres [3, 101, 102]. These options, however, are beyond the scope of this thesis. Interested readers are referred to a recent review and the references therein [3].

2.1.4 Conclusions

The hybrid effect is now clearly established. There are three main hypotheses explaining its presence, with the failure procedure considered to be the most important one, thermal residual stresses considered to play a secondary role, and dynamic effects whose importance is still to be clarified. The main influencing parameters on the hybrid effect are identified in the literature. Different studies have clearly demonstrated that a lower *HVF*, a wider strength scatter, a larger failure strain ratio, a larger ratio between the Young's modulus of the LE fibre over the HE and a higher degree of dispersion of the fibres should increase the hybrid effect. The mode II interlaminar fracture toughness, as well as the layer thickness in interlayer hybrids, are also key parameters, while other properties such as the fibre-matrix interphase strength are not clear. The influence of size effects, matrix plasticity, debonding, matrix cracking as well as viscoelasticity has not yet been investigated.

Many authors have obtained hybrid composites exhibiting a ductile behaviour, both numerically and experimentally. Therefore, fibre hybridisation is a feasible solution to the lack of toughness in composite materials. Nearly all the research has demonstrated that a small percentage of LE fibres is required to achieve a ductile response. A large strength scatter is also critical. In the case of interlayer hybrid composites, a small ply thickness for the LE fibre is necessary as well as good bonding between plies to avoid unstable delaminations, and to allow a progressive fragmentation of the LE fibres. Last but not least, a continuity between the failure of the LE and HE fibres is also mandatory to avoid load drops and allow a gradual failure. In theory, a larger hybrid effect should translate into a larger ductility of the composite. Hence, pseudo-ductility

should be influenced by the material parameters in the same way the hybrid effect is. However, more work needs to be carried out to prove this hypothesis. In addition, while modelling results have mainly focused on intrayarn hybrid composites, experimental testing has focused on interlayer hybrids. More experimental evidence, with intralayer and intrayarn hybrid configurations, is therefore necessary. Likewise, modelling work with interlayer and intralayer hybrid composites using a realistic random distribution of fibres should be addressed, instead of considering a regular packing [15, 31]. A direct comparison of the effect the hybrid configuration has on the ductile response of a hybrid composite should be performed.

Despite the tremendous advances made in recent years, more work is needed. More accurate and realistic models, incorporating the effects influencing the tensile failure of hybrid composites, need to be developed. Currently the state of the art of hybrid composites is behind the state of the art of non-hybrid composites. The development of more advanced models together with more accurate experimental data should allow this gap to be closed further.

2.2 Statistical models for modelling the tensile strength of fibres

As discussed in Section 2.1.1.1, the strength of brittle fibres is not determined due to the presence of flaws, and follows a statistical distribution exhibiting weakest-link characteristics. This implies that a fibre breaks as soon as the weakest link is overloaded. Such strength scatter has been widely described by means of a Weibull distribution [103]. In the following, this distribution and their variations are discussed.

2.2.1 Traditional Weibull distribution

The most widely used statistical distribution for representing the strength of brittle fibres is the traditional Weibull distribution [103]. Accordingly, the failure probability of a fibre segment of length L, with strength σ^{u}, is

$$P = 1 - \exp\left(-\frac{L}{L_0}\left(\frac{\sigma^{\mathrm{u}}}{\sigma_0}\right)^{m}\right) \tag{2.3}$$

where m is the Weibull modulus, σ_0 is the characteristic Weibull fibre strength and L_0 is the characteristic gauge length. Very high Weibull modulus leads to a low strength variability, for instance, in metals where m is around 20. However, low Weibull modulus, i.e. values between 3 and 9, lead to high strength dispersions like in composite materials, see Fig. 2.8. Moreover, a longer length L reduces the strength, since the probability of having a weak link is greater.

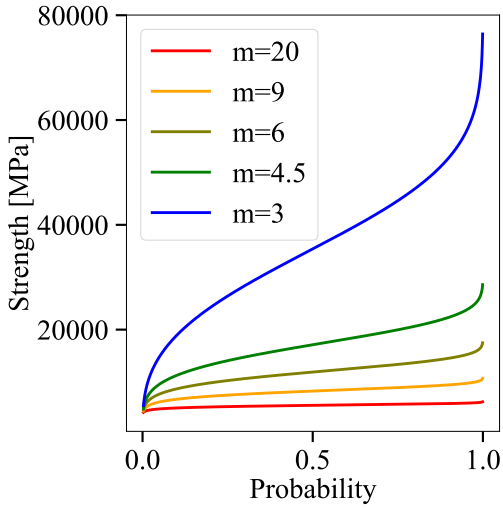

Figure 2.8: Example of the strength scatter of a fibre following a Weibull distribution with different Weibull modulus m, considering $\sigma_0 = 4000$ MPa, $L_0 = 10$ mm and $L = 10 \cdot 10^{-3}$ mm. A smaller Weibull modulus m markedly increases the strength scatter.

It has already been reported in the literature that this distribution overestimates the strength for very low values of gauge lengths L [5, 37, 52, 104–106]. This could be because of variations in the fibre diameter, variations in the Weibull distribution from fibre to fibre and/or the presence of different flaw populations [5]. Consequently, some authors proposed modified Weibull distributions which attempt to solve these issues. In the next section, these are discussed.

2.2.2 Modified Weibull distributions

One of the modified Weibull distribution functions proposed in the literature is known as the 'Power Law Accelerated Weibull distribution' (PLAW). This distribution adds a correction factor into the Weibull equation to be able to characterise the fibre strength at short gauge lengths without overestimating the

strength [52, 104, 105]. Within this, the failure probability becomes

$$P = 1 - \exp\left(\left(-\frac{L}{L_0}\right)^{\alpha_w}\left(\frac{\sigma^u}{\sigma_0}\right)^{m}\right) \tag{2.4}$$

where α_w is the correction factor, which commonly varies between 0.6 and 0.9 [52, 104, 105]. This distribution has mainly been employed in micromechanical simulations where the gauge length, L, tends to be small. Although this equation may improve the extrapolation into short gauge lengths, it adds the need to experimentally determine the value of α_w. Another issue with this distribution is its physical background since it is based on pure fitting.

Curtin [107] presented another model known as the 'Weibull of Weibull' (WOW) which reverts into the PLAW but with a solid physical background. In the WOW model, the strength distribution along a fibre follows a traditional Weibull distribution with modulus m', whereas the characteristic strength of the fibre follows another Weibull distribution with modulus ρ_w. Within these considerations, the distribution given by Curtin reverts to the PLAW with

$$m = \frac{\rho_w m'}{(\rho_w^2 + m'^2)^{1/2}} \qquad \alpha_w = \frac{\rho_w}{(\rho_w^2 + m'^2)^{1/2}} \tag{2.5}$$

The main issue of this model is that more parameters are necessary, since ρ_w and m' must be determined as to characterise the strength of the fibres.

To consider that more than one population flaw is present in the fibres, multimodal Weibull distributions were formulated, from which the bimodal Weibull distribution is the most common [108–111]. Within this, the failure probability becomes

$$P = 1 - \exp\left(-\left(\frac{L}{L_0}\right)\left(\frac{\sigma^u}{\sigma_{01}}\right)^{m_1} - \left(\frac{L}{L_0}\right)\left(\frac{\sigma^u}{\sigma_{02}}\right)^{m_2}\right) \tag{2.6}$$

where σ_{01}, σ_{02}, m_1 and m_2 are the characteristic fibre strength and Weibull modulus of each population flaw, respectively. The second population flaw of this Weibull distribution determines the strength at short gauge lengths. According to Harlow and Phoenix [112], this distribution puts an upper limit into the strength at short gauge lengths, and thus may be more realistic than the traditional Weibull function. The rate at which the strength at short gauge lengths levels off, depends on the magnitude of the Weibull modulus m_2 [5]. Again, the main issue with this equation is that many different parameters must be

determined.

Besides the named statistical distributions, there is some work which has incorporated minor variations into the Weibull distribution [113–115]. Further to this, other authors have also proposed the use of a normal distribution [36, 116]. According to R'Milli *et al.* [116], the Gaussian probability density function is

$$P = \frac{1}{SD\sqrt{2\pi}} \exp\left(-\frac{(\varepsilon^{u} - \mu_{n})^{2}}{2SD^{2}}\right) \tag{2.7}$$

where μ_{n} is the mean, SD is the standard deviation and ε^{u} is the fibre failure strain. R'Milli *et al.* [116] determined that the normal distribution is appropriate to describe the flaw strength in brittle fibres. Furthermore, they also claimed that the Weibull distributions are a good approximation and easier to apply.

Finally, other authors have proposed alternative distributions [117–119]. In practice, these are not used, since they are either too complex mathematically or they need more complicated experimental testing to determine all the parameters involved.

2.2.3 Conclusions

Despite the enormous number of statistical distributions available to date, there is not any agreement as to which distribution would be the best one to use. Some studies suggest that the traditional Weibull distribution overpredicts the strength at short gauge lengths and that the bimodal Weibull distribution is in better agreement with experimental data [108]. Other authors have pointed out that the WOW model yields better predictions of the strength of composites than the other Weibull distributions do [39, 52]. Nonetheless, the traditional Weibull distribution is still the most widely used. This is, however, an important and critical topic, specially for modelling the failure of composite materials. Reliable data is mandatory if the strength is meant to be predicted with accuracy [5].

Even a small error in determining the Weibull distribution could lead to massive errors in the input data for models [5]. The problem is that performing experimental tests to determine the Weibull distribution is no trivial task. Firstly, a large number of experimental tests are mandatory to accurately determine

the Weibull parameters, albeit most authors perform fewer tests than what are needed [120]. Secondly, clamping effects may occur during the test. Finally, a minimum strength is needed to extract a fibre from a yarn to perform the test. This is known to cause non-linearity at low fibre strengths in Weibull plots [52, 105, 119]. Therefore, the literature clearly needs to draw further attention to this topic and precisely propose the best distribution to use, as well as to accurately determine, all the parameters related.

2.3 Micromechanical modelling of the tensile failure of composite materials

In this section, an overview of the most important models presented in the literature that are able to reproduce the tensile failure of UD composite materials is provided. Some models are limited to non-hybrid composites, while others do not face such limitations. Here, the models that are able to consider hybrid composites will always be emphasised. Although this thesis deals with hybrid composites, it is still important to review models for non-hybrid composites as well since they may be able to be extended to hybrids. It is also worth noting that each model possesses unique features and limitations, and thus each model is able to capture different failure mechanisms.

Composite materials can be studied on three levels: micromechanical, mesomechanical and macromechanical. On the micromechanical level, the fibre and matrix are represented and their interaction can be studied. However, on the mesomechanical level, the fibres and matrix are considered as a unique material with homogeneous mechanical properties at the layer level. This allows the interaction between layers, but not between fibres and matrix, to be captured. Finally, on the macromechanical level, the scale of the global structure or mechanical component is taken into consideration using, for instance, laminate theory [121], see Fig. 2.9. Since the failure of composite materials is a micromechanical problem which involves the formation of clusters, the focus here is placed on the different micromechanical models published in the literature.

There are many micromechanical models with different modelling considerations. In this thesis, two main groups are considered: Global Load Sharing (GLS) models, and Local Load Sharing (LLS) models. In the GLS models, the

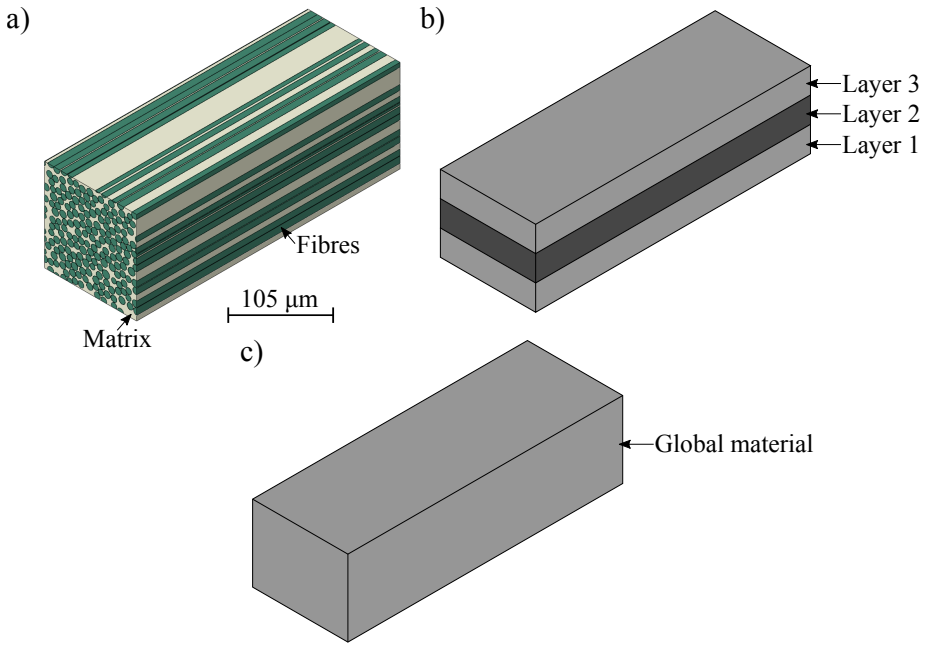

Figure 2.9: The three mechanical levels for studying composite materials: a) micromechanical, where fibres and matrix are represented, b) mesomechanical, where fibres and matrix are an homogeneous material at each ply or layer and c) macromechanical, where a homogeneous material is considered for the entire structure.

load loss by a broken fibre is equally redistributed around all intact fibres. This is a simple, but unrealistic approach which does not allow the formation of clusters to be captured. As a result, these models can only predict the failure when the interaction of fibres is low. Instead, in the LLS models the load of a broken fibre is redistributed around the neighbouring intact fibres which allows the formation of clusters to be captured. While this approach is more accurate, it is more challenging to model. Moreover, analysing the results is also a difficult task [31]. Additionally, shear-lag models which are able to predict the ineffective length of broken fibres, as well as analytical stress concentration factor models which predict the *SCF* around broken fibres, are also discussed.

When a composite material is studied on the micromechanical scale, the fibres and matrix are usually represented by generating what is called a 'Representative Volume Element' (RVE). An RVE may be defined as a *volume representing* a real material i.e. a bundle containing fibres and a matrix in the field of composite materials. This part should be representative, that is, it should be big enough to capture all the physics involved [122, 123]. Nevertheless, its size still needs

to be computationally workable since studying an RVE comprising the real size of the material is generally not feasible. According to some studies, the size of the RVE should be fifty times the fibre radius to accurately capture the elastic properties of the material [122, 123]. Nonetheless, when dealing with damage, the size may need to be far larger than that to accurately capture the stress redistribution around breaks. Moreover, size effects can occur. Thus, ideally the size of the RVE should be equal to the real material specimen. It is worth noting that in some cases the RVE can only contain the fibres, since the matrix may be physically omitted. A very important detail when generating the RVE, is the spatial position of the fibres being taken into consideration. In a 1D RVE, only one row of fibres is considered, as illustrated in Fig. 2.10a. A more realistic representation is obtained with a 2D RVE. In this last case, the fibres can be allocated within a square, an hexagonal or a random packing, as shown in Figs. 2.10b-d, respectively. The latter is the most realistic representation of a composite material, since the spatial allocation of the fibres is always random, and allows the stress to be captured more accurately [124, 125].

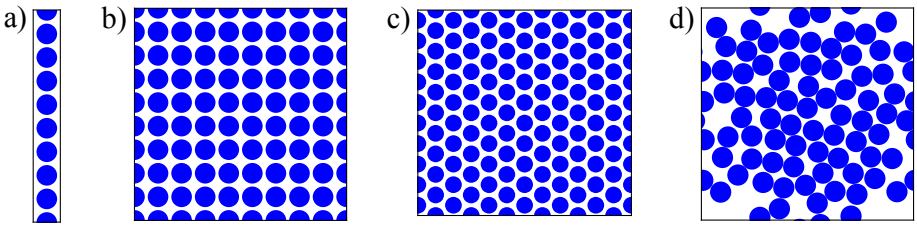

Figure 2.10: Examples of different fibre packings: a) a 1D packing of fibres with a regular spacing, b) a 2D square packing of fibres, c) a 2D hexagonal packing of fibres and d) a 2D random packing of fibres.

While generating an RVE with hexagonal or square packing is straightforward, it is not so with random packing. To generate RVEs containing a random distribution of fibres, different methods are available in the literature. One possibility is to employ digital image analysis which requires the use of sophisticated software [126–130]. Another possibility is to use an algorithmic method. With the latter, two main approaches exist: the 'hard-core' model, or the 'shaking' model. In the hard-core models, random fibre coordinates are continuously generated inside the RVE. These fibres are then accepted as long as they do not overlap with any previous existing fibre in the domain [124, 127, 128, 131–133]. In some models, different criteria are used to move the fibres around to fill empty places in order

to add more fibres until the requested fibre volume fraction is reached. On the other hand, the shaking models have a given square or hexagonal distribution of fibres that is then shaken to obtain a random one [134–139]. Currently, the most widely-acknowledged model, which employs a 'hard-core' approach, is that developed by Melro *et al.* [124] and extended by Tavares *et al.* [35], to generate hybrid intrayarn composites. The algorithm is quite powerful because it was statistically validated against experimental RVEs [126], and is capable of reaching a fibre volume fraction over 65% [124]. In any case, as will be seen in the following subsections, most authors have employed models considering hexagonal and square packings because of their simplicity compared to random packings.

2.3.1 Global load sharing models

Daniels [140] presented the first GLS model. An RVE of parallel fibres of length L without a matrix was considered, see Fig. 2.11a. Daniels assumed that the strength of the fibres follows a Weibull distribution, while the tensile strength of a bundle with infinite fibres may be represented by a normal distribution. With these considerations, the strength of a bundle with infinite fibres is

$$\sigma^{\text{ult}} = \frac{\sigma_0 \left(L/L_0\right)^{-\frac{1}{m}}}{m^{\frac{1}{m}} e^{\frac{1}{m}}} \tag{2.8}$$

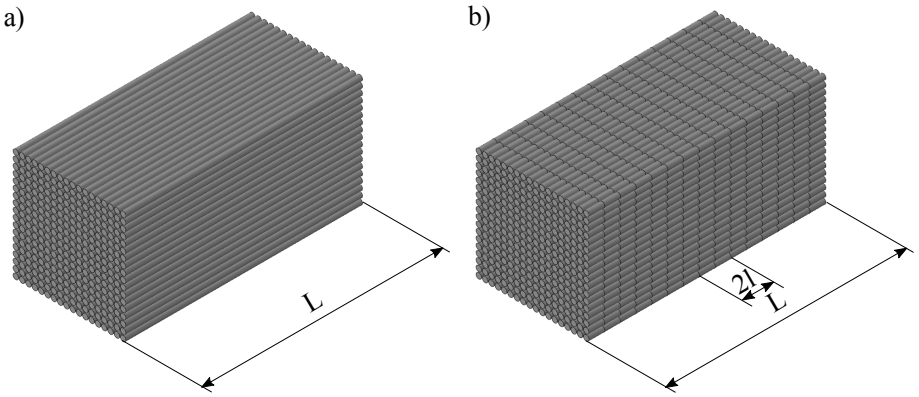

Figure 2.11: Schematic example of a bundle of parallel fibres of length L, a) as in Daniels' model [140], and b) as in Rosen's model [141], where the fibres are divided into a chain of bundles of length l.

This equation is not accurate for several reasons. Firstly, since the matrix is

omitted, when a fibre breaks the fibre is not able to carry load far from the break, which is not realistic. Thus, the ineffective length of the fibres is not captured. Secondly, it cannot deal with hybrid composites nor predict the failure curve of composite materials.

Later on, Rosen [141] improved Daniels' model by adding the effect of the matrix through a shear-lag model assuming an elastic matrix behaviour. Rosen considered a bundle of parallel fibres with length L divided into a chain of bundles with lengths $l = L/L^{\text{in}}$, where L^{in} is the ineffective length of the fibres defined as the distance from the break to which the fibre recovers a percentage, ζ, of the remote stress (Fig. 2.11b). Rosen found that the ineffective length can be estimated with

$$L^{\text{in}} = \frac{d_{\text{f}}}{2}\sqrt{\frac{1-\sqrt{V_{\text{f}}}E_{\text{f}}}{\sqrt{V_{\text{f}}}G_{\text{m}}}}\ln\left[\frac{1}{1-\zeta}\right] \tag{2.9}$$

where d_{f} is the fibre diameter, V_{f} is the fibre volume fraction, E_{f} is the fibre Young's modulus and G_{m} is the shear modulus of the matrix. Following the weakest link theory and considering a large number of fibres, Rosen reached a similar solution to that obtained by Daniels except it accounted for the ineffective length:

$$\sigma^{\text{ult}} = \frac{\sigma_0\left(L^{\text{in}}/L_0\right)^{-\frac{1}{m}}}{m^{\frac{1}{m}}e^{\frac{1}{m}}} \tag{2.10}$$

Even though this equation is more realistic than that of Daniels, it is still not enough to accurately capture the strength.

Later, Curtin also attempted to model the strength of composite materials [107, 142–148]. In his extensive work, Curtin considered another RVE with parallel fibres under a GLS rule. The matrix was hypothesised to break into short slabs relative to the fibre fragments lengths. The load of a broken fibre was then transferred by frictional shear coupling through these matrix slabs into all the surviving fibres. Consequently, the matrix behaviour considered is more realistic than the elastic matrix assumed in Daniels' and Rosen's models. With all these considerations, the mean fibres stress, $\bar{\sigma}_{\text{f}}$, at a certain applied strain, ε^0, is

$$\bar{\sigma}_{\text{f}} = E_{\text{f}}\varepsilon^0 - mE_{\text{f}}\varepsilon^0 L^{\text{in}} + mE_{\text{f}}\varepsilon^0\int_0^{2L^{\text{in}}} P\left(x, E_{\text{f}}\varepsilon^0\right)\left(L^{\text{in}} - x + \frac{x^2}{4L^{\text{in}}}\right)\mathrm{d}x \tag{2.11}$$

where $P\left(x, E_f\varepsilon^0\right)$ is the fragment length distribution, x is the fragment length and L^{in} is again the ineffective length, given by Kelly-Tyson shear-lag model [149] with

$$L^{in} = \frac{R_f E_f}{2\tau}\varepsilon^0 \tag{2.12}$$

where R_f is the fibre radius and τ is the acting shear stress. This shear stress can be considered in different ways. It may be taken as the matrix shear yield stress, as the interfacial shear strength, or as a debonded frictional shear stress (in this case it is the latter). By applying the rule of mixtures, and neglecting the matrix term, the stress of the composite becomes $\sigma^0 = V_f\bar{\sigma}_f$.

Curtin, proposed an approach to obtain the fragment length distribution, $P\left(x, E_f\varepsilon^0\right)$, which was assumed to be exact until the publication of Hui *et al.* [150], who provided the exact solution. Alternatively, a simplified analytical equation to predict the stress-strain behaviour without having to integrate, by neglecting the third term in the right hand side of Eq. (2.11), was also derived [107]

$$\bar{\sigma}_f = E_f\varepsilon^0\left(1 - \frac{1}{2}D\right) \tag{2.13}$$

where the damage variable, D, is

$$D = \left(\frac{E_f\varepsilon^0}{\sigma_R}\right)^{m+1} \tag{2.14}$$

and where σ_R is a reference strength [143, 148]

$$\sigma_R = \left(\frac{L_0\tau\sigma_0^m}{R_f}\right)^{\frac{1}{m+1}} = \sigma_0\left(\frac{2L_0\tau}{d_f\sigma_0}\right)^{\frac{1}{m+1}} \tag{2.15}$$

Moreover, the strength of the composite considered as the maximum in the stress-strain curve was determined with [143]

$$\sigma^{ult} = V_f\sigma_R\frac{m+1}{m+2}\left(\frac{2}{m+2}\right)^{\frac{1}{m+1}} \tag{2.16}$$

The model proposed by Curtin is relatively powerful, allowing the strength and the entire stress-strain curve of a non-hybrid composite to be estimated. Nonetheless, due to the GLS conditions assumed, such a model is limited to

composites with a very low interaction of fibre breaks. Additionally, size effects are not captured.

Later on, Neumeister [151] presented a similar analytical model able to predict the stress-strain behaviour, but without having to integrate. As in the model of Curtin, the matrix-shear interface is modelled by friction, assuming a constant frictional shear stress. Within this, Neumeister obtained that the composite stress is given by

$$\sigma^0 = V_f E_f \varepsilon^0 \left[\frac{1}{D+1} + \frac{1}{2\ln(D+1)} \left(\frac{D}{D+1} \right)^2 \right] \tag{2.17}$$

The term inside the square brackets on Eq. (2.17) represents the softening, and when no damage is present it is equal to 1, while it tends to zero for very large strains. Neumeister's model is able to predict the stress-strain of non-hybrid composites without solving differential equations, by taking into account the recovery zone of the fibres and the stress carried by the fibre fragments shorter than twice the stress recovery. However, the model faces the same limitations as that of Curtin. In addition, it does not yield good results for Weibull modulus lower than 2, and the strain to failure may jump to infinitum depending on the fibre properties because of the slip of fibres in the matrix.

Hui *et al.* [150] obtained an exact closed form solution for the fibre fragmentation phenomenon. Their work is very similar to that carried out by Curtin [148], except that the fragment length distribution derived, $P\left(x, E_f\varepsilon^0\right)$, is exact. They also provided simplifications and different limiting cases. Accordingly, the simplified average fibre stress is

$$\bar{\sigma}_f = E_f \varepsilon^0 \left(1 + \frac{1}{2} D + \Theta \cdot D^2 \right) e^{-D\left(1 - \frac{1}{8}\Xi D\right)} \tag{2.18}$$

where

$$\Theta = \frac{7m+12}{24(2m+3)} \qquad \Xi = \frac{m}{m+1} \tag{2.19}$$

For the derivation of the exact solution, the reader is referred to Hui *et al.* [150]. Even though the model takes into account the exact fragment length distribution, it is still limited due to not considering a local load sharing rule, nor capturing

size effects, like in the Curtin and Neumeister models. This model was extended to hybrid composites by Swolfs *et al.* [34], which will be reviewed later.

More recently, Turon *et al.* [1] presented another analytical model based on the fragmentation of a single fibre. Unlike the previous work, the model of Turon *et al.* considered the length of the composite, L, allowing size effects to be captured. By assuming that fibre strength follows a Weibull distribution, while the number of fibre breaks follows a Poison law, the average fibre stress becomes

$$\bar{\sigma}_{\mathrm{f}} = E_{\mathrm{f}}\varepsilon^{0}\left(\frac{1-e^{-2L^{\mathrm{in}}\rho_{\mathrm{b}}}}{2L^{\mathrm{in}}\rho_{\mathrm{b}}} + \rho_{\mathrm{b}}L^{\mathrm{in}}e^{-L\rho_{\mathrm{b}}}\right) \tag{2.20}$$

where

$$2L^{\mathrm{in}}\rho_{\mathrm{b}} = D \qquad L^{\mathrm{in}} = \frac{R_{\mathrm{f}}E_{\mathrm{f}}}{2\tau}\varepsilon^{0} \tag{2.21}$$

and where ρ_{b} is the fibre break density.

The authors found that a higher Weibull modulus leads to a narrower stress-strain curve, but to a higher strength. This is caused by the wideness of the stochastic fibre strength. For large Weibull modulus m all fibres break at once since the scatter is very low, the contrary occurs for a small m [1]. Moreover, Turon *et al.* [1] discussed the importance of the fibre length. When a fibre is longer, the stiffness loss is larger, since the number of breaks along the fibre increases. However, the stiffness loss due to the presence of a break is smaller in a longer fibre than in a shorter one [1]. Although this model takes into account the length of the fibres, it, like all GLS models, still faces the limitation of not capturing the formation of clusters. This model was extended by Tavares *et al.* [35], to work with hybrid composites and which will be reviewed later.

De Morais [152] considered an RVE consisting of parallel fibres of length equal to the ineffective length and with stochastic strength following a Weibull distribution. An elastic-plastic stress transfer model was taken into account for calculating the stress recovery of the fibres. By neglecting the elastic stress transfer and the contribution of broken fibres, the composite strength becomes

$$\sigma^{\mathrm{ult}} = V_{\mathrm{f}}\left[\frac{16\tau^{2}L_{0}\sigma_{0}^{m}}{(m+2)\,d_{\mathrm{f}}^{2}}\right]^{\frac{1}{m+2}} e^{\left(-\frac{1}{m+2}\right)} \tag{2.22}$$

The model derived is quite similar to the one given by Curtin shown in Eq. 2.16, sharing the same limitations.

In an attempt to improve the inaccuracies of GLS models, Koyanagi *et al.* [153] proposed the Simultaneous Fibre-Failure (SFF) model. The authors assumed that the composite fails when a certain number of simultaneous fibre breaks, n^{ult}, occurs. An expression to estimate n^{ult} was empirically deduced from different experimental tests, leading to

$$\ln n^{\text{ult}} = 4.2 \ln \left(\frac{\tau}{\sqrt{\sigma_0 \sigma_{\text{m}}^{\text{u}}}} \right) + 12.6 \tag{2.23}$$

where $\sigma_{\text{m}}^{\text{u}}$ is the matrix longitudinal strength. The composite tensile strength is then

$$\sigma^{\text{ult}} = \sigma_{\text{R}} \frac{m+1}{m+2} \left(\frac{2}{(m+2)\left(n^{\text{ult}}\right)^2} \sqrt{\frac{V_{\text{f}} + n^{\text{ult}} - 1}{V_{\text{f}}}} \right)^{\frac{1}{m+1}} \tag{2.24}$$

Although this model may be more accurate in terms of predicting the strength of non-hybrid composites, it is still severely limited since it cannot predict the softening curve of composite materials nor the formation of clusters. It is also difficult to judge if the fitting for estimating n^{ult} is accurate enough for any material combination.

By extending Hui *et al.*'s [150] model to hybrids, Swolfs *et al.* [34] developed the first GLS model able to simulate the tensile failure of hybrid composites. The analytical model shares the same assumptions performed in [150]. Thus, the model omits size effects, dynamic effects, stress concentrations and thermal residual stresses. Moreover, due to the GLS rule, the position of the fibres is irrelevant, meaning it can predict neither the effect of the dispersion of the fibres, nor the effect of the hybrid configuration. Therefore, the hybrid composite consists of two parallel sub-composites, one which contains all the LE fibres and the other which contains all the HE fibres. The stress of the hybrid composite is then given by the rule of mixtures

$$\sigma^0 = \frac{\bar{\sigma}_{\text{LE}} V_{\text{LE}} + \bar{\sigma}_{\text{HE}} V_{\text{HE}}}{V_{\text{f}}} \tag{2.25}$$

where $\bar{\sigma}_{\text{LE}}$ and $\bar{\sigma}_{\text{HE}}$ are the average stress of the LE and HE sub-composites, respectively. These are calculated according to the fragmentation solution of

Hui *et al.* [34, 150], using the corresponding properties of each fibre type.

With the model, Swolfs *et al.* predicted a hybrid effect up to 15% for a carbon-glass hybrid. The carbon fibre strength scatter had a large impact on the hybrid effect, while the scatter in the glass fibre showed no importance at all as long as the failure of both fibres took place at different strains. These facts correspond well to the general findings seen in the literature and which were discussed in Section 2.1. The influence the failure strain ratio has on the hybrid effect was insignificant. Nonetheless, this was proved to be wrong in a future work with a more sophisticated model [33]. In accordance, the hybrid effect is influenced by four parameters [33]: the Weibull shape modulus of both LE and HE fibres and two non-dimensional parameters. For an LE Weibull modulus of 5 or higher, the hybrid effect only depends on the LE Weibull modulus and the ratio of fibre stiffness times the relative volume fraction of the LE and HE fibres.

Some time later, Tavares *et al.* [35] presented a GLS model capable of reproducing the stress-strain curve in hybrid and non-hybrid composites. Their work is based on that of Calard and Lamon [154]. An RVE of parallel fibres of length L, with no matrix, is generated. A strength, σ_q^{u}, is then assigned to each fibre q following a Weibull distribution according to the length of the fibres with $P_q = 1 - \exp\left(-\left(L/L_0\right)\left(\sigma_q^{\mathrm{u}}/\sigma_0\right)^m\right)$, where P_q is a random number between 0 and 1, and L_0, σ_0 and m are the Weibull parameters of the fibre q. These can be different for each fibre q in the case of a hybrid composite. A uniaxial tensile strain is then applied in small increments. At each strain increment, the stress of each fibre q is $\sigma_q = E_q\varepsilon^0$, where E_q is the Young's modulus of the fibre q. All fibre stresses are then compared with their own strength, σ_q^{u}. When the stress of a fibre is higher than its strength, the fibre breaks and the number of broken fibres is incremented. Considering a GLS rule, the stress of the broken fibre is proportionally split into the remaining fibres by means of a proportion between the number of active fibres and the total number of fibres. When no more breaks occur, the strain is incremented. Since a GLS rule is considered, the spatial distribution of fibres is not relevant. Therefore, the stress of the composite at each strain iteration is given by

$$\sigma^0 = V_{\mathrm{f}}\frac{\left(N_{\mathrm{q}}^{\mathrm{LE}} - N_{\mathrm{b}}^{\mathrm{LE}}\right)A_{\mathrm{LE}}E_{\mathrm{LE}} + \left(N_{\mathrm{q}}^{\mathrm{HE}} - N_{\mathrm{b}}^{\mathrm{HE}}\right)A_{\mathrm{HE}}E_{\mathrm{HE}}}{N_{\mathrm{q}}\left(A_{\mathrm{LE}}V_{\mathrm{LE}} + A_{\mathrm{HE}}V_{\mathrm{HE}}\right)}\varepsilon^0 \tag{2.26}$$

where N_q^{LE} and N_q^{HE} are the number of LE and HE fibres, respectively, N_b^{LE} and N_b^{HE} are the number of broken LE and HE fibres, respectively, A_{LE} and A_{HE} are the cross-sectional area of the LE and HE fibres, respectively, and N_q is the total number of fibres.

The model is quite simple, however, as the interaction between fibres and the presence of the matrix are omitted, the accuracy of the results is compromised. By using this model, the authors found that a continuity between the failure of the LE and HE fibres is necessary to achieve pseudo-ductility. In addition, the Weibull scale parameter, σ_0, had an effect on the average fibre strength, while the shape parameter, m, changed both the average failure strain and the strength dispersion. A larger strength dispersion caused an earlier failure initiation and a more progressive failure. The gauge length, L, had a similar impact to that of σ_0.

In the same work, Tavares *et al.* [35] extended Turon *et al.*'s [1] analytical model to hybrid composites. Like in the work of Swolfs *et al.* [34], the hybrid composite consists of two parallel sub-composites, one which contains all the LE fibres and the other which contains all the HE fibres. The global response of the hybrid composite is then obtained by applying the rule of mixtures, while the reponse of each sub-composite is given by the model of Turon *et al.* [1]. It was found that to achieve pseudo-ductility, the failure strains of both fibres must be different and a low LE content may enhance the hybrid effect. All of these agree well with the literature, as discussed in Section 2.1.

Recently, Vanegas *et al.* [155] modified the models of Neumeister [151] and Turon *et al.* [1] by assuming that failure takes place when a critical density of fibre breaks is reached. This critical density was obtained by fitting an empirical law into experimental data. The modified Neumeister and Turon models become, respectively

$$\begin{aligned}\sigma^0 &= V_f\left(\rho_b L_0\right)^{1/m}\sigma_0\left[\frac{1}{2L^{in}\rho_b+1}+\frac{1}{2\ln\left(2L^{in}\rho_b+1\right)}\left(\frac{2L^{in}\rho_b}{2L^{in}\rho_b+1}\right)\right]\\ \sigma^0 &= V_f\left(\rho_b L_0\right)^{1/m}\sigma_0\left[\frac{1-e^{-2L^{in}\rho_b}}{2L^{in}\rho_b}+\rho_b L^{in}e^{-L_0\rho_b}\right]\end{aligned} \tag{2.27}$$

where L^{in} is calculated with Eq. (2.21). Unlike other work, in the model of Vanegas *et al.* the composite stress is calculated as a function of the density of

breaks, ρ_b, instead of the applied strain. Although the model improves on the results of those of Neumeister [151] and Turon *et al.* [1], it still shares the same issues present in the original models. Furthermore, the fitting employed may compromise the results.

To summarise, there are a large number of GLS models in the literature, although only a few of them can simulate the stress-strain curve of hybrid composites [34, 35]. The main issue of these models is that the formation of clusters is neglected, and consequently, GLS models are too simple to accurately simulate the tensile failure of composites. Additionally, the majority of these models do not consider a finite number of fibres, nor the length of the composite which does not allow size effects to be captured. Nevertheless, these models need few computational resources which makes them suitable for performing multiple parametric analysis. For other contributing work, the reader is referred to references [156–158].

2.3.2 Local load sharing models

In the case of LLS models, many different modelling assumptions and backgrounds exist. In this thesis, models are classified as analytical models, fibre bundle models, spring element models or finite element models [37]. These are reviewed in the following subsections. Note that, models have been classified here according to the author's own opinion, thus some models could be placed into a different category. Since the majority of the models omit the dynamic effects due to broken fibres, which ones take them into account will always be specified.

2.3.2.1 Analytical models

There are few analytical models that take into account an LLS rule. This is because obtaining a closed form solution with such a complicated stress redistribution around broken fibres is generally impossible.

Zweben [22] extended a shear-lag model to hybrid composites in an attempt to obtain the hybrid effect analytically. The author modelled a 1D packing of LE fibres (one row of parallel fibres), and compared it with an alternating packing of LE and HE fibres (Fig. 2.12).

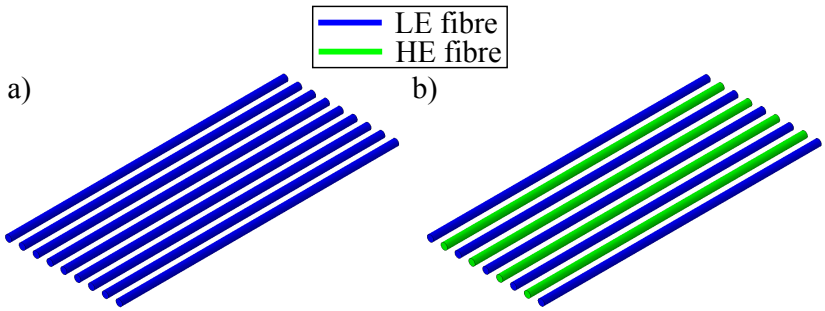

Figure 2.12: The 1D fibre packing model assumed by Zweben to obtain the hybrid effect. a) a non-hybrid composite of LE fibres and b) a hybrid composite of alternating LE and HE fibres.

Assuming that the composite fails when the first HE fibre breaks, the hybrid effect can be computed with

$$R_\varepsilon = \sqrt{\frac{\varepsilon_{\mathrm{HE}}^{\mathrm{ult}}}{\varepsilon_{\mathrm{LE}}^{\mathrm{ult}}}} \left(\frac{L_{\mathrm{H}}^{\mathrm{in}} \left(\varepsilon CF_{\mathrm{H}}^{m} - 1 \right)}{2L^{\mathrm{in}} \left(\varepsilon CF^{m} - 1 \right)} \right)^{-\frac{1}{2m}} \tag{2.28}$$

where $\varepsilon_{\mathrm{HE}}^{\mathrm{ult}}$ is the mean failure strain of the HE non-hybrid composite. The ineffective length of the hybrid composite, $L_{\mathrm{H}}^{\mathrm{in}}$, and that of the non-hybrid composite, L^{in}, are given by

$$\begin{aligned} L^{\mathrm{in}} &= 1.531 \sqrt{\frac{E_{\mathrm{LE}} A_{\mathrm{LE}} s}{G_{\mathrm{m}} h_{\mathrm{m}}}} \\ L_{\mathrm{H}}^{\mathrm{in}} &= \frac{2 \left(k_{\varepsilon 2}^2 - k_{\varepsilon 1}^2 \right)}{\sqrt{k_\varepsilon} \left(k_{\varepsilon 1} \left(2 - k_{\varepsilon 1}^2 \right) - k_{\varepsilon 2} \left(2 - k_{\varepsilon 2}^2 \right) \right)} \sqrt{\frac{E_{\mathrm{LE}} A_{\mathrm{LE}} s}{G_{\mathrm{m}} h_{\mathrm{m}}}} \end{aligned} \tag{2.29}$$

where s is the average fibre spacing and h_{m} is the thickness of the matrix. The ratio of stiffness, k_ε, and the two associated constants, $k_{\varepsilon 1}$ and $k_{\varepsilon 2}$, are

$$k_\varepsilon = \frac{E_{\mathrm{LE}} A_{\mathrm{LE}}}{E_{\mathrm{HE}} A_{\mathrm{HE}}} \quad k_{\varepsilon 1} = \sqrt{\frac{k_\varepsilon + 1 + \sqrt{k_\varepsilon^2 + 1}}{k_\varepsilon}} \quad k_{\varepsilon 2} = \sqrt{\frac{k_\varepsilon + 1 - \sqrt{k_\varepsilon^2 + 1}}{k_\varepsilon}} \tag{2.30}$$

Finally, the strain concentration factor of the hybrid, $\varepsilon CF_{\mathrm{H}}$, and that of the non-hybrid, εCF, are

$$\varepsilon CF = 1.293 \quad \varepsilon CF_{\mathrm{H}} = 1 + \frac{k_{\varepsilon 2} - k_{\varepsilon 1}}{k_{\varepsilon 1} \left(2 - k_{\varepsilon 1}^2 \right) - k_{\varepsilon 2} \left(2 - k_{\varepsilon 2}^2 \right)} \tag{2.31}$$

In accordance with Swolfs *et al.* [3], if Zweben's model is analysed, the follow-

ing can be concluded:

- The strain concentration factor depends only on the ratio of the normalised stiffness of both fibre types, therefore, if both fibres have the same stiffness, the strain concentration factors between the hybrid and non-hybrid composite are equal.
- The hybrid effect greatly increases with the ratio of failure strains. Thus, a large HE fibre failure strain should be very effective. In practice, this is probably overestimated. Swolfs *et al.* [33] demonstrated that the hybrid effect increases with the failure strain ratio up to a plateau which is obtained for a ratio of 2.
- The term $-1/2m$ tends to be small, meaning that the ineffective length and *SCF* have a small influence on the hybrid effect. This is known not to be true, since the hybrid effect strongly depends on the damage development [33–35].
- Fibres with small Weibull modulus m should produce a larger hybrid effect. This is something that has been proved to be true [25, 33–35, 64].

As the conclusions show, Zweben's model is severely limited [3]. Owing to the alternating packing considered, the fibre volume fraction and the effect of dispersion cannot be studied and this may compromise the accuracy of the results. Moreover, both LE and HE fibres are assumed to have the same Weibull modulus which would be unlikely in the case of a real material. In addition, the model assumes an unrealistic elastic matrix to obtain the *SCFs* and ineffective lengths.

Fukuda [25] attempted to improve Zweben's model further, which led to

$$R_\varepsilon = \left(\frac{L_{\mathrm{H}}^{\mathrm{in}} \left(\varepsilon C F_{\mathrm{H}}^m - 1 \right)}{2L^{\mathrm{in}} \left(\varepsilon C F^m - 1 \right)} \right)^{-\frac{1}{2m}} \tag{2.32}$$

Fukuda's equation is quite similar to that of Zweben's, albeit, the strain concentration and ineffective length are calculated more accurately [25]. Moreover, the failure strain ratio of the fibres is not included. This implies that the hybrid effect does not depend on the failure strain of the fibres which is not realistic [3]. As demonstrated by Swolfs *et al.* [33], Fukuda's model underestimates the importance of the failure strain ratio, while Zweben's model overestimates

it. Therefore, these two models may be taken as lower and upper bounds for estimating the hybrid effect.

More recently, Pimenta and Pinho [159] presented the Hierarchical Scaling Law (HSL) model, which was able to predict the tensile failure strength of non-hybrid composites of any size. The model was subsequently refined, allowing the entire stress-strain curve and damage progression of non-hybrid composites of any size [54] to be simulated. The HSL considers a perfectly plastic matrix, and takes into account that the ineffective length grows with the applied strain and the number of broken fibres in the cluster [4]. The model pairs the fibres, whose strength follows a Weibull distribution, into hierarchical bundles (Fig. 2.13). Thus, the total number of fibres in a level-[i_b] bundle is $n^{[i_b]} = 2^{i_b}$. Failure is assumed to propagate in a hierarchical way, that is, the failure description of a level-[1] bundle is extrapolated to define the failure of any generic level-[$i_b + 1$]. Therefore, the survival probability, $S_{U,c}^{[i_b+1]}$ of the generic level-[$i_b + 1$] under an applied stress σ^∞ is

$$S_{U,c}^{[i_b+1]}(\sigma^\infty) = \left(S_{U,e}^{[i_b]}(\sigma^\infty)\right)^4 + 2\left[1 - \left(S_{U,e}^{[i_b]}(\sigma^\infty)\right)^2\right] S_{U,e}^{[i_b]}(\sigma^\infty)\, S_{K,e}^{[i_b]}(\sigma^\infty) \quad (2.33)$$

where $S_{U,e}^{[i_b]}(\sigma^\infty)$ is the survival probability of a level-[i_b] bundle and $S_{K,e}^{[i_b]}(\sigma^\infty)$ is its survival probability under linear stress concentrations. The reader is referred to Pimenta [54] for a description of the entire model.

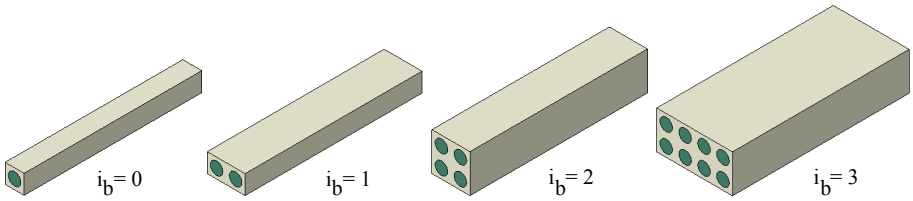

Figure 2.13: Hierarchical scaling law bundle schema. A level-[0] bundle contains only one fibre. Two level-[0] bundles can be grouped to form a level-[1] bundle. Likewise, two level-[1] bundles are paired to form a level-[2] bundle and so on. Notice that the fibre packing used (in this illustration square) does not affect the modelling predictions.

The authors found that there is no universal size for the critical cluster that leads to final failure. This implies that the weakest link theory cannot be used to extrapolate the results of a small bundle to a very large structure [159]. Compared against experiments, the model slightly underpredicted the formation of large clusters, and overpredicted the formation of individual fibre breaks.

This is in-line with other similar models in the literature [39, 41]. Further to this, the model was recently compared against blind and detailed experimental results in the *I international benchmarking exercise for strength models of UD composites* [4]. Although the model had good correlation with experimental data, some discrepancies between models and experiments were still evident. Overall, models failed to consistently and accurately capture failure and fibre-breakage accumulation altogether.

That said, the HSL model is remarkable. Since it is analytical, it is computationally efficient, allowing bundles with thousands of fibres to be simulated in few seconds. Moreover, the model has been shown to be reasonably close to experiments and it also takes into account that the ineffective length grows with the cluster size, which is omitted by many models. Nonetheless, it has some shortcomings. First of all, it assumes a regular distribution of fibres, which does not allow hybrid composites with different radius to be simulated. Secondly it assumes that all clusters are co-planar (i.e. all breaks occur on the same plane) and the *SCF* carried by intact fibres is assumed to be equal to 2 [54]. That is a very large value, especially for a plastic matrix [37], even if dynamic effects are taken into account [63].

2.3.2.2 Fibre bundle models

Fibre Bundle Models (FBM) consider an RVE containing a number of parallel fibres with stochastic strength loaded under uniaxial tension. When a fibre fails, the load is redistributed into the neighbouring intact fibres. After the load redistribution, if no more breaks are encountered, the strain is increased. The procedure is repeated until a finish criterion is satisfied. The main difference in between all the models is related to the way the load of a broken fibre is redistributed over the intact fibres. In some models, this is calculated using known data from a finite element simulation run a priori, while in other models it is calculated either with an analytical equation, or inherently from the equilibrium equations of the model.

Fukuda and Chou [24] proposed one of the earliest models able to deal with hybrid composites. An RVE containing a 1D packing of parallel fibres with alternating layers of LE and HE fibres is considered. The fibres are divided into elements of length $2L^{\text{in}}$, where L^{in} is the ineffective length. The elements are

labelled with subindices p,q according to their position, see Fig. 2.14a.

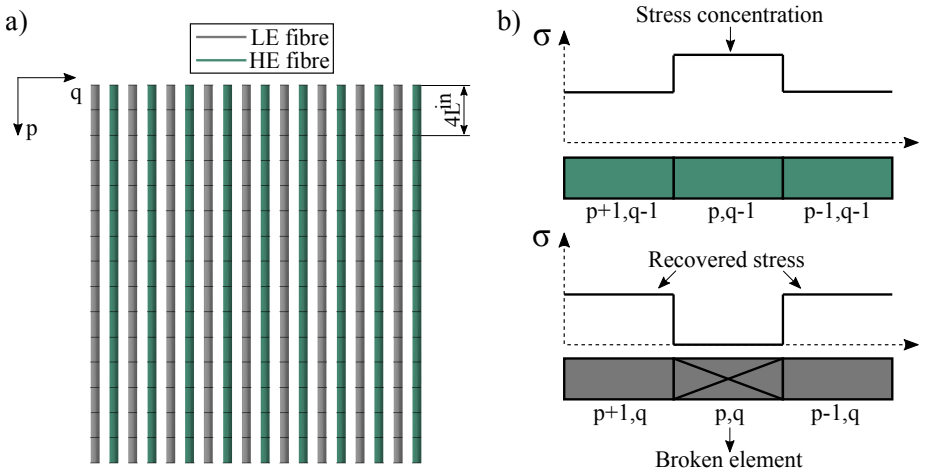

Figure 2.14: Schema of the model developed by Fukuda and Chou [24]. a) a bundle of alternating layers of LE and HE fibres is created, with the fibres divided into elements of length $2L^{in}$ and b) assumed load redistribution around a broken element.

A stochastic strength is assigned to each element. Following this, a uniform strain controlled simulation is started. At the beginning, the *SCF* of all elements are equal to 1 since there are no broken fibres. When an element p,q fails, the element carries no more stress, and then the neighbouring elements to the broken one, i.e. the elements at $p,q-1$ and $p,q+1$, carry an *SCF* larger than 1. This *SCF* around broken fibres was estimated prior to the simulation using shear-lag equations [46], considering an elastic matrix, and taking into account the elastic properties of the LE and HE fibres as well as different break patterns. Since the length of the elements is equal to the entire stress recovery of the fibres, the stress in the broken fibre is directly recovered. This means that the elements at $p+1,q$ and $p-1,q$ carry the nominal stress. Thus, the ineffective length is not explicitly captured. This leads to an unrealistic, but simple, load redistribution (Fig. 2.14b). The simulation continues until all elements in a plane p are broken.

The model demonstrated that the failure strain of hybrid composites can be enhanced thanks to the fact that the cluster development is slower than that of non-hybrid composites, as discussed previously in Section 2.1. Even though this model is relatively advanced for capturing the hybrid effect, it is too simplistic. It considers an unrealistic 1D regular packing of alternating fibres, not allowing for hybrid composites with an *HVF* different than 50% to be simulated. The

stress recovery of the fibres is also not captured. Thus, more refined models were needed.

Curtin *et al.* [144] developed a more advanced LLS model for non-hybrid composites. They considered a 3D RVE with a square or hexagonal fibre packing. Here, the fibres are divided into elements of length l, with l being much smaller than the ineffective length of the fibres. A stochastic strength is applied to each element according to their length l. A uniaxial strain controlled simulation is then started. When a fibre fails, the fibre is assumed to slip within the matrix. Consequently, the ineffective length of the fibres is computed with Eq. 2.12. Along the ineffective length, the stress dropped by the broken fibre is redistributed into the neighbouring fibres by means of stress concentration. This *SCF* is estimated using the model of Hedgepeth and Van Dyke [160]. Nevertheless, another model could be used instead since the longitudinal and transverse behaviour is decoupled. Afterwards, a matrix equation is solved to obtain the stress transferred to the intact fibres around the broken fibres. The simulation is conducted until the composite fails.

The authors found that the overall strength did not depend on the fibre geometry (square or hexagonal). This was also confirmed by Swolfs *et al.* [120]. The size scaling of strength proved to be nearly-independent as well. Despite these findings, it is clear that such facts do not apply to hybrid composites where the LE and HE have a different radius. In such composites, a random distribution of fibres is necessary to properly represent the geometry of the material. In any case, the model developed presents noteworthy features. Unlike the model of Fukuda and Chou [24], Curtin's model captures the stress recovery of broken fibres. Moreover, since the transverse and longitudinal directions are decoupled, stress redistribution around breaks can be changed without having to reformulate the model. Finally, a more realistic packing of fibres was considered, together with a plastic or debonded matrix.

Behzadi *et al.* [36] employed a finite element model to calculate both the *SCF* around multiple broken fibres and the ineffective length, taking matrix yielding into account. These were used as input data in an FBM consisting of parallel fibres with length equal to the ineffective length, see Fig. 2.15a. This is an interesting approach since it allows the accuracy of finite elements to be exploited while still using a simple model. In the finite element model, the

authors predicted an ineffective length of $L^{in} = 0.0745$ mm (measured at 90% of stress recovery) and an increase of *SCF* from 1.09, around a single broken fibre, to 1.36, around three broken fibres (Fig. 2.15b). These values of *SCF* were larger with an elastic matrix, corresponding well to the literature [37, 39].

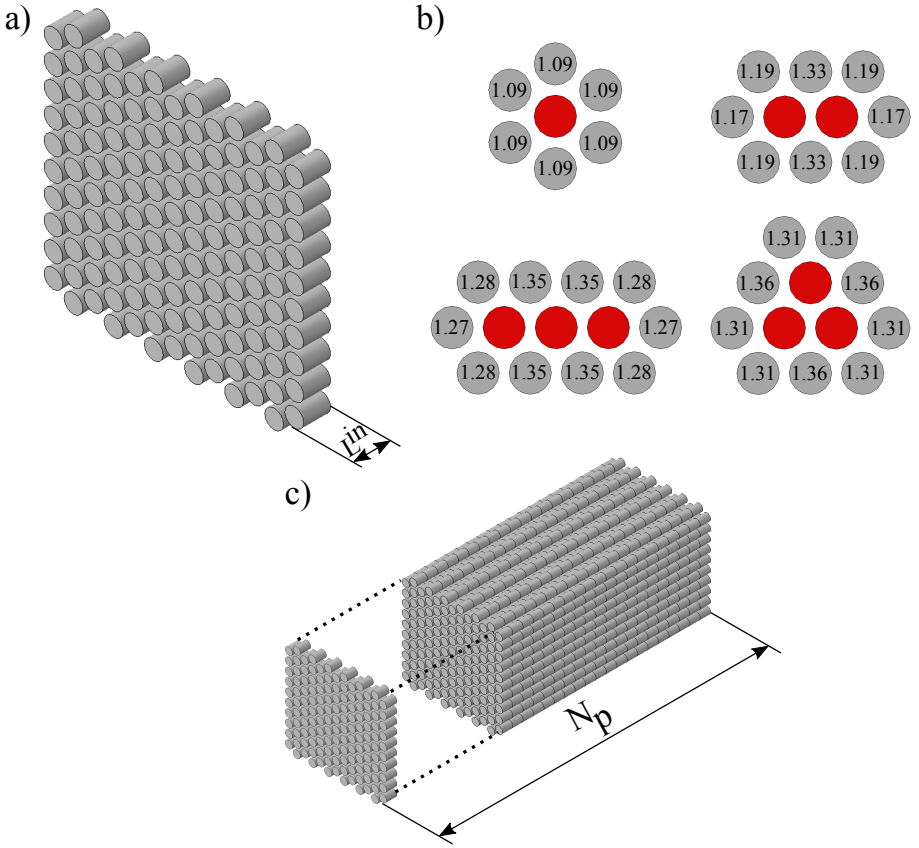

Figure 2.15: Model from Behzadi *et al.* [36], a) a bundle of parallel fibres in a hexagonal packing is considered with length equal to the ineffective length L^{in}, b) *SCF* obtained around different broken fibres (in red) using a finite element model, and c) stacking of single bundles to form a large UD composite.

Unlike the majority of the models, the strength of the fibres was modelled within a normal distribution

$$\varepsilon_q^u = \mu_n + P_q SD \tag{2.34}$$

where ε_q^u is the failure strain of fibre q, μ_n and SD are the mean and standard variation of failure strains of the fibre at a length equal to the ineffective length and P_q is a random number between 0 and 1. At each loading step, the stress

of each fibre q is $\sigma_q = SCF_q E_q \varepsilon^0$, where E_q is the fibre Young's modulus and SCF_q is the stress concentration applied to the fibre. When a fibre fails, its stress is set equal to zero, and the surrounding fibres receive *SCF* according to the finite element model data. Unfortunately the authors did not explain how they obtained the SCF_q for different combinations of broken fibres other than the ones shown in Fig. 2.15b [5]. The FBM is run until an unstable cluster propagates. After that, a fixed number N_p of RVEs are stacked together to form a piece of UD composite of known length (Fig. 2.15c). In accordance with the weakest link theory, failure of the UD composite is triggered whenever one of the bundles fails, since the interaction between bundles is not considered [36].

The authors concluded that matrix yielding reduces the *SCF* in the fibres. The presence of an elasto-plastic matrix surrounding the fibres leads to an increase in the composite failure strain compared to the elastic matrix case. This does not correspond well to the observations of recent work [4, 37], which must be attributed to the omission of the stress recovery of the fibres. Since this effect is omitted, and the *SCF* is larger with an elastic matrix, it is not surprising that the model of Behzadi *et al.* predicted lower failure strains with an elastic matrix. The authors themselves pointed out that a better description of the ineffective length was needed to improve the results, along with the interaction between the composite bundles. These, together with the very short length of the bundle, are the majors flaws of the model. The modelling approach can easily be extended to work with a random packing of fibres in hybrid composites, as long as a proper stress redistribution around breaks is considered.

Mishnaevsky and Dai [32] proposed a model considering an RVE containing a given number of fibres which were assigned either carbon or glass fibre properties. The fibres in the RVE were randomly located and misaligned. Like the majority of the models, the strength of the fibres was considered to follow a Weibull distribution. At each strain increment the stress of a fibre q is

$$\sigma_q = E_q \varepsilon^0 + \Delta\sigma_q \tag{2.35}$$

where here, the fibre Young's modulus, E_q, is calculated as a function of the fibre misalignment [32] and $\Delta\sigma_q$ is the increase of stress carried by the fibre due to the surrounding broken fibres. This increase was calculated using a power-law function [32, 161].

The authors found that hybrid carbon-glass composites can have a lower failure strength and strain than the all-glass non-hybrid composite. Likewise, the strength of the hybrid can be lower than that of the all-carbon non-hybrid composite. In addition, the failure strain of the hybrid composite decreased by increasing the *HVF*. The results were validated against data in the literature and a finite element simulation. Although the model can simulate hybrid composites it is too simple, since the ineffective length of the fibres is not included, and does not allow their stress recovery to be simulated. The load sharing around the surrounding fibres is also quite simplistic. A good point of the model is, nonetheless, the inclusion of the fibre misalignment, which is generally omitted.

One of the most acknowledged and advanced FBMs is that developed by Swolfs *et al.* [31, 33, 40, 41, 120]. An RVE consisting of parallel fibres is generated, which can contain fibres of a different type or of the same type, and is either a hybrid or a non-hybrid composite. Moreover, fibres may be distributed within a hexagonal, square or a random packing. The fibres are divided into elements of length l along the fibre longitudinal direction, see Fig. 2.16. Like in the majority of the models, dynamic effects and thermal residual stresses are omitted. Nonetheless, their flexible formulation allows for their future incorporation.

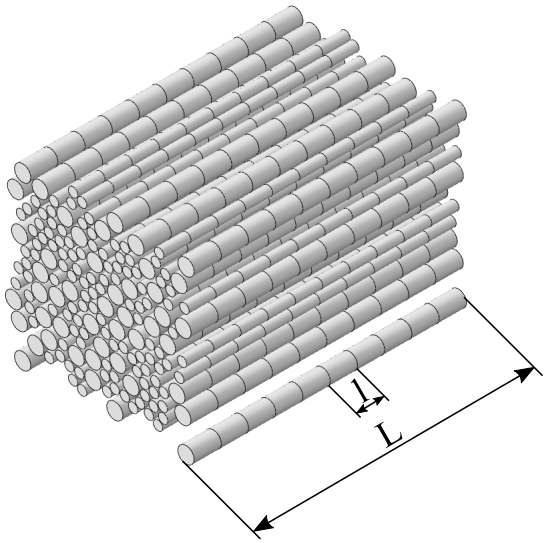

Figure 2.16: The fibre bundle model of length L proposed by Swolfs *et al.* [31]. The fibres are divided into elements of length l, with l being significantly smaller than the ineffective length of the fibres.

A stochastic strength is assigned to each fibre element according to the length of the element, and a uniaxial strain controlled simulation is started. At each strain increment, the stress of each fibre element, σ_q, is

$$\sigma_q = E_q SCF_q \varepsilon^0 \tag{2.36}$$

where E_q is the Young's modulus of element q and SCF_q is the stress concentration factor carried by element q. At each iteration the model checks if any element, q, is carrying a stress higher than its strength. If not, the strain is incremented. Otherwise, the new broken elements are assigned an $SCF_q = 0$, so that they no longer carry any stress. The model then searches for clusters. Two broken fibres are considered to be part of the same cluster if the in-plane distance between the centre of the two fibres, d_r, is below 4 times the smallest fibre radius and the axial distance between break planes, d_l, is less than 10 times the smallest fibre radius, see Fig. 2.17. This is a somewhat arbitrary approach to define clusters. Nonetheless, it is based on finite element simulations describing the stress redistribution around the breaks [45, 68].

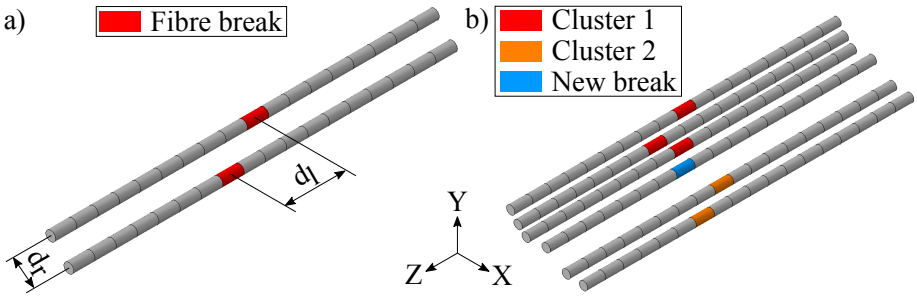

Figure 2.17: Determination of clusters of broken fibres. a) Two broken elements belong to the same cluster if d_r and d_l are equal to or smaller than a certain distance threshold, and b) a new fibre break may appear that complies with the distance threshold conditions for one break in 'cluster 1' and for another break in 'cluster 2', and thus, all broken elements are merged together into a single cluster.

The model subsequently calculates the *SCF* carried by all elements. This is done in two steps. In the first step, the SCF_q are calculated for all elements according to the stress fields obtained in a finite element model that is run prior to the simulation [45, 68]; like in the model of Behzadi *et al.* [36]. In most of the work of Swolfs *et al.*, this stress field was computed by assuming an elastic matrix and perfect interphase bonding. In some studies, a small matrix crack was also added around the broken fibre [40, 41]. These finite element models will be

described further in Section 2.3.4. The ineffective length was also calculated in the finite element model, and the same value was always used in the FBM irrespectively of the applied strain level. For an elastic matrix this is clearly a good approximation. Nonetheless, this is not the case for a plastic matrix where the ineffective length grows with the applied strain [37, 54]. To apply the ineffective length onto the broken fibres, the SCF_q carried by the broken fibre is adjusted from 0, at the position of the break, to 1, at the end of the ineffective length according to the finite element data. The SCF_q carried by these elements inside the ineffective length is therefore smaller than 1, see Fig. 2.18a. As a result, these elements cannot receive *SCF* from other surrounding broken fibres since their stress is limited by shear-lag. Instead, for each intact fibre element, the SCF_q is given by the linear superposition of the *SCF* it receives from all broken fibres according to the stress fields obtained in the finite element model, see Fig. 2.18b. Therefore, the *SCF* is smaller than 1 for elements inside the stress recovery of a broken fibre, while it may be equal to or larger than 1 for intact elements that are under stress concentration due to surrounding broken fibres.

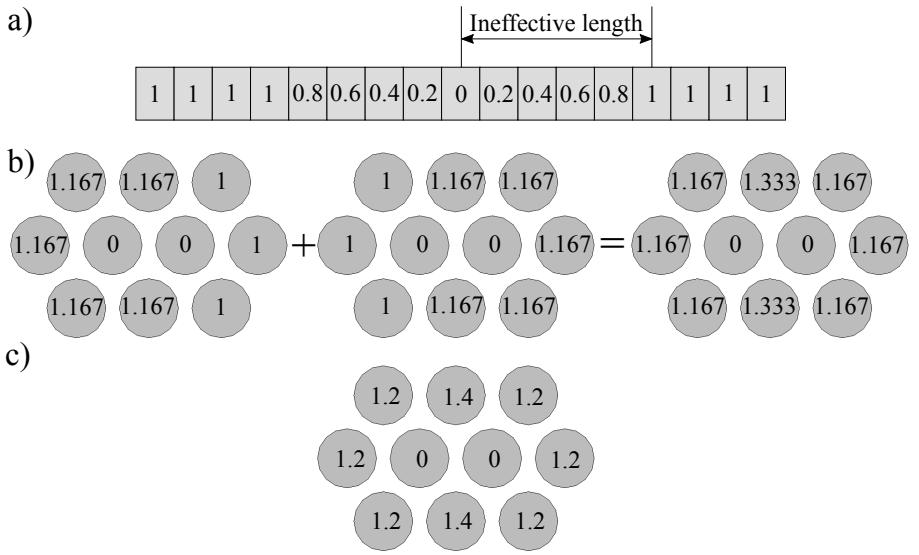

Figure 2.18: Schema of the stress redistribution considered by Swolfs *et al.* [31], a) the *SCF* along a broken fibre determines the stress recovery, b) step 1: the increase of *SCF* caused by the different broken fibres to the intact fibres is summed up by linear superposition, and c) step 2: the *SCFs* obtained in step 1 are modified to achieve load equilibrium. The broken fibres carry an $SCF = 0$.

In the second step, the SCF_q obtained from the first step are modified using an 'enhanced superposition principle' which takes into account the interaction between all fibre breaks. The basic idea is that the SCF_q carried by intact fibres, based on the linear superposition solution computed in the first step, are corrected to achieve load equilibrium, see Fig. 2.18c. This is explained in great detail in Swolfs *et al.* [31]. Although the SCF_q is calculated taking the number of breaks into account, the ineffective length is not. This means that the model omits the increase of ineffective length with the increase of cluster size. This is a common assumption in many models, although recent work has shown that it underpredicts the ineffective length [37]. Along the ineffective length, the SCF_q carried by intact fibres decreases accordingly to the load loss by the broken fibres respecting load equilibrium. The model continues the entire process until an unstable cluster of LE fibres propagates. Finally, to avoid unrealistic stress concentrations at the boundaries, a layer of unbreakable fibres is included on the perimeter of the model. Their stress is not considered.

In the first version of the model, hybrid carbon-glass composites with all fibres having the same radius in a hexagonal packing were simulated [31]. A very local load sharing rule was considered to predict the *SCF* around the broken fibres based on the results of the finite element model [45, 68]. In the case of a hexagonal packing, this means that all six neighbours around a broken fibre are proportionally affected by the stress concentration. Therefore, the *SCF* for a carbon fibre around a broken carbon fibre is $7/6$, while for a glass fibre around a broken carbon fibre it is $1+E_{\mathrm{LE}}/(6E_{\mathrm{HE}})$. In the case of a carbon fibre around a broken glass fibre, the *SCF* for the carbon is the opposite: $1+E_{\mathrm{HE}}/(6E_{\mathrm{LE}})$, while for the glass it is $7/6$ again, where E_{LE} is the Young's modulus of the carbon (LE) fibre and E_{HE} is the Young's modulus of the glass (HE) fibre. The final *SCF* is obtained with the enhanced superposition method as previously explained. Within these considerations, the authors studied the influence that fibre dispersion has on the hybrid effect and, according to the results, it has a significant influence. For intrayarn hybrids, the hybrid effect was up to 9%, nonetheless, the highest hybrid effect was 16% when using an interlayer hybrid configuration of one layer thick. Furthermore, they determined that, although the critical cluster size did not depend on the fibre dispersion, it was a function of the *HVF*.

In a further work, Swolfs *et al.* [41] employed synchrotron radiation computed tomography to analyse fibre break accumulation and cluster formation in a UD non-hybrid composite loaded in tension. The authors compared their experimental data against their modelling results given by the FBM. In this case, a realistic random distribution of fibres was considered instead of a simplistic hexagonal packing. The *SCF* around the breaks was again calculated according to finite element data, but this time a very local load sharing rule was not considered. Instead, the *SCF* was computed as a function of the distance to the broken fibre. This was a major improvement compared to the state of the art models. The failure strain predicted by the model slightly overpredicted the experimental failure strain. However, the fibre break density was too high compared to the experiment, which was attributed to errors in the Weibull distribution. In addition, the formation of clusters was analysed and compared. The authors defined two type of clusters: co-planar and diffuse. A cluster was assumed to be co-planar if the axial distance between fibre breaks was less than 3.5 μm, otherwise it was assumed to be diffuse. While 70% of the clusters were co-planar in the experiments, the model only predicted between 20-30% of co-planar clusters. Swolfs *et al.* suggested that this may be caused by the omission of dynamic effects, and the averaging of the *SCF* over the entire cross-section of each fibre [41]. The maximum cluster predicted was in good agreement with the experiments. Nonetheless, the formation of larger clusters was constantly underestimated by the model. This suggests the presence of larger *SCFs* than the ones used in their model.

In a subsequent study, Swolfs *et al.* [33] investigated the effect that the LE fibre strength scatter, HE fibre stiffness and failure strain ratio have on the hybrid effect using their FBM. A random distribution of fibres, with each fibre having their respective radius, was considered. The *SCF* around the fibre breaks was again calculated according to finite element data, and as a function of the distance to the broken fibre, taking into account the elastic and geometrical properties of the fibres. This allowed a major improvement to be made over state of the art models. Accordingly, if all parameters except the failure strain, HE fibre stiffness and LE fibre strength scatter are kept constant, the ways to increase the hybrid effect are [33]:

– A large LE fibre strength scatter.

– A sufficient high failure strain ratio. In their study, a value of 2 proved to be successful.
– A high HE fibre stiffness reduces the *SCF* on the LE fibres.

Such findings correspond well to what was discussed in Section 2.1. Nevertheless, the authors claimed that a parametric study should be carried out.

The model developed by Swolfs *et al.* presents many good features, since it is relatively simple and computationally efficient, and yet still makes the most from using the accurate stress fields obtained by a finite element model. Nevertheless, it also presents some shortcomings. First of all, running the finite element model to obtain the stress fields is time consuming. Secondly, the ineffective length does not grow with either the applied strain or the cluster size. Nonetheless, the flexible formulation of the model allows such missing features, together with other phenomena like dynamic effects, to be implemented. Indeed, an important shortcoming of the model was that it could not capture the stiffness loss due to broken fibres, thus not predicting pseudo-ductility. This limitation has been lately addressed [100]. The model was recently compared against detailed and blind experimental simulations in the *I international benchmarking exercise for strength models of UD composites*, showing that there is still a large gap between models and experiments [4]. The formation of clusters and damage accumulation predicted by the model did not correlate well with the experiments as was the case with the experimental comparison performed in [41].

To sum up, there are many FBMs in the literature, with the model of Swolfs *et al.* being the most advanced for predicting hybrid effects and formation of clusters. For other notable work, the reader is referred to the literature and references therein [9, 43, 62, 64, 71, 106, 114, 117, 157, 162–188].

2.3.2.3 Spring element models

The Spring Element Model (SEM) is one of the most widely-acknowledged models in the literature. In the SEM, an RVE that contains parallel fibres of a certain length divided into fibre elements of length l is considered. The fibres are connected by means of matrix shear springs. Such geometry leads to a lattice of nodes longitudinally joined by fibre springs and transversely by matrix springs, as illustrated in Fig. 2.19. Thus, unlike FBMs, the matrix is physically

represented by shear springs.

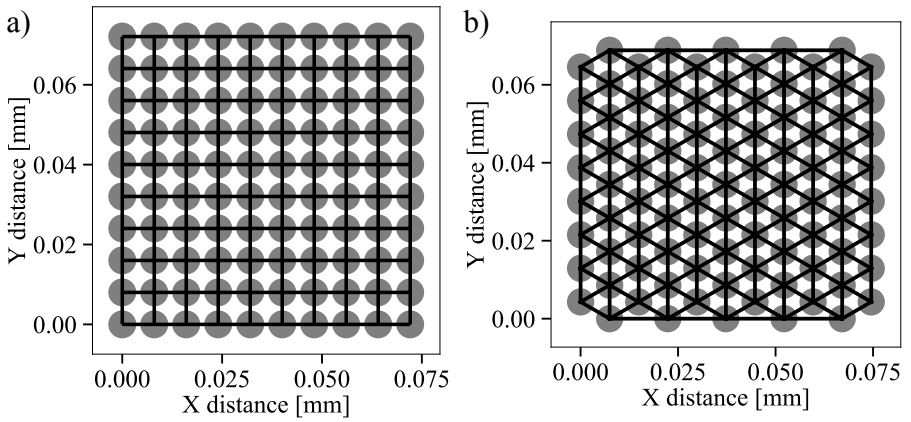

Figure 2.19: A cross-section example of the spring element model showing the fibres (nodes) connected by matrix shear springs, a) square packing, and b) hexagonal packing.

The first SEM was presented by Okabe *et al.* [76]. The model can be seen as an evolution of the Lattice Green's function model [189, 190], which is itself similar to the quadratic influence superposition technique [75] and other influence functions or shear-lag based models [85, 113, 115, 191–193]. In the first SEM presented, the fibres were uniformly spaced in a square arrangement, like in Fig. 2.19a. The model was formulated based on shear-lag theory, including matrix yielding and/or debonding. The model was later refined further by formulating it in a finite element form, thus making it more robust, and compatible with the finite element method [194]. Compared to 3D finite element simulations available in the literature, the model captured the stress fields around broken fibres well. Likewise, the strength and size effects of a carbon FRP were well captured using the WOW model [52, 107, 195] compared against experiments. Although the SEM is an elegant and advanced model, allowing the stress redistribution around breaks to be captured inherently from the equilibrium equations, the SEM by Okabe *et al.* [194] is limited to regular fibre packings (Fig. 2.19) thus not allowing hybrid composites to be simulated.

To allow the study of hybrid composites, a new SEM, able to take into account a random distribution of fibres with their own radius, was developed by Tavares *et al.* [39]. To do so, the length of all matrix shear springs (transverse elements) is different to accommodate the random fibre distribution and radius of each fibre. This leads to an irregular triangular mesh, which can be generated by

performing a Delaunay triangulation [196], see Fig. 2.20.

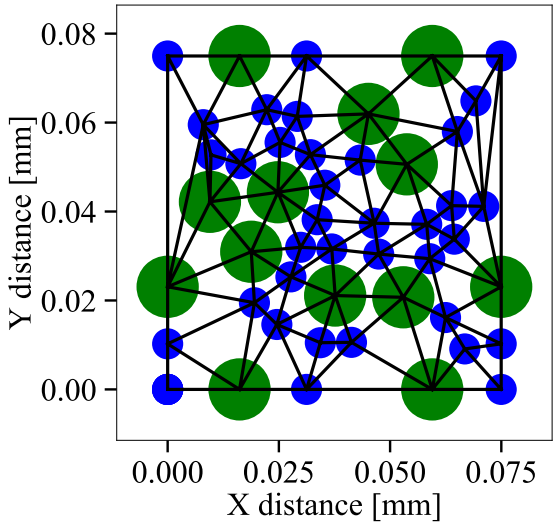

Figure 2.20: A cross-section example of the spring element model developed by Tavares *et al.* [39] showing the fibres (nodes) connected by matrix shear springs of different lengths with a random fibre packing. As a result, an irregular triangular mesh is created.

In the new SEM, the stiffness matrix for the fibre elements, K_{f}^{e}, and for the matrix elements, K_{m}^{e}, are given by

$$K_{\mathrm{f}}^{e} = \frac{A_{\mathrm{f}}^{e} E_{\mathrm{f}}^{e}}{l} \begin{bmatrix} 1 & -1 \\ -1 & 1 \end{bmatrix} \quad K_{\mathrm{m}}^{e} = \frac{G_{\mathrm{m}} \left(A_{\mathrm{m}_2} - A_{\mathrm{m}_1} \right)}{\left(d^{\mathrm{c}} - R_{\mathrm{f}}^{(1)} - R_{\mathrm{f}}^{(2)} \right) \ln \left(\dfrac{A_{\mathrm{m}_2}}{A_{\mathrm{m}_1}} \right)} \begin{bmatrix} 1 & -1 \\ -1 & 1 \end{bmatrix} \tag{2.37}$$

where A_{m_1} and A_{m_2} are the associated matrix area of the two different fibres connected by the transverse spring and d^{c} is the centre-to-centre distance between the two fibres. These areas can be estimated as a function of the number of fibres connected to the two fibres, $N_{\mathrm{s}}^{(1)}$ and $N_{\mathrm{s}}^{(2)}$, and their respective fibre radius, $R_{\mathrm{f}}^{(1)}$ and $R_{\mathrm{f}}^{(2)}$

$$A_{\mathrm{m}_1} = \frac{2\pi R_{\mathrm{f}}^{(1)} l}{N_{\mathrm{s}}^{(1)}} \qquad A_{\mathrm{m}_2} = \frac{2\pi R_{\mathrm{f}}^{(2)} l}{N_{\mathrm{s}}^{(2)}} \tag{2.38}$$

At each strain increment the equilibrium equation reads

$$F = Ku \tag{2.39}$$

where u and F are the nodal displacement and load vectors, while K is the global

stiffness matrix

$$K = \sum_{e=1}^{N_L - N_b} K_f^e + \sum_{e=1}^{N_T} K_m^e \tag{2.40}$$

where N_L is the number of fibre or longitudinal elements, N_b is the number of broken elements and N_T is the number of matrix or transverse elements. The matrix is considered to be either elastic or elasto-plastic according to a given matrix shear yield stress. These behaviours are implemented using a sequentially linear analysis [197]. A uniaxial strain is slowly applied. At each strain increment, Eq. (2.39) is solved to obtain the nodal displacements and thereafter the stress of each fibre element is computed by $\sigma^e = E_f B_f u$, where the strain-displacement transformation matrix is $B_f = [1/l \quad -1/l]$. If a fibre element fails or any matrix shear element exceeds the shear yield stress, τ_y, then the number of broken elements, N_b, and the stiffness of the broken matrix elements are updated. After that, the global stiffness matrix, K, is recalculated and Eq. (2.39) is again solved. This iterative process is repeated until no more fibre or matrix elements fail, and then, a new strain increment is started.

The model formulation is very robust, since it inherently captures the effect that the different material parameters (matrix and fibres) have on the stress redistribution around breaks from the equilibrium equations. Moreover, it allows hybrid and non-hybrid composites with a random distribution of fibres to be simulated. Compared to experimental data, the model overpredicted the fibre break density and underpredicted the formation of larger clusters as well as the number of co-planar clusters, as occurred with other similar models [4, 41, 54]. The omission of dynamic effects and matrix cracking were identified as being the main explanations for such discrepancies.

Later, the authors performed an in-depth study of the stress redistribution around broken fibres in non-hybrid composites with different material parameters [37]. The fibre volume fraction had a massive influence on the *SCF*. A smaller volume fraction increased the *SCF*, since less fibres are available to share the load of the broken fibre. This agrees well with the results of Swolfs *et al.* [68]. Adding matrix yielding heavily reduced the *SCF*, since the shear stress transfer is limited by the shear yield stress. Hence, adding matrix yielding is necessary for predicting an accurate load redistribution. Other material parameters did not have a significant effect on the *SCF*. The ineffective length depended mainly on

the fibre Young's modulus and the matrix shear yield stress. A larger Young's modulus increases the ineffective length since a larger stress must be recovered. Similarly, reducing the shear yield stress led to a larger ineffective length due to a smaller shear stress transfer. In addition, the cluster size had a powerful effect on the ineffective length, as has been pointed out by other authors [54, 198].

In a future contribution, Tavares *et al.* [63] would improve the SEM by including, for the first time in the literature, the dynamic effects associated to the fibre failure in a model able to predict the tensile failure of composites. The model is itself the same as the previous SEM [39], but with the inertial term added to capture the dynamic effect. The fibre and matrix stiffnesses are therefore calculated as in Eq. (2.37). The mass matrix of the fibre elements, M_{f}^{e}, and that of the matrix, M_{m}^{e}, are computed with

$$\begin{aligned} M_{\mathrm{f}}^{e} &= A_{\mathrm{f}}^{e}\rho_{\mathrm{f}}^{e}l\begin{bmatrix} 1/3 & 1/6 \\ 1/6 & 1/3 \end{bmatrix} \\ M_{\mathrm{m}}^{e} &= \rho_{\mathrm{m}}\left(d^{\mathrm{c}} - R_{\mathrm{f1}} - R_{\mathrm{f2}}\right)\begin{bmatrix} 1/12\left(3A_{\mathrm{m_1}} + A_{\mathrm{m_2}}\right) & 1/12\left(A_{\mathrm{m_1}} + A_{\mathrm{m_2}}\right) \\ 1/12\left(A_{\mathrm{m_1}} + A_{\mathrm{m_2}}\right) & 1/12\left(A_{\mathrm{m_1}} + A_{\mathrm{m_2}}\right) \end{bmatrix} \end{aligned} \tag{2.41}$$

where ρ_{f}^{e} is the density of fibre element e, while ρ_{m} is the density of the matrix. Rayleigh damping is introduced into the model to avoid dynamic instability with

$$C = \alpha^{\mathrm{r}}M + \beta^{\mathrm{r}}K \tag{2.42}$$

where K is given as in Eq. (2.40), α^{r} and β^{r} are the mass and stiffness proportional damping coefficients and M is the global mass matrix

$$M = \begin{cases} \sum_k M_{ik} & i = j \\ 0 & i \neq j \end{cases} \tag{2.43}$$

where M_{ij} are the individual elements of the global mass matrix [63].

Finally, the equilibrium equation, now incorporating the inertial term, reads

$$M\ddot{u} + C\dot{u} + Ku = F \tag{2.44}$$

where $\ddot{u}$ and $\dot{u}$ are the nodal acceleration and velocity vectors, respectively. A linear velocity is slowly applied to the RVE. At each increment, Eq. (2.44) is solved using an explicit integration scheme based on the central difference method to obtain the displacement, velocities and accelerations [63]. Subsequently, the

stresses of the fibre and matrix elements are determined.

The authors found that the maximum *SCF* is always larger in the dynamic model than in the static one, and with this increase being dependent on the material. On average, the dynamic *SCF* was 1.83 times larger than the static for an elastic matrix, and 1.43 for a plastic matrix. The dynamic effects had an influence on the tensile behaviour and final failure of the material if an elastic matrix was considered. Nonetheless, with a plastic matrix the effect was not significant. Including dynamic effects led to an earlier formation of clusters than with the static model, making the results closer to the experimental ones. Nonetheless, the formation of large clusters was still underpredicted compared to the experiments. The formation of co-planar clusters did not improve either compared to the static model. This occurred both with an elastic and a plastic matrix.

The latest SEM developed is clearly one of the most robust and advanced models in the literature, since it captures the stress fields around broken fibres inherently from the equilibrium equations, and takes into account dynamic effects. In addition, it can capture the entire stress-strain curve and the stiffness loss of a composite material. Nonetheless, it also presents some disadvantages. The model is computationally limited in comparison with other simpler models. Solving RVEs with a large number of fibres is not feasible unless a super computer is used. This is the case for both the static and dynamic models. In the static model, a large stiffness matrix, K, must be inverted, which is computationally expensive. Otherwise, an iterative procedure must be used to obtain the displacement of the fibres. In the dynamic model, the explicit formulation avoids having to invert the stiffness matrix. Nonetheless, since the time increment is very small to avoid instability, the computational time is still compromised. Finally, due to the complex formulation involved, adding new effects may not be straightforward.

2.3.2.4 Finite element models

In this section different micromechanical Finite Element Models (FEM) able to simulate the fibre tensile failure of composite materials are discussed. Developing such a micromechanical FEM is a challenging task. Firstly, one must choose the appropriate size of the RVE so that it can be representative of the

true material but small enough to reduce computer time. Secondly, the computational resources needed to fully characterise a material with damage in the fibres, matrix and the fibre-matrix interphase are incredibly high. That said, one way to overcome this issue would be the use of super-computation such as the Alya system [199]. Because of this, only a few studies have successfully modelled the fibre tensile failure process using a micromechanical FEM, and in all cases, the RVE employed was excessively small. Notwithstanding, there is a lot of work which has used RVEs to obtain the elastic properties of composite materials [124, 200–202], or to simulate fibre-matrix debonding [203–207] or other loading conditions [208–213]. These studies will not be discussed here, as they are not relevant for this thesis. Interested readers are referred to the cited articles and references therein. Likewise, other non-micromechanical FEMs, able to simulate the failure of hybrid composites are also outside the scope of this review. Interested readers are again referred to the literature [15, 96].

Mishnaevsky and Brøndsted [214] performed a parametric study to investigate the damage evolution of glass FRP. The effect that the fibre strength scatter, viscosity of the polymer matrix, and the fibre matrix interface have on composite strength were investigated. To do so, a three-dimensional micromechanical FEM was developed [215]. To model fibre failure, damageable planes (layers of elements) were introduced into several sections of fibres at random locations. To model fibre-matrix interphase cracking, a damageable thin layer between the fibre and the matrix was added (Fig. 2.21). The remainder of the model was always elastic. This means that damage can only occur in certain locations of the model. The damage evolution for the fibres and interphase was implemented assuming that the stiffness is reduced if a stress or a damage parameter in the element or a nodal point exceeds a critical level [216–220].

The authors concluded that if all fibres have the same strength, the strength of the composite after the pre-critical load increases, while fibres with stochastic strength increase the composite strength post-critical load. The matrix viscosity increased the damage rate in the fibres. The inclusion of matrix defects was not significantly important compared to the fibre strength variability. Nonetheless, the presence of interface cracks had a considerable effect on fibre failure and matrix cracking. According to the authors, these observations suggest that an interface with varied strength and weak local areas can delay both matrix and

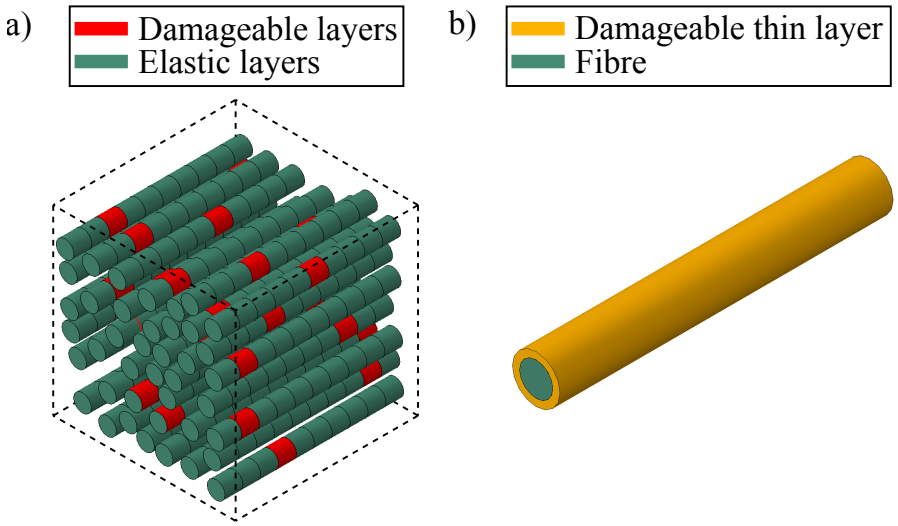

Figure 2.21: Schema of the finite element model employed by Mishnaevsky and Brøndsted [214]: a) damageable layers are introduced at random planes in the fibres, and b) a thin damageable layer is added between the fibre and matrix to simulate interphase failure. The RVE is small, containing around 20 fibres with a length of few microns.

fibre failure and increase composite strength.

Qing and Mishnaevsky [139] performed more numerical investigations within the same approach, using a random distribution of fibres. The influence the random position of the fibres and the strength scatter have on the mechanical response and strength of glass FRP was investigated. The results obtained showed that the variability of the microstructure has a significant influence on the composite strength and the mechanical behaviour after the beginning of damage growth in the fibres. These results prove that an accurate microstructure should always be aimed.

In a future work, Mishnaevsky and Dai would simulate the mechanical response of a carbon-glass hybrid composite using the same modelling approach [32]. The aim was mainly to compare the FEM against an FBM, which was reviewed in Section 2.3.2.2. In this case, crack evolution was implemented within a 3D power law [221], using a linear elastic fracture mechanics approach together with the extended-FEM method. In addition, the virtual crack closure technique was also used to calculate the strain energy release rate. RVEs with an *HVF* of 0, 25, 50, 75 and 100% were simulated, showing a ductile response at low *HVF*.

An alternative approach to reduce computational effort is to create a coupled two-scale FEM. These models separate micromechanical and macromechanical geometries and couple them, so that the results of one simulation are the inputs of the other at each load increment. One of the latest two-scale FEM was presented by Thionnet *et al.* [222], who studied the effects of the accumulation of fibre breakage in UD carbon fibre composites. Their model included stochastic fibre strength, matrix shear failure, interfacial debonding and matrix viscosity, making it a robust and complete model. The authors found that the failure of a UD composite material is a consequence of random fibre breaks which at high loads lead to the formation of clusters of broken fibres. The kinetics of fibre failure were different under steady loading, but still, failure of the structure was controlled by the viscoelasticity nature of the matrix leading to the development of clusters of broken fibres. Like the models of Pimenta [54] and Swolfs *et al.* [33], this model was also compared against blind data in the *I international benchmarking exercise for strength models* [4]. The model overpredicted the formation of larger clusters, and predicted an excessive non-linear stress-strain response, albeit the failure strength was relatively close to the experimental one.

The most recent and complete work to date concerning the damage development and failure in hybrid and non-hybrid composites under longitudinal tension is that published by Tavares *et al.* [35]. In their study, a micromechanical FEM able to reproduce fibre-matrix debonding by means of cohesive elements, and matrix cracking and yielding was developed by using a constitutive model developed by Melro *et al.* [207]. The fibres, randomly placed in the RVE within their respective radius, were modelled as transversally isotropic with a stochastic strength assigned for each fibre element. In addition, dynamic effects were considered. The authors concluded that, in order to obtain a ductile behaviour, the strength dispersion of the LE fibre was a key parameter. A wider strength scatter led to a wider damage progression and to a larger ductility.

Although some authors have been able to simulate the damage progression in composite materials using an FEM, performing such simulations is still too demanding, even if a super computer is employed. All the work carried out considered RVEs that were too small to be representative of real materials, and therefore, care must be taken when interpreting the FEM results. In any case, these models may be more useful in the future when the computational power

increases enough to allow larger RVEs to be simulated. For other notable work, the reader is referred to references [223–226].

2.3.3 Shear-lag theory

When a fibre breaks, the stress along the fibre is recovered over a distance called ineffective length (Fig. 2.22), thanks to the shear stress transfer occurring in the matrix. Shear-lag models attempt to estimate this stress recovery. Thus, these models are important because, coupled with an FBM and an appropriate load sharing rule, they can predict the tensile failure of composite materials. Some of these models can also estimate the *SCF* around fibre breaks. However, most studies only consider a fibre embedded in a portion of matrix and, consequently, just predict the stress recovery of the broken fibre. In this section, different shear-lag models that are solely able to predict the stress recovery of broken fibres are reviewed.

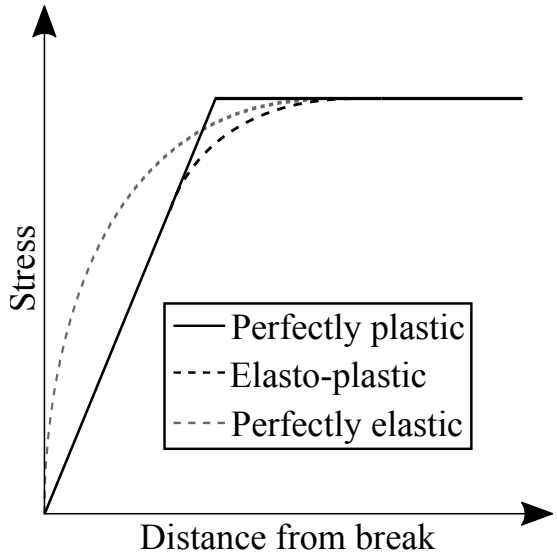

Figure 2.22: Examples of stress recovery in a broken fibre. An elastic matrix leads to an exponential stress recovery, while a perfectly plastic matrix leads to a linear stress recovery. An elasto-plastic matrix leads to a combination of the previous two extreme cases, leading to a linear region (yielded matrix) and an exponential zone (elastic matrix). More complex profiles can be obtained by adding a debonded region (not shown).

The first shear-lag model was presented by Cox [227]. This theory considered a perfectly-bonded elastic fibre in an elastic matrix. Thus, no upper limit was included for generating the interfacial shear stresses. In other words, the matrix

shear yield stress is 'infinite'. In addition, the matrix was assumed to carry only shear loads; a very common supposition in shear-lag models. In general, this is reasonable, since the tensile stresses carried by polymer matrices are negligible compared to those of the fibres. Given these considerations, the stress in the broken fibre, σ_f, along its length is

$$\sigma_f = E_f \varepsilon^0 \left(1 - \exp\left(-\frac{z}{R_f}\sqrt{\frac{2G_m R_f}{E_f(s-2R_f)}}\right)\right) \tag{2.45}$$

where z is the longitudinal distance from the break plane. This kind of model would correspond to the perfectly elastic case in Fig. 2.22. In practice, this theory may apply at very low loads, but at higher loads, the matrix will undoubtedly yield, since the matrix shear yield stress of polymers is very low (typical values range between $20-100$ MPa [37]). Therefore, more advanced theories, including matrix yielding were needed.

Rosen [141], developed a similar model, by assuming a fibre which was surrounded by an elastic matrix which was itself surrounded by a material with the composite properties. With these considerations, Rosen derived Eq. (2.9) to predict the ineffective length of the broken fibre, see Section 2.3.1.

One of the most widely-acknowledged shear-lag models in the literature is the one given by Kelly-Tyson [149]. In this model, a perfectly plastic matrix was assumed for the first time, together with a perfect fibre-matrix bonding. In this way, linear forces occur at the fibre-matrix interphase leading to a linear stress recovery within a constant acting shear stress (Fig. 2.22). Within these considerations, the ineffective length of a broken fibre, L^{in}, and its stress, σ_f, along its length are

$$L^{in} = \frac{E_f R_f}{2\tau}\varepsilon^0 \qquad \sigma_f = \begin{cases} \dfrac{2\tau z}{R_f} & 0 \le z \le L^{in} \\ E_f \varepsilon^0 & L^{in} < z \le \infty \end{cases} \tag{2.46}$$

where τ is, here, the matrix shear yield stress. Thanks to the plastic flow, the model includes an upper limit for the interfacial shear stress, allowing for a better estimation of the stress recovery. Nonetheless, it also presents some flaws. The model assumes that the matrix yields along the entire ineffective length. In reality, the shear stress will decrease down to zero in some region close to the end of the ineffective length. In that region, no yielding will occur,

since the shear stress will not exceed the yield stress. Such a feature cannot be captured by this model. It is worth mentioning that fibre-matrix debonding can also be simulated by this model by assuming that a constant debonded shear stress occurs instead of using the shear yield stress. This is something that was discussed in Section 2.3.2.

Later Piggott [228] presented another model including a debonded region. In Piggott's work, interfacial shear stresses appear thanks to the frictional stresses at the debonded region, whereas elastic stress transfer appears in the perfectly bonded region. The model was subsequently refined by different authors [229–232]. The stress recovery profile for these models combining a debonded and an elastic region is illustrated in Fig. 2.23.

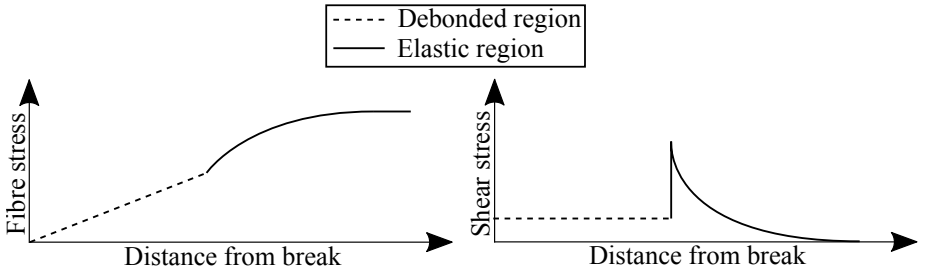

Figure 2.23: Schema of the stress profile assumed by some authors [228–232]. A debonded region, which may follow a constant shear stress or not, is followed by a well-bonded elastic region.

According to Lacroix [230], debonding occurs over a distance $\varsigma L/2$ with $0 \leq \varsigma \leq 1$. The stress for the fibre in the debonding region at a distance z, and along the elastic region is

$$\begin{aligned} \sigma_{\mathrm{f}} &= 4\tau_{\mathrm{s}}\frac{(L/2)-z}{d_{\mathrm{f}}} && \forall z : \varsigma\frac{L}{2} \leq z \leq \frac{L}{2} \\ \sigma_{\mathrm{f}} &= E_{\mathrm{f}}\varepsilon^{0} - \left(E_{\mathrm{f}}\varepsilon^{0} - 2\tau_{\mathrm{s}}\frac{L}{d_{\mathrm{f}}}\varsigma\right)\frac{\cosh\left(2\beta^{\mathrm{L}}z/d_{\mathrm{f}}\right)}{\cosh\left(\beta^{\mathrm{L}}\dfrac{L}{d_{\mathrm{f}}}(1-\varsigma)\right)} && \forall z : z \leq (1-\varsigma)\frac{L}{2} \end{aligned} \tag{2.47}$$

where the debonded shear stress is calculated with

$$\tau_{\mathrm{s}} = -\mu\left(\sigma_{\nu} + \sigma_{\mathrm{f}}^{\mathrm{r}}\right) \tag{2.48}$$

whereas $\sigma_{\mathrm{f}}^{\mathrm{r}}$ is the thermal residual stress, μ is the friction coefficient and

$$\sigma_{\nu} = \frac{E_{\mathrm{f}}E_{\mathrm{m}}\left(\nu_{\mathrm{f}} - \nu_{\mathrm{m}}\right)}{E_{\mathrm{f}}\left(1+\nu_{\mathrm{m}}\right) + E_{\mathrm{m}}\left(1+\nu_{\mathrm{f}}\right)\left(1-2\nu_{\mathrm{f}}\right)}\varepsilon^{0} \tag{2.49}$$

while ν_f and ν_m are the fibre and matrix Poisson's ratio, respectively. The shear-lag parameter, β^L, and the debonded coefficient, ς, are, respectively,

$$\beta^L = \sqrt{\frac{E_m}{E_f(1+\nu_m)\ln(2s/d_f)}} \quad \varsigma = \frac{E_f\varepsilon^0 - 2\dfrac{\tau_s^{ult}}{\beta^L}\coth\left(\beta^L(L/d_f)(1-\varsigma)\right)}{2\tau_s(L/d_f)} \tag{2.50}$$

where τ_s^{ult} is the interfacial shear strength. Thus, when the shear stress reaches the shear strength, debonding occurs. In order to obtain ς from Eq. 2.50, an iterative procedure is necessary. Unfortunately, this makes the model infeasible to be used with FBMs.

A rather similar model was presented by Ivens [229]. The stress along the debonded region and along the elastic region are

$$\begin{aligned} \sigma_f &= \frac{\sigma_s}{L_s^{in}} z && \forall z: \quad z \le L_s^{in} \\ \sigma_f &= E_f\varepsilon^0 - \left(E_f\varepsilon^0 - \sigma_s\right)\exp\left(\frac{\beta^I\left(L_s^{in} - z\right)}{s}\right) && \forall z: \quad z > L_s^{in} \end{aligned} \tag{2.51}$$

where σ_s is the fibre stress at the end of the debonded region and β^I is a shear-lag parameter similar to that of Lacroix [230]

$$\sigma_s = \frac{\beta^I E_f\varepsilon^0 - 2\tau_s^{ult}}{\beta^I} \quad \beta^I = \sqrt{\frac{2E_m}{E_f(1+\nu_m)\ln\left((5s/R_f)^2\right)}} \tag{2.52}$$

The length of the elastic region is

$$L_e^{in} = \frac{R_f}{\beta^I}\ln\left(\frac{10\left(E_f\varepsilon^0 - \sigma_s\right)}{E_f\varepsilon^0}\right) \tag{2.53}$$

whereas the length of the debonded region, L_s^{in}, is obtained from solving the following system of equations:

$$\begin{aligned} \sigma_s &= \gamma_s\left(1 - \exp\left(-\alpha_s L_s^{in}\right)\right) - \beta_s\left(L_s^{in} - \frac{1}{\alpha_s}\left(1 - \exp\left(-\alpha_s L_s^{in}\right)\right)\right) \\ \varepsilon_m &= 2\varepsilon^0 + \frac{2R_f\left(E_f\varepsilon^0 - \sigma_s\right)}{\beta^I E_f L_s^{in}}\left(1 - \exp\left(-\frac{\beta^I L_e^{in}}{R_f}\right)\right) - \frac{\sigma_s}{E_f} \end{aligned} \tag{2.54}$$

where

$$\alpha_s = \frac{2\mu\chi E_m\nu_f}{R_f E_f} \quad \beta_s = \frac{\nu_m E_f}{\nu_f L_s^{in}}\left(\varepsilon_m - \frac{\sigma_s}{E_f}\right) \quad \gamma_s = \frac{E_f}{\nu_f}\left(\nu_m\varepsilon_m - \frac{\sigma_f^r}{\chi E_m}\right) \tag{2.55}$$

and where χ is a constant which depends on the material and the geometrical properties [229]. Because it introduces debonding, the model is powerful like the one proposed by Lacroix [230], nonetheless, it is relatively complex and obtaining L_s^{in} is not straightforward.

Nairn [233] developed a three-dimensional axisymmetric model taking into account all the components of the fibre stress, and improving the interfacial stress at the fibre breaks. The model also included thermal residual stresses and assumed an elastic matrix. The model was later extended to include matrix plasticity with and without debonding obtaining good agreement with a finite element model [234]. The final model is relatively advanced since it includes yielding and debonding. Nonetheless, its complex formulation makes it challenging to implement in FBMs.

Landis and McMeeking [235] included matrix yielding in Cox's [227] shear-lag model, leading to an elasto-plastic shear-lag equation. Within this, matrix yielding occurs when the applied strain, ε^0, is larger than the matrix shear yield strain, ε_y^{ult}, given by

$$\varepsilon_y^{ult} = 2\frac{\tau}{E_f}\sqrt{\frac{E_f(s-2R_f)}{G_m d_f}} \tag{2.56}$$

When yielding occurs, the stress in the fibre at a distance z from the break is

$$\sigma_f = \begin{cases} \dfrac{4\tau}{d_f} z & 0 \le z \le L_s^{in} \\ E_f\varepsilon^0 - 2\tau\sqrt{\dfrac{E_f(s-2R_f)}{G_m d_f}}\exp\left[2\sqrt{\dfrac{G_m d_f}{E_f(s-2R_f)}}\left(\dfrac{L_s^{in}-z}{d_f}\right)\right] & z \ge L_s^{in} \end{cases} \tag{2.57}$$

where the slip length, i.e. the length where matrix yielding has occurred, L_s^{in}, is

$$L_s^{in} = \frac{d_f}{4}\left(\frac{E_f\varepsilon^0}{\tau} - 2\sqrt{\frac{E_f(s-2R_f)}{G_m d_f}}\right) \tag{2.58}$$

where τ is, here, the matrix shear yield stress. Note that, when yielding does not occur, i.e. $\varepsilon^0 \le \varepsilon_y^{ult}$, the fibre stress is given as in Eq. 2.45. Within this model, the stress recovery profile corresponds to the elasto-plastic curve in Fig. 2.22 when yielding occurs, and to the perfectly elastic curve when no yielding appears. In practice the model may also be used to simulate debonding instead

of yielding, by inserting a debonded shear stress for τ instead of the matrix shear yield stress.

Although this model adds an upper limit to the shear stress, the model implies that yielding occurs in a thin layer around the broken fibre while the rest of the matrix is elastic [235]. To resolve this issue, Landis and McMeeking [235] presented a new model based on the work of Cox [227]. The authors obtained a non-linear partial differential equation to describe the load recovery. Since a closed form solution is not available for the developed equation, the authors fitted a power-law function to describe the model in a simple way. Their results were in a good agreement with a finite element analysis.

De Morais [236] developed a more refined model which included a debonded region, a plastic region, and a final elastic region in the broken fibre. Along the debonded length, a decreasing interfacial shear stress is derived from Poisson contractions and Coulomb friction, similar to the model of Lacroix [230]. The debonded region is followed by a matrix yielding zone, where the interfacial shear stress is assumed to be equal to the matrix shear yield stress. Finally, there is an elastic part, where the interfacial shear stress follows an exponential law. The model was in good agreement with a 3D FEM. The approach presented is very robust since it includes debonding with an elasto-plastic matrix. Nonetheless, the model was developed for a regular packing of fibres, was derived for non-hybrid composites, and must be solved numerically, making it impractical to be used with FBMs.

More recently St-Pierre *et al.* [198] presented a shear-lag model to predict the ineffective length. In their work, the Kelly-Tyson model was modified by including a scaling factor, which increases the ineffective length with the number of broken fibres in the cluster. Thus, the ineffective length becomes

$$L^{\text{in}} = \frac{n\pi d_{\text{f}}^2 E_{\text{f}}}{4C\tau}\varepsilon^0 \tag{2.59}$$

where C is the shear-lag profile, $C = 4s\sqrt{n}$, s is the mean distance between fibre centres, $s = R_{\text{f}}\sqrt{\pi/V_{\text{f}}}$, n is the number of broken fibres in the cluster and τ is here again the matrix shear yield stress, see Fig. 2.24. For other ways to estimate the shear-lag profile, the reader is referred to Pimenta and Pinho [159]. The model developed is remarkable, since it includes the effect of the cluster size in

a simple analytical equation. When more than one broken fibre is present, the ineffective length of the broken fibres increases [37, 159]. This is well captured by this model. Moreover, the plastic limit is included, allowing for a more realistic representation than the elastic models. The outcomes of the model were validated against finite element data obtaining good agreement.

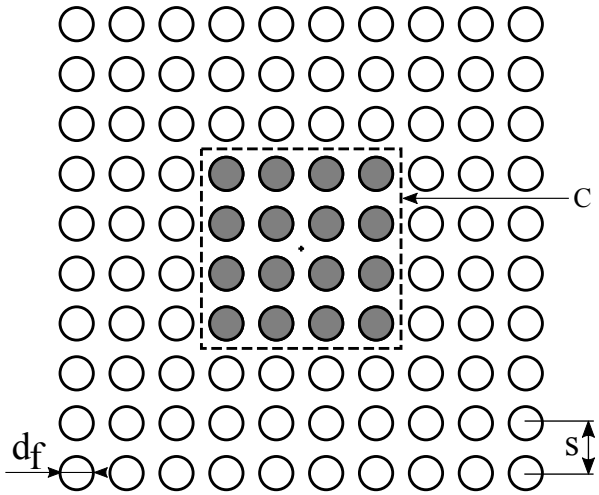

Figure 2.24: A cross-section example of the model assumed by St-Pierre *et al.* [198]. A bundle of 100 fibres is shown, with a cluster of 16 broken fibres (coloured grey) centred into the bundle. The model estimates the ineffective length of the planar cluster of broken fibres, with corresponding shear-lag perimeter *C*.

Even though the state of the art in shear-lag models has advanced and new and more refined models have been developed, the Kelly-Tyson shear-lag model [149] is still the most commonly used to date thanks to its simplicity. By combining shear-lag models with a statistical strength distribution and a load sharing rule, it is possible to simulate the tensile failure of composite materials. According to Xia *et al.* [237] shear-lag models are generally accurate for high fibre/matrix stiffness ratios, high fibre volume fractions, and/or when global matrix yielding proceeds fibre breaking. Thus, shear-lag models should be mostly accurate in FRP. Overall, many shear-lag models present the following issues [5]:

- Matrix plasticity is sometimes omitted.
- Fibre-matrix debonding is sometimes not considered.
- Matrix cracking is neglected.
- Matrix viscosity effects are not taken into account.

- Anisotropic fibre properties are not possible.
- An ordered fibre packing is generally considered.
- A combination of an elasto-plastic matrix behaviour with debonding is usually not considered.
- The increase of ineffective length with the number of broken fibres is generally omitted.
- All fibres are assumed to be of the same material.

As has been seen, some authors have tried to overcome some of these issues. Nevertheless, more work is needed. More refined models, simpler to use and incorporating an elasto-plastic matrix with debonding, matrix cracking and the cluster size should be addressed in the future. Viscosity effects may also need to be included. Moreover, there is not a single analytical model which takes into account the existence of fibres with different mechanical properties, like in a hybrid composite. For other notable work the reader is referred to references [191, 231, 232, 238–242].

2.3.4 Stress concentration factor models

Different authors have derived analytical equations for predicting the *SCF* around broken fibres, taking into account several features. This is also a relevant topic, since an analytical equation can be used in an FBM together with a shear-lag model for simulating the tensile failure of a composite material. It is worth mentioning that, the *SCF* is defined here as the ratio between the local stress in an intact fibre over the applied far-field stress. It should also be noted that the *SCF* can be either dynamic or static. Most of the work found in the literature has focused on static *SCF*, although some authors have also attempted to model the dynamic *SCF*. Thus, the models which take dynamic effects into account will be emphasised. In the following, some of the available models, mainly analytical, able to predict the *SCF* around fibre breaks are summarised. Note that this topic is interrelated with the shear-lag theory, since some models are obtained by shear-lag considerations.

Hedgepeth [56] developed the first model able to predict the *SCF* around broken fibres. The author modelled a 1D packing of fibres embedded in an elastic matrix. According to Hedgepeth, the static *SCF* in an intact fibre around n

broken fibres is

$$SCF = \prod_{j=1}^{n} \frac{2j+2}{2j+1} \tag{2.60}$$

while the dynamic *SCF* is given by

$$SCF^{\mathrm{d}} = M_{\mathrm{d}} SCF \tag{2.61}$$

where M_{d} is a dynamic factor which ranges between 1.15 and 1.2 depending on the number of simultaneous breaks [56]. Although the model is somewhat powerful, it is limited because of the following reasons. It does not consider the distance between fibres (since it is a 1D fibre packing), neither the effect of the fibre content nor the physical properties. Moreover, the matrix is treated as an elastic solid. Thus, the model is unsuitable to perform accurate simulations. Nonetheless, this model is one of the very few which includes dynamic effects.

Later, Hedgepeth and Van Dyke [160] extended their previous work to 2D square and hexagonal fibre packings. Unlike the original model, the effect of matrix yielding was included in their predictions as well. This allowed a more realistic static *SCF* to be predicted, allowing the decrease in *SCF* due to the matrix yielding to be captured. Nevertheless, the model is still limited since it does not take into account a random distribution of fibres, and considers a non-hybrid composite. Furthermore, the model is not purely analytical, making it challenging to use with FBMs.

A further simple approach was given by Harlow and Phoenix [243]. By assuming that the load released by a broken fibre is only transferred onto the two nearest neighbouring fibres, the static *SCF* becomes

$$SCF = 1 + \frac{n}{2} \tag{2.62}$$

By analysing this equation it is clear that it is too simplistic. As with the work of Hedgepeth and Van dyke, such a method considers neither the fibre spacing, nor the properties of the material or the matrix behaviour.

Fukuda and Kawata [69, 70] included the effect of the fibre content and the material parameters, and studied their influence on the static *SCF*. Decreasing the interfibre spacing was seen to increase the *SCF* around breaks. Likewise, increasing the number of broken fibres also increased the *SCF*, since more

load needs to be redistributed. A larger ratio of fibre Young's modulus over matrix Young's modulus also increased the *SCF*. The effect of random spacing on the *SCF* was also studied [67], demonstrating that the *SCF* depends on the distance between broken and intact fibres, and hence it should be treated statistically. Most of these effects have been confirmed by different studies [37, 68]. Although the model is powerful, taking into account many effects, it is not purely analytical which makes it difficult to use. The model was also applied to establish the *SCF* in hybrid composites [46].

Xing *et al.* [26] extended Hedgepeth's [56] 1D packing approach to hybrid composites, consisting of one row of LE fibres and another row of HE fibres in an elastic matrix and including dynamic effects. The model showed that the dynamic *SCF* may be smaller in hybrid composites than in non-hybrids, which should lead to hybrid effects, as discussed in Section 2.1.1.2. Further refinements were performed in Ji *et al.* [57]. The main drawbacks of these models is that they are not analytical, assume simplistic regular packings of fibres and an elastic matrix. The good point is that they take into account the dynamic effect.

Another simple model for predicting the static *SCF* was presented by Pitkethly and Bader [30] with

$$SCF = 1 + \frac{\sqrt{n}}{\Upsilon} \tag{2.63}$$

where Υ is an experimentally determined load function depending on the geometrical and material properties. Therefore, such a model includes, in a semi-empirical way, the geometry and material characteristics. While this model is fairly simple, it is impractical, since it enforces the need to obtain Υ.

Soon after, Wagner and Eitan [244] developed a more advanced model for predicting the static *SCF* based on shear-lag theory considering an elastic matrix. The authors derived a function depending upon the interfibre distance, the matrix and fibre properties as well as the ineffective length. The static *SCF* around a broken fibre was derived as

$$SCF = 1 + \frac{\arcsin\left(R_f/d^c\right)}{\pi} \frac{\sinh\left(\beta^c\left(L^{in} - z\right)\right)}{\sinh\left(\beta^c L^{in}\right)} \tag{2.64}$$

where β^c is cox's shear-lag parameter [227]

$$\beta^c = \frac{1}{R_f}\sqrt{\frac{2G_m}{E_f \ln\frac{d^c}{2R_f}}} \tag{2.65}$$

and d^c is the centre-to-centre distance from the broken to the intact fibre. For long fibres $\beta^c \gg 1$. The model is somewhat powerful since it takes into account the material properties and the distance between fibres by using simple analytical equations. Thus, it can be used, to some extent, with hybrid and non-hybrid composites. Nonetheless, it considers an elastic matrix, and the model was derived from a 1D planar array of fibres. That is known to overpredict the *SCF* [37]. It also omits the fibre volume fraction, which is known to have a very considerable impact on the *SCF* [37, 68].

The importance of including matrix yielding was also highlighted by Nedele and Wisnom [245]. In their work, a finite element model was used to study the static *SCF* around a broken fibre. The model consisted of an axisymmetric single broken fibre surrounded by a matrix which was itself surrounded by either concentric cylinders representing the fibres or a perfect composite material. Their results showed that the *SCF* is dependent on the assumed fibre-matrix bonding and on the matrix behaviour. For all cases the static *SCF* predicted was lower than that of Hedgepeth and Van Dyke [160]. Moreover, it was found that only half of the ineffective length presented an excess of stress, and that the stress actually decreases from the nominal value farther away.

Grubb *et al.* [246] simplified Eitan and Wagner's approach using a similar idea to that of Pitkethly and Bader [30]. The static *SCF* becomes

$$SCF = 1 + \frac{1}{\pi}\arccos\left(\frac{d^c}{2R_e}\right) \tag{2.66}$$

where R_e is an experimentally determined fibre-fibre interaction radius. The authors compared the predictions of their new model against that of Eitan and Wagner as well as experimental data obtained by Raman Spectroscopy. The new model was closer to the experimental results than the model of Eitan and Wagner, but had as a drawback the fibre-fibre interaction radius.

Van den Heuvel *et al.* experimentally obtained the static *SCF* by using Raman Spectroscopy data [82, 83, 247–250] and studied the influence of inter-fibre

spacing on the *SCF* resulting from a break. According to their data, the state of the art models were not accurate enough.

Zhou and Wagner [251] improved the model of Eitan and Wagner [252] by adding a given debonded region followed by an elastic region in the broken fibre. The model was again derived from a 1D fibre packing, using shear-lag theory. Overall, the model is quite similar to the one presented in Eitan and Wagner, except that a more advanced shear-lag parameter is used, and debonding is included. With these considerations, the static *SCF* around n adjacent broken fibres is

$$\begin{aligned} SCF = 1 + \sum_{i=1}^{n} \frac{2\arcsin\left(\frac{R_q}{d^{c(i)}}\right)}{\pi} \Bigg[\left(1 - \frac{\mu L_s^{in(i)}}{R_j^{(i)}}\right) \frac{\cosh \beta_q^N z}{\cosh \beta_q^N \frac{L_s^{in(i)}}{2}} + \\ + \frac{2\mu R_j^{(i)}}{R_q^2} \left(\frac{L_s^{in(i)}}{2} - z\right) \Bigg] \quad 0 \le z \le \frac{L_s^{in(i)}}{2} \\ SCF = 1 + \sum_{i=1}^{n} \left(1 - \frac{\mu L_s^{in(i)}}{R_j^{(i)}}\right) \frac{2\arcsin\left(\frac{R_q}{d^{c(i)}}\right) \sinh \beta_j^{N(i)} \left(L^{in(i)} + \frac{L_s^{in(i)}}{2} - z\right)}{\pi \sinh \beta_j^{N(i)} L^{in(i)}} \dots \\ \dots \quad z \ge \frac{L_s^{in(i)}}{2} \end{aligned} \tag{2.67}$$

where R_j and R_q are the radius of the broken and intact fibres, respectively, β_j^N and β_q^N are Nayfeh's shear-lag parameter [253] for the broken and intact fibre, respectively, as given in Zhou and Wagner [251], and L_s^{in} is the length of the debonded region. For all equations, $L_s^{in} \le R_j/\mu$ should be satisfied.

A maximum *SCF* of 1.33 was predicted when one fibre break was present and the radiuses of the broken and intact fibres were the same, agreeing well with Hedgepeth [56]. Overall, results were in better agreement with experimental data than the model of Eitan and Wagner [244]. Later, the model was extended to work with hybrid composites by simply adding an extra term taking into account the difference of stiffness between the broken and intact fibres [254]. However, such model is still not enough, because, besides not including matrix yielding, it omits the volume fractions of the fibres which affect the *SCF* [45].

Ohno *et al.* [255] also derived equations for estimating the static *SCF* around a broken fibre. A hexagonal fibre-array model containing a broken fibre was

considered with interfacial slip and matrix yielding. Two approximate solutions were found for predicting the *SCF* in the closest neighbour to the break with

$$\begin{aligned} SCF &= \frac{1-e^{-\sqrt{3}L^{\text{in[-]}}}}{6\sqrt{3}L^{\text{in[-]}}} && \text{solution 1} \\ SCF &= \frac{\kappa_1\eta_1\left(1-e^{-\eta_3 L^{\text{in[-]}}}\right)-\kappa_3\eta_3\left(1-e^{-\eta_1 L^{\text{in[-]}}}\right)}{6\left(\kappa_1-\kappa_3\right)\eta_1\eta_3 L^{\text{in[-]}}} && \text{solution 2} \end{aligned} \tag{2.68}$$

where

$$\begin{bmatrix}\eta_1\\ \eta_2\end{bmatrix} = \pm\left(\frac{7-\sqrt{19}}{2}\right)^{\frac{1}{2}} \qquad \begin{bmatrix}\eta_3\\ \eta_4\end{bmatrix} = \pm\left(\frac{7+\sqrt{19}}{2}\right)^{\frac{1}{2}} \tag{2.69}$$

$$\kappa_n = \frac{3-\eta_n^2}{3} \quad n = 1,2,3,4$$

and where $L^{\text{in[-]}}$ is a dimensionless ineffective length [255]. The authors found solution 2 to be in good agreement with 3D finite element simulations. Nonetheless, as in the case of previous work, this model was derived for a regular packing of fibres, making it impractical for models with a random fibre packing. Moreover, it does not directly take into account the material properties or the distance between fibres.

An in-depth work of the static *SCF* around broken fibres was performed by Swolfs *et al.* in different publications [40, 45, 68]. In a first contribution, Swolfs *et al.* [68] studied the static *SCF* around a single broken fibre within a realistic random distribution of fibres embedded in an elastic matrix using an FEM. Hence this was the first time in the literature that a realistic fibre distribution was used for studying the *SCF*, see Fig. 2.25a. By fitting their results, the *SCF* around a broken fibre in a non-hybrid composite becomes

$$\begin{aligned} SCF &= -3.92\ln\left(\frac{d^c-R_j-R_q}{R_j}\right)+3.84 && \text{if} \quad V_f = 30\% \\ SCF &= -2.87\ln\left(\frac{d^c-R_j-R_q}{R_j}\right)+2.86 && \text{if} \quad V_f = 50\% \\ SCF &= -2.12\ln\left(\frac{d^c-R_j-R_q}{R_j}\right)+1.78 && \text{if} \quad V_f = 70\%. \end{aligned} \tag{2.70}$$

The results obtained show that ordered fibre packings lead to higher *SCF* than random packings at the same normalised distance from a broken fibre. However,

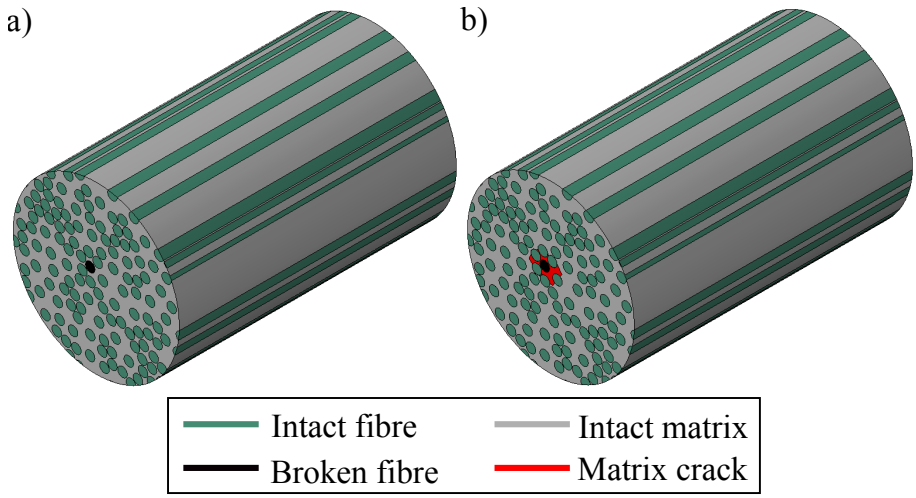

Figure 2.25: Schema of the finite element model developed by Swolfs *et al.* [40, 68]: a) general model, and b) including a matrix crack around the broken fibre.

the maximum *SCF* was approximately 70% higher in random packings due to the fibres being closer to the broken one. The fibre volume fraction had a significant impact on the *SCF*, the ineffective length and overload length (the longitudinal distance in intact fibres presenting an excess of stress). Thus, models should clearly include the effect of the volume fraction and fibre distance. However, the fibre stiffness had a negligible impact on the *SCF* but an important influence on both the ineffective length and overload length. Finally, including anisotropic elastic properties for the fibres produced a higher *SCF*, ineffective and overload lengths. Although the FEM developed to predict the *SCF* is quite advanced, the authors did not include matrix plasticity in their modelling results. Moreover, the obtained equations are a fitting for a specific material case. Thus, the FEM must be run for each material configuration, to obtain the proper *SCF*.

A similar study was later carried out by Swolfs *et al.* [45], but with different hybrid composites. In this new study, the effect of the *HVF*, the elastic properties and the assumption of having the same radius for both fibres or not was studied. The authors found that the *HVF* has a small impact on the stress redistribution, however, a small increase of the *SCF* on both fibre types was noted with decreasing the LE fibre content. The ineffective length was not affected. In addition, a stiffer HE fibre reduced the *SCF* on the HE fibres around a broken LE fibre, while this influence for the *SCF* carried by LE fibres was smaller. Finally, the authors attributed the discrepancies between their results and the ones in the

literature to the use of a more realistic fibre packing.

Later, a matrix crack around the broken fibre was added into their FEM [40] and their presence on the load redistribution was explored (Fig. 2.25b). The addition of matrix cracks increased the *SCF* although the effect was small. However, the authors highlighted that more work was needed as the matrix cracks were assumed to occur around fibre breaks and, alternatively, the matrix could yield or debond. For this case, the *SCF* around a broken fibre was fitted as

$$\begin{aligned} SCF &= -3.67\ln\left(\left(d^{\mathrm{c}} - R_j - R_q\right)/R_j\right) + 6.36 \quad \text{with matrix crack} \\ SCF &= -3.30\ln\left(\left(d^{\mathrm{c}} - R_j - R_q\right)/R_j\right) + 5.76 \quad \text{without matrix crack.} \end{aligned} \tag{2.71}$$

One of the most relevant analytical models in the literature was recently developed by St-Pierre *et al.* [198]. The authors formulated an analytical model capable of predicting the static *SCF* around a planar cluster of broken fibres of any size, as shown in Fig. 2.26. Accordingly, the *SCF* around a cluster of broken fibres follows a power-law with

$$SCF = 1 + I\left(\frac{R_{\mathrm{b}}}{r}\right)^{\alpha} \tag{2.72}$$

where

$$I = \begin{cases} \dfrac{1}{2\ln\left(R_{\mathrm{t}}/R_{\mathrm{b}}\right)} & \text{if } \alpha = 2 \\ \dfrac{(2-\alpha)R_{\mathrm{b}}^{2-\alpha}}{2\left(R_{\mathrm{t}}^{2-\alpha} - R_{\mathrm{b}}^{2-\alpha}\right)} & \text{otherwise,} \end{cases} \tag{2.73}$$

where r is the in-plane distance from the centre of the cluster to the centre of the intact fibre, R_{b} is the equivalent radius of the cluster of broken fibres, $\pi R_{\mathrm{b}}^2 = ns^2$, R_{t} is the equivalent radius of the composite, $\pi R_{\mathrm{t}}^2 = N_{\mathrm{q}}s^2$, n is the number of broken fibres in the cluster, s is the average distance between fibre centres, $s = R_{\mathrm{f}}\sqrt{\pi/V_{\mathrm{f}}}$, and α is a power-law exponent which controls the maximum value of *SCF* and the shape of the curve. Its value depends mainly on the matrix properties and behaviour. According to St-Pierre *et al.* [198], such a parameter is equal to 2 for an elasto-plastic matrix, whilst according to Tavares *et al.* [37] it is 3.8 for an elastic matrix. The analytical model was in good agreement with an FEM for different cluster sizes. By analysing this model, it is clear that it is one of the most robust in the literature. It is simple and analytical, it takes into account the cluster size, composite size, fibre volume fraction, fibre radius

and it can be further calibrated by adjusting the value of α, allowing different matrix behaviours or features not directly accounted such as matrix cracks to be taken into account. The formulation is flexible, allowing for it to be extended to hybrid composites. Thus, this model can easily be applied to FBMs.

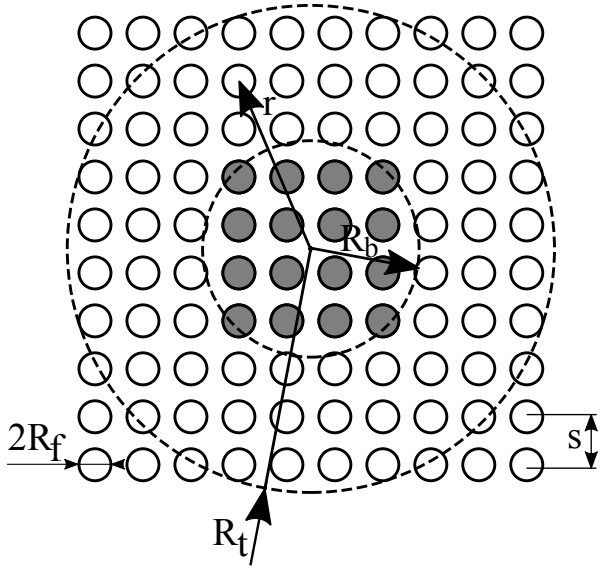

Figure 2.26: A cross-section example of the model assumed by St-Pierre *et al.* [198]. A bundle of 100 fibres is shown, with a planar cluster of 16 broken fibres (coloured grey) centred into the bundle. The model estimates the *SCF* carried by any fibre in the bundle caused by the entire cluster.

To summarise, there are different models to predict the *SCF* around a broken fibre. Most work omits the dynamic *SCF*, focusing only on the static. Some models are based on mathematical considerations without taking into account geometrical and/or material properties, while other models take them into account leading to more complex and realistic models. Currently, there is not a single analytical model which can predict the *SCF* around a cluster of broken fibres in a hybrid composite taking into account the elastic and geometrical properties of the two fibres in the hybrid as well as the matrix behaviour (perfectly elastic or elasto-plastic/perfeclty-plastic). Models taking debonding and matrix cracking into account are also scarce. Thus, new models should be developed. For other relevant work the reader is referred to references [37, 63, 95, 256].

2.3.5 Conclusions

This section has focused on the available models able to predict the failure and damage progression in UD composite materials under fibre tensile loading. Clearly, predicting the failure of composite materials is not an easy task. The most difficult challenges are to accurately calculate the stress redistribution around broken fibres and to take the interaction between the fibres and matrix into account.

Different models attempt to capture the failure of composites. GLS models are computationally inexpensive, simple and easy to use. However, they cannot capture the formation of clusters, which severely limits them. At best, these can be used to perform some parametric analyses. In contrast, LLS models can predict the formation of clusters and are more advanced than GLS. Nonetheless, they are also computationally more expensive. LLS models can be classified into diverse categories according to the considerations involved: analytical models, fibre bundle models, spring element models and finite element models. Analytical models may be more limited in terms of features, since different assumptions need to be considered so as to obtain an analytical solution (e.g. assuming that all clusters are planar as in the work of Pimenta [54]). The advantage is that they are computationally less expensive than the others. Fibre bundle models can be very sophisticated, and may take into account several features, but they need larger computational resources. Spring element models are even more sophisticated than fibre bundle models, but need even larger computational resources due to the presence of the matrix. Finally, finite element models should be the most accurate, yet computational power nowadays is not substantial enough to perform studies with large RVEs. In some models, post-processing the results is also a difficult task since the amount of data is very large. Visualising and determining the formation of clusters is generally not straightforward.

At present, the majority of the models in the literature were developed for non-hybrid composites, although some are able to deal with hybrids [33, 39]. Hybrid composite materials are more complex to simulate than non-hybrids, since the difficult interaction between both LE and HE fibres must be captured. Moreover, if both fibres have a different radius, the geometry is further complicated,

especially if random packings are used. Currently, (besides FEM) the spring element model developed by Tavares *et al.* [39, 63] is one of the few models able to predict the pseudo-ductile behaviour of a hybrid composite with a random distribution of fibres. The model of Swolfs *et al.* [31, 33] can accurately predict hybrid effects, but it can only capture the ductile behaviour of the material when an interlayer hybrid configuration is considered [100]. Thus, new models able to predict the ductility of hybrid composites and less expensive than the spring element model are yet to be developed.

Shear-lag models can describe the stress recovery in a broken fibre. At present, diverse shear-lag models have been formulated including different features such as matrix yielding, debonding or the size of the cluster of broken fibres. Nonetheless, there is a lack of models taking into account many of the features collectively. Analytical models considering fibres of different types have not yet been developed.

Models for predicting the *SCF* around broken fibres also exist in the literature. Very few models are able to predict the *SCF* when taking into account the distance between broken fibres, as well as the elastic and geometrical properties of the composite. At present, no analytical model can predict the *SCF* in a hybrid composite by accurately considering the elastic and geometrical properties of the fibres as well as the volume fraction of each constituent. Additionally, most models omit dynamic effects.

Currently there are a number of different issues and problems arising from attempting to simulate the tensile failure of composite materials. This is well discussed in Bunsell *et al.* [4]. Firstly, many models do not use an accurate random distribution of parallel fibres. Although that is a reasonable approach for non-hybrid composites, it should be avoided with hybrid composites as to allow a more realistic stress redistribution [45, 68]. Moreover, there are several defects such as fibre waviness, voids, resin-rich regions, etc., that are neither included nor investigated [4]. Secondly, the majority of the models assume a traditional Weibull distribution or a modified Weibull distribution to characterise the strength of the fibres. This is a key input parameter in the models, nonetheless, the proper distribution to use is not yet clarified [4, 5]. In addition, the matrix microscale properties are also not simple to determine. In general, macroscale resin properties are entered into the micromechanical

models, although the microscale resin properties could be different to that of the macroscale properties [4, 5]. Many models, assume simplistic elastic stress redistribution around the broken fibres, omitting matrix yielding, matrix cracks and debonding. These phenomena should be incorporated into the models. Likewise, the inclusion of dynamic effects has been scarce, which would affect the formation of clusters in the models.

Compared against experiments, models are sometimes satisfactorily compared against one set of data, but fail to accurately predict failure for a different material [4]. All current state of the art models underpredict the formation of larger clusters as well as the number of co-planar clusters compared to the experiments [4, 39, 41]. Although this discrepancy was originally considered to be caused by the omission of dynamic effects, recent work has shown there may be other reasons behind this [63]. Overall, models have been compared against only a single specimen. To take into account the strength variability, they should be compared against a number of identical specimens rather than against a single one [4]. Another issue is the size of the RVE. Models usually consider small RVEs containing hundreds or thousands of fibres, while real composites commonly contain millions of fibres. Because of the presence of size effects, RVEs with the size of the real material specimen should be attempted. A more objective definition of what determines a cluster of broken fibres is also necessary [4, 37]. At present, this is usually determined by a distance criteria, which is sometimes differently considered by the authors and hinders the comparison with experimental data [4]. Finally, whether final failure is triggered due to the accumulation of damage and clusters or due to the propagation of a large cluster should be determined [4].

2.4 Literature review conclusions

Fibre hybridisation is a potential solution to the inherent quasi-brittle behaviour and low toughness of composite materials. With the correct design, the failure process of non-hybrid composites can be altered, leading to hybrid effects and a ductile failure. The relative fibre volume fraction, elastic properties, failure strains, degree of dispersion and fibre strength scatter are the main parameters affecting the hybrid effect and have been studied in depth. Other phenomena such as matrix cracks, debonding or yielding need yet further investigation.

Currently, it is well known that a lower number of LE fibres, a large strength scatter, higher fibre dispersion and larger ratio of failure strain between the fibres, among others, should increase the hybrid effect. The three hypothesis to explain the hybrid effect, mainly the changes in the failure development, residual stresses and dynamic effects, are clearly pointed out in the literature. The failure development has been well studied, and its significant importance is very clear. Residual stresses are known to be secondary, whereas the dynamic effects have not been properly studied yet.

There are different models with which to study the failure of hybrid and non-hybrid composites. Two main modelling groups can be defined: GLS and LLS models. GLS models are simple and computationally efficient, but cannot capture the formation of clusters leading to a large overprediction of the strength. Meanwhile, LLS models can capture the formation of clusters and the stress redistribution around broken fibres, but their complexity is greater which, in general, leads to computationally expensive models. While the majority of models are developed for non-hybrid composites, only few are intrinsically capable of taking hybrid composites into account. The development of accurate LLS models able to capture the fibre tensile failure and damage development in hybrid composites with a low computational effort is necessary.

The stress recovery of broken fibres can be predicted by means of shear-lag models, while the stress concentration around broken fibres carried by the surrounding intact fibres can be estimated using *SCF* models. Combining both, it is possible to compute the entire stress redistribution around broken fibres. In general, these models are developed for non-hybrid composites. New models taking into account the presence of different fibres are yet to be seen.

At this point, the development of more advanced and accurate models in the literature is needed. As discussed in Section 2.3.5, there is still a large gap between models and experiments. As a summary, models present different issues. Firstly, the failure of the material is not predicted with enough accuracy for blind material design. Secondly, the formation of larger clusters and the number of co-planar clusters are significantly underestimated, while, the fibre break density is generally overestimated. Thirdly, dynamic effects are generally omitted. Moreover, models should objectively determine when final failure occurs, as well as include realistic fibre geometries (random fibre packings,

including matrix rich regions, voids, etc.). Finally, all models need accurate fibre strength data and matrix properties as input parameters.

Part II

Publications

3

Paper A – A 3D Progressive Failure Model for predicting pseudo-ductility in hybrid unidirectional composite materials under fibre tensile loading

The paper has been published in *Composites Part A: Applied Science and Manufacturing* 107 (2018) 579–591.

Overview

One of the main objectives of this thesis is to develop a suitable model which can simulate the fibre tensile failure and damage development in hybrid composite materials containing fibres with different elastic and geometrical properties.

Currently, few models in the literature are able to predict the fibre tensile failure and damage development in hybrid composites. Some models can only predict failure up to the onset of the LE fibre failure, not allowing to capture pseudo-ductility [33]. Finite element models and spring element models do not face this limitation, but are heavily bounded computationally [35, 39]. Other more simplistic models cannot capture the formation of clusters, making them unrealistic [34, 35].

To obtain a model capable of predicting the formation of clusters and damage development, while still being computationally efficient, developing a fibre bundle model using a local load sharing rule seems to be the best option.

In this chapter a novel 3D progressive failure model able to simulate the tensile failure and damage progression in hybrid and non-hybrid unidirectional composite materials is developed. The model is based on a fibre bundle model, and considers a representative volume element containing a given number of parallel fibres with their own radius and elastic properties. The model captures the formation of clusters of broken fibres using known functions to calculate the stress redistribution around breaks. The stiffness loss of the materials is computed by associating a damage variable to the loss of stress transfer capability along the ineffective length of broken fibres. The model is validated against experimental data and finite element simulations showing a good agreement with the different hybrid and non-hybrid composites analysed.

A 3D Progressive Failure Model for predicting pseudo-ductility in hybrid unidirectional composite materials under fibre tensile loading

Jose M. Guerrero[a,*], Joan A. Mayugo[a], Josep Costa[a], Albert Turon[a]

[a] *AMADE, Polytechnic School, Universitat de Girona, Campus Montilivi s/n, E-17003 Girona, Spain*

Abstract

This paper presents a three-dimensional Progressive Failure Model based on the chain of bundles able to represent the stiffness loss in unidirectional composite materials loaded in the fibre direction. A representative volume element with a random distribution of fibres with their own radius is considered. Complete stress distributions around fibre breaks are obtained by associating a damage variable to the loss of stress transfer capability along the ineffective length and applying local stress concentrations. The model has been validated by comparing it against the literature results and exhibits good agreement with hybrids and non-hybrid composites. The aim of this model is to simulate the tensile response of unidirectional composite systems dominated by fibre fragmentation mechanisms using a very reduced computational effort, even for larger representative volume elements, compared to micro-mechanical finite element models.

keywords: Hybrid, Polymer-matrix composites (PMCs), Computational modelling, Micro-mechanics

3.1 Introduction

Fibre Reinforced Polymers (FRP) are widely used in lightweight structures mainly thanks to their high specific strength and stiffness. However, their quasi-brittle behaviour and low toughness leads to fibre tensile failure with hardly any prior damage symptoms, thus limiting their use and applicability [1]. One potential way to solve this problem is with fibre hybridisation [3]. In a hybrid composite, two kinds of fibres with different longitudinal failure strains are

* Corresponding author
Paper published in: *Composites Part A 107 (2018) 579–591*
Doi: https://doi.org/10.1016/j.compositesa.2018.02.005

mixed. The mixture can be arranged on three different scales [3], which are also able to be combined into: i) interlayer or layer-by-layer i.e. by mixing layers of different fibres, ii) intralayer or yarn-by-yarn i.e. by mixing the fibres within the layers but not within the separate yarns, and iii) intrayarn or fibre-by-fibre i.e. by mixing the fibres completely at the yarn/tow.

A low elongation fibre (LE) has a low failure strain and a high elongation fibre (HE) has a high failure strain. Thanks to this combination, the LE failure strain in a hybrid can be larger than that in a non-hybrid composite. This phenomenon is known as the hybrid effect [33]. Moreover, with the appropriate hybridisation design, a progressive failure of fibres under tensile load can be induced leading to pseudo-ductile behaviour [16]. Currently [3], to explain the hybrid effect the scientific community outlines three main reasons: i) changes in the development of the failure, ii) thermal residual stresses and iii) dynamic effects.

Nowadays, changes in the failure propagation are assumed to be the main reason for the hybrid effect. Because of the presence of flaws, the strength of brittle fibres is not deterministic and follows a statistical distribution. When a fibre breaks, shear stresses are transferred from the fibre to the matrix. As a consequence, the broken fibre recovers its stress in a distance called the ineffective length, whereas the surrounding fibres withstand stress concentration. Eventually, the neighbouring fibres of each broken fibre fail, thus initiating several clusters of broken fibres which grow further upon loading. When one of these clusters reaches a certain size, it propagates unstably and leads to the final failure. Other phenomena, such as debonding, matrix cracking or yielding and fibre pullout, may also contribute. Notwithstanding, in a hybrid composite the differences between the elastic and geometrical properties and the failure strains can alter and delay the formation of clusters. Moreover, by reducing the quantity of LE fibres in the hybrid, LE failure strain can also be increased because of the size effects [31].

An additional and secondary cause of the hybrid effect is related to the residual stresses generated during the manufacturing process [3]. Residual stresses appear when mixing different populations of fibres with dissimilar thermal expansion coefficients, which leads to different residual stresses in each fibre population.

The third reason given for the hybrid effect is the dynamic effect in the process of tensile failure. When a fibre breaks, the elastic energy that was sustained by that fibre is released and becomes kinetic energy which dampens after some time. During this period, dynamic loads propagate through the composite and increase the probability of failure. However, in the case of a hybrid composite, the dynamic phenomena can be altered. Xing *et al.* [26] demonstrated that in a hybrid composite two out-of-phase stress waves, one for each fibre population, propagate after an LE fibre break. If both waves compensate each other, lower dynamic loads are produced, leading to larger failure strains. However, this topic has not been studied in depth and its importance remains unclear [3, 5].

In addition, the hybrid effect is also influenced somewhat by different parameters which include the relative volume fraction between both fibres, strength distribution, fibre dispersion, fibre stiffness ratios and the failure strain ratio. Other parameters, such as the matrix stiffness or debonding, have no clear influence [33]. Moreover, the specimen size effect on the hybrid effect is also unknown [15].

Over the past decades different authors have attempted to study hybrid composites under fibre tensile loading. Hayashi [23] was the first author who observed the hybrid effect in a carbon-glass layer-by-layer hybrid in an experimental test. Later, Zweben [22] extended a shear-lag model to hybrid composites to obtain the hybrid effect analytically. While Fukuda [25] improved the model further, it still has major limitations. According to Swolfs *et al.* [33], Fukuda's and Zweben's models can be used as the upper and lower bounds for predicting the hybrid effect.

Recently, Tavares *et al.* [35] presented a fibre-by-fibre micro-mechanical finite element model (FEM) simulating fibre, matrix and fibre-matrix interphase damage [206]. The results demonstrated the importance of the failure strain ratio of both fibres, the statistical strength distribution and a progressive failure between both HE and LE fibres in obtaining pseudo-ductility. However, the model requires high computational resources and is limited to simulating a small number of fibres.

Okabe *et al.* [76, 194] presented an advanced shear-lag model able to represent the fibre failure process of composite materials. The model represents the fibres

through tensile springs and the matrix through shear springs. The advantage of these types of models is that they are simpler, faster and cheaper in computational cost than FEM models are. Furthermore, they are still able to simulate the key physics involved, without being limited to only a few fibres as in the FEM approach. However, Okabe *et al.*'s model is limited to hexagonal or square packings, which do not allow hybrid composites with fibres of different radii to be studied.

Swolfs *et al.* [31, 33, 40, 41, 120] presented a strength model under the assumption of a local load sharing rule, based on the chain of bundles approach from Rosen [141], Okabe *et al.* [76, 194] and others [43, 175]. Unlike the model of Okabe *et al.*, a random fibre packing with each fibre with its own radius was considered. With their model, Swolfs *et al.* demonstrated that larger LE strength dispersions, lower number of LE fibres, higher HE fibre stiffness or larger failure strain ratios all ultimately lead to greater hybrid effects. Fibre dispersion also showed an evident impact. However, Swolfs' model [31, 33, 40, 41, 120] attempts to predict the behaviour only up to the onset of LE fibre fragmentation, because it does not capture a non-linear response attributable to fragmentation mechanisms. Thus, it is unable to predict pseudo-ductility.

In recent years, an increase in the amount of experimental work conducted concerning fibre hybridisation has also been seen. Czél and Wisnom [18] hybridised thin carbon fibre prepreg plies with standard thick plies of glass fibres. They found pseudo-ductility with specimens of one and two plies of thin carbon. However, specimens with three and four plies failed with unstable delamination. Later, Wisnom *et al.* [15] obtained similar findings. Moreover, they compared their results with a simplified version of Swolfs *et al.* [31] strength model and obtained good agreement. Yu *et al.* [17] also manufactured intermingled hybrid composites using aligned discontinuous fibres. By combining high-modulus carbon and E-glass in the hybrid, good pseudo-ductile responses were also obtained as a result of the carbon fibres fragmentation. Further to this, Jalalvand *et al.* [11] developed a new simple analytical method to predict all possible damage mode maps in unidirectional hybrid composites. By using the method as a design guideline, new hybrid specimens of a standard-thickness glass/thin-ply carbon hybrid were manufactured and tested, leading to a good pseudo-ductile response. Quite recently, Fotouhi *et al.* [12] tested quasi-isotropic

high performance thin-ply carbon/glass hybrid laminates. Pseudo-ductility was also obtained in all fibre orientations under tensile loading. Last but no least, Czél *et al.* [16] hybridised thin-ply unidirectional interlayer all carbon-epoxy composites comprising high modulus and high strength. Again, large pseudo-ductile responses were obtained.

Despite advances in the modelling and understanding of hybrid composites, there is no local load sharing model for these materials that is capable of representing the pseudo-ductile behaviour within a random distribution of fibres. At the moment, the exception to this are the micro-mechanics FEM models which require huge computational resources and so are unsuitable as a design tool or to perform parametric studies.

In the present work, the authors propose a new three-dimensional Progressive Failure Model, (called here PFM) based on the chain of bundles which is able to accurately represent both progressive damage and pseudo-ductile behaviour in unidirectional composites. The proposed model implicitly allows fibre fragmentation mechanisms to be captured, thus estimating multiple breaks along the length of the fibre. A random distribution of fibres of a given radius is considered. The methodology leads to different deformations along the model, using the hypothesis that fibres work in parallel but taking into account the local stress fields around each fibre break. The complete stress distribution around the fibre breaks is obtained through two dependent approaches. Firstly, a damage variable related to fibre breaks and to a shear-lag model is computed. Secondly, local stress concentrations are applied through all stress recoveries. Thermal residual stresses and dynamic loads are omitted but the model framework allows for its future implementation. The remainder of this paper is as follows: firstly, we present the model, which we then validate by comparing it with the literature results, and finally some conclusions are drawn.

3.2 Chain of bundles progressive failure model

3.2.1 Definition of the fibre random distributed RVE

A representative volume element (RVE) with a random distribution of fibres is generated to capture the interaction between the fibres and the matrix. The RVE represents, on a micro-mechanical scale, a portion of a real material model

containing the matrix and a sufficient number of fibres. According to Trias *et al.* [122] and Zangernberg *et al.* [123], the minimum transversal size of the RVE in an elastic model should be 50 times the fibre radius ($50 \times R_f$). However, in a model with damage, the minimum size of the RVE could be even larger to capture the fibre effects. Similarly, the RVE length in the fibre longitudinal direction should be long enough to ensure that the ineffective length will be well captured. Some studies employed RVEs with a length of between $15 \times R_f$ and $40 \times R_f$ [35, 68]. However, an RVE using these length values does not ensure a good prediction of the fibre fragmentation. A congruent RVE length depends on the fibre and matrix elastic properties as well the ineffective and debonding lengths. Thus, RVEs length with an order of magnitude equal to several times the ineffective length should be used [31, 41]. Furthermore, size effects may occur. Therefore, the RVE must be big enough to capture the micro-mechanisms of the damage, the stress redistribution around the broken fibres during the failure process, and the clusters of fibre breaks on the different planes.

The model proposed considers an RVE that contains a certain number of parallel fibres randomly allocated, with a total length L, height a, and width b. All the fibres are divided into elements of constant length l. This leads to a domain consisting of a number of *fibres* working in parallel and divided into different *planes* working in series, also known as chain of bundles [141]. The RVE may represent a hybrid, where each fibre has its own radius and properties, or a non-hybrid composite. Each fibre element is noted by the sub-indices (p,q), where p is the plane identity ranging from 1 to N_p, with N_p being the total number of planes, and q is the fibre identity ranging from 1 to N_q, with N_q being the total number of fibres. The matrix is not really represented, but it is accounted for by means of its stiffness and a shear-lag model. Fibres at the outskirts of the RVE are cut and symmetric so that the geometry obtained is completely periodic. This schema is illustrated in Fig. 3.1. The random distribution of fibres is generated using the formulation of Melro *et al.* [124], and extended to hybrid composites by Tavares *et al.* [35].

Because of the strength scatter of the fibres, each fibre element has a different tensile strength, $\sigma^u_{p,q}$. To do this, a random number between 0 and 1 is applied to all elements, $P_{p,q}$. Then, the strength $\sigma^u_{p,q}$ of each element is obtained according to a statistical distribution, the element length l and $P_{p,q}$. Any statistical

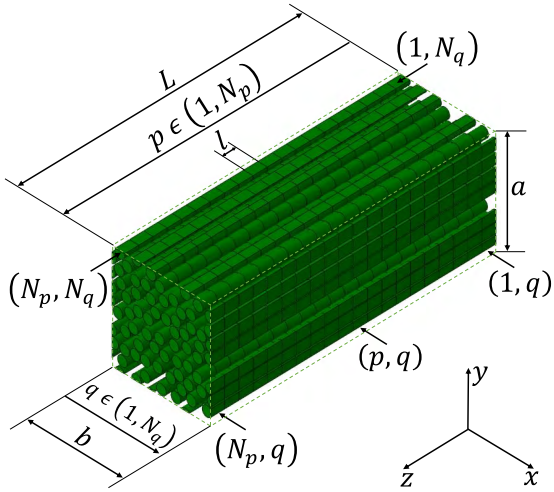

Figure 3.1: Schema of the RVE for the Progressive Failure Model. The enumeration of the planes is sorted from 1 to N_p, with plane 1 always being the plane to the extreme right and plane N_p to the extreme left. Fibre numeration is random from 1 to N_q.

distribution could be adopted and implemented in the proposed model. In the literature, the Weibull distribution [103] is most commonly used to represent fibre strength, although other variants such as the bimodal and the power-law accelerated Weibull distribution are also employed [104, 112].

3.2.2 Constitutive equation

The model assumes the complete stress distribution on the RVE in two dependent ways. On the one hand, when a fibre breaks, shear-lag stresses are transferred between the fibre and the matrix, which can lead to debonding, matrix cracking, yielding, or a combination of these [76, 149, 227]. Consequently, an ineffective length appears so that the stress in the fibre is recovered. A shear-lag model is used to obtain the ineffective length of a broken fibre element. According to Xia *et al.* [237], shear-lag models are accurate in polymer matrix composites if the fibre stiffness is much larger than the matrix, the matrix yields and the fibre volume fraction is relatively high. Assuming that the loss of stress transfer capability produces a reduction in local effective stiffness, the shear-lag model is implemented by simply updating the damage variable of all the elements inside the ineffective length of the broken fibre. On the other hand, local Stress Concentration Factors (*SCF*) are applied through all stress recoveries, so that the neighbouring fibres to a break are locally overloaded, increasing their failure

probability. Therefore, the (SCF) is assumed as a dimensionless parameter equal to 1 if the fibre element is not affected by any break, or higher than 1 if it is affected by breaks. In the literature, the $SCF_{p,q}$ is measured as the ratio between the real local fibre stress, $\sigma_{p,q}$, and the fibre far field stress, $\sigma^{\infty}_{p,q}$, where the stress is not influenced by the damage, fibre breaks or stress concentration

$$\sigma_{p,q} = SCF_{p,q}\sigma^{\infty}_{p,q} \tag{3.1}$$

In this work, the main hypothesis is that all fibre elements in each plane work in parallel, while all planes work in series. This means that all fibre elements in the plane undergo the same deformation, ε_p, (evaluated in Section 3.2.4). As damage is different on each plane, a different deformation is obtained along the model. Therefore, the effective stress is given by relating the effective Young's modulus and the deformation of the plane

$$\tilde{\sigma}_{p,q} = E_q\,(1 - D_{p,q})\,\varepsilon_p \tag{3.2}$$

where E_q is the Young's modulus of fibre q and $D_{p,q}$ is the state damage variable on element p,q. Therefore, the effective stress, $\tilde{\sigma}_{p,q}$, depends on the stiffness and damage distribution: the plane stiffness -by ε_p-, and the element stiffness -directly by $D_{p,q}$-, but it does not take into account the stress concentration.

To obtain the real fibre stress, $\sigma_{p,q}$, it is necessary to relate the effective stress $\tilde{\sigma}_{p,q}$, and the far-field stress, $\sigma^{\infty}_{p,q}$, that appear in the definition of $SCF_{p,q}$. To do that, a stress ratio, Ω_p, is defined

$$\Omega_p = \frac{\tilde{\sigma}_{p,q}}{\sigma^{\infty}_{p,q}} \tag{3.3}$$

The stress ratio associated to each plane p is evaluated according to the plane level equilibrium condition explained in Section 3.2.4. By putting together Eqs. (3.1)–(3.3), the constitutive equation of a fibre element relates the real local longitudinal fibre stress with the longitudinal plane strain

$$\sigma_{p,q} = \frac{SCF_{p,q}}{\Omega_p} E_q\,(1 - D_{p,q})\,\varepsilon_p \tag{3.4}$$

When the element's tensile stress $\sigma_{p,q}$ exceeds its strength $\sigma^{\mathrm{u}}_{p,q}$, the element fails and its damage variable $D_{p,q}$ is set equal to 1. This causes an ineffective length in the broken fibre which is represented as damage in all the elements inside the

ineffective length. Therefore, damage is equal to 0 for a pristine fibre element, equal to 1 for a broken fibre element, or between 0 and 1 for a fibre element that is influenced by the ineffective length predicted by a shear-lag model. In the following, how to evaluate $D_{p,q}$ and $SCF_{p,q}$ is explained.

The PFM is able to use any model to predict the ineffective length. In this work, the widely used Kelly-Tyson [149] shear-lag model is adopted, which assumes a perfectly plastic matrix leading to a linear stress recovery. Therefore, the ineffective length $L^{\text{in}}_{p,q}$ of a broken fibre is given by

$$L^{\text{in}}_{p,q} = \frac{E_q R_q}{2\tau_q}\varepsilon_p \tag{3.5}$$

where τ_q is the shear yield strength of the matrix for fibre q and R_q is the radius of fibre q. Note that both can be different for each fibre population in the case of a hybrid composite. The Kelly-Tyson model leads to different ineffective lengths depending on the elastic and geometrical properties and increases with the strain as the load is incremented.

As previously outlined, the damage variable, (calculated assuming the loss of stress transfer capability in the ineffective length), produces a reduction of local effective stiffness. Thus, a gradual decrease of damage from 1 at the position of the break, to 0 at both ends of the ineffective length (see Fig. 3.2a and Fig. 3.2b) is applied. As fibres may fail many times along their length, different ineffective lengths may overlap. Then, the highest damage always prevails for each element inside overlapping stress recoveries. Another potential case is an element failure located close to the boundaries of the model. In that case, the ineffective length is not fully recovered, (see Fig. 3.2c). According to these hypotheses, an element p,q is affected by each break in the fibre q at each plane i with

$$D_{p,q} = \begin{cases} \max\left(\dfrac{L^{\text{in}}_{i,q} - |i-p|\,l}{L^{\text{in}}_{i,q}}\right) & \forall i : (D_{i,q} = 1) \cup \left(|i-p|\,l < L^{\text{in}}_{i,q}\right) \\ 0 & \text{otherwise.} \end{cases} \tag{3.6}$$

In general, according to the literature [68, 251, 252], the SCF of an affected fibre element (p,q) around a broken element (i,j) can be predicted with two interacting functions: one which depends on the radial distance between both

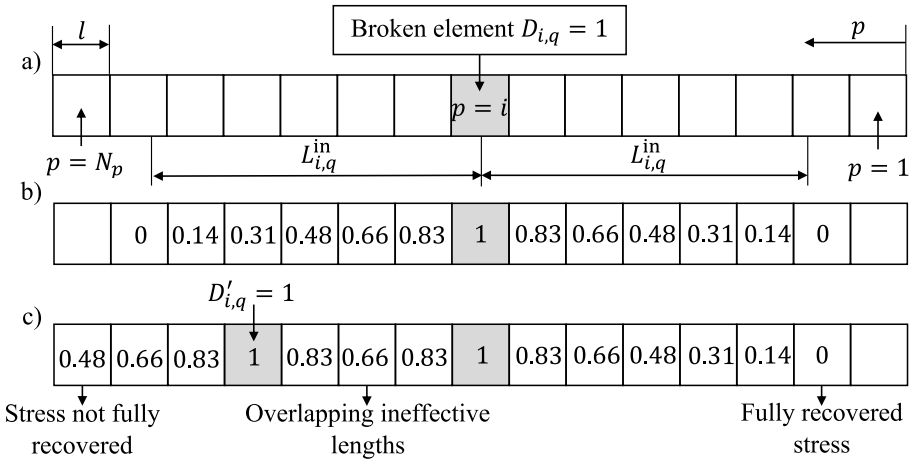

Figure 3.2: a) Schema of the ineffective length around a broken element, b) resultant damage distribution, c) overlapping ineffective lengths and not fully-recovered stresses in a fibre with two breaks.

fibres, $\delta_{(q-j)}$, and the other which depends on the plane position along the ineffective length, $\lambda_{(p-i)}$. A schematic example of the *SCF* for a fibre around a broken one is shown in Fig. 3.3. The interaction functions $\delta_{(q-j)}$ and $\lambda_{(p-i)}$ can be parametrised with computational micro-mechanics studies (for example the work of Swolfs *et al.* [40, 41, 45, 68]), or can be formulated with analytical approaches (such as the Zhou and Wagner [251], and Eitan and Wagner [252] models). The corresponding functions are shown in Table 3.1.

It should be highlighted that in order to simplify the model, the widely used Kelly-Tyson shear-lag model was adopted to predict the ineffective length. Nonetheless, the *SCF* models of Eitan and Wagner and Zhou and Wagner are based on Cox's shear-lag model [227, 252] and Nayfeh's shear-lag model [251] respectively. This means that the *SCFs* are calculated using a different physical principle than the ineffective length. Nevertheless, we assume it is a reasonable approach considering the complexity involved in the process of fibre breakage. In any case, the functions to predict the *SCF* and the ineffective length are an 'exchangeable part' in the proposed Progressive Failure Model. Thus, any another model to predict the *SCF* or the ineffective length could be used instead.

Whenever different broken fibres are present, the *SCF* of an affected fibre (p,q) is obtained by assuming a linear superposition of the contribution given by all the breaks on the fibres. However, the *SCF* is bounded by the limitation of

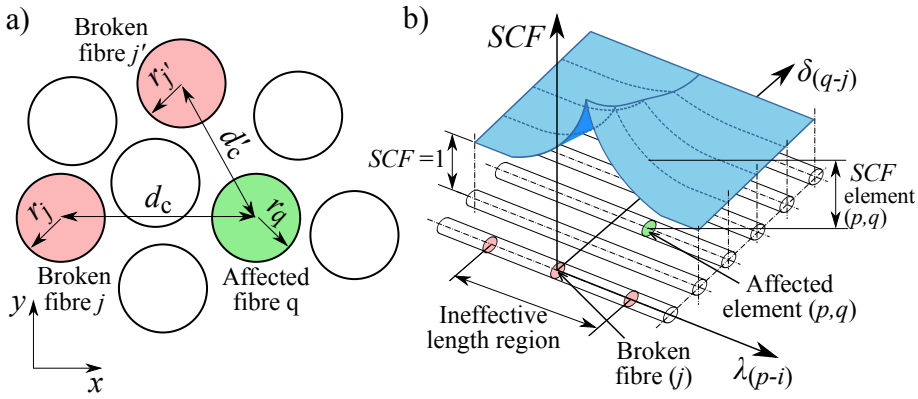

Figure 3.3: a) In-plane separation between broken and affected fibre, b) stress concentration schema for intact fibres around a broken fibre depending on the in-plane distance and the position along the ineffective length.

transfering load to the fibre by shear-lag. On the one hand, the elements inside any ineffective length (elements where $0 < D_{p,q} < 1$) have their stress limited by the shear-lag model. Therefore, only intact fibre elements ($D_{p,q} = 0$) can be over loaded by the *SCF*. On the other hand, another important related fact is to secure the stress continuity at the end of an ineffective length of a broken fibre. In the last element in the ineffective length region, no *SCF* is applied, but the subsequent elements can cover part of the *SCF*. To achieve this continuity, *SCF* is limited in the elements close to ineffective length regions also in accordance with the shear-lag limitation over load transfer to the fibre. Thus, the $SCF_{p,q}$ expressed in a general form is

$$SCF_{p,q} = \begin{cases} \min\left(SCF^{0}_{p,q}, SCF^{\mathrm{L}}_{p,q}\right) & \forall p,q : D_{p,q} = 0 \\ 1 & \text{otherwise,} \end{cases} \tag{3.7}$$

where $SCF^{0}_{p,q}$ is the *SCF* predicted by the linear superposition of the contribution of all the fibre breaks using the interacting functions as

$$SCF^{0}_{p,q} = 1 + \sum_{i=1}^{N_\mathrm{p}} \sum_{j=1}^{N_\mathrm{q}} \delta_{(q-j)}\, \lambda_{(p-i)}\, [D_{i,j} = 1] \tag{3.8}$$

where here $[\bullet]$ are the Iverson brackets and define 1 if $\bullet$ is true, and 0 if it is false. $SCF^{\mathrm{L}}_{p,q}$ is the *SCF* limit according to the shear-lag capacity to transfer load to the fibre, and is calculated as the slope defined by the stress gradient of

Table 3.1: Functions to obtain the stress concentration factor according to three different models. (*) Swolfs *et al.* [41] function along the ineffective length has been assumed. (**) Zhou and Wagner [251] provided equations for debonding and non-debonding regions. Here, only non-debonding regions are considered.

SCF model	Functions: radial distance $\delta_{(q-j)}$ and ineffective length $\lambda_{(p-i)}$
Swolfs *et al.* [41] (*)	$\delta_{(q-j)} = -P_1 \ln\left(\frac{d^{\mathrm{c}}_{q-j} - (R_j + R_q)}{R_j}\right) + P_2$ where P_1 and P_2 are two constants from a micro-mechanic model and d^{c}_{q-j} is the centre-to-centre distance between fibres q and j $\lambda_{(p-i)} = \frac{L^{\mathrm{in}}_{i,j} - l\,\lvert i-p\rvert}{L^{\mathrm{in}}_{i,j}} \quad \forall (i,j) : l\,\lvert i-p\rvert < L^{\mathrm{in}}_{i,j}$
Eitan and Wagner [252]	$\delta_{(q-j)} = \frac{\varphi_j}{\pi}$ where $\varphi_j = \arcsin\left(R_j / d^{\mathrm{c}}_{q-j}\right)$ $\lambda_{(p-i)} = \frac{\sinh \beta^{\mathrm{c}}_{(q-j)} \left(L^{\mathrm{in}}_{i,j} - l\,\lvert i-p\rvert\right)}{\sinh \beta^{\mathrm{c}}_{(q-j)} L^{\mathrm{in}}_{i,j}} \quad \forall (i,j) : l\,\lvert i-p\rvert < L^{\mathrm{in}}_{i,j}$ where $\beta^{\mathrm{c}}_{(q-j)}$ is Cox's [227] shear-lag parameter: $\beta^{\mathrm{c}}_{(q-j)} = \frac{1}{R_j}\sqrt{\frac{2G_{\mathrm{m}}}{E_j \ln \frac{0.5 d^{\mathrm{c}}_{q-j}}{R_j}}}$ where G_{m} is the matrix shear modulus.
Zhou and Wagner [251] (**)	$\delta_{(q-j)} = \left(1 - \frac{\mu l}{R_j}\right)\frac{2\varphi_j}{\pi}$ where μ is a friction coefficient $\lambda_{(p-i)} = \frac{\sinh \beta^{\mathrm{N}}_j \left(L^{\mathrm{in}}_{i,j} + 0.5l - l\,\lvert i-p\rvert\right)}{\sinh \beta^{\mathrm{N}}_j L^{\mathrm{in}}_{i,j}} \quad \forall (i,j) : l\,\lvert i-p\rvert < L^{\mathrm{in}}_{i,j}$ where β^{N}_j is Nayfeh's shear-lag parameter, as given in [251]: $\left(\beta^{\mathrm{N}}_j\right)^2 = \frac{2}{R_j^2 E_j E_{\mathrm{m}}}\left(\frac{E_j \frac{R_j^2}{R_{\mathrm{m}}^2} + E_{\mathrm{m}}\left(1 - \frac{R_j^2}{R_{\mathrm{m}}^2}\right)}{\frac{1}{4G_j}\left(1 - \frac{R_j^2}{R_{\mathrm{m}}^2}\right) + \frac{1}{2G_{\mathrm{m}}}\left(\frac{R_{\mathrm{m}}^2}{R_{\mathrm{m}}^2 - R_j^2}\ln\left(\frac{R_{\mathrm{m}}^2}{R_j^2}\right) - \frac{1}{2}\left(3 - \frac{R_j^2}{R_{\mathrm{m}}^2}\right)\right)}\right)$ where G_j and R_{m} are the broken fibre shear modulus and the radius of the shear-carrying matrix cylinder

the nearest ineffective length:

$$SCF^{\mathrm{L}}_{p,q} = \min\left(\frac{1}{L^{\mathrm{in}}_{i,q}}\,\lvert i-p\rvert\, l\right) \quad \forall i : D_{i,q} = 1 \tag{3.9}$$

The constitutive equation presented here allows the fibre fragmentation mechanism to be captured by means of the fibre breaks and its associated damage variable. The redistribution of stress using the shear-lag model permits several

breaks along the length of any fibre. However, other mechanisms, such as delamination, are ignored by the model. Nonetheless, neglecting delamination is an acceptable assumption in the failure prediction of non-hybrids and of an intrayarn hybrid, where the different fibre populations are mixed at the fibre level. In other hybrid configurations, such as an interlayer hybrid where the different fibres are located in different layers, delamination should be considered.

3.2.3 Element stiffness, plane stiffness and global RVE stiffness

As previously mentioned, the proposed methodology leads to different elongations through the domain, causing a dissimilar strain for each plane ε_p. The approach proposed is to compute the strains of each plane according to the element's stiffness and the initial hypothesis that fibres work in parallel and planes in series.

The progressive failure is formulated using the stiffness damage of each fibre element, $D_{p,q}$. To do so, Hooke's law of an element under tensile stress defines the longitudinal stiffness of a single fibre element, $k_{p,q}$, with

$$k_{p,q} = E_q \left(1 - D_{p,q}\right) \frac{A_q}{l} \tag{3.10}$$

where A_q is the cross-sectional area of fibre q given by $A_q = s_q\prime\, \pi R_q^2$, and where $s_q\prime$ is a factor which guarantees the appropriate area of not entire fibres on the domain will be considered ($s_q\prime = 1$ for entire fibres and $s_q\prime < 1$ for fibres located at the corners, or the outskirts of the RVE).

The total stiffness of each plane can be obtained by assuming that all fibre elements in the plane and the matrix stiffness work in parallel

$$k_p = \sum_{q=1}^{N_\mathrm{q}} k_{p,q} + E_\mathrm{m} \frac{A_\mathrm{m}}{l} \tag{3.11}$$

where the matrix behaviour is assumed to be linear elastic, with E_m being the matrix Young's modulus, and A_m the matrix cross-sectional area of the RVE, $A_\mathrm{m} = a\, b - \sum_{q=1}^{N_\mathrm{q}} A_q$.

Similarly, the total stiffness is calculated by assuming that all planes work in

series

$$K = \left(\sum_{p=1}^{N_\mathrm{p}} \frac{1}{k_p} \right)^{-1} \tag{3.12}$$

3.2.4 External and internal equilibrium

Because of mechanical equilibrium, the internal force of each plane, F_p, must be equal to the total external force, F, sustained by the system so that $F = F_p$. The total external force can be found by relating the current total stiffness, K, and the global longitudinal homogenised strain, ε^0, given in Section 3.2.6. Similarly, the force of each plane can also be obtained by relating the plane stiffness and the strain of the plane leading to

$$F = F_p \qquad K\,\varepsilon^0\,L = k_p\,\varepsilon_p\,l \tag{3.13}$$

Therefore, ε_p is obtained as a function of ε^0 with

$$\varepsilon_p = \frac{K\,L}{k_p\,l}\varepsilon^0 \tag{3.14}$$

To maintain local load equilibrium, the aggregation of the loads of the fibres and the matrix, must be equal to the load of the plane, therefore

$$F_p = k_p\,\varepsilon_p\,l = \sum_{q=1}^{N_\mathrm{q}} \sigma_{p,q} A_q + \varepsilon_p E_\mathrm{m} A_\mathrm{m} \tag{3.15}$$

By substituting Eq. (3.4) in (3.15), and re-organizing, Ω_p can be found as

$$\Omega_p = \frac{\sum_{q=1}^{N_\mathrm{q}} SCF_{p,q} E_q\,(1 - D_{p,q})\,A_q}{k_p\,l - E_\mathrm{m} A_\mathrm{m}} \tag{3.16}$$

where Ω_p as result of a plane level equilibrium becomes constant to all fibre elements in plane p. An additional formulation of Ω_p is obtained by substituting (3.11) in (3.16) leading to

$$\Omega_p = \frac{\sum_{q=1}^{N_\mathrm{q}} SCF_{p,q} E_q\,(1 - D_{p,q})\,A_q}{\sum_{q=1}^{N_\mathrm{q}} E_q\,(1 - D_{p,q})\,A_q} \tag{3.17}$$

Once Ω_p has been evaluated, all $\sigma_{p,q}$ can be calculated from Eq. (3.4) and compared with their strength $\sigma^\mathrm{u}_{p,q}$. It is worth mentioning that small deformations

are assumed. Thus, the element length l, total RVE length L and cross-sectional areas A_q, A_m remain constant.

3.2.5 Composite homogenised stress and break density

The homogenised composite stress is obtained as an average of both element stresses and matrix stress, weighed by their volume fraction. For a non-hybrid, this leads to

$$\sigma^0 = \frac{V_\mathrm{f}}{N_\mathrm{p} N_\mathrm{q}} \sum_{p=1}^{N_\mathrm{p}} \sum_{q=1}^{N_\mathrm{q}} \sigma_{p,q} + \frac{1 - V_\mathrm{f}}{N_\mathrm{p}} \sum_{p=1}^{N_\mathrm{p}} E_\mathrm{m} \varepsilon_p \tag{3.18}$$

where V_f is the total fibre volume fraction.

For a hybrid composite, the average of the fibre stress must be calculated independently for each fibre type to capture the differences in the cross-sectional area

$$\sigma^0 = \frac{V_\mathrm{f1}}{N_\mathrm{p} N_1} \sum_{p=1}^{N_\mathrm{p}} \sum_{q \in \mathrm{f1}} \sigma_{p,q} + \frac{V_\mathrm{f2}}{N_\mathrm{p} N_2} \sum_{p=1}^{N_\mathrm{p}} \sum_{q \in \mathrm{f2}} \sigma_{p,q} + \frac{1 - V_\mathrm{f1} - V_\mathrm{f2}}{N_\mathrm{p}} \sum_{p=1}^{N_\mathrm{p}} E_\mathrm{m} \varepsilon_p \tag{3.19}$$

where V_f1 and V_f2 are the relative fibre volume fractions of each fibre population in the case of a hybrid, and N_1 and N_2 are the number of fibres in populations f1 and f2, respectively.

The break density is calculated by dividing the number of broken elements into the total RVE volume as

$$\rho_\mathrm{b} = \frac{1}{a\, b\, L} \sum_{p=1}^{N_\mathrm{p}} \sum_{q=1}^{N_\mathrm{q}} [D_{p,q} = 1] \tag{3.20}$$

where $[\bullet]$ is the Iverson bracket. In the case of a hybrid composite, the break density of each population can also be calculated with the respective number of broken elements.

3.2.6 Algorithm procedure

A controlled monotonic increment of longitudinal displacement is performed along z direction to guarantee a stable tensile damage process. Hence, each new loading step t starts by increasing the current longitudinal displacement applied,

$(u)_t$, with

$$(u)_t = (u)_{t-1} + (\Delta u)_t \tag{3.21}$$

where $(u)_{t-1}$ is the displacement from the previous step, and $(\Delta u)_t$ is the displacement increment. In each load step, the longitudinal displacement and the global longitudinal homogenised strain, ε^0, assuming a uni-axial behaviour, are both related by the total length of the model with

$$\left(\varepsilon^0\right)_t = \frac{(u)_t}{L} \tag{3.22}$$

Following this, the stiffness, forces, strains and Ω_p are first estimated with the damage variable and the *SCF* from the previous step with Eqs. (3.10)–(3.12), (3.14) and (3.17). Note that, in the first step $t = 1$, all damage variables $D_{p,q}$ are equal to zero, and all $SCF_{p,q}$ are equal to one. If there are broken elements, then the ineffective length, damage variable and the *SCF* are calculated with the estimated stiffness, forces, strains and Ω_p using Eqs. (3.5)–(3.7). As the damage has changed, the stiffness, forces, strains and Ω_p are re-calculated to obtain the true actual current magnitudes. Next, the element stresses are computed with Eq. (3.4). If no elements break, the composite stress and break densities are evaluated with Eqs. (3.18)–(3.20). If new elements fail, the damage $D_{p,q}$ of all new broken elements is set equal to 1 and the same procedure is repeated without increasing the applied displacement and with the current damage and latest calculated *SCF*, until no more failures happen in the current step. When no new elements fail, a new step is started by updating $(u)_t$ and $\left(\varepsilon^0\right)_t$ with Eqs. (3.21) and (3.22). This procedure is shown in the flowchart in Fig. 3.4. The model stops when either all elements in a plane are damaged, or the composite stress has decreased by a pre-defined percentage of maximum load value. For non-hybrid composites, where a brittle failure is expected, the simulation is stopped when the stress decreases 10% from the maximum reached. In a hybrid composite, LE fibre population could fail originating a large load drop. To avoid an early end of the simulation before HE fibre failure, the calculation is stopped when the stress decreases more than 80%. The model was implemented in MatLab (The MathWorks Inc., USA) [257] and Python programming language (Python Software Foundation, https://www.python.org/). The results can be exported into ParaView (Kitware Inc., USA) [258] for visual post-processing.

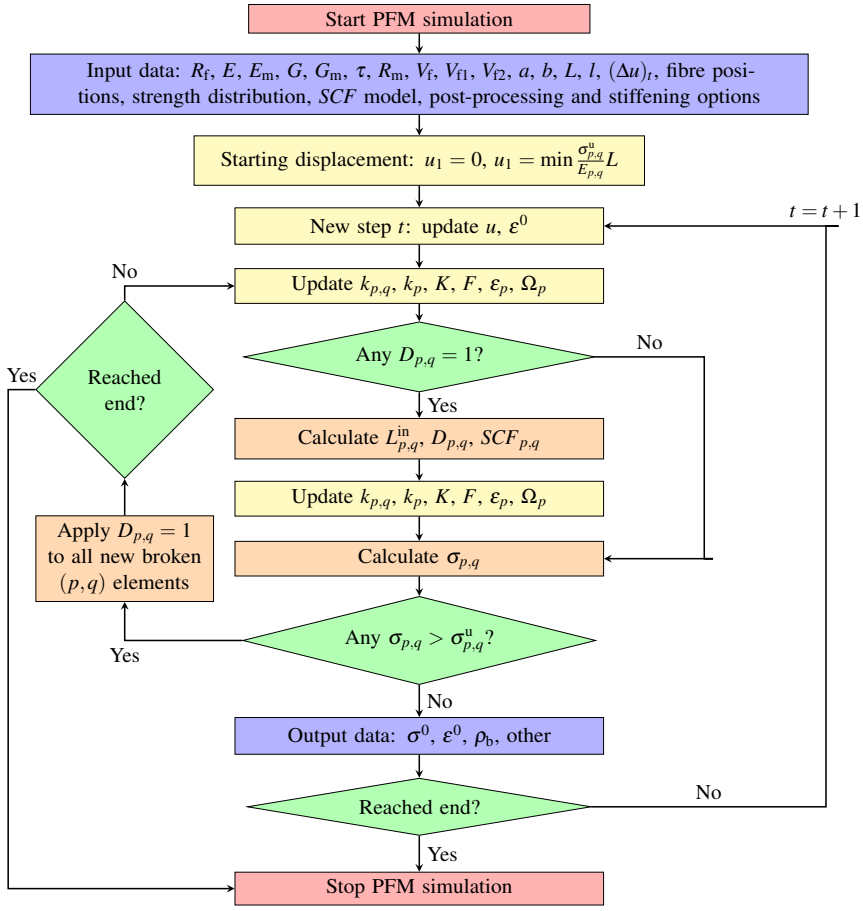

Figure 3.4: Progressive Failure Model flowchart.

3.3 Results and discussion

3.3.1 Non-hybrid UD T700S and M40 carbon fibre epoxy

Two different non-hybrid UD composites consisting of T700S-Epoxy and M40-Epoxy were simulated using the proposed PFM. The results were compared with the reported experimental data in Swolfs *et al.* [41] and Koyanagi *et al.* [153] respectively, in an attempt to validate the model. All model properties shown in Table 3.2, except the estimated matrix and *SCF* related properties, were also taken from [41] and [153]. The tensile behaviour of each composite system was performed with all three models shown in Table 3.1 to observe their impact on the final failure. The parameters P_1 and P_2 were taken to be $P_1 = 6.12$ and $P_2 = 7.74$, as in [41].

Table 3.2: UD composites and model properties.

Composite	Fibre properties			Weibull properties			Matrix properties			*SCF* properties		RVE data	
	E, E_0 [GPa]	G [GPa]	R_f [μm]	m [-]	σ_0 [MPa]	L_0 [mm]	E_m [GPa]	G_m [GPa]	τ [MPa]	R_m [μm]	μ [-]	L [mm]	V_f [%]
T700S-Epoxy	197.9	78.53	3.5	$m_1 = 4.8$ $m_2 = 12$	$\sigma_{01} = 5200$ $\sigma_{02} = 6100$	10	3.0	1.11	40	42	0.5	1.54	55
M40-Epoxy	392.0	155.55	3.0	16	4500	25	3.5	1.29	50	36	0.18	25	60
AS4 -Epoxy	234.0	92.85	3.5	10.7	4275	12.7	3.76	1.39	50	-	-	$15 \times R_f$	60
M50S	480.0	190.48	2.65	9	4600	10				-	-		

Like [41], a bimodal Weibull distribution was applied to assign the strength, $\sigma^{\mathrm{u}}_{p,q}$, to each fibre element of the T700S composite with

$$P_{p,q} = 1 - \exp\left(-\left(\frac{l}{L_0}\right)\left(\frac{\sigma^{\mathrm{u}}_{p,q}}{\sigma_{01}}\right)^{m_1} - \left(\frac{l}{L_0}\right)\left(\frac{\sigma^{\mathrm{u}}_{p,q}}{\sigma_{02}}\right)^{m_2}\right) \tag{3.23}$$

Whereas, according to [153], a traditional Weibull distribution was applied for the M40 composite using

$$P_{p,q} = 1 - \exp\left(-\frac{l}{L_0}\left(\frac{\sigma^{\mathrm{u}}_{p,q}}{\sigma_0}\right)^{m}\right) \tag{3.24}$$

where $P_{p,q}$ is a random number between 0 and 1, L_0, m, σ_0, σ_{01}, m_1, σ_{02} and m_2 are Weibull parameters and $\sigma^{\mathrm{u}}_{p,q}$ is the corresponding strength of the fibre element.

A stiffening effect was assumed for the T700S composite only, to be consistent with [41]. Hence, the Young's modulus of the fibres at a step t was given as described in Toyama and Takatsubo [259]

$$(E_q)_t = E_0 + 1000\left(4133.6\left(\varepsilon^0\right)_t - 70331\left(\varepsilon^0\right)_t^2\right) \tag{3.25}$$

The initial Young's modulus, E_0, was chosen to be consistent with [41].

The main issue in defining the model was to decide on the appropriate width, thickness and length of the RVE. These dimensions had to be as close as possible to the real specimen but still ensure that the model would be workable. To observe the influence the RVE size has on the results, RVEs of a width and thickness of $50\times R_{\mathrm{f}}$, $100\times R_{\mathrm{f}}$, $150\times R_{\mathrm{f}}$ and $200\times R_{\mathrm{f}}$ —where R_{f} is the fibre radius— were generated. Fig. 3.5 shows a cross-section view of an example of the fibre distributions obtained.

The RVE length of the T700S was 1.54 mm for all cases, which corresponded to the length of the testing coupon [41]. However, for the M40, the experimental length was 150 mm [153], which is too long to be simulated while maintaining an appropriate small element length. Thus, a first previous study was performed with the M40 composite to determine the sensitivity of the results for both the RVE length L and the element length l. The results obtained from this analysis (Fig. 3.6) suggested that an element length below $3\times R_{\mathrm{f}}$ is small enough, while an RVE length of 25 mm is acceptably long enough. Hence, the RVE length L

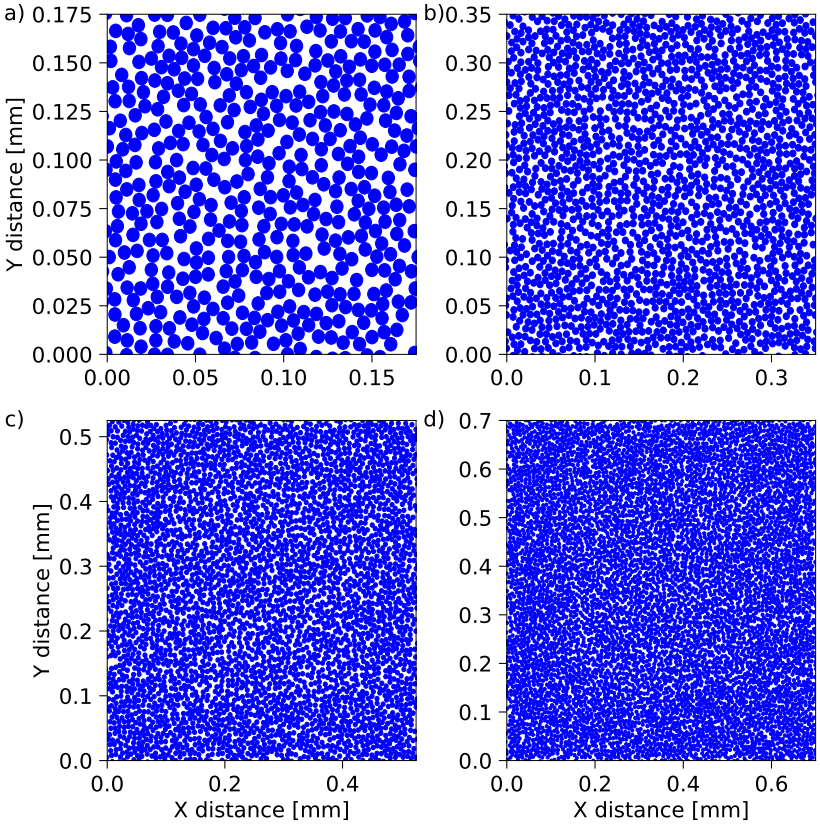

Figure 3.5: Cross-section view examples of RVEs with T700S fibre a) $50\times R_{\mathrm{f}}$, b) $100\times R_{\mathrm{f}}$, c) $150\times R_{\mathrm{f}}$, d) $200\times R_{\mathrm{f}}$.

of the M40 composite was set to 25 mm. Consequently, an element length l of 3.5×10^{-3} and 8.3×10^{-3} mm for the T700S and M40 composites, respectively, was applied. These values were taken as a compromise between accuracy and computational time.

In addition, the variability in the results caused by the randomness of fibre position and fibre strengths had to be considered. Thus, all simulations of each size and *SCF* model were solved 40 times with different fibre distributions, leading to a total of 480 simulations for each composite.

Considering all the inevitable inaccuracies in the modelling assumptions and in the input data, the predicted ultimate strain and strength presented remarkable agreement with the given experimental data for both the T700S and M40 composites, especially for the largest RVE sizes. For the T700S composite, the proposed PFM predicted in the largest RVE, a mean failure strain of 2.14% with

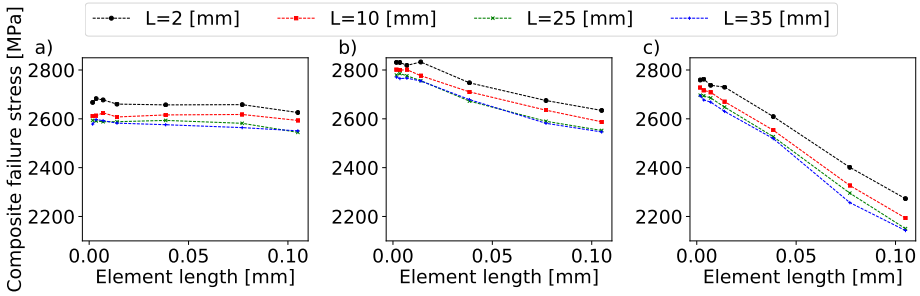

Figure 3.6: Influence of the total RVE length (L) and element length (l) on the failure strength for the M40 composite. The mean result for 20 simulations is shown. The RVE width and thickness were $50 \times R_f$. a) Using the Swolfs *et al.* *SCF* model, b) using the Eitan and Wagner *SCF* model, and c) using the Zhou and Wagner *SCF* model.

the Swolfs *SCF* model, and of 2.07%, using the Eitan *SCF* and the Zhou *SCF* models which over-predict the experimental result of 1.89%, but are close to the 2.17% prediction of Swolfs' strength model [41]. Similarly, for the M40 composite the models predicted a mean failure strength between 2511 MPa and 2572 MPa, albeit with a small over-prediction of 2310 MPa for the experimental one as well.

The obtained failure strain and stress decreased as the RVE cross-sectional size increased; which is coherent with the size effect. These findings suggest that an RVE with a width and thickness size of $50 \times R_f$ (adequate for elastic predictions according to [122, 123]) is not enough to predict unidirectional composite failure mechanisms. The error bars within the 95% confidence intervals in Figs. 3.7 and 3.8, decrease with larger RVE sizes.

The size effect was remarkably less pronounced in the Swolfs *et al.* [41] *SCF* model. To better understand the differences between the *SCF* models implemented, a plot example of the predicted *SCF* with all models is shown in Fig. 3.9. As can be seen, the Swolfs *SCF* model predicts a much larger *SCF* at a smaller centre-to-centre distance, d^c_{q-j}, to the broken fibre. However, the *SCF* decreases much faster by increasing, d^c_{q-j}, in comparison to the other models. Therefore, the Swolfs *SCF* model is more localised than the others. This should explain why the size effect is smaller with the Swolfs model: causing *SCF* in a smaller centre-to-centre distance means that fewer fibres are needed to accurately represent stress re-distribution around fibre breaks. The Zhou and Wagner and Eitan and Wagner *SCF* models both estimate the same stress peak,

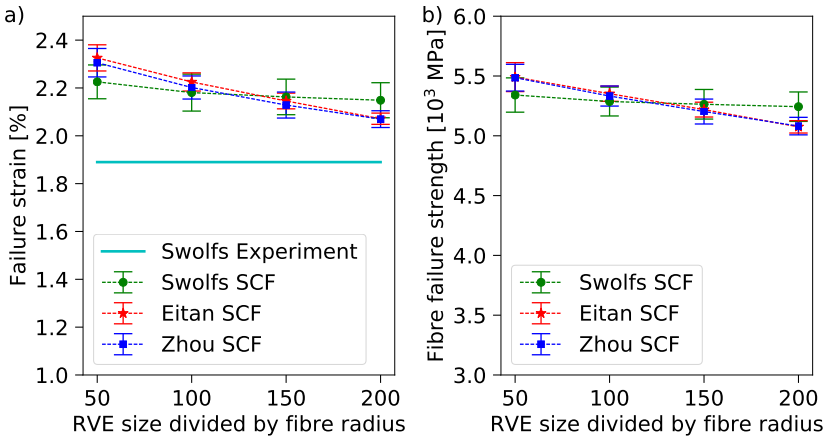

Figure 3.7: T700S error bars for 40 simulations at each simulated RVE size for each *SCF* model compared with Swolfs *et al.* [41] experimental results, a) failure strain, b) fibre failure stress.

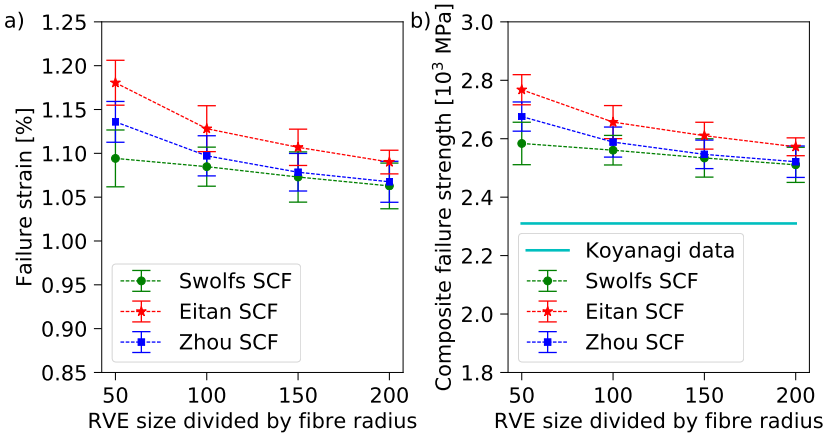

Figure 3.8: M40 error bars for 40 simulations for each simulated RVE size for each *SCF* model compared with Koyanagi *et al.* [153] experimental results, a) failure strain, b) composite failure stress.

but the *SCF* along the ineffective length is different. For the Eitan and Wagner model, the *SCF* distribution along the ineffective length is narrower and affects only a small region of the intact fibres close to the broken fibre. By increasing d^{c}_{q-j}, the *SCF* distribution along the ineffective length tends to coincide with the Zhou and Wagner model.

The cluster evolutions, with the T700S composite for each *SCF* model, are shown at different instants close to final failure in Fig. 3.10. It can be observed that groups of clusters formed with all models. These clusters increased in size

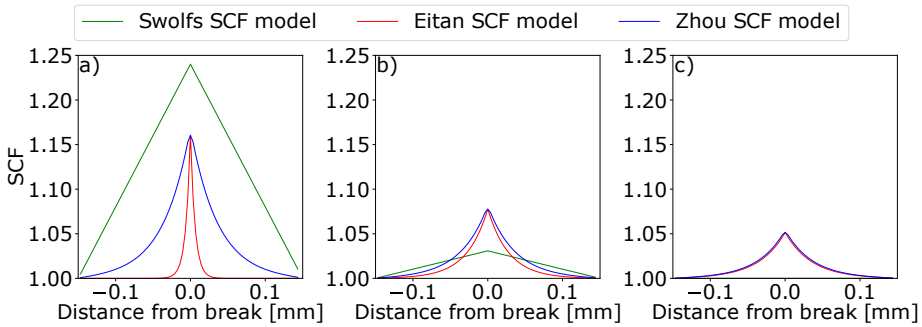

Figure 3.9: Predicted *SCF* to an intact fibre at different centre-to-centre distances, d^{c}_{q-j}, according to the Zhou and Wagner, Eitan and Wagner and Swolfs *et al.* models. a) $d^{c}_{q-j} = 2.07R_f$, b) $d^{c}_{q-j} = 4.14R_f$, c) $d^{c}_{q-j} = 6.21R_f$. The *SCF* is shown along the ineffective length of a 0.15 mm broken fibre, with all material data corresponding to the T700S fibre in Table 3.2.

as the load was incremented until a critical cluster propagated and led to final failure. Even though the same fibre strengths were used with all three *SCF* models, the failure procedure was clearly different. Not only was the failure strain different, but so too were the clusters formed at the different places in the model. Moreover, final failure, due to unstable cluster propagation, also happened at a different location.

By observing the results obtained, it is not possible to conclude if an *SCF* approach is more accurate than the others. Indeed, the results show that the *SCF* model has only a relative influence on the predicted failure. The significant difference between the *SCF* models analysed is the formulation basics and the nature of the identification parameters. The Zhou and Wagner model and the Eitan and Wagner model are formulations totally based on theoretical shear-lag assumptions. These models need a major number of parameters, which are not always simple to estimate, such as μ or R_m. However, the Swolfs *SCF* model proposes a completely different approach, by where the *SCF* is obtained by fitting results from a micro-mechanic finite element analysis using a relatively large RVE with hundreds of fibres and a long length.

Both composites presented a different failure. The T700S composite experimented some stiffness loss before final failure, whereas the M40 composite exhibited a very brittle failure, as seen in Figs. 3.11a and 3.12a. This effect is highlighted by the evolution of the break densities in Figs. 3.11b and 3.12b, as the curve of the M40 presents a more sudden degradation than that of T700S.

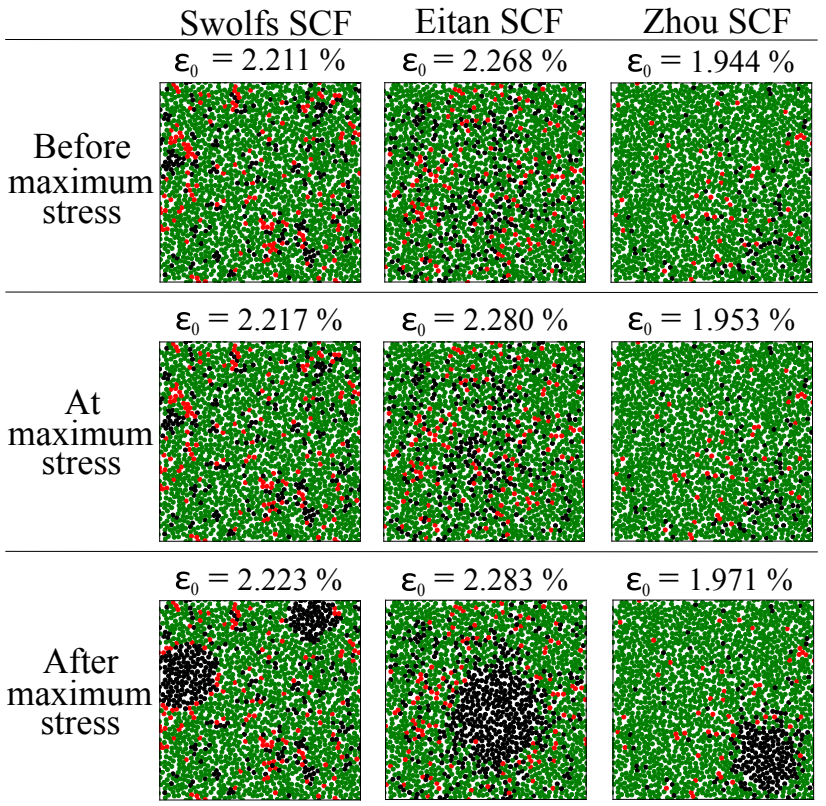

Figure 3.10: Cluster evolution at different stages during final failure within 16% of total length in each direction of the section with largest break density for the T700S composite. Broken fibres in black, damaged fibres in red and intact fibres in green. RVE size corresponds to $100 \times R_f$.

The break density of T700S was over-predicted by the model compared to the experimental results, as in Swolfs *et al.* [41], which could be the consequence of inaccuracies in the model or in the experimental data. A summary of the results obtained is presented in Table 3.3. The total computational time is also shown for each set of simulations and presented a strong exponential increase by increasing the width/thickness of the RVE. The simulations using the Swolfs *SCF* model needed smaller computational time in the PFM. However, it must be remarked that the two constants (P_1 and P_2) used by this *SCF* model are obtained from micromechanical finite element analyses which represent a considerable effort.

Table 3.3: Obtained failure strains and stress with 95% normal distribution confidence intervals for 40 realizations of each RVE size and *SCF* model. T700S failure stress corresponds to the fibre failure stress, whereas M40 corresponds to the composite failure stress. The CPU times are the mean values for each realization (simulation). Simulations were run on an Intel i7-5820K 3.3GHz processor. (*) Estimated values.

Composite	Experimental test	*SCF* model	Variable	RVE width and thickness size (R_f is the fibre radius)			
				$50\times R_f$	$100\times R_f$	$150\times R_f$	$200\times R_f$
T700S-Epoxy	1.89 % [41]	Swolfs *et al.*	Failure strain [%]	2.23 ± 0.07	2.18 ± 0.08	2.16 ± 0.07	2.15 ± 0.07
			Failure stress [MPa]	5341 ± 143	5287 ± 121	5264 ± 124	5243 ± 123
			CPU time [h:mm:ss]	0:01:28	0:06:00	0:15:10	0:34:50
	4740 MPa (*)	Eitan and Wagner	Failure strain [%]	2.33 ± 0.05	2.22 ± 0.04	2.15 ± 0.03	2.07 ± 0.02
			Failure stress [MPa]	5491 ± 121	5352 ± 64	5219 ± 62	5075 ± 52
			CPU time [h:mm:ss]	0:03:20	0:28:12	1:49:47	4:37:00
		Zhou and Wagner	Failure strain [%]	2.31 ± 0.06	2.20 ± 0.05	2.13 ± 0.05	2.07 ± 0.04
			Failure stress [MPa]	5486 ± 112	5332 ± 84	5203 ± 104	5081 ± 73
			CPU time [h:mm:ss]	0:03:14	0:25:59	1:40:16	4:59:00
M40-Epoxy	0.976 % (*)	Swolfs *et al.*	Failure strain [%]	1.09 ± 0.03	1.08 ± 0.02	1.07 ± 0.03	1.06 ± 0.03
			Failure stress [MPa]	2584 ± 73	2561 ± 51	2534 ± 66	2511 ± 60
			CPU time [h:mm:ss]	0:02:08	0:13:36	0:45:41	1:09:00
	2310 MPa [153]	Eitan and Wagner	Failure strain [%]	1.18 ± 0.03	1.13 ± 0.03	1.11 ± 0.02	1.09 ± 0.01
			Failure stress [MPa]	2768 ± 52	2657 ± 57	2610 ± 46	2572 ± 31
			CPU time [h:mm:ss]	0:03:42	0:22:43	0:42:28	2:53:00
		Zhou and Wagner	Failure strain [%]	1.14 ± 0.02	1.10 ± 0.02	1.08 ± 0.02	1.07 ± 0.02
			Failure stress [MPa]	2676 ± 50	2589 ± 51	2546 ± 49	2521 ± 54
			CPU time [h:mm:ss]	0:02:51	0:27:26	0:24:22	2:30:00

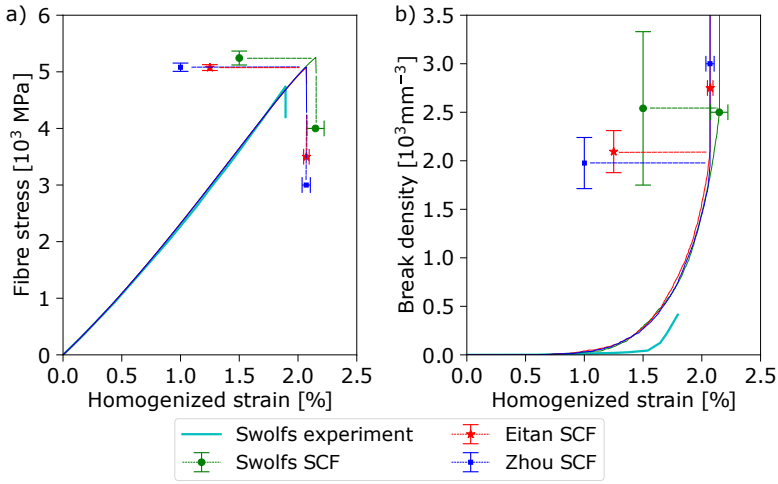

Figure 3.11: T700S closest curve to the mean from all 40 simulations with a size of $200 \times R_f$ for each *SCF* model compared against the experimental results from Swolfs *et al.* [41], a) mean stress-strain curve, b) mean break density curve.

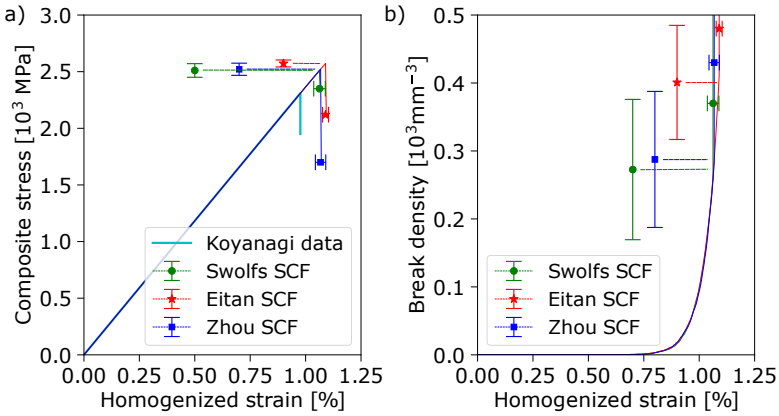

Figure 3.12: M40 closest curve to the mean from all 40 simulations of size $200 \times R_f$ for each *SCF* model compared against the experimental results from Koyanagi *et al.* [153], a) mean stress-strain curve, b) mean break density curve. The experimental stress-strain curve was assumed to be linear from the experimental strength with Young's modulus given by the rule of mixtures.

3.3.2 Hybrid UD AS4-M50S carbon fibres/epoxy

A UD intrayarn hybridisation within M50S carbon (LE fibre) and AS4 Carbon (HE fibre) with epoxy matrix was simulated at different LE relative hybrid volume fractions. All data, shown in Table 3.2, was taken from Tavares *et al.* [35]. In order to carry out a clean comparison with [35] FEM results, the

simulations were performed using the same RVE dimensions. Thus, RVEs with width, thickness and length of $15 \times R_f$ were generated, with R_f being the largest fibre radius in the RVE. It is important to remark that while such a small RVE is not big enough to properly represent the failure process accurately, it is the appropriate configuration to compare the PFM simulation with the micro-mechanical FEM results. A Weibull distribution extrapolated to the total gauge length (instead of the element length) was also used:

$$P_{p,q} = 1 - \exp\left(-\frac{L}{L_0}\left(\frac{\sigma^u_{p,q}}{\sigma_0}\right)^m\right) \tag{3.26}$$

where the element length l was set to 0.35×10^{-3} mm.

The *SCF* model used was from Swolfs *et al.* [41]. In a hybrid composite the appropriate *SCFs* profiles depend on the stiffness ratio between the broken and the intact fibre (E_j/E_q). Three combination cases are then possible: i) a broken LE fibre causing *SCF* to an HE fibre ($E_j/E_q = 2.05$), ii) a broken HE fibre causing *SCF* to an LE fibre ($E_j/E_q = 0.49$), and iii) a broken fibre (LE or HE) causing *SCF* to a fibre of the same population ($E_j/E_q = 1$). Swolfs *et al.* [45] provided the *SCF* for $E_j/E_q = 3.71$ and $E_j/E_q = 1.85$. Thus, interpolation and extrapolation was performed in between to obtain the *SCF* for $E_j/E_q = 2.05$ and $E_j/E_q = 0.49$, respectively. These profiles are shown in Fig. 3.13a. When either a broken LE fibre causes *SCF* to an intact LE, or a broken HE fibre causes *SCF* to an intact HE fibre, the profile shown in Fig. 3.13b was assumed, which was also taken from [45]. Thus, the corresponding parameters P_1 and P_2 from Table 3.1 are $P_1 = 2.982, P_2 = 3.068$ for $E_j/E_q = 3.71$, $P_1 = 1.908, P_2 = 1.975$ for $E_j/E_q = 1.85$, and $P_1 = 3.656, P_2 = 3.053$ for the *SCF* profile between fibres of the same population. Note that for the two non-hybrid cases (a 100% HE composite and a 100% LE composite), the same Swolfs *et al.* [41] *SCF* model used in Section 3.3.1 was applied. Moreover, it is worth mentioning that the stress re-distribution between fibres of the same type (Fig. 3.13b), which share the same stiffness and radius, differs from the one obtained between fibres of different type (Fig. 3.13a), with distinct stiffness and fibre radii. Therefore, the *SCF* for $E_j/E_q = 1$ does not fit in between the curves of $E_j/E_q = 0.49$ and $E_j/E_q = 1.85$.

Within each hybrid relative volume fraction modelled (see Fig. 3.14), 40 simulations were solved leading to a total of 360 simulations, with each set of

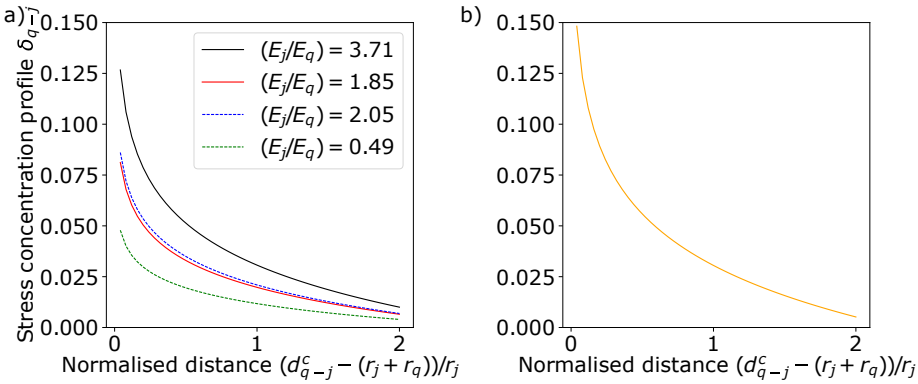

Figure 3.13: Hybrid stress concentration profiles. a) for different ratios E_j/E_q between broken and intact fibres when both fibres belong to different fibre populations, b) for the same fibre population.

40 simulations taking approximately 9 minutes to be completed. The tensile stress-strain curves obtained are shown and compared with the [35] FEM results in Fig. 3.14 at LE hybrid volume fractions of 0, 25, 50, 75 and 100%. A good agreement was obtained, which led to similar failure responses.

Pseudo-ductility was predicted at LE relative volume fractions between 10 and 30%. The other composites either failed prematurely, or the interaction between fibres was not evident enough. This failure process is highlighted in Fig. 3.15. For nearly all the hybrid configurations it is possible to observe that the LE fibre break density does not increase once a certain point is reached. That means that the LE fibre is fully fragmented and is incapable of breaking further, even when the applied load is incremented. At low LE volume fractions between 10 and 30%, the breaks of the LE fibre saturated while the HE fibre was failing, which led to pseudo-ductility until the final failure. However, at higher LE volume fractions the failure was sudden and brittle. These results demonstrate that the proposed model is able to capture fibre fragmentation, which is one of the most relevant mechanisms associated to pseudo-ductility.

The hybrid failure strain is also presented in Fig. 3.16. For LE volume fractions lower than 70%, the hybrid failure strain was considered as the corresponding strain at the second maximum in the stress-strain curve, which corresponded to the failure of the HE fibre in the hybrid. However, for larger LE volume fractions, the first maximum was considered as failure strain instead, because the drop in stress afterwards did not show any evidence of a second maximum.

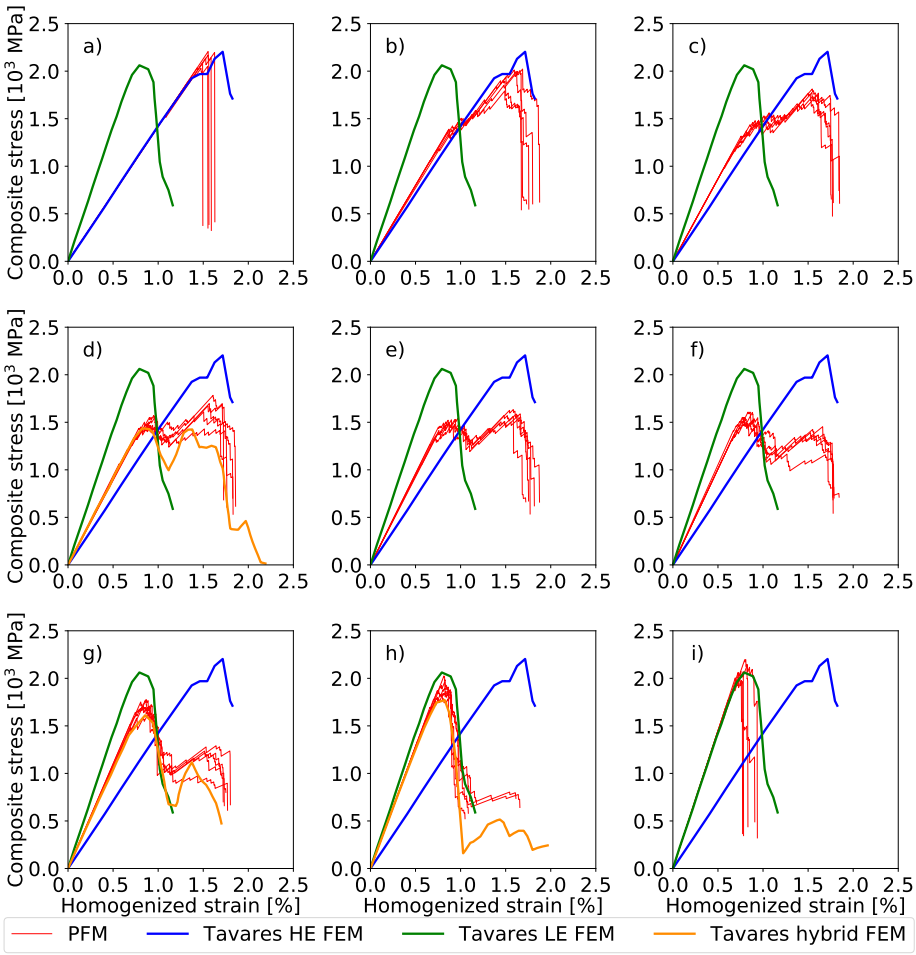

Figure 3.14: Stress-strain curves obtained for hybrid M50S-AS4 fibre compared with Tavares *et al.* [35] FEM when varying the relative LE hybrid fibre volume fraction. a) 0%LE, b) 10%LE, c) 20%LE, d) 25%LE, e) 30%LE, f) 40%LE, g) 50%LE, h) 75%LE, i) 100%LE. For the sake of readability only 5 realisations are shown.

These failure strain values correspond to the failure of the LE fibres.

The small discrepancies between PFM and FEM are attributed to the shear-lag model, the prediction of *SCF* and, in particular, the omission of dynamic phenomena. Nonetheless, the proposed model predicted similar results using a very simple model that can be run on a regular computer in a short time, whereas Tavares *et al's* [35] model requires an enormous computational effort in a high power computational facility.

Future work should try to address the problems omitted here such as matrix

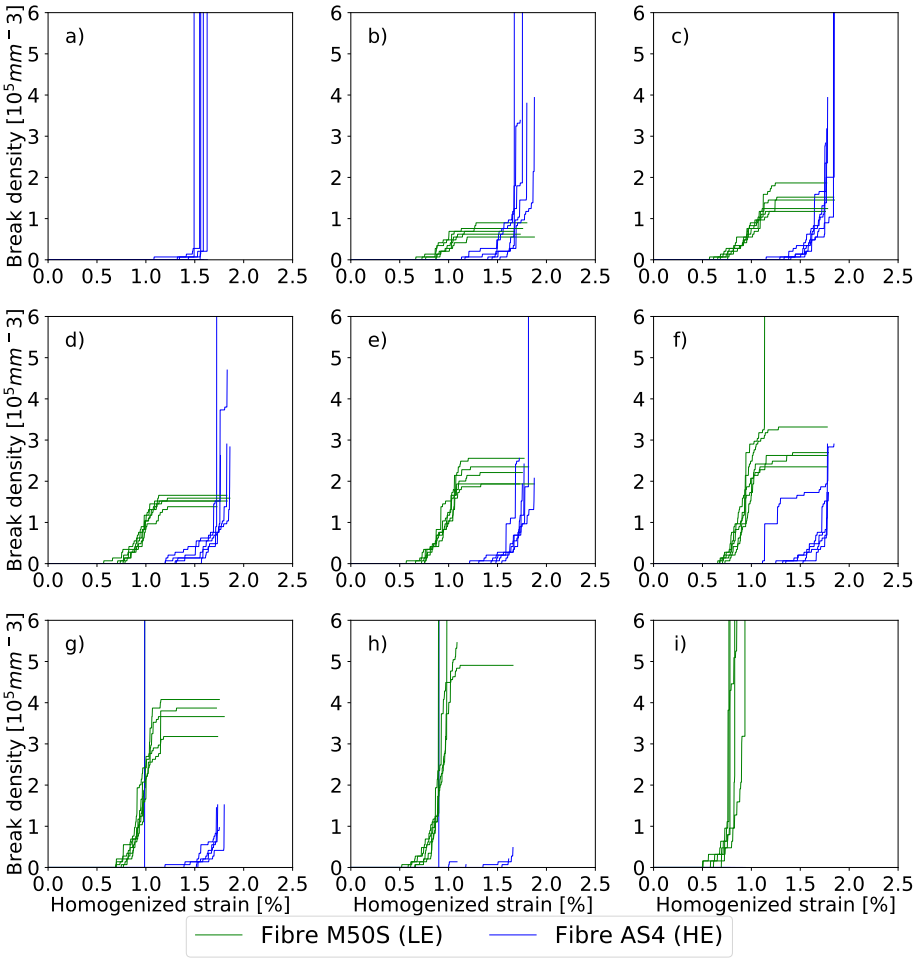

Figure 3.15: Break density-strain curves obtained for hybrid M50S-AS4 fibre composite when varying the relative hybrid fibre volume fraction. a) 0%LE, b) 10%LE, c) 20%LE, d) 25%LE, e) 30%LE, f) 40%LE, g) 50%LE, h) 75%LE, i) 100%LE. For the sake of readability only 5 realisations are shown.

damage, thermal residual stresses and dynamic effects. Further parametric studies to design hybrid configurations to maximise pseudo-ductility and the effect of unknown parameters such as the effect of debonding or the effect of the size in the hybrid effect should also be included.

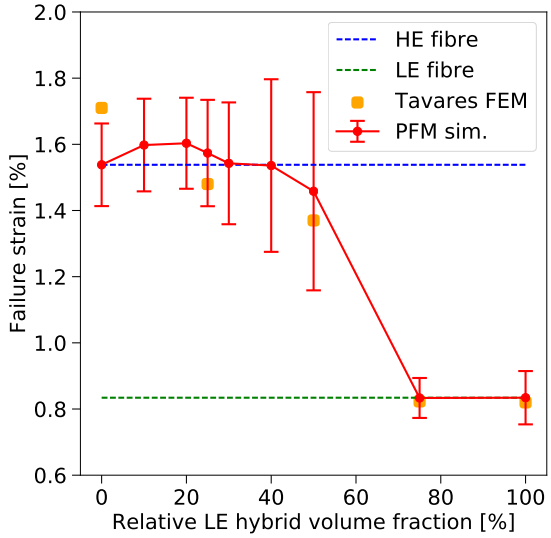

Figure 3.16: Hybrid failure strain obtained for different LE and HE relative volume fractions. The results of the simulations are compared with [35] FEM results. The error bars are shown within the 95% confidence intervals for 40 realizations.

3.4 Conclusions

A 3D progressive failure model based on the chain of bundles approach [141], was developed and validated. The model accurately represents the failure curve of unidirectional composite materials with a random distribution of fibres. A complete stress distribution is obtained by associating a damage variable to the loss of stress transfer capability along the ineffective length, which produces a reduction of local effective stiffness. Consequently, local stress concentrations are applied through all stress recoveries, so that the neighbouring fibres are locally overloaded. The method, formulated in an explicit form, leads to different deformations along the length of the model.

The model has been validated with results available in the literature. Each simulation, with different random distribution of fibres, has been repeated multiple times to evaluate the uncertainly of the results. For non-hybrids, T700S-Epoxy and M40-Epoxy UD composites were simulated and compared to results from Swolfs *et al.* [41] and Koyanagi *et al.* [153], respectively. Moreover, an RVE size with transversal dimensions larger than $200 \times R_f$ is needed to capture the size effect inherent to the failure process, which is more exigent than the required $50 \times R_f$ for elastic RVE predictions according to [122, 123]. Three *SCF*

models corresponding to the models of Swolfs *et al.* [41], Zhou and Wagner [251] and Eitan and Wagner [252] were compared and found to have a slightly different failure prediction. A significant difference between these formulations is the parameters identification method. The Zhou and Wagner model and the Eitan and Wagner model are entirely based on theoretical assumptions. They need a significant number of parameters and some of them are not easy to calculate or estimate. Meanwhile, the Swolfs *SCF* model is parametrised with a simpler set of values. The exact identification of these must be performed by a micro-mechanical finite element approach. However, all three models led to a similar failure procedure which showed a tendency to form clusters of broken fibres and which led to final failure. In any case, the Swolfs *SCF* model generates more localised stress concentration factors, leading to predictions significantly less sensitive to the size effect when compared to the other models. Finally, a hybrid carbon-carbon (M50S-AS4) epoxy composite was simulated and pseudo-ductility was obtained at LE volume fractions between 10 and 30%. The results were compared with those of Tavares *et al.* [35] micro-mechanical FEM and also obtained good agreement, but with a much faster and simpler model than the FEM is.

Acknowledgements

The authors would like to acknowledge P.P. Camanho, A.R. Melro and R.P. Tavares for their permission to use their random fibre generator. The authors acknowledge the financial support from the Spanish 'Ministerio de Ciencia e Innovación' (MINECO) under the projects MAT2015-69491-C3-1-R and TRA2015-71491-R co-financed by the European Regional Development Fund (ERDF). The first author would like to acknowledge the predoctoral Grant BES-2016-078270 from the 'Subprograma Estatal de Formación del MICINN' co-financed by the European Social Fund.

4

Paper B – An analytical model to predict stress fields around broken fibres and their effect on the longitudinal failure of hybrid composites

The paper has been published in *Composite Structures* 211 (2019) 564–576.

Overview

One of the objectives of this thesis is to develop an analytical model for predicting the stress redistribution around a cluster of broken fibres in hybrid composites, taking into account the geometrical and elastic properties of the fibres. And, derived from this, to understand the influence that the matrix behaviour (elastic or plastic), has on the load redistribution around broken fibres, as well as on the damage evolution in different hybrid composites.

Currently, some analytical models exist in the literature which are able to predict this load redistribution, but they do not take into account either the geometrical and elastic properties of the fibres or the volume fraction of each constituent [198, 251, 252]. In addition, many models consider an elastic matrix instead of a more realistic plastic matrix. However, the validity of omitting matrix yielding for simulating hybrid composites is not yet established. Thus, to predict an accurate stress redistribution around fibre breaks in hybrid composites, a new model which takes into account all relevant material properties as well as the matrix behaviour, must be developed.

In this chapter, an analytical model for predicting the stress redistribution around clusters of broken fibres is developed. The model takes into account the cluster size, RVE size, volume fractions, fibre radius and elastic properties of each fibre population in the hybrid with simple analytical equations. Moreover, it can represent different matrix behaviours or effects not directly present into the model. The analytical model is entered into the progressive failure model previously presented in Chapter 3, to predict more accurately the fibre tensile failure and cluster development in hybrid composites. The results demonstrate that the stiffness ratio between both fibres as well as the matrix behaviour considered (plastic or elastic) have a significant impact on the load redistribution around breaks. This further leads to a different damage development and failure process, being a plastic matrix more realistic compared to experimental data. The model is validated by comparing with a spring element model.

An analytical model to predict stress fields around broken fibres and their effect on the longitudinal failure of hybrid composites

Jose M. Guerrero[a,*], Rodrigo P. Tavares[a,b,c], Fermin Otero[c,d], Joan A. Mayugo[a], Josep Costa[a], Albert Turon[a], Pedro P. Camanho[b,c]

[a] *AMADE, Polytechnic School, Universitat de Girona, Campus Montilivi s/n, E-17003 Girona, Spain*

[b] *DEMec Faculdade de Engenharia, Universidade do Porto, Rua Dr. Roberto Frias, 4200–465 Porto, Portugal*

[c] *INEGI, Rua Dr. Roberto Frias, 400, 4200–465 Porto, Portugal*

[d] *Centre Internacional de Mètodes Numèrics a l'Enginyeria (CIMNE), Edifici C1, Campus Nord UPC C/ Gran Capità S/N, 08034 Barcelona, Spain*

Abstract

This paper presents an analytical model to predict the stress redistribution around broken fibres in hybrid polymer composites. The model is used under the framework of a progressive failure approach to study the load redistribution around breaks in hybrid composites. The outcomes of the model are validated by comparing it with a spring element model. Moreover, the approach is further used to study the tensile behaviour of different hybrid composites. The results obtained show that the load redistribution around breaks depends on the stiffness ratio between both fibres as well as the matrix behaviour considered and the hybrid volume fraction. Furthermore, the different material parameters have a large effect on the tensile behaviour, with an increase of ductility achieved if the failure process of the two fibres is gradual.

keywords: Stress concentration, Hybrid composites, Modelling, Micro-mechanics

* Corresponding author

Paper published in: *Composite Structures 211 (2019) 564–576*
Doi: https://doi.org/10.1016/j.compstruct.2018.12.044

4.1 Introduction

Fibre hybridisation is a potential solution to the quasi-brittle behaviour of Fibre Reinforced Polymers (FRP), resulting in fibre tensile failure with hardly any previous damage symptoms [1, 4, 41, 42, 260]. In a hybrid composite, a Low Elongation (LE) fibre is combined with a High Elongation (HE) fibre. This combination may lead to a larger failure strain of baseline composites based on LE fibres, resulting in a hybrid effect. Moreover, the failure process of the material can become gradual leading to an increase of ductility [16, 18]. It is currently accepted that progressive failure, dynamic effects, and thermal residual stresses are the main reasons to explain the hybrid effect [3, 4, 26].

The strength of the fibres is not deterministic and follows a statistical distribution. When a fibre fails, the fibre locally loses its loading capability, which is recovered by shear transfer in the matrix over a distance called ineffective length. In this region the neighbour intact fibres are subjected to stress concentrations. As the load is incremented, clusters of broken fibres are created increasing the stress concentration in intact fibres even further. In a non-hybrid composite this process quickly leads to final failure, whilst in a hybrid composite the stress redistribution around broken fibres is altered due to the presence of fibres with different mechanical and geometrical properties [45]. These differences may alter and delay the formation of clusters leading to hybrid effects [15, 31, 33]. However, it remains to be understood if final failure happens either by the accumulation of damage and clusters or by the unstable propagation of a large critical cluster [4].

Different models that attempt to represent the failure process of composite materials and the stress redistribution around breaks are available in the literature. These models can be classified as Global Load Sharing (GLS) and Local Load Sharing (LLS). In GLS models, the stress loss by a broken fibre is redistributed equally among all intact fibres [1, 142, 150, 151, 155]. As a consequence, such models cannot predict the formation of clusters, which in general leads to a large overprediction of the failure strength. Nonetheless, GLS models can capture some trends affecting the failure process such as fibre fragmentation or the effect of the fibre strength variation [34, 35].

In the LLS models, the load of broken fibres is redistributed into the closest

intact fibres allowing to capture the formation of clusters. In these models, different modelling approaches exist [37]: analytical models [54, 159, 198], spring element models [39, 76, 194], fibre bundle models [33, 260] and micromechanical finite element models [35, 214, 222]. Though all methods, in general, predict the failure strength accurately, all predict different cluster formation and evolution due to the different modelling strategies. Moreover, all models omit the dynamic effects and overpredict the fibre break density compared with experiments [4, 41].

Currently there is not any analytical model that can predict accurately the Stress Concentration Factor (*SCF*) around clusters of broken fibres in hybrid composites taking into account the differences in elastic and geometrical properties of the two fibres in the hybrid [45]. Moreover, in depth parametric analysis of the load redistribution around breaks in hybrid composites, and their effect on the tensile response still remain scarce [31, 33, 35, 39, 260]. Furthermore, recent simulations showed that the load redistribution around breaks in non-hybrid composites is heavily influenced by the matrix behaviour [37]. However, such effects have not been studied with hybrid composites. It is, therefore, vital to further understand the load redistribution and to improve the available tools to predict this load redistribution as this is believed to be the main mechanism that triggers final failure of composites.

In this work, a new analytical model to compute the load redistribution around a cluster of broken fibres in a hybrid composite is presented. The model is an extension of the non-hybrid model presented in St-Pierre *et al.* [198]. The analytical model is used within the framework of a progressive failure model approach [260] to study the load redistribution around broken fibres in different hybrid composites using both a plastic and an elastic matrix. The model is validated by comparing with the extension of the Spring Element Model (SEM) to hybrid composites proposed by Tavares *et al.* [39]. Furthermore, the tensile failure of different hybrid composites is simulated using the same approach with the objective of understanding the influence of the modelling parameters on the macroscopic response. These simulations are also validated and compared with the SEM.

4.2 Modelling strategy

In this work, a new analytical model to predict the *SCF* around broken fibres in hybrid composites is presented. The analytical model is used within the framework of a Progressive Failure Model (PFM) [260]. In the PFM, a three dimensional Representative Volume Element (RVE) containing a random distribution of fibres is used. By applying known functions to predict the load redistribution around broken fibres, the PFM can simulate the tensile failure process of composite materials, capturing fibre clustering, fibre fragmentation and stiffness loss. This model is reviewed in the next sections where also the new analytical model to predict the *SCF* around breaks is presented.

To validate the new proposed model used in PFM, the obtained results are compared with the SEM. The SEM was firstly developed by Okabe *et al.* [76, 194, 195] and was recently extended to hybrid composites, damageable interfaces, and random fibre microstructures by Tavares *et al.* [39]. The SEM consists of a more complex three dimensional RVE where the fibres are longitudinal tensile springs connected by transverse springs representing the matrix. Unlike the PFM, the SEM can predict the load redistribution around breaks inherently from the equilibrium equations, being a finite element model. However, SEM is computationally more expensive than PFM. Further details of the SEM can be seen in Tavares *et al.* [39].

4.2.1 Progressive Failure Model

The PFM consists of a RVE of width a, height b and length L containing a random distribution of fibres of a given radius. The fibres are divided into elements of length l along their longitudinal direction, leading to a succession of planes. Each fibre is denoted with the sub-index $q \in [1, ..., N_q]$, while each plane is denoted with the sub-index $p \in [1, ..., N_p]$, where N_q and N_p are the number of fibres and planes respectively, see Fig. 4.1. Each element has a different strength according to a statistical distribution. Once an element fails, a damage distribution is applied over the ineffective length of the broken fibre, whereas stress concentration is applied into the neighbouring intact fibre elements.

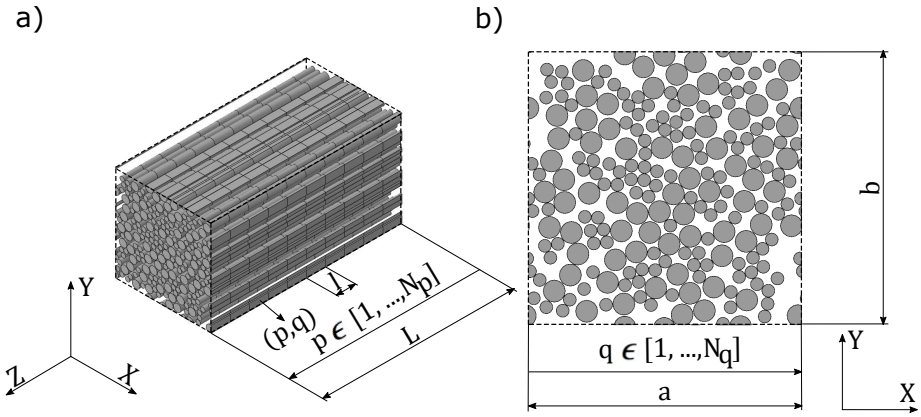

Figure 4.1: Schema of the RVE used in the PFM: a) 3D view, b) plane view.

4.2.1.1 Constitutive equation

The constitutive equation relating the stress of each element, $\sigma_{p,q}$, and the strain ε_p is

$$\sigma_{p,q} = \frac{SCF_{p,q}}{\Omega_p} E_q \left(1 - D_{p,q}\right) \varepsilon_p \tag{4.1}$$

where $SCF_{p,q}$ is the stress concentration factor of element p,q, E_q is the Young's modulus of fibre q, $D_{p,q}$ is the state damage variable, which is equal to 1 for broken elements, equal to 0 for intact elements and in between for elements in any stress recovery, ε_p is the strain of the plane (which is considered to be the same for all elements of plane p) and Ω_p is a stress ratio which enforces load equilibrium by modifying the stress concentration according to the strain level. Readers are referred to Guerrero *et al.* [260] for an in-depth description of the model.

The evolution of $D_{p,q}$ and $SCF_{p,q}$, depends on the model used to predict the ineffective length and the *SCF* around breaks, respectively. Even though any model may be applied to predict both, it is important to use models that are consistent for both parameters. In the following section, the model to predict damage is explained, whereas the new model for predicting the *SCF* is explained in Section 4.2.1.3.

4.2.1.2 Functions for ineffective length

In this work two different behaviours to simulate damage are considered, i.e. the matrix is plastic or the matrix is elastic.

When the matrix is plastic, a modified version of Kelly-Tyson shear-lag model [149] is adapted as given in St-Pierre *et al.* [198]. This approach adds a factor, H, which scales the ineffective length with cluster size. Here, two broken fibre elements belong to the same cluster (c), if the distance between the centres of both fibres is below four times the fibre radius and both elements are in the same plane p. Each cluster is represented with the sub-index p,c, with $c \in \left[1,...,N_p^{\mathrm{c}}\right]$ where N_p^{c} is the number of clusters at plane p. This means that the scaling effects depend on the element length, l. Nonetheless, it was verified that varying the element length does not significantly change neither the macroscopic response of the composite nor the damage development. The ineffective length of a broken fibre in cluster p,c is then

$$L_{p,q}^{\mathrm{in}} = \frac{R_q E_q}{2\tau_q} H_{p,c}\varepsilon_p = \frac{n_{p,c}\pi R_q^2 E_q}{C_{p,c}\tau_q}\varepsilon_p \tag{4.2}$$

where τ_q is the matrix shear yield stress, R_q is the fibre radius, $C_{p,c} = 4s\sqrt{n_{p,c}}$, where $n_{p,c}$ is the number of broken fibres on cluster p,c and s is the mean centre-to-centre distance between each fibre and its closest neighbour. Here, it is estimated with $s = \left(\left(R_{\mathrm{f1}}V_{\mathrm{f1}} + R_{\mathrm{f2}}V_{\mathrm{f2}}\right)/V_{\mathrm{f}}\right)\sqrt{\pi/V_{\mathrm{f}}}$, where R_{f1} and R_{f2} are the fibre radius of fibre populations 1 and 2 respectively, V_{f} is the overall fibre volume fraction and V_{f1} and V_{f2} are the fibre volume fraction of each population respectively $(V_{\mathrm{f}} = V_{\mathrm{f1}} + V_{\mathrm{f2}})$. It is worth mentioning that here, s, is not the average inter-fibre spacing of the cluster, but the average inter-fibre spacing of the overall RVE. That is, because the ineffective length should depend not only on the fibres in the broken cluster but also on the fibres that surround it.

The damage of element p,q according to each break in the fibre q at each plane i follows a linear recovery with

$$D_{p,q} = \begin{cases} \max\left(\dfrac{L_{i,q}^{\mathrm{in}} - |i-p|\,l}{L_{i,q}^{\mathrm{in}}}\right) & \forall i:\ (D_{i,q}=1)\cup\left(|i-p|\,l < L_{i,q}^{\mathrm{in}}\right) \\ 0 & \text{otherwise.} \end{cases} \tag{4.3}$$

If the matrix behaves elastically, the Cox's shear-lag model [227, 235] is adapted as in [37]. Then the ineffective length is

$$L_{p,q}^{\text{in}} = H_{p,c}\sqrt{\frac{E_q R_q}{2G_{\text{m}}}\left(s - 2\frac{R_{\text{f1}}V_{\text{f1}} + R_{\text{f2}}V_{\text{f2}}}{V_{\text{f}}}\right)}\ln\left(\frac{1}{1-0.999}\right) \tag{4.4}$$

where G_{m} is the matrix shear modulus. It should be noted that this length corresponds to a recovery of 99.9% of the fibre stress [37]. The damage is then computed with

$$D_{p,q} = \begin{cases} \max\left(\exp\left(-\dfrac{|i-p|\,l}{H_{p,c}R_q}\sqrt{\dfrac{2G_{\text{m}}R_q}{E_q\left(s - 2\dfrac{R_{\text{f1}}V_{\text{f1}} + R_{\text{f2}}V_{\text{f2}}}{V_{\text{f}}}\right)}}\right)\right) \ldots \\ \ldots \quad \forall i : (D_{i,q} = 1) \cup \left(|i-p|\,l < L_{i,q}^{\text{in}}\right) \\ 0 \quad \text{otherwise.} \end{cases} \tag{4.5}$$

4.2.1.3 Stress concentration factor model

Different approaches have been used to predict the *SCF* around breaks [41, 198, 251, 252]. Recently, St-Pierre *et al.* [198] presented a model capable of predicting the *SCF* around co-planar clusters of broken fibres in non-hybrid composites. St-Pierre's *et al.* [198] approach is adapted and extended here to work with hybrid composite materials. The reason why this model was chosen over others is related to the fact that the model predicts the *SCF* around clusters instead of isolated fibre breaks, and it is built on a simple but solid physical background. The model assumes that the *SCF* around a cluster of broken fibres takes a power-law shape.

In this work, the increment of *SCF* for an intact element p,q due to cluster i,c is represented with two functions, δ and λ, so that $\Delta SCF = \delta \cdot \lambda$. The function δ depends on the in-plane distance (r_{q-c}) between the geometrical centre of coordinates of cluster i,c and intact element p,q, while λ depends on the plane position along the ineffective length. As each cluster may contain broken fibres of each type, an intact element may receive *SCF* from broken fibres of the same

population or the other, leading to four combinations of δ

$$\begin{aligned}
\delta_{11_{(q-c)}} &= I_{11_{i,c}} \left(\frac{R_{i,c}}{r_{q-c}} \right)^{\alpha} \qquad \delta_{22_{(q-c)}} = I_{22_{i,c}} \left(\frac{R_{i,c}}{r_{q-c}} \right)^{\alpha} \\
\delta_{12_{(q-c)}} &= I_{12_{i,c}} \left(\frac{R_{i,c}}{r_{q-c}} \right)^{\alpha} \qquad \delta_{21_{(q-c)}} = I_{21_{i,c}} \left(\frac{R_{i,c}}{r_{q-c}} \right)^{\alpha}
\end{aligned} \tag{4.6}$$

where $\delta_{11_{(q-c)}}$ and $\delta_{22_{(q-c)}}$ represent the increment of *SCF* that an intact element of fibre population 1 and 2 respectively receives due to broken fibres of its own type in cluster i,c, while $\delta_{12_{(q-c)}}$ and $\delta_{21_{(q-c)}}$ are the increment of *SCF* that an element of fibre population 1 and 2 respectively receives due to broken fibres of different type in cluster i,c. $R_{i,c}$ is the equivalent radius of the cluster, estimated with $\pi R_{i,c}^2 = n_{i,c} S_{i,c}^2$, where $S_{i,c}$ is the average fibre spacing of the cluster, $S_{i,c} = \left(\left(n_{1_{i,c}} R_{\mathrm{f1}} + n_{2_{i,c}} R_{\mathrm{f2}} \right) / n_{i,c} \right) \sqrt{\pi / V_{\mathrm{f}}}$, where $n_{1_{i,c}}$ and $n_{2_{i,c}}$ are the number of broken fibres of population 1 and 2 respectively in cluster i,c and $n_{i,c} = n_{1_{i,c}} + n_{2_{i,c}}$. The exponent α is an input parameter which controls the maximum value of *SCF* and the shape of the curve. According to the literature, this value can be adopted as $\alpha = 2$ for a plastic matrix and $\alpha = 3.8$ for elastic matrix [37, 198]. The terms I are constants, which are determined later in this section, see Eq. (4.10).

Similarly, as there are two fibre populations, each cluster i,c has two ineffective lengths, the ineffective length of broken elements of type 1, $L_{1_{i,c}}^{\mathrm{in}}$, and that of broken elements of type 2, $L_{2_{i,c}}^{\mathrm{in}}$. Therefore, two functions appear for λ as

$$\lambda_{1_{(p-i)}} = \begin{cases} \dfrac{L_{1_{i,c}}^{\mathrm{in}} - l\,|i-p|}{L_{1_{i,c}}^{\mathrm{in}}} & \forall (i,c) : l\,|i-p| < L_{1_{i,c}}^{\mathrm{in}} \quad \text{Plastic matrix} \\ \exp\left(-\dfrac{|i-p|\,l C_{i,c}}{2\pi n_{i,c} R_{\mathrm{f1}}^2} \sqrt{\dfrac{2 G_{\mathrm{m}} R_{\mathrm{f1}}}{E_{\mathrm{f1}} \left(s - 2 \dfrac{R_{\mathrm{f1}} V_{\mathrm{f1}} + R_{\mathrm{f2}} V_{\mathrm{f2}}}{V_{\mathrm{f}}} \right)}} \right) \ldots & \\ \ldots \quad \forall (i,c) : l\,|i-p| < L_{1_{i,c}}^{\mathrm{in}} \quad \text{Elastic matrix,} \end{cases}$$

$$\lambda_{2_{(p-i)}} = \begin{cases} \dfrac{L_{2_{i,c}}^{\mathrm{in}} - l\,|i-p|}{L_{2_{i,c}}^{\mathrm{in}}} & \forall (i,c) : l\,|i-p| < L_{2_{i,c}}^{\mathrm{in}} \quad \text{Plastic matrix} \\ \exp\left(-\dfrac{|i-p|\,l C_{i,c}}{2\pi n_{i,c} R_{\mathrm{f2}}^2} \sqrt{\dfrac{2 G_{\mathrm{m}} R_{\mathrm{f2}}}{E_{\mathrm{f2}} \left(s - 2 \dfrac{R_{\mathrm{f1}} V_{\mathrm{f1}} + R_{\mathrm{f2}} V_{\mathrm{f2}}}{V_{\mathrm{f}}} \right)}} \right) \ldots & \\ \ldots \quad \forall (i,c) : l\,|i-p| < L_{2_{i,c}}^{\mathrm{in}} \quad \text{Elastic matrix,} \end{cases} \tag{4.7}$$

where $\lambda_{1_{(p-i)}}$ represents the evolution of $\delta_{11_{(q-c)}}$ and $\delta_{21_{(q-c)}}$ along $L^{\text{in}}_{1_{i,c}}$, while $\lambda_{2_{(p-i)}}$ represents the evolution of $\delta_{22_{(q-c)}}$ and $\delta_{12_{(q-c)}}$ along $L^{\text{in}}_{2_{i,c}}$. E_{f1} and E_{f2} are the Young's modulus of fibre type 1 and 2 respectively.

Because of load equilibrium, the load loss of each fibre population in the cluster, must be redistributed into the remaining intact fibres at same plane. Thus, the following equilibrium equations arise

$$\begin{aligned}
\pi R^2_{\text{f1}} n_{1_{i,c}} \sigma^{\infty}_1 = &\int_{R_{i,c}}^{R_{\text{t}}} I_{11_{i,c}} \left(\frac{R_{i,c}}{r_{q-c}}\right)^{\alpha} \sigma^{\infty}_1 V_{\text{f1}} 2\pi r_{q-c}\, \mathrm{d}r_{q-c} + \\
&+ \int_{R_{i,c}}^{R_{\text{t}}} I_{21_{i,c}} \left(\frac{R_{i,c}}{r_{q-c}}\right)^{\alpha} \sigma^{\infty}_2 V_{\text{f2}} 2\pi r_{q-c}\, \mathrm{d}r_{q-c} \\
\pi R^2_{\text{f2}} n_{2_{i,c}} \sigma^{\infty}_2 = &\int_{R_{i,c}}^{R_{\text{t}}} I_{22_{i,c}} \left(\frac{R_{i,c}}{r_{q-c}}\right)^{\alpha} \sigma^{\infty}_2 V_{\text{f2}} 2\pi r_{q-c}\, \mathrm{d}r_{q-c} + \\
&+ \int_{R_{i,c}}^{R_{\text{t}}} I_{12_{i,c}} \left(\frac{R_{i,c}}{r_{q-c}}\right)^{\alpha} \sigma^{\infty}_1 V_{\text{f1}} 2\pi r_{q-c}\, \mathrm{d}r_{q-c}
\end{aligned} \tag{4.8}$$

where R_{t} is the RVE equivalent radius, $R_{\text{t}} = \sqrt{(a \cdot b)/\pi}$, while σ^{∞}_1 and σ^{∞}_2 are the stress at infinite for each fibre population respectively. Assuming that the strain is the same for both fibre populations, $\sigma^{\infty}_1/E_{\text{f1}} = \sigma^{\infty}_2/E_{\text{f2}}$. In addition, it is assumed that two intact fibre elements of different type located at the exact same distance to the same break, receive the same increment of force due to the break. This assumption means that the overload transferred from a break to an intact fibre is independent of both the Young's modulus and the fibre radius of the intact fibre. This fact is supported by the results presented in Swolfs *et al.* [45]. As isostrain conditions are considered, force equality implies that the increment of stress concentration solely depends on the stiffness and cross-sectional area of both fibres leading to

$$I_{21_{i,c}} = \frac{E_{\text{f1}} R^2_{\text{f1}}}{E_{\text{f2}} R^2_{\text{f2}}} I_{11_{i,c}} \qquad I_{12_{i,c}} = \frac{E_{\text{f2}} R^2_{\text{f2}}}{E_{\text{f1}} R^2_{\text{f1}}} I_{22_{i,c}} \tag{4.9}$$

These conditions imply that a fibre with lower stiffness located at the same distance to the break is subjected to a higher *SCF* than a fibre with a higher stiffness, which is consistent to the general observations seen in the literature [31, 45]. By substituting the relation between σ^{∞}_1 and σ^{∞}_2 and Eq. (4.9) into Eq. (4.8), the constants $I_{11_{i,c}}, I_{22_{i,c}}, I_{12_{i,c}}$ and $I_{21_{i,c}}$ are obtained as functions of α:

$$
I1_{i,c} = \begin{cases} \dfrac{n1_{i,c} R_{f1}^2 R_{f2}^2}{2R_{i,c}^2 \ln\left(R_t/R_{i,c}\right)\left(R_{f1}^2 V_{f2} + R_{f2}^2 V_{f1}\right)} & \text{for } \alpha = 2 \\ \dfrac{n1_{i,c} R_{f1}^2 R_{f2}^2 R_{i,c}^{-\alpha}\left(\alpha - 2\right)}{2\left(R_{i,c}^{2-\alpha} - R_t^{2-\alpha}\right)\left(R_{f1}^2 V_{f2} + R_{f2}^2 V_{f1}\right)} & \text{otherwise,} \end{cases}
$$

$$
I2_{i,c} = \begin{cases} \dfrac{E_{f1} n1_{i,c} R_{f1}^4}{2E_{f2} R_{i,c}^2 \ln\left(R_t/R_{i,c}\right)\left(R_{f1}^2 V_{f2} + R_{f2}^2 V_{f1}\right)} & \text{for } \alpha = 2 \\ \dfrac{E_{f1} n1_{i,c} R_{f1}^4 R_{i,c}^{-\alpha}\left(\alpha - 2\right)}{2E_{f2}\left(R_{i,c}^{2-\alpha} - R_t^{2-\alpha}\right)\left(R_{f1}^2 V_{f2} + R_{f2}^2 V_{f1}\right)} & \text{otherwise,} \end{cases}
$$

$$
I1_{i,c} = \begin{cases} \dfrac{n2_{i,c} R_{f1}^2 R_{f2}^2}{2R_{i,c}^2 \ln\left(R_t/R_{i,c}\right)\left(R_{f1}^2 V_{f2} + R_{f2}^2 V_{f1}\right)} & \text{for } \alpha = 2 \\ \dfrac{n2_{i,c} R_{f1}^2 R_{f2}^2 R_{i,c}^{-\alpha}\left(\alpha - 2\right)}{2\left(R_{i,c}^{2-\alpha} - R_t^{2-\alpha}\right)\left(R_{f1}^2 V_{f2} + R_{f2}^2 V_{f1}\right)} & \text{otherwise,} \end{cases}
$$

$$
I2_{i,c} = \begin{cases} \dfrac{E_{f2} n2_{i,c} R_{f2}^4}{2E_{f1} R_{i,c}^2 \ln\left(R_t/R_{i,c}\right)\left(R_{f1}^2 V_{f2} + R_{f2}^2 V_{f1}\right)} & \text{for } \alpha = 2 \\ \dfrac{E_{f2} n2_{i,c} R_{f2}^4 R_{i,c}^{-\alpha}\left(\alpha - 2\right)}{2E_{f1}\left(R_{i,c}^{2-\alpha} - R_t^{2-\alpha}\right)\left(R_{f1}^2 V_{f2} + R_{f2}^2 V_{f1}\right)} & \text{otherwise.} \end{cases} \tag{4.10}
$$

The model is very powerful as it takes into account the cluster size, RVE size, volume fractions, fibre radius and elastic properties of each fibre population with simple analytical equations. Moreover, it can represent different matrix behaviours or effects not present into the model by adjusting the value of α.

As there can be multiple clusters along the RVE, a superposition rule is considered. Therefore, the total *SCF* for an intact fibre element is obtained by linear superposition of the *SCF* of all clusters. Nonetheless, the *SCF* of a given element is bounded according to shear-lag transfer. This limitation ensures that there is a stress continuity between elements inside any ineffective length (elements where $0 < D_{p,q} < 1$) that are not affected by *SCF*, and subsequent intact elements ($D_{p,q} = 0$), which can be affected by the *SCF*. Thus, the total *SCF* of an intact element p,q is given by

$$
SCF_{p,q} = \begin{cases} \min\left(SCF_{p,q}^0, SCF_{p,q}^L\right) & \forall p,q : D_{p,q} = 0 \\ 1 & \text{otherwise,} \end{cases} \tag{4.11}
$$

where $SCF^{0}_{p,q}$ is the *SCF* predicted by the linear superposition of the contribution of all clusters using the previous δ and λ functions given by

$$\begin{aligned} SCF^{0}_{p,q} &= 1+\sum_{i=1}^{N_{\mathrm{p}}}\sum_{c=1}^{N_i^{\mathrm{c}}} \delta 11_{(q-c)}\,\lambda 1_{(p-i)} + \delta 12_{(q-c)}\,\lambda 2_{(p-i)} \quad \forall i,c : n_{i,c}>0 \quad \& \quad q \in \mathrm{f1} \\ SCF^{0}_{p,q} &= 1+\sum_{i=1}^{N_{\mathrm{p}}}\sum_{c=1}^{N_i^{\mathrm{c}}} \delta 22_{(q-c)}\,\lambda 2_{(p-i)} + \delta 21_{(q-c)}\,\lambda 1_{(p-i)} \quad \forall i,c : n_{i,c}>0 \quad \& \quad q \in \mathrm{f2} \end{aligned} \tag{4.12}$$

where f1 and f2 are fibre populations 1 and 2 respectively. $SCF^{\mathrm{L}}_{p,q}$ is the *SCF* limitation for broken fibre q to achieve stress continuity. This limit for intact element p,q is calculated according to the slope of the stress gradient of the nearest ineffective length, $1/L^{\mathrm{in}}_{i,q}$, in the fibre q, multiplied by the distance between planes i and p:

$$SCF^{\mathrm{L}}_{p,q} = \min\left(\frac{1}{L^{\mathrm{in}}_{i,q}}\,|i-p|\,l\right) \quad \forall i : D_{i,q}=1 \tag{4.13}$$

It should be noted that the broken and damaged fibre elements are not excluded from Eq. (4.8). Therefore, the *SCF* of each intact element is computed independently of the percentage of broken and damaged elements. However, the percentage of broken and damaged elements is taken into account to compute the strain of each plane, ε_p, and the stress ratio, Ω_p, which affect the final stress of the elements, $\sigma_{p,q}$. This is explained in detail in Guerrero *et al.* [260].

4.3 Methodology

In a hybrid composite the stress redistribution around broken fibres depends mainly on the elastic and geometrical properties of both fibres, the matrix behaviour (plastic or elastic), the hybrid volume fraction as well as the local fibre arrangement [33, 45]. All these properties will affect the creation and propagation of clusters that lead to final failure. In this work, the effects of the Young's modulus of the fibres, matrix shear strength (plastic or elastic) and hybrid volume fraction on the stress redistribution around a broken fibre are investigated in detail. Later, their effect on the tensile failure behaviour are also evaluated. The simulations are performed with the PFM using the new *SCF* model presented in previous section 4.2.1.3. All simulations are compared with the SEM [39] to validate the results.

A modified version of Melro's *et al.* [124] random fibre generator is used to create a RVE of width, thickness and length of $75 \times 75 \times 300$ times the fibre radius. The element length is always 2 times the fibre radius, with both fibres in the RVE having the same radius. The same RVE is used for both PFM and SEM when studying the same problem. Note however that a new RVE is generated for each case in study. To observe the differences in load redistribution and failure process with different properties, three hybrid composites are considered by combining different fibres. These hybrids correspond to AS4-Eglass, M50S-AS4 and AS4-T800G, whose properties are shown in Table 4.1. In all cases, the matrix corresponds to epoxy with elastic properties $E_{\mathrm{m}} = 1260$ MPa and $G_{\mathrm{m}} = 450$ MPa. To understand the impact of the matrix behaviour, all cases are simulated with plastic ($\tau_q = 50$ MPa) and elastic matrix ($\tau_q \to \infty$). In addition, each hybrid is simulated with a HE hybrid volume fraction of 25%, 50% and 75%. Here, the HE Hybrid Volume Fraction (HVF_{HE}) is referred to be as the percentage of HE fibre volume fraction, V_{HE}, over the total fibre volume fraction, $HVF_{\mathrm{HE}} = (V_{\mathrm{HE}}/V_{\mathrm{f}}) \cdot 100$.

Table 4.1: Fibre properties.

Fibre type	Fibre properties		Weibull properties		
	E_{f} [GPa]	R_{f} [μm]	m [-]	σ_0 [MPa]	L_0 [mm]
AS4	230	3.5	10.7	4275	12.7
M50S	480		9	4600	10
T800G	295		4.8	6800	10
E-glass	70		6.34	1550	24

In the case of SEM, the model calculates all unknown variables directly from the equilibrium equations, as a function of the material properties and RVE geometry, being a very robust tool. However, it is less efficient computationally than the PFM. For the PFM instead, the ineffective length and *SCF* need to be applied according to the matrix behaviour. In all cases where the matrix is plastic ($\tau_q \neq \infty$), the ineffective length and damage are simulated within Eqs. (4.2) and (4.3). In these cases, the *SCF* is calculated using $\alpha = 2$. However, when the matrix is elastic ($\tau_q = \infty$), then the ineffective length and damage are simulated with Eqs. (4.4) and (4.5) and $\alpha = 3.8$. It is worth mentioning that, when the matrix is plastic, its behaviour is considered to be perfectly plastic in the PFM, whilst it is elastic-plastic in the SEM.

To investigate the stress redistribution around breaks, a broken fibre is arbitrarily placed around the middle of the RVE for each hybrid composite. This broken fibre is either the fibre with lower Young's modulus (LM) or the fibre with higher Young's modulus (HM). Usually, the LM fibre corresponds to the fibre with larger failure strain, i.e. the HE fibre, whereas the HM fibre corresponds to the fibre with smaller failure strain, i.e. the LE fibre. Even tough the LE fibres will break before the HE fibres, it is important to study the HE fibre load redistribution as well as towards final failure the HE fibre also fails. A remote tensile strain, ε^0, of 2% is applied and the consequent obtained load redistribution around the broken fibre is characterised with three different metrics. The first one is the maximum *SCF* obtained on intact LM and HM fibres. The *SCF* is calculated as the ratio between the actual stress on the fibre over the stress if there were no breaks, i.e. $E_\mathrm{f}\varepsilon^0$. The second metric is the ineffective length of the broken fibre, which is defined as the distance where the broken fibre recovers 90% of the nominal load, whereas the last metric is the radial influence length. This is defined as the maximum distance in the break plane in which the *SCF* is higher than 1%. The results shown for both the ineffective length and radial length are normalised by the fibre radius. Ten realisations are performed for each case, leading to a total of 360 simulations.

To understand the influence of the modelling parameters on the tensile failure process, the same hybrid composites are simulated under fibre tensile loading. Moreover, non-hybrid composites of each fibre type are also simulated. To do so, a random strength, $\sigma^\mathrm{u}_{p,q}$, is generated for each element in the RVE according to the Weibull distribution [103] with $P_{p,q} = 1 - \exp\left(-\left(l/L_0\right)\left(\sigma^\mathrm{u}_{p,q}/\sigma_0\right)^m\right)$, where $P_{p,q}$ is a random number between 0 and 1, while σ_0, L_0 and m are the corresponding Weibull parameters of the fibre element shown in Table 4.1. To compare the results between simulations, different metrics are proposed based on literature [14]. The first metric is the yield stress, σ^y, which is understood as the knee point where the stress-strain curve deviates from the initial linear elastic regime at a strain of 0.1%. The second metric is the ductile strain, ε^d, defined as the strain difference between the strain at peak stress, and the initial slope line at the failure stress level $\left(\varepsilon^\mathrm{d} = \varepsilon^\mathrm{ult} - \sigma^\mathrm{ult}/E_0\right)$, where E_0 is the initial Young's modulus of the composite given by the rule of mixtures. The third metric is the peak stress, σ^ult, whereas the fourth metric is the strain at peak stress, ε^ult. These metrics are summarised in Fig. 4.2. The fifth metric is the

cluster size at peak stress, N^{c}. Here, two broken fibres belong to the same cluster if the distance between centres is smaller than 4 times the fibre radius and the axial distance between break planes is smaller than 10 times the fibre radius [37, 39, 41]. It should be noted that the definition of clusters used to assess the damage evolution explained in this section, is different than the one used for calculating the *SCF* and ineffective length shown in previous Section 4.2.1.2. This is done to allow a fair comparison between the analytical and numerical model, and other models in the literature. The sixth and final metric is the fibre break density at peak stress, ρ_{b}^{ult}. Five realisations are performed for each case in study, leading to 110 simulations in total.

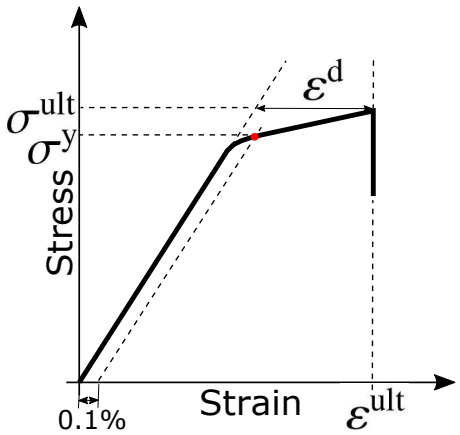

Figure 4.2: Main metrics used to characterise the tensile behaviour of hybrid composites.

4.4 Stress redistribution around breaks

In this section the stress redistribution around a broken fibre is analysed. A comparison of the results between the SEM and the analytical *SCF* model used in the framework of the PFM is performed to asses the validity of the analytical model. The overall volume fraction considered was 60% for all cases studied. It should be noted that in this section, because the fibres have no strength, the HVF_{HE} is referred to be as the percentage of LM fibre volume fraction over the total fibre volume fraction.

4.4.1 Stress concentration factor

The trends predicted by both PFM and SEM are the same for all hybrid materials and matrix behaviour, even though the absolute values are not the same. However, their relative difference is remarkably small considering the simplicity of the analytical model. These results justify the assumption done in Eq. 4.9.

In Fig. 4.3, the *SCF* around a broken HM fibre is shown with a plastic matrix and an elastic matrix as a function of the HVF_{HE} for the different hybrids in study. The *SCF* calculated is larger for the LM fibres when compared with the HM fibres. As the LM fibres have a lower stiffness, their stress before the break was lower compared with the HM fibre. Hence, the relative increase of stress is larger on the LM fibre causing a larger *SCF* [45].

Interestingly, the *SCF* on HM fibres decreases when adding LM fibres, while the opposite happens for the *SCF* on LM fibres. That should be related to the fact that by increasing the LM fibre content, the distance of the HM fibre to the break increases, and the load to redistribute is mainly taken by the LM fibres. This will cause larger hybrid effects at smaller HM volume fractions as has already been reported in literature [31, 33, 35, 260]. Moreover, the *SCF* on HM fibres is not strongly affected by the LM stiffness, whereas the opposite happens with the *SCF* on LM fibres. The larger the ratio between the stiffness of the HM and LM fibre is, the larger is the *SCF* obtained on the LM fibres. This fact agrees well with the findings of Swolfs *et al.* [45].

The matrix behaviour i.e. plastic or elastic changes the maximum value of *SCF*, being larger with elastic matrix, however, the trends are the same. The reason for this difference is the fact that, in an elastic matrix, there is no upper limit for shear stress transfer between fibre and matrix, hence causing a more localised effect and larger *SCF*.

In Fig. 4.4 the *SCF* around a broken LM fibre is shown with both plastic and elastic matrix for different HVF_{HE} and materials. The *SCF* on HM fibres again decreases by increasing the content of LM fibres, whilst the opposite happens with the LM fibres. Interestingly, the *SCF* on both HM and LM fibres are smaller than in the previous case. That is related to the fact that the LM fibre carried less load than the HM fibre before failure, hence resulting in smaller *SCF*. It should

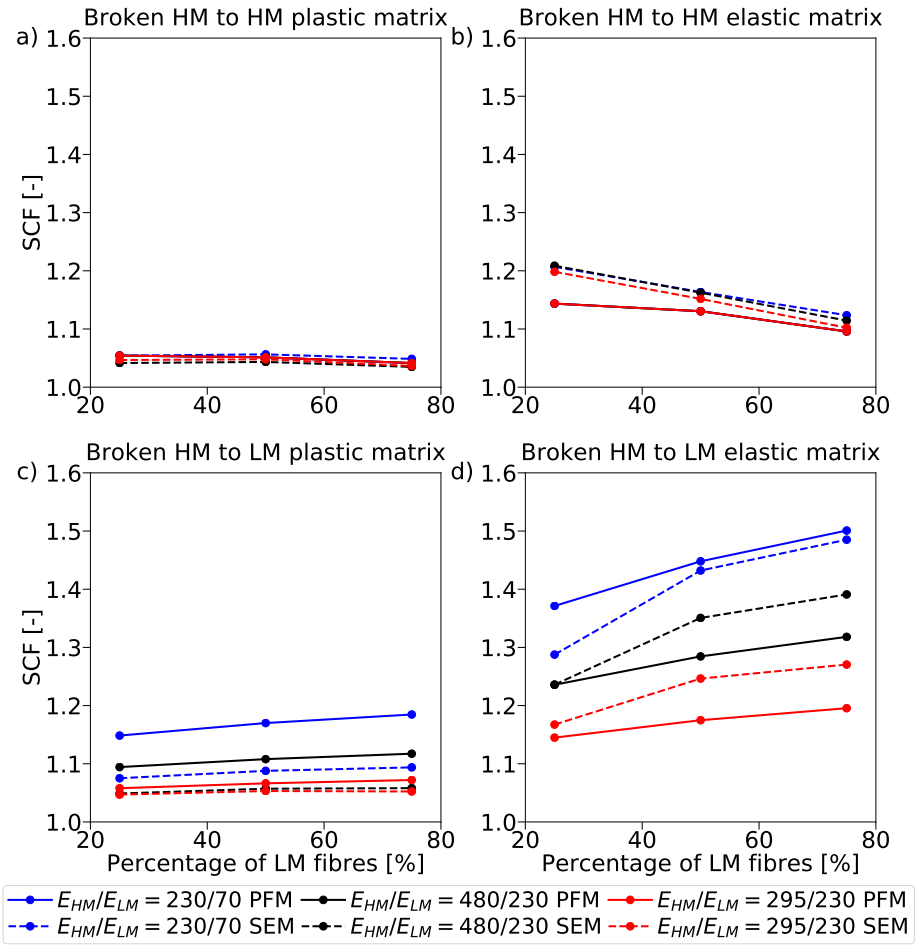

Figure 4.3: Maximum stress concentration factors around a broken HM fibre as a function of the HE hybrid volume fraction for different hybridisations: a) on HM fibres with plastic matrix, b) on HM fibres with elastic matrix, c) on LM fibres with plastic matrix, d) on LM fibres with elastic matrix. The average of 10 realisations are shown ($\tau_q = 50$ MPa for plastic matrix). Note that in a) and b), all PFM results are the same.

be noted however, that in reality the LM fibres usually fail after the failure of multiple HM fibres. Thus, the *SCF* obtained will be much larger than the ones predicted here, as the HM fibres no longer support load. The *SCF* on the LM fibre is not strongly affected by the stiffness of the HM fibre. Nonetheless, the *SCF* on the HM fibre is highly influenced by the stiffness of the LM fibre. A smaller stiffness ratio between HM and LM fibre leads to a larger *SCF* on the HM fibres, which is the opposite as observed in the previous case.

Although the models are able to take into account fibres with different radii

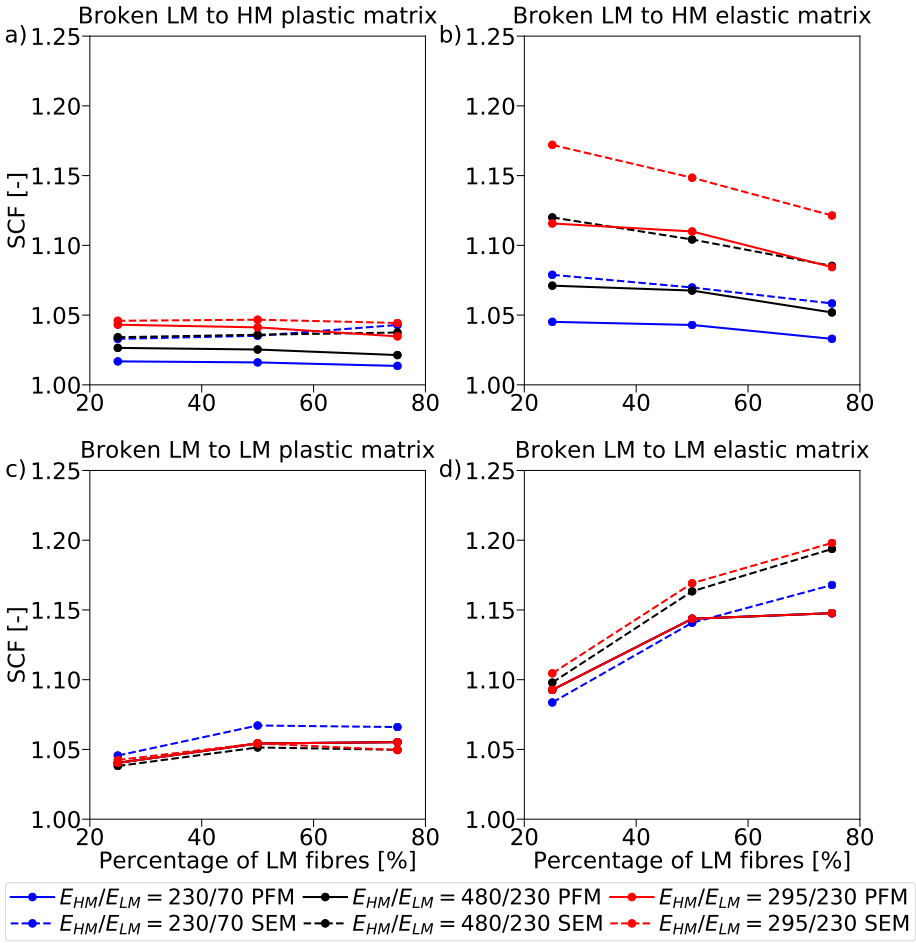

Figure 4.4: Maximum stress concentration factors around a broken LM fibre as a function of the HE hybrid volume fraction for different hybridisations: a) on HM fibres with plastic matrix, b) on HM fibres with elastic matrix, c) on LM fibres with plastic matrix, d) on LM fibres with elastic matrix. The average of 10 realisations are shown ($\tau_q = 50$ MPa for plastic matrix). Note that in c) and d), all PFM results are the same.

[39, 260], in this study the fibres were considered to always have the same radii. Otherwise, it would add another layer of complexity due to higher differences in the microstructures of the composites analysed.

4.4.2 Ineffective length

In Fig. 4.5 the ineffective length is shown for a broken HM fibre and a broken LM fibre with both plastic and elastic matrix as a function of the HVF_{HE} for each material system.

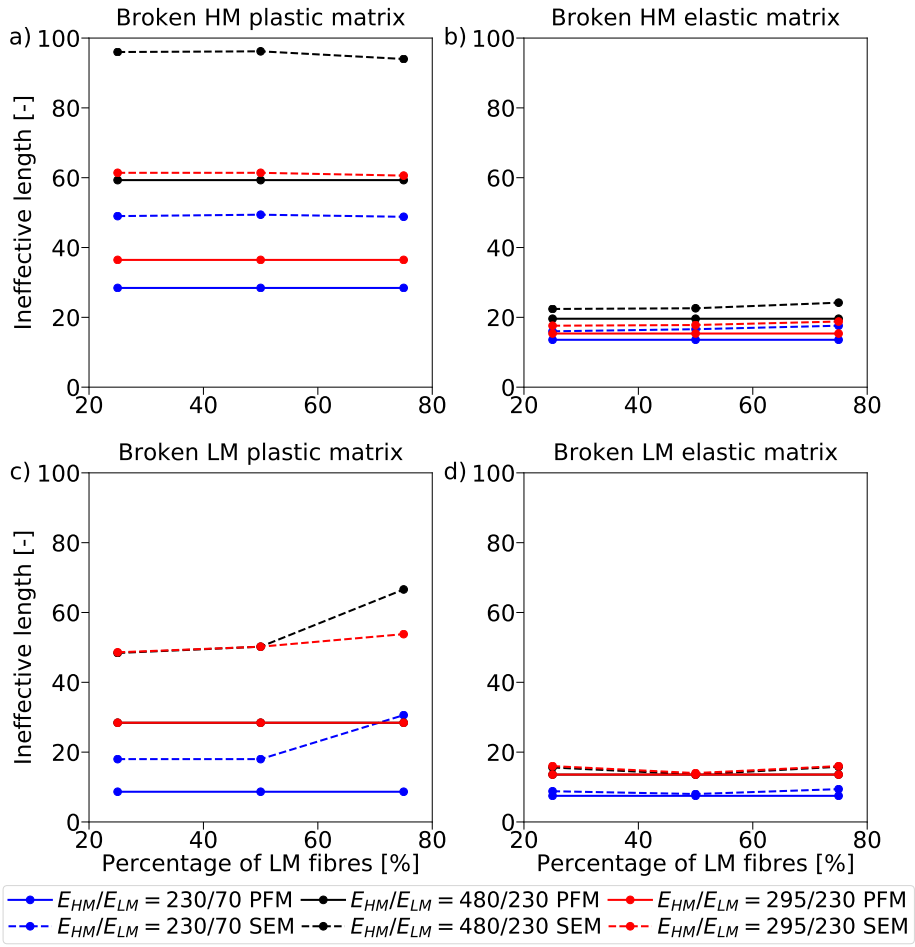

Figure 4.5: Normalised ineffective length at 90% of load recovery: a) broken HM fibre and plastic matrix, b) broken HM fibre and elastic matrix, c) broken LM fibre and plastic matrix, d) broken LM fibre and elastic matrix. The average of 10 realisations are shown ($\tau_q = 50$ MPa for plastic matrix). Note that in c) and d), the results for $E_{HM}/E_{LM} = 480/230\,PFM$ and $E_{HM}/E_{LM} = 295/230\,PFM$ are the same.

The ineffective length is larger for the HM fibre than for the LM fibre. That is due to its stiffness: a larger stiffness means that a larger load needs to be recovered, hence causing a larger ineffective length. Interestingly, the ineffective length is not significantly affected by the stiffness of the other fibre in the hybrid, which corresponds well to the findings of Swolfs *et al.* [45]. Similarly, the HVF_{HE} has a small effect on the ineffective length. In Fig. 4.5 d), a minimum can be observed for the SEM at $HVF_{\mathrm{HE}} = 50\%$, however, the difference is small compared to other volume fractions. In the same way, in Fig. 4.5 b) and c) a small increase of ineffective length is observed in the SEM for $HVF_{\mathrm{HE}} = 75\%$.

In any of these cases, the small difference in ineffective length due to the HVF_{HE} should be related to the changes in the microstructure, as the ratio between HM and LM fibres is different.

The ineffective length exhibits a large change between plastic and elastic matrix, the same trend that was observed for the *SCF*. The ineffective length is smaller for an elastic matrix, as there is no limit in shear stress transfer, making it possible for the stress to be recovered in the broken fibre in a shorter region. With the plastic matrix the shear transfer is limited by the matrix shear strength resulting in a larger ineffective length. In any case the trends remain the same for both matrix behaviours.

In general, the results predicted between the SEM and the analytical models in PFM follow similar trends, although some differences are observed. In the PFM the ineffective length is always smaller than in SEM. This is specially evident for the plastic matrix cases. There are two main reasons which can explain this difference. Firstly, with a plastic matrix, the behaviour of the matrix is elastic-plastic in the SEM, whilst it is perfectly plastic in PFM. Because of this, the shear stress is constant along the ineffective length, causing an underprediction of the ineffective length. This issue could in principle be improved by using an elastic-plastic model in PFM instead of a perfectly plastic. The second reason could be related to the microstructure. In the SEM, the ineffective length of each broken fibre depends on the local stiffness around the broken fibre. This means that if the broken fibre is surrounded by more LM fibres (with lower stiffness), then the ineffective length of the broken fibre is higher. This explains why the SEM predicts an increase in ineffective length at larger HVF_{HE}. However, this effect is unlikely to be captured by a simple analytical model.

4.4.3 Radial influence length

The radial influence length for each material system, as a function of the HVF_{HE} is shown in Fig. 4.6.

As it can be observed, the radial influence length is larger when a HM fibre is broken than when a LM fibre is. That is because the HM fibre has a larger stiffness, causing a larger load to be redistributed over intact fibres leading to a larger radial length. In most cases a small increase of the radial length can be

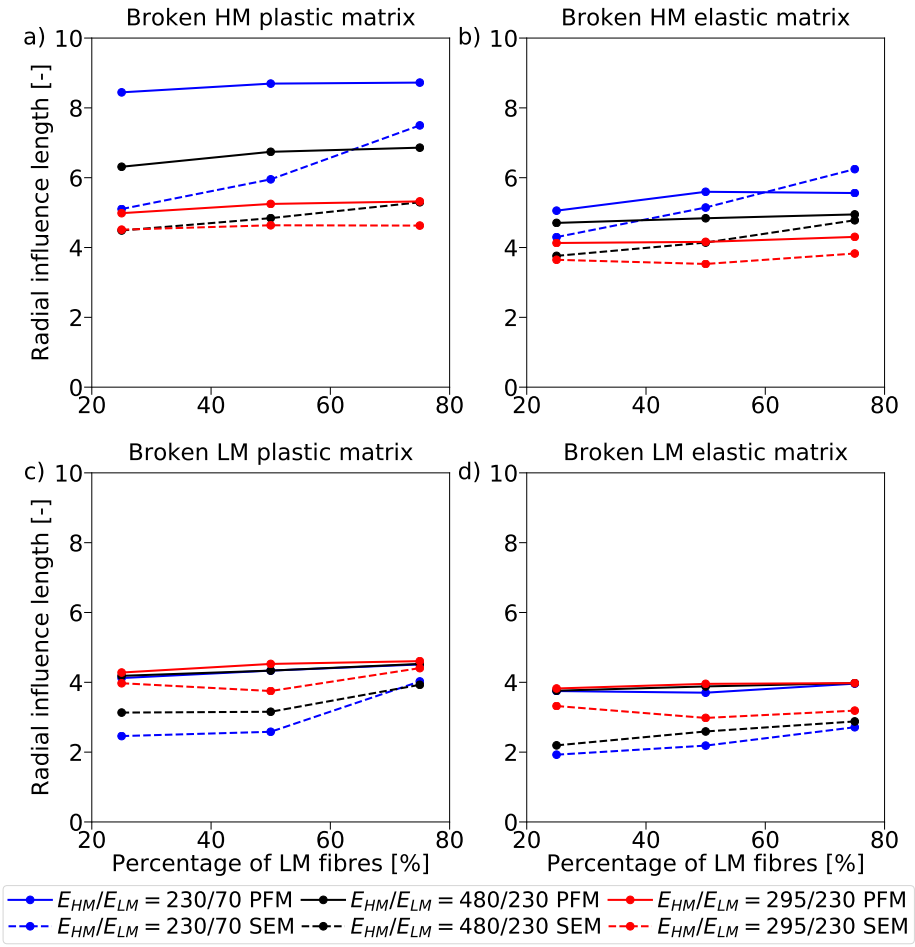

Figure 4.6: Normalised radial influence length: a) broken HM fibre and plastic matrix, b) broken HM fibre and elastic matrix, c) broken LM fibre and plastic matrix, d) broken LM fibre and elastic matrix. The average of 10 realisations are shown ($\tau_q = 50$ MPa for plastic matrix).

observed by increasing the HVF_{HE}. This increase is larger for the SEM than for the PFM, although overall the trends are similar. In general, the radial influence length is slightly larger for the PFM than for SEM.

Overall the radial length is affected by the stiffness of the fibres. A larger ratio of stiffness between HM and LM fibres causes a larger radial influence length when the HM fibre is broken. The opposite trend is observed when the LM fibre is broken. This observation corresponds well to what was observed with the *SCF*.

Changing the matrix from elastic to plastic maintains the same trends as it was seen with the *SCF* and ineffective length. As expected, the radial length is smaller with an elastic matrix, which is again caused by the no upper limit in shear transfer between fibre and matrix. In any case, the radial influence length is heavily dependent on the microstructure and its average value for each realization performed presents an error of approximately ± 1 mm/mm.

4.5 Tensile behaviour

In this section the tensile failure of the hybrid materials cases used in Section 4.4 is simulated under strain controlled conditions. A comparison of results is performed between SEM and PFM. In this section, the total fibre volume fraction considered is 50%.

A summary of all the results obtained for the hybrid materials with plastic matrix is presented in Table 4.2, while the results with elastic matrix are shown in Table 4.3. The results for the non-hybrid cases are summarised in Table 4.4. The presented results, correspond to the average of 5 realisations for each case. The average computational time for performing one run of the cases studied was 1314 s for the SEM, whereas it was 114 s for the PFM. Therefore, the simplified model is approximately 10 times faster.

The stress-strain curves obtained for all materials with a plastic matrix are shown in Fig. 4.7. The tensile behaviour predicted by the two modelling approaches is in good agreement for all cases despite of the differences in the modelling assumptions. In general, the PFM overpredicts the final failure of the composite, leading to larger peak stresses, yield stresses, strain and break densities, when compared with the SEM.

The failure process is seen to be very different for each hybrid configuration and varies greatly with the HVF_{HE}. For the AS4-Eglass hybrid, no ductility is observed at the different HVF_{HE} simulated. However, at a $HVF_{\mathrm{HE}} = 75\%$, there is a larger stiffness loss when compared with $HVF_{\mathrm{HE}} = 50\%$ and $HVF_{\mathrm{HE}} = 25\%$ before the final load drop, which suggests that ductility could be present for $HVF_{\mathrm{HE}} > 75\%$. This is also indicated by the fibre break density evolution presented in Fig. 4.8. As it can be seen, the fibre break density increases exponentially for all HE hybrid volume fractions leading to a brittle failure,

Table 4.2: Obtained results for all hybrid materials with plastic matrix.

Material	HVF_{HE} [%]	SEM						PFM					
		σ^{y} [MPa]	σ^{ult} [MPa]	ε^{d} [%]	$\varepsilon^{\mathrm{ult}}$ [%]	N^{c} [-]	$\rho_{\mathrm{b}}^{\mathrm{ult}}$ [mm^{-3}]	σ^{y} [MPa]	σ^{ult} [MPa]	ε^{d} [%]	$\varepsilon^{\mathrm{ult}}$ [%]	N^{c} [-]	$\rho_{\mathrm{b}}^{\mathrm{ult}}$ [mm^{-3}]
Hybrid AS4-Eglass	25	1844	1858	0.101	2.026	5.2	2880	2009	2025	0.134	2.251	10.4	6195
	50	1481	1494	0.101	2.067	4.4	2380	1624	1660	0.192	2.388	9.4	6712
	75	1144	1153	0.124	2.201	4.0	2480	1239	1299	0.316	2.653	14.2	8141
Hybrid M50S-AS4	25	2163	2163	0.065	1.098	10.6	4235	2310	2321	0.091	1.199	8.6	7063
	50	1955	1966	0.109	1.210	14.8	6435	2052	2060	0.119	1.275	7.0	6922
	75	1680	1897	0.525	1.808	14.4	9692	1817	2020	0.517	1.893	60.2	16229
Hybrid AS4-T800G	25	2432	2444	0.115	2.076	7.2	3831	2604	2614	0.112	2.223	33.8	6397
	50	2687	2720	0.157	2.213	7.0	4719	2880	2908	0.141	2.345	11.6	7439
	75	2978	3222	0.646	2.949	8.8	10670	3213	3533	0.760	3.282	31.0	21340

Table 4.3: Obtained results for all hybrid materials with elastic matrix.

Material	HVF_{HE} [%]	SEM						PFM					
		σ^{y} [MPa]	σ^{ult} [MPa]	ε^{d} [%]	ε^{ult} [%]	N^{c} [-]	ρ_{b}^{ult} [mm^{-3}]	σ^{y} [MPa]	σ^{ult} [MPa]	ε^{d} [%]	ε^{ult} [%]	N^{c} [-]	ρ_{b}^{ult} [mm^{-3}]
Hybrid AS4-Eglass	25	2001	2002	0.070	2.144	16.2	5661	1927	1927	0.022	2.038	9.4	2471
	50	1627	1635	0.102	2.253	18.6	6585	1648	1652	0.061	2.246	77.2	5739
	75	1247	1315	0.531	2.900	135.2	22360	1290	1349	0.221	2.648	132.6	17150
Hybrid M50S-AS4	25	2278	2313	0.074	1.180	30.8	7958	2237	2237	0.039	1.107	33.2	5979
	50	2069	2090	0.157	1.327	34.8	13141	2060	2075	0.064	1.229	116.0	8625
	75	1923	2078	0.299	1.706	42.8	19782	1876	1893	0.069	1.358	80.0	6977
Hybrid AS4-T800G	25	2602	2656	0.063	2.194	49.3	9242	2583	2585	0.042	2.130	115.2	6073
	50	2969	3495	1.557	4.199	4745.0	92451	3006	3414	0.539	3.127	1136.0	56394
	75	3447	4576	1.054	4.326	159.0	63661	3525	4484	0.991	4.192	3909.8	78179

Table 4.4: Obtained results for all non-hybrid materials with plastic ($\tau_q = 50$) and elastic matrix ($\tau_q = \infty$).

Material	τ_q	SEM						PFM					
	[MPa]	σ^{y} [MPa]	σ^{ult} [MPa]	ε^{d} [%]	ε^{ult} [%]	N^{c} [-]	ρ_b^{ult} [mm^{-3}]	σ^{y} [MPa]	σ^{ult} [MPa]	ε^{d} [%]	ε^{ult} [%]	N^{c} [-]	ρ_b^{ult} [mm^{-3}]
AS4	50	2252	2252	0.094	2.018	4.2	3265	2383	2391	0.105	2.172	14.2	5927
	∞	2397	2397	0.065	2.114	14.0	6482	2173	2173	0.009	1.887	8.2	1413
T800G	50	3605	3950	0.377	3.055	3.4	4940	3873	4388	0.416	3.376	6.0	7864
	∞	4615	5613	0.671	4.476	75.5	31195	4725	5708	0.935	4.785	1035.8	45807
M50S	50	2388	2388	0.059	1.054	5.2	3477	2590	2592	0.074	1.150	8.0	7187
	∞	2599	2599	0.058	1.141	17.4	7900	2385	2385	0.015	1.005	5.2	2604
E-glass	50	1043	1111	0.251	3.426	10.6	9479	1168	1263	0.316	3.859	22.0	18335
	∞	1222	1301	0.246	3.964	47.8	26062	1244	1311	0.217	3.895	177.0	25973

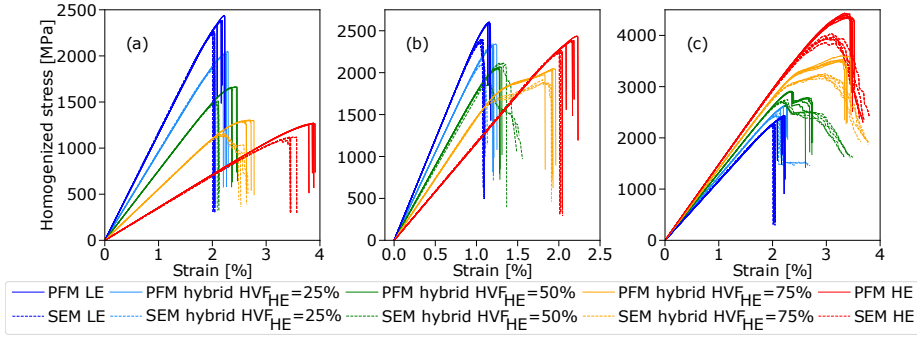

Figure 4.7: Simulated stress-strain curves for different hybrid materials at different HE hybrid volume fractions (HVF_{HE}) using a plastic matrix. (a) hybrid AS4-Eglass, (b) hybrid M50S-AS4, and (c) hybrid AS4-T800G. The non-hybrid composites are also shown.

nonetheless, this increase is less abrupt for $HVF_{\mathrm{HE}} = 75\%$.

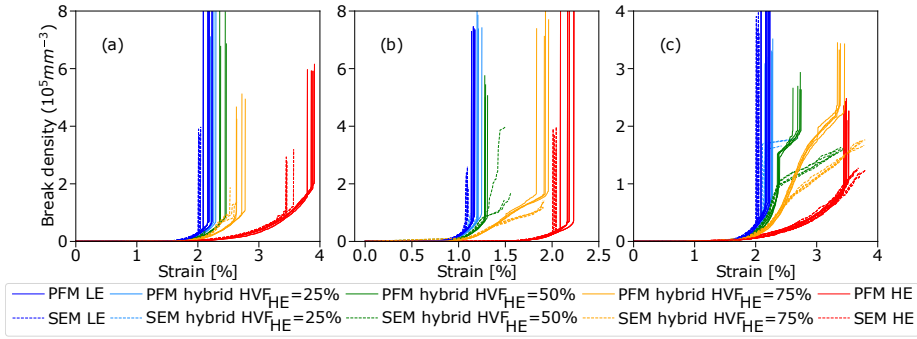

Figure 4.8: Simulated break-density curves for different hybrid materials at different HE hybrid volume fractions (HVF_{HE}) using a plastic matrix. (a) hybrid AS4-Eglass, (b) hybrid M50S-AS4, and (c) hybrid AS4-T800G. The non-hybrid composites are also shown.

For the M50S-AS4 hybrid, brittle failures are also obtained at HVF_{HE} of 25% and 50%. Nonetheless, a rather large ductility of around 0.5% is predicted by the models for $HVF_{\mathrm{HE}} = 75\%$, meaning that for this composite material the failure process is gradual. This is clearly demonstrated by the evolution of fibre break density, which increases linearly but not exponentially, until final failure.

Similarly, a ductility of around 0.7% is observed within the AS4-T800G hybridisation at a $HVF_{\mathrm{HE}} = 75\%$. However, by decreasing the HVF_{HE} brittle failures are obtained. In the case of $HVF_{\mathrm{HE}} = 25\%$, the failure is completely brittle whereas for the $HVF_{\mathrm{HE}} = 50\%$ two load drops can be observed. The first load drop corresponds to the failure of the LE fibres, whilst the second one

corresponds to the failure of the HE fibres. Nevertheless this case cannot be considered as ductile because the failure is not really continuous.

In general, the predicted cluster size is larger for the PFM than for SEM. The reason for this is likely to be related to the fact that final failure occurs later in PFM. In any case, the cluster size predicted are in general in good agreement with results of non-hybrid composites [41]. Similarly, the fibre break density is in general larger for the PFM for the same reason, although in this case both models predict larger values than seen in the literature [41]. The fibre break density seems to increase with ductility. The larger is the ductile strain, the larger is the break density. This is caused by the fact that final failure is being delayed, leading to larger break densities. For the M50S-AS4 hybrid, the fibre break density at maximum stress for $HVF_{\mathrm{HE}} = 75\%$ is more than 2 times larger compared to $HVF_{\mathrm{HE}} = 25\%$, being this increase from 4235 to 9692 mm^{-3} for SEM and from 7063 to 16229 mm^{-3} for PFM. Similarly, for the AS4-T800G hybrid, the fibre break density at $HVF_{\mathrm{HE}} = 75\%$ is approximately 3 times larger than at $HVF_{\mathrm{HE}} = 25\%$, with an increase from 3831 to 10670 mm^{-3} and 6397 to 21340 mm^{-3} for SEM and PFM respectively. It is worth mentioning that both the cluster size and fibre break density are here being compared with results of non-hybrid composites, which are brittle and less damage tolerant than the analysed hybrids. Therefore, this comparison should be taken with care. Nonetheless, although there is no certainty in the results for hybrid composites, the models seem to partially capture the results in non hybrid composites and their application to hybrid composites, although debatable, can lead to important insights.

The predicted stress-strain curves using an elastic matrix are shown in Fig. 4.9, while the fibre break density can be seen in Fig. 4.10. Both models are again in good agreement for most material configurations, although now the PFM is in general underpredicting final failure compared to SEM. Nonetheless, the obtained stress-strain curves and failure process differ greatly from the ones observed by using a plastic matrix. Unlike the plastic matrix case, some ductility appears within the AS4-Eglass hybrid at a $HVF_{\mathrm{HE}} = 75\%$. However, a very small ductility is predicted for the M50S-AS4 hybrid at a $HVF_{\mathrm{HE}} = 75\%$ compared to the plastic matrix case. The differences between plastic and elastic matrix are even larger for the AS4-T800G hybrid. With this material, the ductile

strain at a $HVF_{\mathrm{HE}} = 75\%$ is of 1%, which is much larger than the 0.7% predicted for plastic matrix. Similarly, at a $HVF_{\mathrm{HE}} = 50\%$ a large ductility of 1.5% for SEM and 0.5% for PFM is predicted whilst no ductility was present with a plastic matrix.

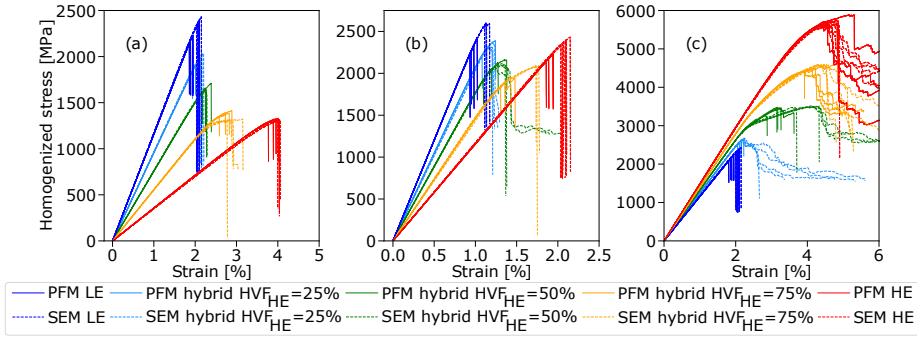

Figure 4.9: Simulated stress-strain curves for different hybrid materials at different HE hybrid volume fractions (HVF_{HE}) using an elastic matrix. (a) hybrid AS4-Eglass, (b) hybrid M50S-AS4, and (c) hybrid AS4-T800G. The non-hybrid composites are also shown.

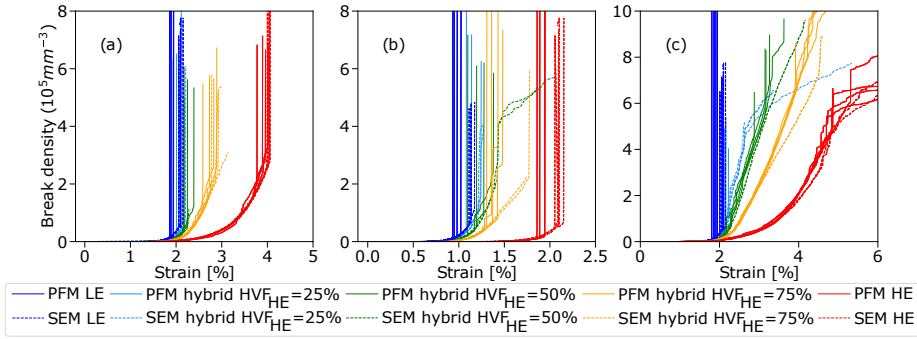

Figure 4.10: Simulated break-density curves for different hybrid materials at different HE hybrid volume fractions (HVF_{HE}) using an elastic matrix. (a) hybrid AS4-Eglass, (b) hybrid M50S-AS4, and (c) hybrid AS4-T800G. The non-hybrid composites are also shown.

By further analysing the cluster evolution and break density with an elastic matrix, larger differences appear in comparison with the plastic matrix. For the ductile cases, the models with an elastic matrix predict a much larger break density than with a plastic matrix. The cluster size is also unrealistically large compared with experimental data [41]. This is especially evident for the AS4-T800G hybrid, in which the cluster size predicted by the models exceeds the number of fibres in the RVE for $HVF_{\mathrm{HE}} = 75\%$ and $HVF_{\mathrm{HE}} = 50\%$. This

means that in some cases, some fibres were broken more than once over the 10 axial element lengths considered, corresponding to 20 times the fibre radius. Therefore, the same fibre was broken multiple times in the same cluster. This effect is even more exaggerated due to the small Weibull modulus, m, of the T800G fibre which causes a large strength variation for that fibre. However, it should be highlighted again that both the cluster size and fibre-break density are being compared with results of non-hybrid composites which are brittle and less damage tolerant than the simulated hybrids.

For the cases of the non-hybrid composites the models are again in good agreement. For these materials the final failure is brittle for all cases, being similar between elastic and plastic matrix. However, the fibre break density and cluster size are again very large for some cases with elastic matrix and do not correspond well to data available in the literature [41].

The large differences of results between plastic and elastic matrix highlight that the differences in load redistribution, seen in previous Section 4.4, lead to very different failure progression. In an elastic matrix, the shear stress transfer between fibre and matrix is not limited which causes the stress redistribution to be always very localised around the break. As a consequence, many isolated clusters along the model appear which need to grow very large in size to propagate unstably. This is the reason why the cluster size is usually larger for the elastic matrix cases. Similarly, it should also explain why larger ductilities are observed with an elastic matrix. In a real composite however, the shear stresses are limited by the matrix strength, like it is the case with a plastic matrix approach. Results of this work suggest that, while an elastic matrix may lead to similar failure prediction in non-hybrid composites compared to a plastic matrix, the use of an elastic matrix can lead to inaccurate results when modelling hybrid composites. Nonetheless, it is impossible to further validate the results due to the lack of experimental data. Furthermore, a better definition of cluster size is needed to avoid clusters larger than the number of fibres.

4.6 Conclusions

In this work, a new analytical model for predicting the *SCF* around clusters of broken fibres in hybrid unidirectional composites was presented. The model was used within the framework of a PFM [260] to study the stress redistribution around breaks in different hybrid composites and their effect on the tensile response and failure process. The results were validated by comparing with the SEM [39].

The predicted stress redistribution around broken fibres in hybrid composites was seen to vary with the stiffness ratio of the fibres on the hybrid, the matrix behaviour being plastic or elastic, the broken fibre stiffness as well as the HE hybrid volume fraction. Three different metrics were used to quantify this load redistribution: maximum *SCF* on HM and LM fibres, ineffective length and radial length.

The *SCF* on an intact fibre with different stiffness than the broken fibre is affected by the stiffness ratio of both fibres. The larger the ratio, the larger the *SCF* when the HM fibre is broken, whereas the opposite happens when the LM fibre is broken. Adding LM fibres into the hybrid composite decreases the *SCF* on HM fibres, which should lead to larger hybrid effects. When a HM fibre is broken, the *SCF* is larger on the LM fibres than on the HM fibres. However, the *SCFs* are smaller in both populations when the LM fibre is broken. Changing the matrix from plastic to elastic has an important impact on the *SCF*. With an elastic matrix, the *SCF* is larger due to the fact that there is no limit in shear stress transfer. The new proposed analytical model predicted well the trends and stress redistribution in all cases and is in good agreement with the SEM. Moreover, assuming that the overload carried by an intact fibre due to a break does not depend on its Young's modulus and radius, provides a good correlation between the analytical model and the SEM.

The ineffective length was found to depend mainly on the stiffness of the broken fibre. The larger the stiffness, the larger the ineffective length. As a difference from the *SCF*, the stiffness of the hybridisation fibre and the HVF_{HE} has no significant impact on the ineffective length. However, the matrix behaviour has a strong effect, being the ineffective length smaller with an elastic matrix. Finally, the radial influence length follows the same trends as the *SCF* and is smaller

with an elastic matrix.

In addition, a simulation of the fibre tensile failure of different hybrid materials was performed under strain controlled conditions. Different ductile responses were predicted for some composites at high HVF_{HE}, whereas in other cases brittle and sudden failures were obtained. The ductile composites presented a gradual and progressive increase of fibre break density, whereas an exponential increase was obtained for the brittle materials.

Large differences were again found between plastic and elastic matrix, meaning that the differences in load redistribution lead to different failure progression. When the matrix was considered elastic, many isolated clusters appeared along the model. These clusters needed to grow very large in size before unstable propagation. As a consequence, unrealistically large cluster size and break densities were predicted for some simulations. This wasn't the case with a plastic matrix, which presented more realistic results compared to experiments [41]. Therefore, results suggest that using an elastic matrix may lead to erroneous predictions when modelling hybrid composites. Additional experimental data is required to further validate and improve the different models for hybrid composites.

Acknowledgements

The authors of Universitat de Girona acknowledge the financial support from the Spanish Ministerio de Economía, Industria y Competitividad (MINECO) under the projects MAT2015-69491-C3-1-R and TRA2015-71491-R co-financed by the European Regional Development Fund (ERDF). Jose M. Guerrero acknowledges the predoctoral Grant BES-2016-078270 from the Subprograma Estatal de Formación del MICINN cofinanced by the European Social Fund. Rodrigo P. Tavares acknowledges the support of the Portuguese Government's Fundação para a Ciência e Tecnologia, under the Grant SFRH/BD/115872/2016. Fermin Otero acknowledges the funding of Project NORTE-01-0145-FEDER-000022 SciTech Science and Technology for Competitive and Sustainable Industries, cofinanced by Programa Operacional Regional do Norte (NORTE2020), through ERDF. Pedro P. Camanho acknowledges the funding of Project PTDC/EMS-PRO/4732/2014, cofinanced by Programa Operacional Competitividade e Internacionalização and Programa Operacional Regional de Lisboa, through

ERDF and by National Funds through FCT - Fundação para a Ciência e Tecnologia.

Data availability

The raw/processed data required to reproduce these findings cannot be shared at this time due to legal or ethical reasons.

5

Paper C – Failure of hybrid composites under longitudinal tension: Influence of dynamic effects and thermal residual stresses

The paper has been published in *Composite Structures.* In Press, journal pre-proof (2019).

Overview

One of the objectives of the present thesis is to investigate the impact that the dynamic effects and thermal residual stresses have on the tensile behaviour of hybrid composites as well as on the formation and development of clusters.

Besides some FEMs [35], the SEM by Tavares *et al.* [63] is the only state of the art model that inherently captures the failure and damage development in composite materials taking into account dynamic effects due to fibre failure. The drawback of either FEM or SEM, is their massive computational requirements. Since none of these models have studied dynamic effects in hybrid composites, their role on the tensile failure and cluster development in hybrid composites is still unknown. Regarding the thermal residual stresses, the majority of the models omit them altogether, since their impact on final failure and on the hybrid effect is known to be small [3]. However, their influence on cluster development is unexplored.

In this Chapter, the latest PFM presented in previous Chapter 4 is enhanced by including dynamic effects due to fibre failure, and thermal residual stresses as a result of the manufacturing process. On the one hand, this should allow to improve the model further, closing the gap to the experiments. On the other hand, it should allow to capture dynamic effects with a low computational effort compared to FEM or SEM. The outcomes of this work show that, albeit the dynamic effects change cluster formation, nonetheless they do not significantly alter the final failure of the material. Although the thermal residual stresses do not affect the formation of clusters, they can delay damage initiation and final failure by inducing compressive stresses into the fibres.

Failure of hybrid composites under longitudinal tension: Influence of dynamic effects and thermal residual stresses

Jose M. Guerrero[a,*], Joan A. Mayugo[a], Josep Costa[a], Albert Turon[a]

[a] *AMADE, Polytechnic School, Universitat de Girona, Campus Montilivi s/n, E-17003 Girona, Spain*

Abstract

A progressive failure model including dynamic effects and thermal residual stresses able to simulate the failure and damage development of hybrid unidirectional polymer composites under fibre tensile loading is presented. The model is used to study the influence dynamic effects and thermal residual stresses have on the development of clusters of fibre breaks and the failure process of different hybrid composites. The results obtained show that while the dynamic effects change cluster formation, nonetheless they do not significantly alter the final failure of the material. Overall, the influence is greater for the more brittle materials. Although the thermal residual stresses do not affect the formation of clusters, they can delay damage initiation and final failure by inducing compressive stresses into the fibres.

keywords: Dynamic effects, Thermal residual stresses, Hybrid, Micro-mechanics

5.1 Introduction

Fibre hybridisation, obtained by mixing a Low Elongation (LE) fibre with a High Elongation (HE) fibre in a single matrix, is a promising strategy that can overcome the inherent quasi-brittle behaviour and low toughness of Fibre Reinforced Polymers (FRP) that leads to fibre tensile failure with hardly any prior damage symptoms [1, 4, 41, 260, 261]. With a certain hybridisation, the failure process of the material can be altered, leading to hybrid effects and an increase in ductility [3, 13, 15–18, 31, 33–35, 39, 260, 261]. At present, changes in failure development, thermal residual stresses and dynamic effects are the

* Corresponding author

Paper published in: *Composite Structures. In Press, journal pre-proof (2019)*
Doi: https://doi.org/10.1016/j.compstruct.2019.111732

main explanations for the so-called effects [3, 22, 26, 44].

The tensile strength of brittle fibres is not deterministic and can be characterised with a statistical distribution. When a fibre breaks, the fibre loses its load carrying capacity over a distance known as ineffective length. Along this length, the neighbouring intact fibres are subjected to stress concentrations. Intrinsically, this stress redistribution is dynamic. When a fibre fails, the strain energy sustained by the fibre is released in the form of a stress wave which dampens after some time. During this period, dynamic stress concentrations, which exceed the static, appear in intact fibres around the broken fibre [26, 56, 57, 60, 61, 63]. Currently, it has been reported that the dynamic stress concentration can be between 10% to 110% higher than the static depending on the configuration of the material [63]. As the load is increased, clusters of broken fibres start to form, which will eventually lead to final failure. It is, however, unclear if final failure is triggered due to the accumulation of damage or the unstable propagation of a large critical cluster [4]. In a non-hybrid composite this failure process occurs quickly, leading to a catastrophic failure. Nonetheless, in a hybrid composite, the formation of clusters can be altered thanks to the difference between the elastic and geometrical properties of the two fibre populations in the hybrid, leading to hybrid effects [15, 17, 18, 31, 33, 35, 260, 261].

Two main modelling approaches can be found in the literature to predict the fibre tensile failure of composites. Global Load Sharing (GLS) [1, 34, 35, 142, 150, 151, 155], which cannot capture the formation of clusters, and Local Load Sharing (LLS) [31–33, 35, 39, 54, 62, 63, 159, 194, 214, 222, 260, 261] which are able to do so. In general, models can predict the failure strength within an accuracy of around 20%, but overpredict the fibre break density at failure and underpredict the formation of co-planar clusters. In addition, compared with experiments, most models predict the formation of larger clusters too late. These issues have been mainly attributed to the omission of the dynamic effects due to fibre failure [4, 37, 41, 260].

To study their importance, Bullegas [62], incorporated for the first time, the dynamic effects in the tensile failure process of non-hybrid composites using a simplified approach. A 10% decrease in strength was found. Moreover, the average distance between consecutive breaks decreased when using the dynamic model. Such findings should have made the modelling results closer to the

experiments. Unfortunately, they did not provide a direct measure of the number of co-planar clusters. Recently, Tavares *et al.* [63], incorporated the dynamic effects in a spring element model using a random distribution of fibres. The dynamic Stress Concentration Factor (*SCF*) with a plastic matrix in a non-hybrid composite was on average 43.2% higher, whereas it was 83.2% higher with an elastic matrix. Even though the dynamic effects caused an earlier formation of larger clusters, the number of co-planar clusters and the fibre break density did not significantly improve compared to the static model when an elasto-plastic matrix was considered. However, the authors did not study the influence the dynamic effects have on the hybrid composites. Therefore, the role of the dynamic phenomenon on the fibre tensile failure and cluster development of hybrid composites remains unexplored. Moreover, if the dynamic *SCF* is smaller in hybrid composites than in non-hybrids, hybrid effects may occur [26], but the importance of this has not yet been clarified.

Another common assumption in models is to neglect the thermal residual stresses resulting from the manufacturing process, which appear because of the different thermal expansion coefficient of the constituents. Different authors have demonstrated that the thermal residual stresses are secondary, since they can only account for up to 10% of the hybrid effects [7, 8, 22]. Nonetheless, their influence on cluster development has yet to be studied.

In this work, a progressive failure model [37, 260, 261], including thermal residual stresses and dynamic effects, is formulated. Their influence on the tensile failure process of hybrid composite materials is then investigated. The paper is organised as follows: firstly, the progressive failure model, including dynamic effects and thermal residual stresses, is presented. After that, some hybrid materials are simulated under fibre tensile loading to assess their influence and finally some conclusions are drawn.

5.2 Modelling approach

In this section the modelling strategy of this work is presented. Firstly, an analytical equation to determine thermal residual stresses for each fibre population derived from the manufacturing process is developed. Secondly, a progressive failure model [260, 261] is reviewed and modified by including thermal residual stresses and dynamic effects. To take the dynamic effects into account, a

simple approach is considered based on Bullegas' work [62]. After a fibre fails, a dynamic iteration is performed in which the static *SCF* caused by the new failures is increased by a given dynamic factor. If at the end of the iteration no new failures occur, then the *SCF* values are reverted into the static conditions.

5.2.1 Analytical determination of thermal residual stresses

To determine the thermal residual stresses in a hybrid composite, two main hypothesis are applied following the approach in Prussak *et al.* [262]. Firstly, the force equilibrium in the fibre direction should lead to the summary of the force of all constituents (each fibre population and matrix) equal to zero, thus leading to

$$V_{\mathrm{f1}}\sigma_{\mathrm{f1}}^{\mathrm{r}} + V_{\mathrm{f2}}\sigma_{\mathrm{f2}}^{\mathrm{r}} + V_{\mathrm{m}}\sigma_{\mathrm{m}}^{\mathrm{r}} = 0 \tag{5.1}$$

Secondly, both fibre populations and matrix should have the same strain (including mechanical and thermal), thus

$$\frac{\sigma_{\mathrm{f1}}^{\mathrm{r}}}{E_{\mathrm{f1}}} + \alpha_{\mathrm{f1}}\left(T - T_{\mathrm{r}}\right) = \frac{\sigma_{\mathrm{f2}}^{\mathrm{r}}}{E_{\mathrm{f2}}} + \alpha_{\mathrm{f2}}\left(T - T_{\mathrm{r}}\right) = \frac{\sigma_{\mathrm{m}}^{\mathrm{r}}}{E_{\mathrm{m}}} + \alpha_{\mathrm{m}}\left(T - T_{\mathrm{r}}\right) \tag{5.2}$$

where V_{f1}, V_{f2}, V_{m} are the volume fractions ($V_{\mathrm{f1}} + V_{\mathrm{f2}} + V_{\mathrm{m}} = 1$), $\sigma_{\mathrm{f1}}^{\mathrm{r}}$, $\sigma_{\mathrm{f2}}^{\mathrm{r}}$, $\sigma_{\mathrm{m}}^{\mathrm{r}}$ are the longitudinal residual stresses, E_{f1}, E_{f2} and E_{m} are the Young's modulus whilst, α_{f1}, α_{f2} and α_{m} are the coefficient of thermal expansion, where sub-indices f1, f2 and m refer to fibre populations 1 and 2, and the matrix, respectively, whereas T is the test temperature and T_{r} is the stress-free reference temperature (usually the cure temperature). By mixing Eq. (5.1) and (5.2), the residual stresses become

$$\begin{aligned}
\sigma_{\mathrm{f1}}^{\mathrm{r}} &= E_{\mathrm{f1}}\frac{V_{\mathrm{f2}}E_{\mathrm{f2}}\left(\alpha_{\mathrm{f2}} - \alpha_{\mathrm{f1}}\right) + V_{\mathrm{m}}E_{\mathrm{m}}\left(\alpha_{\mathrm{m}} - \alpha_{\mathrm{f1}}\right)}{E_{\mathrm{f1}}V_{\mathrm{f1}} + E_{\mathrm{f2}}V_{\mathrm{f2}} + E_{m}V_{m}}\left(T - T_{\mathrm{r}}\right) \\
\sigma_{\mathrm{f2}}^{\mathrm{r}} &= E_{\mathrm{f2}}\frac{V_{\mathrm{f1}}E_{\mathrm{f1}}\left(\alpha_{\mathrm{f1}} - \alpha_{\mathrm{f2}}\right) + V_{\mathrm{m}}E_{\mathrm{m}}\left(\alpha_{\mathrm{m}} - \alpha_{\mathrm{f2}}\right)}{E_{\mathrm{f1}}V_{\mathrm{f1}} + E_{\mathrm{f2}}V_{\mathrm{f2}} + E_{m}V_{m}}\left(T - T_{\mathrm{r}}\right) \\
\sigma_{\mathrm{m}}^{\mathrm{r}} &= E_{\mathrm{m}}\frac{V_{\mathrm{f1}}E_{\mathrm{f1}}\left(\alpha_{\mathrm{f1}} - \alpha_{\mathrm{m}}\right) + V_{\mathrm{f2}}E_{\mathrm{f2}}\left(\alpha_{\mathrm{f2}} - \alpha_{\mathrm{m}}\right)}{E_{\mathrm{f1}}V_{\mathrm{f1}} + E_{\mathrm{f2}}V_{\mathrm{f2}} + E_{m}V_{m}}\left(T - T_{\mathrm{r}}\right)
\end{aligned} \tag{5.3}$$

while the residual strains can be determined with $\varepsilon_{\mathrm{f1}}^{\mathrm{r}} = \sigma_{\mathrm{f1}}^{\mathrm{r}}/E_{\mathrm{f1}}$, $\varepsilon_{\mathrm{f2}}^{\mathrm{r}} = \sigma_{\mathrm{f2}}^{\mathrm{r}}/E_{\mathrm{f2}}$ and $\varepsilon_{\mathrm{m}}^{\mathrm{r}} = \sigma_{\mathrm{m}}^{\mathrm{r}}/E_{\mathrm{m}}$. Note that for a non-hybrid composite the same equations can be applied by simply setting the quantities of one of the fibre populations equal to zero and thus leading to the same equations shown elsewhere as [263, 264].

5.2.2 Progressive Failure Model

The Progressive Failure Model (PFM) [37, 260, 261] is based on the chain of bundles approach and consists of a Representative Volume Element (RVE) of width a, height b and length L which contains a random distribution of fibres of a given radius. The fibres are divided into elements of length l along their longitudinal direction. For each element a different strength is assigned according to a statistical distribution. This leads to a domain of parallel tensile springs divided into planes in series. Each fibre is denoted with the sub-index $q \in [1, ..., N_q]$, which determines the position along the X and Y axes, while each plane is denoted with the sub-index $p \in [1, ..., N_p]$, which determines the position along the Z axis, where N_q and N_p are the number of fibres and planes respectively, see Fig. 5.1. When an element fails, the stress redistribution around the break is simulated by applying damage along the ineffective length of the broken fibre and stress concentration onto the neighbouring intact fibre elements. This approach allows fibre clustering and the stiffness loss of composite materials to be captured in a more computationally efficient way than other more sophisticated models [37, 261].

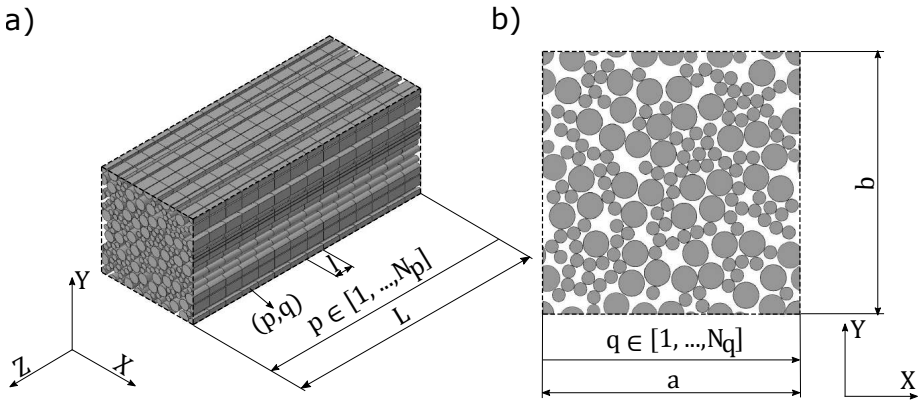

Figure 5.1: Schema of the RVE employed in the PFM: a) isometric view, b) plane view.

5.2.2.1 Constitutive equation

The constitutive equation which relates the element stress, $\sigma_{p,q}$, and the strain, ε_p, taking into account the residual strain now becomes

$$\sigma_{p,q} = \frac{SCF_{p,q}}{\Omega_p} E_q \left(1 - D_{p,q}\right) \left(\varepsilon_p + \varepsilon_q^{\mathrm{r}}\right) \tag{5.4}$$

where $SCF_{p,q}$ is the stress concentration factor (SCF) of element p,q, E_q is the Young's modulus of fibre q, $D_{p,q}$ is the damage state variable which is equal to 1 for broken elements, equal to 0 for intact elements and in between for elements in any stress recovery, ε_p is the mechanical strain of the plane (which is assumed to be the same for all elements of plane p), $\varepsilon_q^{\mathrm{r}}$ is the fibre's thermal residual strain determined with Eq. (5.3) and Ω_p is a stress ratio which enforces load equilibrium at each plane.

Calculating Ω_p and ε_p depends on a load equilibrium condition, whereas calculating $D_{p,q}$ and $SCF_{p,q}$ depends solely on an analytical model that is entered into the PFM. In theory, any model can be applied to predict both of them. Nonetheless, the models used should be consistent between them to obtain reliable results [37].

To take into account the dynamic effects, it is assumed here that the dynamic effects act by increasing the static SCF by a magnification factor, as has been proposed in other work [62]. Thus, after a fibre element fails, a dynamic iteration is performed and the static SCFs caused by the new failures are increased by a given factor. If at the end of the iteration no new failures occur, then the SCFs are reverted into the static values. Therefore the dynamic effects are included in the calculation of the SCF. In the following, the remaining modelling equations and model process are explained.

5.2.2.2 Load equilibrium

Because the amount of damage may be different at each plane, each plane has its own mechanical strain, ε_p. Thus, ε_p is evaluated according to the stiffness of the RVE, the current strain applied at infinity, ε^0, and the residual strains. To do so, first the stiffness of each element, $k_{p,q}$, is calculated by Hooke's law with

$$k_{p,q} = E_q\,(1 - D_{p,q})\,\frac{A_q}{l} \tag{5.5}$$

where A_q is the fibre's cross-sectional area. The stiffness of each plane, k_p, and the stiffness of each plane for fibre populations 1 and 2 (f1 and f2), are then computed by assuming all elements and the matrix in the plane work in parallel

$$k_{p_1} = \sum_{q \in \mathrm{f1}}^{N_q} k_{p,q} \qquad k_{p_2} = \sum_{q \in \mathrm{f2}}^{N_q} k_{p,q} \qquad k_p = k_{p_1} + k_{p_2} + k_{\mathrm{m}} \tag{5.6}$$

where k_m is the matrix stiffness, $k_\mathrm{m} = E_\mathrm{m}A_\mathrm{m}/l$, E_m is the matrix Young's modulus and A_m the matrix's cross-sectional area, $A_\mathrm{m} = a\,b - \sum_{q=1}^{N_q} A_q$. Next, the total stiffness of the system is computed by assuming all planes work in series

$$K = \left(\sum_{p=1}^{N_p} \frac{1}{k_p} \right)^{-1} \tag{5.7}$$

Finally, ε_p can be obtained by load equilibrium, as the total mechanical and thermal force of each plane, $F_p = k_p\varepsilon_p l + k_{p_1}\varepsilon_{\mathrm{f1}}^{\mathrm{r}} l + k_{p_2}\varepsilon_{\mathrm{f2}}^{\mathrm{r}} l + k_\mathrm{m}\varepsilon_\mathrm{m}^{\mathrm{r}} l$, must be equal to the force applied, $F = K\varepsilon^0 L$, leading to

$$\varepsilon_p = \frac{K\varepsilon^0}{k_p}\frac{L}{l} - \frac{k_{p_1}\varepsilon_{\mathrm{f1}}^{\mathrm{r}} + k_{p_2}\varepsilon_{\mathrm{f2}}^{\mathrm{r}} + k_\mathrm{m}\varepsilon_\mathrm{m}^{\mathrm{r}}}{k_p} \tag{5.8}$$

where ε^0 is the applied strain and $\varepsilon_{\mathrm{f1}}^{\mathrm{r}}$, $\varepsilon_{\mathrm{f2}}^{\mathrm{r}}$ and $\varepsilon_\mathrm{m}^{\mathrm{r}}$ are the residual strains of fibre populations 1 and 2, and the matrix, respectively, determined with Eq. (5.3).

To maintain local load equilibrium, the aggregation of the loads of the fibres and the matrix at each plane, p, must be equal to the load of the plane F_p. This condition allows the stress ratio Ω_p to be obtained with

$$\begin{aligned} F_p &= \sum_{q=1}^{N_q} \left(\frac{SCF_{p,q}}{\Omega_p} E_q \left(1 - D_{p,q}\right) \left(\varepsilon_p + \varepsilon_q^{\mathrm{r}}\right) A_q \right) + \left(\varepsilon_p + \varepsilon_m^{\mathrm{r}}\right) E_\mathrm{m} A_\mathrm{m} \\ \Omega_p &= \frac{\sum_{q=1}^{N_q} SCF_{p,q} E_q \left(1 - D_{p,q}\right) \left(\varepsilon_p + \varepsilon_q^{\mathrm{r}}\right) A_q}{\left(k_p\varepsilon_p + k_{p_1}\varepsilon_{\mathrm{f1}}^{\mathrm{r}} + k_{p_2}\varepsilon_{\mathrm{f2}}^{\mathrm{r}} - k_\mathrm{m}\varepsilon_p\right) l} \end{aligned} \tag{5.9}$$

5.2.2.3 Ineffective length and damage

The ineffective length of broken fibres depends mainly on the matrix behaviour, which can be elastic or plastic, as debonding is omitted here [37, 261]. The matrix behaviour is a key factor in the modelling predictions as it changes the ineffective length and the magnitude of the *SCF* over the intact fibres [5, 37, 39, 261].

For a plastic matrix, the model is modified as to include the residual strain. Therefore, the ineffective length corresponds to a modified Kelly-Tyson shear-lag model [149]. The ineffective length includes a scaling factor, H, which scales the ineffective length according to the cluster size [198]. This cluster is calculated assuming that two broken fibre elements belong to the same cluster

(c), if the distance between the centres of both fibres is below four times the smallest fibre radius and both elements are on the same plane p [37, 261]. Each cluster of plane p is represented with the sub-index p,c, with $c \in \left[1,...,N_p^c\right]$ where N_p^c is the total number of clusters on plane p. Thus, the ineffective length of a broken fibre element in cluster p,c is

$$L_{p,q}^{\text{in}} = \frac{R_q E_q}{2\tau_q} H_{p,c} \left(\varepsilon_p + \varepsilon_q^{\text{r}}\right) = \frac{n_{p,c}\pi R_q^2 E_q}{C_{p,c}\tau_q} \left(\varepsilon_p + \varepsilon_q^{\text{r}}\right) \tag{5.10}$$

where τ_q is the matrix shear yield stress, R_q is the fibre radius, $C_{p,c} = 4s\sqrt{n_{p,c}}$, and where $n_{p,c}$ is the number of broken fibres on cluster p,c and s is the overall mean distance between fibre centres, $s = \left[\left(R_{\text{f1}}V_{\text{f1}} + R_{\text{f2}}V_{\text{f2}}\right)/V_{\text{f}}\right]\sqrt{\pi/V_{\text{f}}}$, where R_{f1} and R_{f2} are the fibre radius of fibre populations 1 and 2 respectively and V_{f} is the overall fibre volume fraction, $V_{\text{f}} = V_{\text{f1}} + V_{\text{f2}}$. The damage of element p,q due to each break in the fibre q at each plane i is computed following the ineffective length curve as

$$D_{p,q} = \begin{cases} \max\left(\dfrac{L_{i,q}^{\text{in}} - |i-p|\,l}{L_{i,q}^{\text{in}}}\right) & \forall i:\ (D_{i,q}=1) \cup \left(|i-p|\,l < L_{i,q}^{\text{in}}\right) \\ 0 & \text{otherwise.} \end{cases} \tag{5.11}$$

If an elastic matrix is assumed, then the ineffective length is based on Cox's shear-lag model [227, 235]. For this scenario, the ineffective length depends neither on the residual strain nor on the mechanical strain [37], and is given by [261]

$$L_{p,q}^{\text{in}} = H_{p,c}\sqrt{\frac{E_q R_q}{2G_{\text{m}}}\left(s - 2\frac{R_{\text{f1}}V_{\text{f1}} + R_{\text{f2}}V_{\text{f2}}}{V_{\text{f}}}\right)}\ln\left(\frac{1}{1-\zeta}\right) \tag{5.12}$$

where G_{m} is the matrix shear modulus. It is worth mentioning that this length corresponds to a recovery of ζ percent of the nominal fibre stress (in this work $\zeta = 99.9\%$ of the nominal fibre stress [37, 261]). The damage is then computed with

$$D_{p,q} = \begin{cases} \max\left(\exp\left(-\dfrac{|i-p|\,l}{H_{p,c}}\sqrt{\dfrac{2G_{\text{m}}}{E_q R_q\left(s - 2\dfrac{R_{\text{f1}}V_{\text{f1}} + R_{\text{f2}}V_{\text{f2}}}{V_{\text{f}}}\right)}}\right)\right) \ldots \\ \ldots \quad \forall i:\ (D_{i,q}=1) \cup \left(|i-p|\,l < L_{i,q}^{\text{in}}\right) \\ 0 \quad \text{otherwise.} \end{cases} \tag{5.13}$$

Nonetheless, as was demonstrated in Guerrero *et al.* [261], the use of an elastic matrix may lead to inaccurate results when modelling hybrid composites. Consequently, in this work the matrix is assumed to be plastic and the ineffective length and damage are calculated with Eqs. (5.10) and (5.11).

5.2.2.4 Stress concentration factor and dynamic effects

To predict the static *SCF* around breaks, different models can be found in the literature [41, 198, 251, 252]. In this work, the proposed model, which has been used in previous studies and is based on the work of St-Pierre *et al.* [198], is applied [261]. The model is very powerful as it can predict the static *SCF* around a cluster i,c of broken fibres located on the same plane, taking into account the cluster size, RVE size, volume fractions, fibre radius and elastic properties of each fibre population. Furthermore, it can be calibrated to take into account different effects not present in the model [261].

The complex dynamic effects are simulated in this work in a simple and efficient way by adapting the approach proposed in Bullegas [62]. When a new element fails, a dynamic iteration is started. The static increment of *SCF* produced by the cluster i,c, to which the broken element belongs to, is multiplied by a factor larger than 1, M_{d}. This factor is only applied to the *SCF* produced by clusters i,c with new breaks, while it is equal to 1 for all other clusters i,c with no new broken elements. If no new elements fail at the end of the dynamic iteration, then all factors are set equal to 1 and the model reverts to static conditions. However, if new elements fail, then a new dynamic iteration is started. Hence, the static *SCF* caused by any cluster i,c with new broken fibres is multiplied by M_{d}.

It should be noted that the proposed approach does not allow the entire dynamic process to be captured, as unlike other models [63], the time variable is omitted. Within this approach, only the instant of time at which the maximum dynamic effect is produced is considered. Notwithstanding, that is the only time instant of interest as any new failures will occur when the *SCF* is maximum. Therefore, this method allows for a more efficient simulation process. In addition, it is assumed that the behaviour is quasi-static, since dynamic effects only occur as a result of new breaks and not to the applied load. Further to this, it is considered that the dynamic factor, M_{d}, is independent of the number of simultaneous

breaks that occur in the cluster i,c, in accordance with the results of Tavares *et al.* [63].

The static increment of *SCF* for an intact element p,q due to cluster i,c is given by $\Delta SCF = \delta \cdot \lambda$, where δ and λ are two functions [261]. The function δ is related to the in-plane distance (r_{q-c}) between the geometrical centre of coordinates of cluster i,c and intact element p,q, while λ is related to the plane position along the ineffective length. Because an intact element can receive *SCF* from broken fibres from the same or other population, and each cluster can contain broken fibres of each population, four combinations for δ occur

$$\begin{aligned} \delta_{11_{(q-c)}} &= I_{11_{i,c}} \left(\frac{R_{i,c}}{r_{q-c}} \right)^{\alpha} \qquad \delta_{22_{(q-c)}} = I_{22_{i,c}} \left(\frac{R_{i,c}}{r_{q-c}} \right)^{\alpha} \\ \delta_{12_{(q-c)}} &= I_{12_{i,c}} \left(\frac{R_{i,c}}{r_{q-c}} \right)^{\alpha} \qquad \delta_{21_{(q-c)}} = I_{21_{i,c}} \left(\frac{R_{i,c}}{r_{q-c}} \right)^{\alpha} \end{aligned} \tag{5.14}$$

Similarly, each cluster i,c has two ineffective lengths, the ineffective length of broken elements of type 1, $L^{\text{in}}_{1_{i,c}}$, and that of broken elements of type 2, $L^{\text{in}}_{2_{i,c}}$. Therefore, two combinations for λ occur

$$\lambda_{1_{(p-i)}} = \begin{cases} \dfrac{L^{\text{in}}_{1_{i,c}} - l\,|i-p|}{L^{\text{in}}_{1_{i,c}}} & \forall (i,c) : l\,|i-p| < L^{\text{in}}_{1_{i,c}} \quad \text{Plastic matrix} \\ \exp\left(-\dfrac{|i-p|\,lC_{i,c}}{2\pi n_{i,c} R^2_{\text{f1}}} \sqrt{\dfrac{2G_{\text{m}}R_{\text{f1}}}{E_{\text{f1}}\left(s - 2\dfrac{R_{\text{f1}}V_{\text{f1}} + R_{\text{f2}}V_{\text{f2}}}{V_{\text{f}}} \right)}} \right) \ldots \\ \ldots \quad \forall (i,c) : l\,|i-p| < L^{\text{in}}_{1_{i,c}} \quad \text{Elastic matrix,} \end{cases}$$

$$\lambda_{2_{(p-i)}} = \begin{cases} \dfrac{L^{\text{in}}_{2_{i,c}} - l\,|i-p|}{L^{\text{in}}_{2_{i,c}}} & \forall (i,c) : l\,|i-p| < L^{\text{in}}_{2_{i,c}} \quad \text{Plastic matrix} \\ \exp\left(-\dfrac{|i-p|\,lC_{i,c}}{2\pi n_{i,c} R^2_{\text{f2}}} \sqrt{\dfrac{2G_{\text{m}}R_{\text{f2}}}{E_{\text{f2}}\left(s - 2\dfrac{R_{\text{f1}}V_{\text{f1}} + R_{\text{f2}}V_{\text{f2}}}{V_{\text{f}}} \right)}} \right) \ldots \\ \ldots \quad \forall (i,c) : l\,|i-p| < L^{\text{in}}_{2_{i,c}} \quad \text{Elastic matrix,} \end{cases} \tag{5.15}$$

where $\delta_{11_{(q-c)}}$ and $\delta_{22_{(q-c)}}$ correspond to the static increment of *SCF* that an intact element from fibre populations 1 and 2, respectively, receives due to broken fibres of its own type in cluster i,c, while $\delta_{12_{(p-i)}}$ and $\delta_{21_{(p-i)}}$ are the static increments

of *SCF* that an element of fibre populations 1 and 2, respectively, receives due to broken fibres of a different type in cluster i,c. $\lambda 1_{(p-i)}$ is the evolution of $\delta 11_{(q-c)}$ and $\delta 21_{(q-c)}$ along $L^{\text{in}}_{1_{i,c}}$, while $\lambda 2_{(p-i)}$ is the evolution of $\delta 22_{(q-c)}$ and $\delta 12_{(q-c)}$ along $L^{\text{in}}_{2_{i,c}}$. $R_{i,c}$ is the equivalent radius of the cluster, $\pi R^2_{i,c} = n_{i,c} S^2_{i,c}$, $S_{i,c}$ is the average fibre spacing of the cluster, $S_{i,c} = \left[\left(n_{1_{i,c}} R_{\text{f1}} + n_{2_{i,c}} R_{\text{f2}}\right)/n_{i,c}\right]\sqrt{\pi/V_{\text{f}}}$, $n_{1_{i,c}}$ and $n_{2_{i,c}}$ are the number of broken fibres in populations 1 and 2, respectively, in cluster i,c, and $n_{i,c} = n_{1_{i,c}} + n_{2_{i,c}}$. The exponent α is an input parameter which governs the maximum value of *SCF* and the shape of the curve. Its value can be adopted as $\alpha = 2$ for a plastic matrix or $\alpha = 3.8$ for an elastic matrix [37, 198, 261]. As this work assumes a plastic matrix, $\alpha = 2$ will be used.

The terms I are constants which differ for each cluster i,c and are given by

$$
\begin{aligned}
I11_{i,c} &= \begin{cases} \dfrac{n_{1_{i,c}} R^2_{\text{f1}} R^2_{\text{f2}}}{2R^2_{i,c}\ln\left(R_{\text{t}}/R_{i,c}\right)\left(R^2_{\text{f1}}V_{\text{f2}} + R^2_{\text{f2}}V_{\text{f1}}\right)} & \text{for } \alpha = 2 \\ \dfrac{n_{1_{i,c}} R^2_{\text{f1}} R^2_{\text{f2}} R^{-\alpha}_{i,c}\left(\alpha - 2\right)}{2\left(R^{2-\alpha}_{i,c} - R^{2-\alpha}_{\text{t}}\right)\left(R^2_{\text{f1}}V_{\text{f2}} + R^2_{\text{f2}}V_{\text{f1}}\right)} & \text{otherwise,} \end{cases} \\
I21_{i,c} &= \begin{cases} \dfrac{E_{\text{f1}} n_{1_{i,c}} R^4_{\text{f1}}}{2E_{\text{f2}}R^2_{i,c}\ln\left(R_{\text{t}}/R_{i,c}\right)\left(R^2_{\text{f1}}V_{\text{f2}} + R^2_{\text{f2}}V_{\text{f1}}\right)} & \text{for } \alpha = 2 \\ \dfrac{E_{\text{f1}} n_{1_{i,c}} R^4_{\text{f1}} R^{-\alpha}_{i,c}\left(\alpha - 2\right)}{2E_{\text{f2}}\left(R^{2-\alpha}_{i,c} - R^{2-\alpha}_{\text{t}}\right)\left(R^2_{\text{f1}}V_{\text{f2}} + R^2_{\text{f2}}V_{\text{f1}}\right)} & \text{otherwise,} \end{cases} \\
I22_{i,c} &= \begin{cases} \dfrac{n_{2_{i,c}} R^2_{\text{f1}} R^2_{\text{f2}}}{2R^2_{i,c}\ln\left(R_{\text{t}}/R_{i,c}\right)\left(R^2_{\text{f1}}V_{\text{f2}} + R^2_{\text{f2}}V_{\text{f1}}\right)} & \text{for } \alpha = 2 \\ \dfrac{n_{2_{i,c}} R^2_{\text{f1}} R^2_{\text{f2}} R^{-\alpha}_{i,c}\left(\alpha - 2\right)}{2\left(R^{2-\alpha}_{i,c} - R^{2-\alpha}_{\text{t}}\right)\left(R^2_{\text{f1}}V_{\text{f2}} + R^2_{\text{f2}}V_{\text{f1}}\right)} & \text{otherwise,} \end{cases} \\
I12_{i,c} &= \begin{cases} \dfrac{E_{\text{f2}} n_{2_{i,c}} R^4_{\text{f2}}}{2E_{\text{f1}}R^2_{i,c}\ln\left(R_{\text{t}}/R_{i,c}\right)\left(R^2_{\text{f1}}V_{\text{f2}} + R^2_{\text{f2}}V_{\text{f1}}\right)} & \text{for } \alpha = 2 \\ \dfrac{E_{\text{f2}} n_{2_{i,c}} R^4_{\text{f2}} R^{-\alpha}_{i,c}\left(\alpha - 2\right)}{2E_{\text{f1}}\left(R^{2-\alpha}_{i,c} - R^{2-\alpha}_{\text{t}}\right)\left(R^2_{\text{f1}}V_{\text{f2}} + R^2_{\text{f2}}V_{\text{f1}}\right)} & \text{otherwise,} \end{cases}
\end{aligned}
\tag{5.16}
$$

where R_{t} is the RVE equivalent radius, $R_{\text{t}} = \sqrt{(a \cdot b)/\pi}$.

To take into account the interaction between different clusters, a superposition rule is considered. The total *SCF* for an intact fibre element is obtained by the linear superposition of the *SCF* it receives from all clusters i,c. Nonetheless, to achieve stress continuity between elements inside any ineffective length

(elements where $0 < D_{p,q} < 1$) that are not affected by the *SCF*, and subsequent intact elements ($D_{p,q} = 0$), which can be overloaded by the *SCF*, the *SCF* of an element is limited according to shear-lag transfer [37, 260, 261]. Thus, the total *SCF* of an intact element p,q is

$$SCF_{p,q} = \begin{cases} \min\left(SCF^{0}_{p,q}, SCF^{\mathrm{L}}_{p,q}\right) & \forall p,q : D_{p,q} = 0 \\ 1 & \text{otherwise,} \end{cases} \tag{5.17}$$

where $SCF^{0}_{p,q}$ is the *SCF* predicted by the linear superposition of the contribution of all clusters, taking into account the dynamic effect using the previous δ and λ functions with

$$\begin{aligned} SCF^{0}_{p,q} &= 1 + \sum_{i=1}^{N_p} \sum_{c=1}^{N_i^c} M_{1_{i,c}} \delta 11_{(q-c)} \lambda 1_{(p-i)} + M_{2_{i,c}} \delta 12_{(q-c)} \lambda 2_{(p-i)} \ldots \\ &\ldots \quad \forall i,c : n_{i,c} > 0 \quad \& \quad q \in \mathrm{f1} \\ SCF^{0}_{p,q} &= 1 + \sum_{i=1}^{N_p} \sum_{c=1}^{N_i^c} M_{2_{i,c}} \delta 22_{(q-c)} \lambda 2_{(p-i)} + M_{1_{i,c}} \delta 21_{(q-c)} \lambda 1_{(p-i)} \ldots \\ &\ldots \quad \forall i,c : n_{i,c} > 0 \quad \& \quad q \in \mathrm{f2} \end{aligned} \tag{5.18}$$

where f1 and f2 are fibre populations 1 and 2, respectively, while $M_{1_{i,c}}$ and $M_{2_{i,c}}$ are the dynamic factors caused by new breaks in populations 1 and 2, respectively, in cluster i,c. As detailed at the beginning of this subsection, these factors are equal to 1 for any cluster i,c in which no new breaks occurred. Nevertheless, if any new broken elements of type 1 appear in cluster i,c, then $M_{1_{i,c}} = M_{\mathrm{d}}$. Similarly, if new broken elements of type 2 appear then $M_{2_{i,c}} = M_{\mathrm{d}}$. Therefore, many different combinations may occur because, an intact element may receive dynamic *SCF* from the two populations in the cluster or from only one of them, or it may receive dynamic *SCF* from one cluster and static *SCF* from another different cluster. Finally, $SCF^{\mathrm{L}}_{p,q}$ is the *SCF* limitation for broken fibre q, and it is calculated as in previous work [37, 260, 261]:

$$SCF^{\mathrm{L}}_{p,q} = \min\left(\frac{1}{L^{\mathrm{in}}_{i,q}} |i-p|\, l\right) \quad \forall i : D_{i,q} = 1 \tag{5.19}$$

5.2.2.5 Numerical implementation

A uniaxial strain controlled simulation is performed along the fibre longitudinal direction by slowly increasing the applied strain, ε^0. In this way, a progressive and stable damage process can be simulated. A step-by-step implementation of the model is shown in Algorithm 5.1. Before starting the simulation, the strength of each element is generated following a given statistical distribution, and if they are to be considered the thermal residual stresses are estimated, as given in lines 1-2 of the algorithm. After that, a new loading step is started by applying a uniaxial strain, see line 3. At each new iteration, y, of the model, the objective is to compute the stress of each element by following the procedure shown in lines 5-11 of the algorithm. Next, the stresses are compared with the strengths, as given in line 12. At this point two possibilities may arise: 1) new elements fail and, consequently, lines 13-16 of the algorithm are applied, or 2) no new elements fail, and thus lines 18-20 are employed. If no new elements fail, then the algorithm applies static conditions, i.e. $M_{1_{p,c}} = 1$ and $M_{2_{p,c}} = 1$ for all clusters p, c. Then a new static step, is started by increasing the applied strain. However, if new elements fail, a damage factor equal to 1 is assigned to all new broken elements. Then, all clusters p, c are determined. For the clusters p, c with new breaks of type 1, $M_{1_{p,c}} = M_{\mathrm{d}}$. Similarly for the clusters p, c with new breaks of type 2, $M_{2_{p,c}} = M_{\mathrm{d}}$ is assigned. For all clusters with no new breaks $M_{1_{p,c}} = 1$ and $M_{2_{p,c}} = 1$. The algorithm then starts a dynamic iteration by repeating the whole process. The process shown continues until either all elements in a plane are broken, or the average fibre stress of the HE fibre population has decreased in a single step, t, by a pre-defined percentage of the maximum load value. A small decrease of 10%, is enough to capture the final failure of the material and also allows computational time to be reduced.

5.3 Methodology

To study the influence both thermal residual stresses and dynamic phenomenon have on the tensile failure of hybrid composites, different materials are simulated using the PFM. To quantify their importance separately, the tensile behaviour is simulated three times: a) under static conditions (i.e. $M_{\mathrm{d}} = 1$) and without thermal residual stresses, b) under static conditions with thermal residual stresses, and c) under dynamic conditions (i.e. $M_{\mathrm{d}} \neq 1$) and without thermal residual

Algorithm 5.1 Progressive Failure Model algorithm

Input: RVE domain and model data (material properties, model options, etc.)
Output: Stress-strain curve, break density, cluster progression, etc.

1: Generate the strength of each element, $\sigma^{\mathrm{u}}_{p,q}$
2: Calculate thermal residual stresses with Eq. (5.3) if considered
3: Start new step $t+1$: increase ε^0
4: Start new iteration $y+1$
5: Estimate $k_{p,q}, k_{p_1}, k_{p_2}, k_p, K, \varepsilon_p$ with Eqs. (5.5)–(5.8) using the latest known values of damage, $D_{p,q}$
6: **if** There are broken elements **then**
7: Calculate $L^{\mathrm{in}}_{p,q}, D_{p,q}$ of broken fibres with Eqs. (5.10) and (5.11) if the matrix is plastic, or Eqs. (5.12) and (5.13) if it is elastic
8: Calculate SCF with Eqs. (5.14)–(5.19) using the latest known values of $M_{1_{p,c}}$ and $M_{2_{p,c}}$
9: Re-calculate $k_{p,q}, k_{p_1}, k_{p_2}, k_p, K, \varepsilon_p$ with Eqs. (5.5)–(5.8) using the updated values of damage, $D_{p,q}$
10: **end if**
11: Calculate Ω_p and $\sigma_{p,q}$ with Eqs. (5.4) and (5.9)
12: **if** Any $\sigma_{p,q} > \sigma^{\mathrm{u}}_{p,q}$ **then**
13: Set $D_{p,q} = 1$ to all new broken elements
14: Determine all clusters p, c
15: For all clusters p, c in which new broken elements of type 1 appeared, $M_{1_{p,c}} = M_{\mathrm{d}}$. For all clusters p, c in which new broken elements of type 2 appeared, $M_{2_{p,c}} = M_{\mathrm{d}}$. For all clusters with no new breaks, $M_{1_{p,c}} = 1$ and $M_{2_{p,c}} = 1$
16: Start dynamic iteration: go to line 4 if end criteria is not met, otherwise go to line 22
17: **else**
18: Set all $M_{1_{p,c}} = 1$ and $M_{2_{p,c}} = 1$
19: Reset iteration counter: $y = 0$
20: Start new static iteration: go to line 3 if end criteria is not met, otherwise go to line 22
21: **end if**
22: Output simulation data and stop

stresses. For the dynamic cases, the value of M_{d} is varied between 1.25, 1.43, 1.6 and 2. These values are taken from the literature: 1.43 corresponds to the average result given in Tavares *et al.* [63] using a plastic matrix, while 1.6 corresponds to the result of Hedgepeth [56] and 2 is a theoretical maximum factor for a spring-mass system without damping [62]. Likewise for the thermal residual stresses, two extreme values (a lower bound and an upper bound) for the

coefficient of thermal expansion of both LE and HE fibres in the materials are used to observe their impact. To calculate them, the test temperature is assumed to be $T = 25°C$, whereas the stress-free temperature is $T_r = 150°C$.

To observe the impact of the dynamic phenomenon and thermal residual stresses with diverse material properties, different intrayarn hybrid unidirectional composites are simulated by combining various carbon and glass fibres. These hybrids correspond to X5-T300 (Carbon-Carbon), T300-Eglass (Carbon-Glass) and X5-Eglass (Carbon-Glass). These material combinations are interesting as, in all cases, the failure strain of both fibre populations should be fairly well apart, and all LE fibres have a relatively small Weibull modulus which is known to be positive for the hybrid effect [33–35]. In all cases, the matrix is always Epoxy with properties $E_m = 3760$ MPa, $\tau_q = 50$ MPa and $\alpha_m = 58 \cdot 10^{-6}\ °C^{-1}$ [35, 265]. The corresponding properties of each fibre can be seen in Table 5.1.

Fibre type	Fibre properties				Weibull parameters		
	E_f [GPa]	R_f [μm]	α_f [$°C^{-1}$] Low	α_f [$°C^{-1}$] High	m [-]	σ_0 [MPa]	L_0 [mm]
T300	232	3.5	$-0.7 \cdot 10^{-6}$	$0.7 \cdot 10^{-6}$	5.10	3170	25
X5	520	5.05	$-0.7 \cdot 10^{-6}$	$0.7 \cdot 10^{-6}$	6.1	2500	25
Eglass	72	8	$5 \cdot 10^{-6}$	$10 \cdot 10^{-6}$	13	2500	25

Table 5.1: Fibre properties.

A modified version of Melro's random fibre generator [35, 124] is used to create an RVE of width, thickness and length of (respectively) $75 \times 75 \times 300$ times the largest fibre radius on the RVE. The element length, l, is equal to the smallest fibre diameter in the RVE. The overall volume fraction (V_f) is always 60%. However, because the Hybrid Volume Fraction (HVF) is known to have a considerable impact on the tensile response of hybrid composites [27, 31, 34, 35, 261], each hybrid is simulated with an HVF of 10, 20, 30, 40, 50 and 75%. Here, the HVF is the percentage of LE fibre volume fraction (V_{LE}) over the total volume fraction (V_f), $HVF = (V_{LE}/V_f)$. In addition, a non-hybrid composite of each fibre type is also simulated.

As in other work [37, 39, 41, 260, 261], the strength of each element in the RVE is given by a Weibull distribution [103]. To generate them, a random number between 0 and 1 is assigned for each element, $P_{p,q}$. The strength of the element, $\sigma^u_{p,q}$, is then computed according to the Weibull distribution function with $P_{p,q} = 1 - \exp\left(-\left(l/L_0\right)\left(\sigma^u_{p,q}/\sigma_0\right)^m\right)$, using the corresponding Weibull

properties, σ_0, m, L_0 of the fibre given in Table 5.1. Because of the random nature of the fibre strength and the random position of the fibres, 8 runs are performed for each case in study. For each run, a new RVE and new element strengths are generated. However, the same RVEs and fibre strengths are used for the static, dynamic and thermal residual stress cases to allow for a fair comparison between them.

To compare the results between simulations, different metrics are used [261]. Firstly, the failure strength, σ^{ult}, which corresponds to the maximum stress reached by the material. Secondly, the failure strain, ε^{ult}, which corresponds to the strain at σ^{ult}. Thirdly, the yield stress (σ^{y}), which is defined as the knee point at a strain of 0.1% where the stress-strain curve deviates from the initial linear elastic region. And fourthly, the pseudo-ductile strain ($\varepsilon^{\text{d}} = \varepsilon^{\text{ult}} - \sigma^{\text{ult}}/E_0$), where E_0 is the initial Young's modulus of the composite given by the rule of mixtures.

The fifth metric is the maximum cluster of broken fibres in the RVE, N^{c}, at failure. To track these clusters along the simulation, it is assumed that two broken elements belong to the same cluster if their distance between centres is smaller than 4 times the smallest fibre radius and the distance between break planes is less than 10 times the smallest fibre radius [33, 37, 39, 41, 261]. A cluster is assumed to be co-planar if the axial distance between all brake planes in the cluster is smaller than or equal to one element length, otherwise it is a diffuse cluster [39, 41]. It should be noted that, the maximum cluster size shown in the results is different from the cluster definition that was used in section 5.2.2.3 to calculate the *SCFs* and ineffective length. This was done to allow the damage evolution to be measured in the same way as it has been done in the literature.

It is worth mentioning that the RVE volumes used in this study, which are as small as $0.26 \times 0.26 \times 1.05$ mm and as large as $0.6 \times 0.6 \times 2.4$ mm, and contain as few as 1100 fibres and as many as 4500 fibres, are small compared to a real material specimen. Due to the size effects present in composite materials, the strengths obtained, σ^{ult}, may not be representative of real composites. Moreover, the Weibull distribution used to calculate the fibre strengths is extrapolated to the element length, l, which is very small. This is known to cause an overprediction of the strength. Further discussion related to size effects and Weibull distribution

issues can be found elsewhere [5, 37].

5.4 Results

In this section the influence both thermal residual stresses and dynamic effects have on the failure process and cluster development of broken fibres for the different hybrids simulated is analysed. All results correspond to the average of 8 runs.

5.4.1 Dynamic effects

Overall, the maximum cluster size, shown in Fig. 5.2 a)-c), increases with the dynamic factor. In general, this increase seems to be larger for the composites that are less damage tolerance, i.e. the non-hybrid composites and the hybrids with larger *HVF*. Nevertheless, the formation of co-planar clusters shown in Fig. 5.2 d)-f) presents a negligible variation for the dynamic factor.

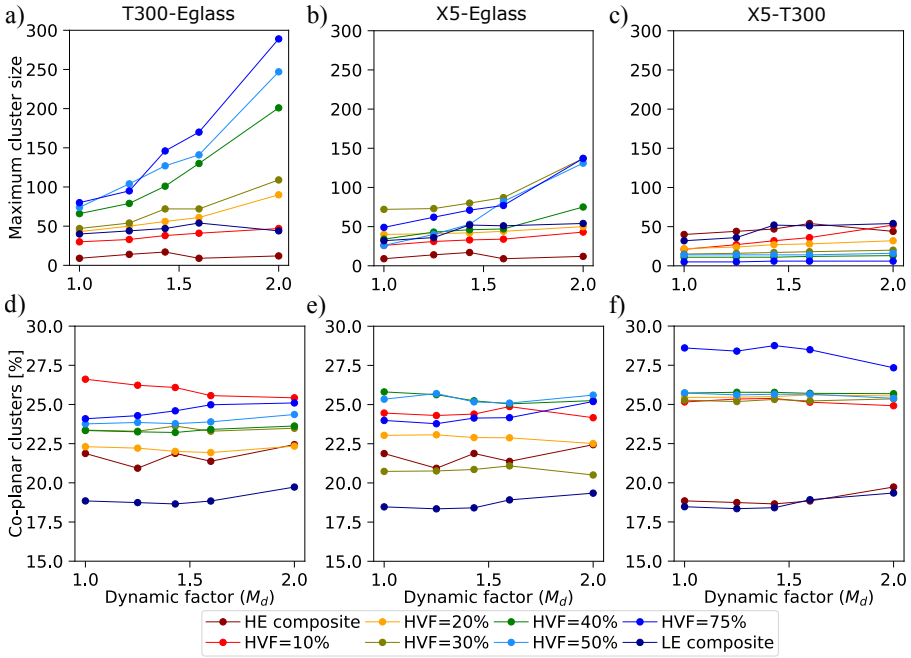

Figure 5.2: Effect of the dynamic factor on the formation of clusters. From a) to c), the maximum cluster size, in number of broken fibres, is shown within the T300-Eglass, X5-Eglass and X5-T300 composites respectively. From d) to f), the percentage of co-planar clusters are shown within the T300-Eglass, X5-Eglass and X5-T300 composites respectively. The average of 8 runs is shown for each material configuration.

The influence of the dynamic effects on the failure strain and ductile strain is shown in Fig. 5.3. Overall, there is a minor decrease in the failure strain when the dynamic factor is increased. For both the X5-Eglass and X5-T300 composites, shown in Fig. 5.3 b) and c), the decrease in failure strain is larger for the non-hybrid composites than it is for the hybrids. However, this does not occur with the T300-Eglass composite shown in Fig. 5.3 a), which presents a larger decrease of failure strain for the hybrid composites with $HVF = 10\%$ and $HVF = 20\%$ than it does for the non-hybrids when $M_{\mathrm{d}} = 2$. Regarding the ductile strain, similar trends are highlighted. In general, there is a minor decrease in the ductile strain when the dynamic factor is increased. This decrease is seen to be larger for the T300-Eglass hybrid composites with $HVF = 10\%$ and $HVF = 20\%$.

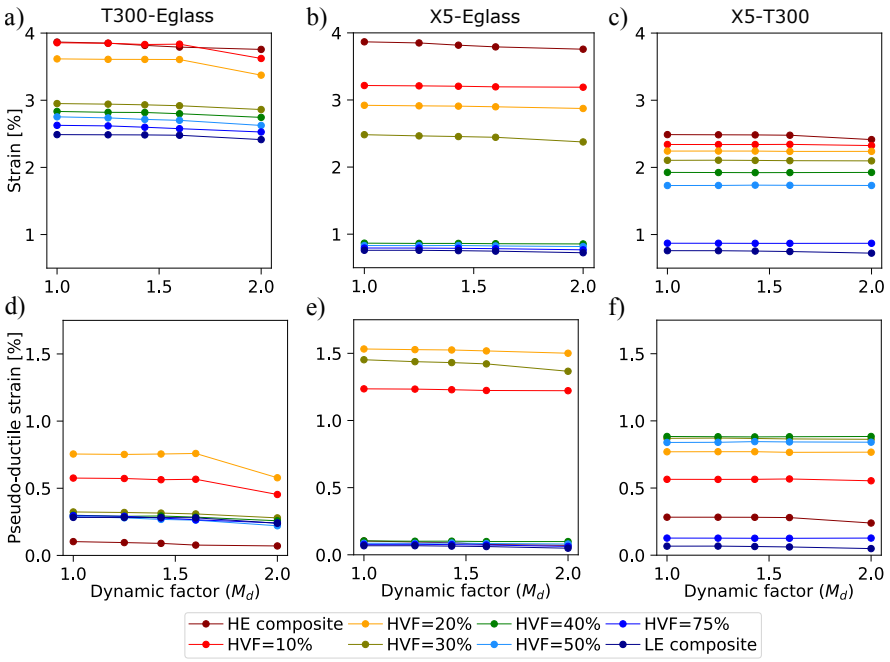

Figure 5.3: Effect of the dynamic factor on the failure strain and ductile strain. From a) to c), the failure strain is shown within the T300-Eglass, X5-Eglass and X5-T300 composites respectively. From d) to f), the ductile strain is shown within the T300-Eglass, X5-Eglass and X5-T300 composites respectively. The average of 8 runs is shown for each material configuration.

The failure stress and yield stress of the simulated composites is shown in Fig. 5.4. As with the failure strain, the failure strength also presents a small decrease when increasing the dynamic factor, although the decrease is mostly negligible.

In regards to the yield stress, no changes at all are observed for the hybrid composites.

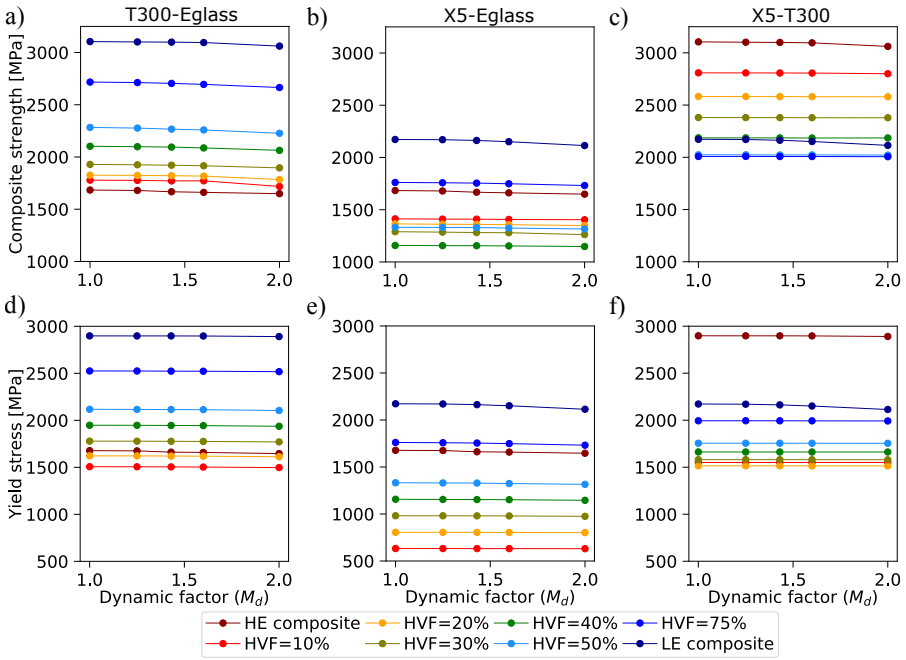

Figure 5.4: Effect of the dynamic factor on the failure stress and yield stress. From a) to c), the failure stress is shown within the T300-Eglass, X5-Eglass and X5-T300 composites respectively. From d) to f), the yield stress is shown within the T300-Eglass, X5-Eglass and X5-T300 composites respectively. The average of 8 runs is shown for each material configuration.

The tensile behaviour predicted for each composite is seen to be very different and to be heavily dependent on the *HVF*, as illustrated in Fig. 5.5. A large pseudo-ductile strain of 0.6-0.8% is predicted with the X5-T300 hybrid for an *HVF* of between 10-50%, whilst at larger *HVF*, brittle behaviours are obtained. An even larger pseudo-ductile strain of 1.25-1.5% can be observed for the X5-Eglass composite for an *HVF* of between 10-30%. For the last hybrid studied, T300-Eglass, a ductile strain of 0.6-0.8% for an *HVF* of between 10-20% is found. As has been discussed, the dynamic effects lead to a slightly earlier failure, but do not significantly change the tensile behaviour.

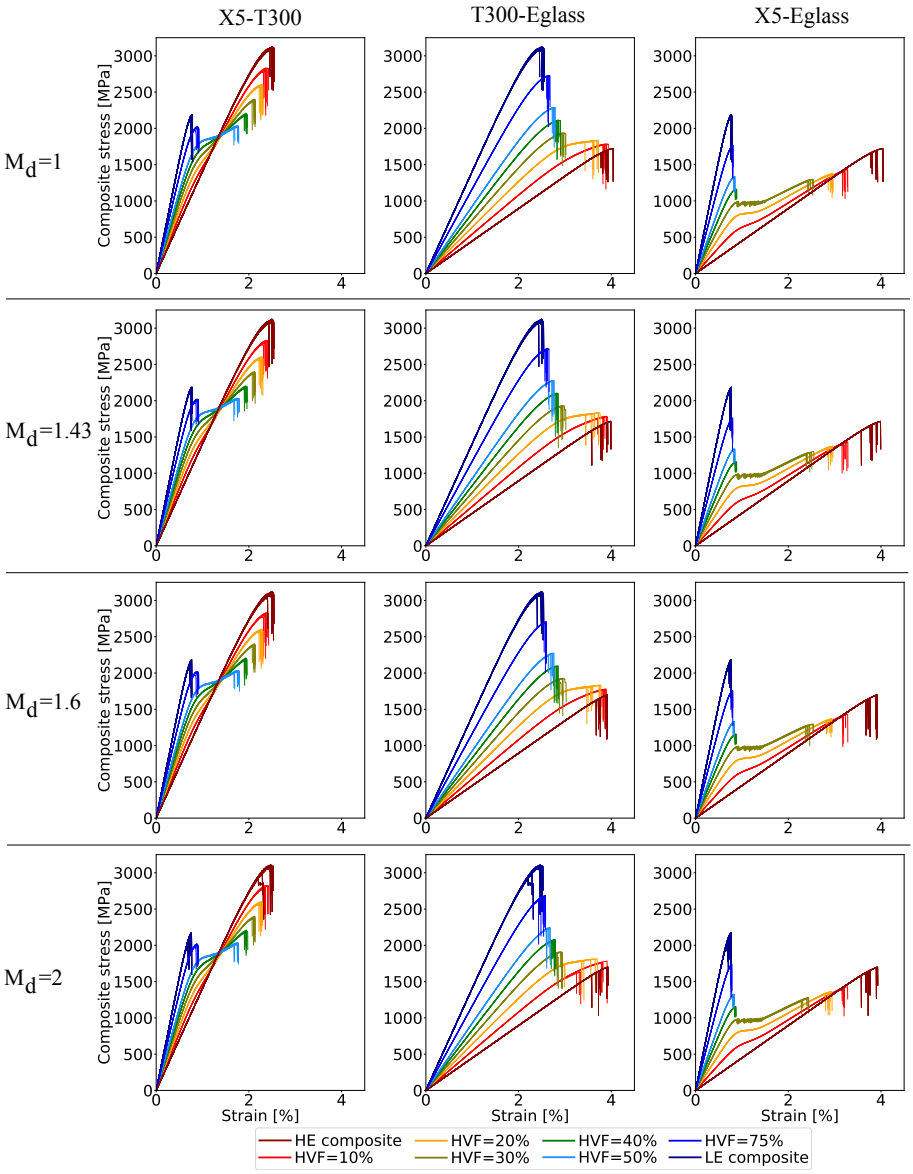

Figure 5.5: Simulated stress-strain curves with each hybrid composite material for different dynamic factors, M_{d}.

5.4.2 Thermal residual stresses

The influence thermal residual stresses have on the formation of clusters is shown in Fig. 5.6. Overall the thermal residual stresses do not have a significant impact on cluster formation. The maximum variation in cluster size can be seen for the X5-Eglass hybrid composite for $HVF = 30\%$, showing a change of 10

fibres compared to the case without thermal residual stresses. For the co-planar clusters, the variation is less than 1% for all composites.

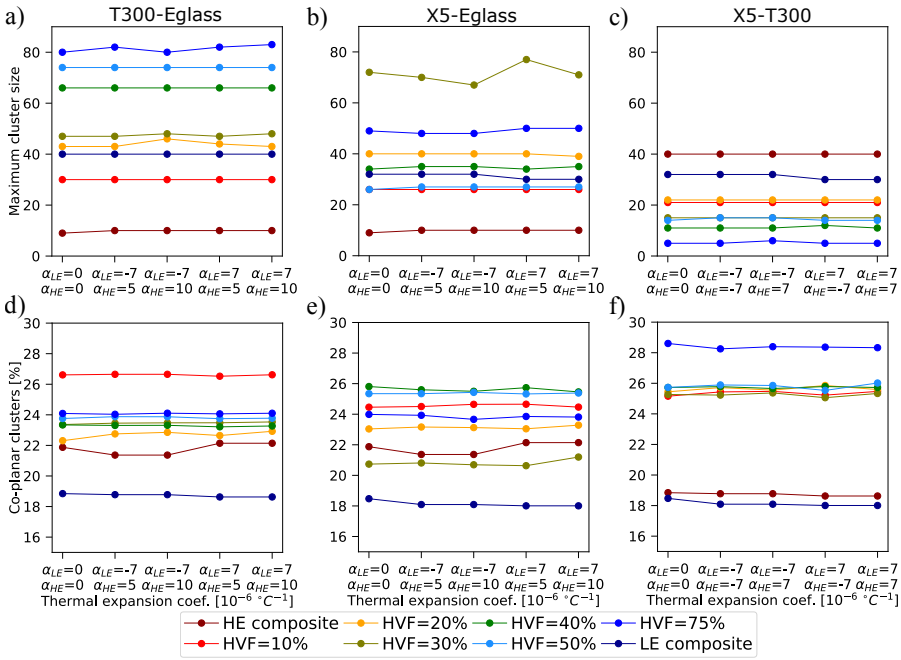

Figure 5.6: Effect of the thermal residual stresses on the formation of clusters. From a) to c), the maximum cluster size, in number of broken fibres, is shown within the T300-Eglass, X5-Eglass and X5-T300 composites respectively. From d) to f), the percentage of co-planar clusters are shown within the T300-Eglass, X5-Eglass and X5-T300 composites respectively. The average of 8 runs is shown for each material configuration.

The influence of thermal residual stresses on the failure and ductile strains is shown in Fig. 5.7. In some composites a minor variation of these two strains is seen when the residual stresses are considered. For the X5-T300 composite, the failure strain and ductile strain present a minor increase when $\alpha_{\mathrm{LE}} = 7 \cdot 10^{-6}\ ^{\circ}C^{-1}$ and $\alpha_{\mathrm{HE}} = -7 \cdot 10^{-6}\ ^{\circ}C^{-1}$ and a small decrease for the opposite combination. For the other two combinations of α_{LE} and α_{HE}, the results lie somewhere in between. The same trend is seen for the X5-Eglass and T300-Eglass composites. The ductile composites, corresponding to $HVF = 10-30\%$, experience an increase in failure strain and ductile strain when $\alpha_{\mathrm{LE}} = 7 \cdot 10^{-6}\ ^{\circ}C^{-1}$ and $\alpha_{\mathrm{HE}} = 5 \cdot 10^{-6}\ ^{\circ}C^{-1}$, and a decrease when $\alpha_{\mathrm{LE}} = -7 \cdot 10^{-6}\ ^{\circ}C^{-1}$ and $\alpha_{\mathrm{HE}} = 10 \cdot 10^{-6}\ ^{\circ}C^{-1}$.

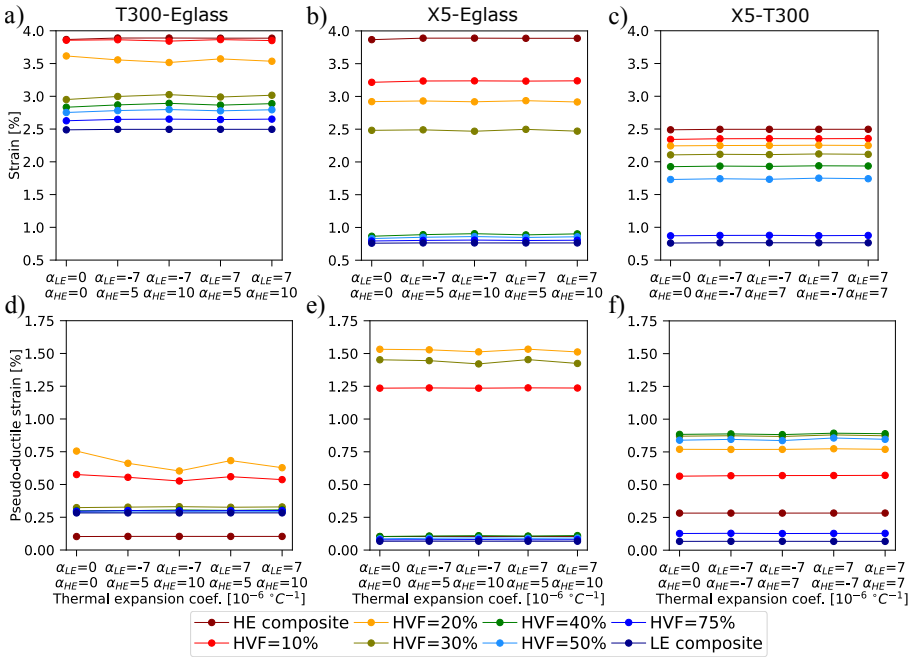

Figure 5.7: Effect of the thermal residual stresses on the failure strain and ductile strain. From a) to c), the failure strain is shown within the T300-Eglass, X5-Eglass and X5-T300 composites respectively. From d) to f), the ductile strain is shown within the T300-Eglass, X5-Eglass and X5-T300 composites respectively. The average of 8 runs is shown for each material configuration.

In regards to the failure stress and yield stress shown in Fig. 5.8, a minor variation can also be observed with the thermal residual stresses. For the X5-T300 composite, the strength and yield stress are the largest when $\alpha_{\mathrm{LE}} = -7 \cdot 10^{-6}$ $^{\circ}C^{-1}$ and $\alpha_{\mathrm{HE}} = 7 \cdot 10^{-6}$ $^{\circ}C^{-1}$, while they are the smallest when $\alpha_{\mathrm{LE}} = 7 \cdot 10^{-6}$ $^{\circ}C^{-1}$ and $\alpha_{\mathrm{HE}} = -7 \cdot 10^{-6}$ $^{\circ}C^{-1}$. Similarly, for the X5-Eglass and T300-Eglass the maximum occurs when $\alpha_{\mathrm{LE}} = -7 \cdot 10^{-6}$ $^{\circ}C^{-1}$ and $\alpha_{\mathrm{HE}} = 10 \cdot 10^{-6}$ $^{\circ}C^{-1}$ and the minimum for the opposite combination. For the other combinations of coefficient of thermal expansion, the results lie between these.

The tensile behaviour obtained is not shown since it is qualitatively the same as that illustrated in Fig. 5.5.

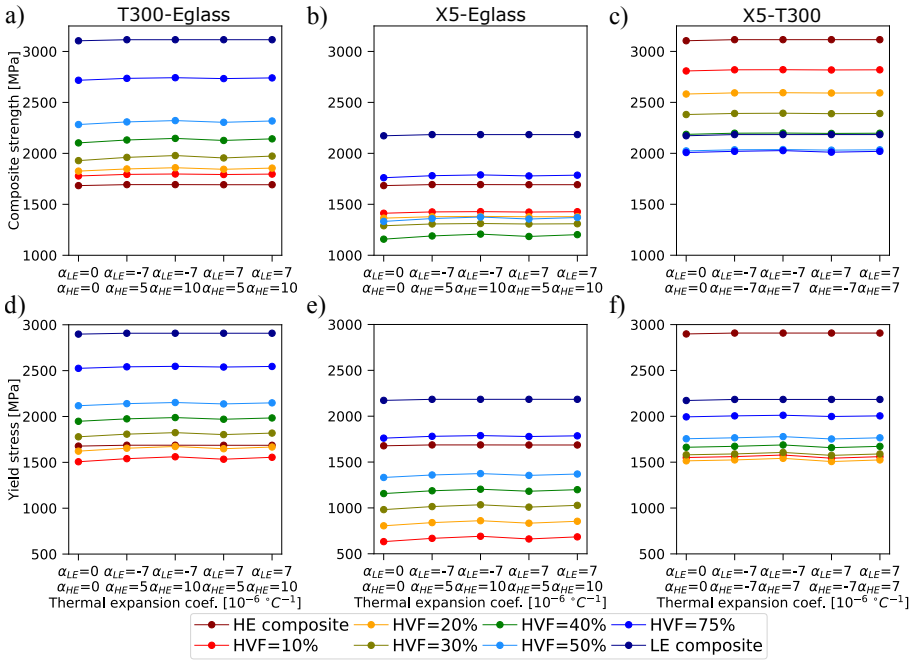

Figure 5.8: Effect of the thermal residual stresses on the failure stress and yield stress. From a) to c), the failure stress is shown within the T300-Eglass, X5-Eglass and X5-T300 composites respectively. From d) to f), the yield stress is shown within the T300-Eglass, X5-Eglass and X5-T300 composites respectively. The average of 8 runs is shown for each material configuration.

5.5 Discussion

5.5.1 Influence of dynamic effects

As proved in Fig. 5.2, the maximum cluster size increases as the dynamic factor does. This can be easily understood. Since increasing the dynamic factor leads to higher *SCF*, the probability of creating larger clusters is also greater. These findings imply that the dynamic effects change the damage development of the materials, leading to an earlier formation of larger clusters in the dynamic model than in the static model. This emphasises the importance of including dynamic effects. Considering them should, in theory, lead to a more realistic formation of clusters compared to experiments. Nevertheless, the formation of co-planar clusters is seen to be unaffected by the dynamic effects. Thus, increasing the dynamic factor does not increase the formation of co-planar clusters, as was supposed in the literature [5, 41]. This corresponds well to the recent findings

of Tavares *et al.* [63]. Such outcomes suggest that, the underprediction of co-planar clusters seen in most of the models in the literature may not be related to the omission of dynamic effects. It should be noted that the formation of clusters depends on the specific RVE and fibre strengths of each run. In other words, owing to the variability of the results, some of the curves in Fig. 5.2 may intersect.

As evidenced in Fig. 5.3, a minor decrease in the failure strain and ductile strain occurs when considering dynamic effects. In some hybrid composites such as the X5-Eglass and X5-T300, the decrease in failure strain is larger for the non-hybrid composites than for the hybrids, which suggests the presence of a small positive hybrid effect caused by the dynamic effects. However, this does not occur with the T300-Eglass composite which presents a larger decrease of failure strain for the hybrid composites comprising a low *HVF*. These results suggest that, although the dynamic effects change the formation of clusters, they do not have any significant influence on the final failure or on the ductility of the composite. This is something that corresponds well to the findings of Tavares *et al.* [63] in non-hybrid composites using an elasto-plastic matrix.

A minor decrease in strength is also seen when considering the dynamic effects as illustrated in Fig. 5.4. The yield stress presents no changes at all due to the dynamic effects. This is because the yield stress depends mainly on the initiation of damage when the number of breaks is still small. At that point, the dynamic effects are not important.

The tensile behaviour predicted for each composite, shown in Fig. 5.5, proves that a ductile failure process can be achieved via fibre hybridisation. A very large ductile strain between 1.25-1.5% is obtained with the X5-Eglass composite for an *HVF* between 10-30%. That large pseudo-ductile strain is possible thanks to the fact that the failure strain of the two fibres in the hybrid is well apart, and the failure process is continuous. In any case, it can be seen that the dynamic effects lead to a slightly earlier failure, but do not significantly change the tensile behaviour.

The results obtained show that the dynamic phenomenon has an effect on the formation of clusters, leading to larger clusters at smaller strains compared to the static model. Nonetheless, final failure is not significantly altered, as the failure

strain and strength are marginally smaller in the dynamic model. The tensile behaviour is also seen to be unaffected. This contradicts the general belief in the literature that the dynamic effects considerably influence final failure [5, 41]. Additionally, if the dynamic factor is smaller in the hybrid composites than that of the baseline non-hybrid composites, as the work of Xing *et al.* [26] suggests, hybrid effects should occur due to the dynamic phenomenon. However, the results presented by varying the dynamic factor, M_{d}, show a very reduced effect. Therefore, the contribution the dynamic phenomenon makes to the hybrid effect seems to be very small. These results have been obtained by using a plastic matrix approach. Using an elastic matrix should lead to the dynamic effects having a greater influence on final failure, as pointed in Tavares *et al.* [63]. Nonetheless, a plastic matrix should be a more realistic representation of the failure process [261]. Adding the dynamic effects should allow a more accurate formation of clusters and, consequently, should be a step forward in modelling predictions.

5.5.2 Influence of thermal residual stresses

As evidenced in Fig. 5.6, the thermal residual stresses do not change damage progression. However, as shown in Fig. 5.7, they can have a minor influence on the failure and ductile strains. In some material combinations, the failure strain and ductile strain increase when the thermal residual stresses are considered. These changes can be understood as being due to the magnitude of the thermal residual stresses. For the X5-T300 hybrid composites, when $\alpha_{\mathrm{LE}} = 7 \cdot 10^{-6}\ ^{\circ}C^{-1}$ and $\alpha_{\mathrm{HE}} = -7 \cdot 10^{-6}\ ^{\circ}C^{-1}$, the HE fibre residual stress is either compressive, or it is tensile albeit smaller than in the other combinations. This, in turn, causes a delay in the initiation of damage for the HE fibre compared to the other scenarios, thus leading to an increase in the failure strain and ductile strain. However, since the magnitude of the thermal stresses is small, the variation in the final failure is very reduced. A similar effect occurs with the X5-Eglass and T300-Eglass composites. When $\alpha_{\mathrm{LE}} = 7 \cdot 10^{-6}\ ^{\circ}C^{-1}$ and $\alpha_{\mathrm{HE}} = 5 \cdot 10^{-6}\ ^{\circ}C^{-1}$, smaller residual stresses in the HE fibre are again induced compared to the other combinations when the *HVF* is low. Therefore, either inducing compressive stresses or smaller tensile stresses into the HE fibre should delay the initiation of damage in the HE fibre, leading to an increase in failure strain and ductile strain.

A similar effect is seen with the failure strength and yield stress. This is again controlled by the magnitude of the thermal residual stresses. Introducing compressive stresses into the LE fibre increases the yield stress and failure strength because the initiation of damage in the LE fibre is delayed. This in itself should also increase the hybrid effect, as pointed out in the literature [7, 8, 22].

The results obtained suggest that the thermal residual stresses have a negligible effect on cluster formation and damage evolution. Nonetheless, they can have a minor effect on final failure [3, 7, 22]. Inducing compressive residual stresses for the LE fibre increases the failure strength and yield stress of the material. Likewise, introducing compressive stresses into the HE fibre increases the failure and ductile strains. A combination of the two cases should lead to the best overall behaviour.

5.6 Conclusions

In this work, a progressive failure model including dynamic effects and thermal residual stresses was developed. The model was used to study the effect the dynamic phenomenon and thermal residual stresses have on the fibre tensile failure process and cluster development of intrayarn hybrid unidirectional composite materials.

Different metrics were used to characterise the failure process of the materials studied: ductile strain, failure strain, yield stress, failure stress, maximum cluster size and the percentage of co-planar clusters. The different hybrids simulated presented a different tensile behaviour, exhibiting a ductile response at low LE hybrid volume fractions. Composites with larger hybrid volume fractions were found to fail in a brittle manner.

The addition of thermal residual stresses had a negligible effect on cluster evolution and damage development. However, they can have some effect on the final failure of the material. Adding compressive residual stresses delays the damage initiation for the LE fibre, leading to an increase in the failure strength and yield stress of the material. That in itself leads to an hybrid effect. Likewise, adding compressive stresses to the HE fibre delays the initiation of damage in the HE fibre, increasing both the failure strain and ductile strain. Combining both scenarios in the right measure should lead to the best overall behaviour.

The dynamic effects were found to have a considerable influence on cluster formation and damage evolution compared to the static model. When the dynamic model was employed, larger clusters were always obtained. Thus, the formation of larger clusters occurred earlier in the dynamic model. This should lead to a more realistic formation of clusters compared to experiments, as was pointed out by Swolfs *et al.* [41]. Nonetheless, the influence on final failure was very minor, with a negligible decrease in failure strain and strength being noted. Despite their minor effect on final failure, a remarkable fact is that some hybrid composites experienced a smaller influence of the dynamic effects compared to the baseline non-hybrid composites, which suggests a small positive hybrid effect caused by the dynamic phenomenon. Therefore, the influence of the dynamic effects on final failure is very dependent on the material system. Although, the impact of the dynamic effect on final failure was negligible, adding dynamic effects should allow a more realistic prediction of cluster formation, thus closing the gap between models and experiments. However, at this point it is impossible to further validate the results from this work due to the lack of experimental data. The literature needs more experimental results, especially with hybrid composites, to be able to improve the available models.

Acknowledgments

The authors acknowledge P.P. Camanho, A.R. Melro and R.P. Tavares for their permission to use their random fibre generator. The authors acknowledge the financial support from the Spanish Ministerio de Economía, Industria y Competitividad (MINECO) under the project TRA2015-71491-R co-financed by the European Regional Development Fund (ERDF). In addition, the authors thank the financial support of the grant RTI2018-097880-B-I00 from the Spanish Ministerio de Ciencia, Innovación y Universidades. The first author also acknowledges the predoctoral Grant BES-2016-078270 from the 'Subprograma Estatal de Formación del MICINN' co-financed by the European Social Fund.

Data availability

The raw/processed data required to reproduce these findings cannot be shared at this time due to legal or ethical reasons.

6

Paper D – Size effects in hybrid unidirectional polymer composites under longitudinal tension: a micromechanical investigation

The paper has been submitted to *Composites Part A: Applied Science and Manufacturing*.

Overview

Another specific objective of this work is to investigate the influence that the specimen size has on the hybrid effect, formation of clusters and damage development in hybrid composites (i.e. the so-called size effect).

Currently it is well known that composite materials exhibit a size effect, which implies that their strength changes with the volume of the material [47–51, 54, 55, 266, 267]. This is an important phenomenon, since small specimens are commonly used to design larger structures. Although size effects have been greatly studied in non-hybrid composites, the importance that the specimen size has on the hybrid effect and damage development in hybrid composites is not clear [15].

In this Chapter, the influence that the specimen size has on the tensile behaviour and cluster development in hybrid unidirectional polymer composites is investigated using the dynamic PFM presented in previous Chapter 5. Results show that increasing the RVE length leads to an earlier failure and to a small decrease of ductility. However, the hybrid effect improves considerably. In contrast, increasing the RVE cross-section leads to smaller hybrid effects, may delay final failure and may increase the ductility of the material. Moreover, incrementing the RVE volume increases the critical cluster size, while the presence of ductility does not change the magnitude of the size effects.

Size effects in hybrid unidirectional polymer composites under longitudinal tension: a micromechanical investigation

Jose M. Guerrero[a,*], Joan A. Mayugo[a], Josep Costa[a], Albert Turon[a]

[a] *AMADE, Polytechnic School, Universitat de Girona, Campus Montilivi s/n, E-17003 Girona, Spain*

Abstract

While fibre hybrid composites result in hybrid effects and improved ductility compared to non-hybrid laminates, it is unclear how specimen size influences hybrid properties (i.e. the so-called 'size effect'). This paper addresses this phenomenon in a carbon-carbon hybrid composite by means of micromechanical modelling using a progressive failure model. Results demonstrate that increasing the length of the virtual specimen causes an earlier failure, slightly decreases the ductility and significantly improves the hybrid effect, whereas increasing the cross-section of the virtual specimen may delay final failure, may increase ductility and reduces the hybrid effect. In addition, increasing the coupon volume results in a higher maximum cluster size, while the presence of ductility does not alter the magnitude of the size effects.

keywords: Size effects, A. Hybrid, C. Computational modelling, C. Micromechanics

SUBMITTED PAPER. EMBARGO UNTIL PUBLICATION DATE

* Corresponding author

Paper submitted to: *Composites Part A (October 2019)*

7

Paper E – The influence the hybrid configuration has on damage development in hybrid polymer composites under fibre tensile loading

The paper is *in preparation for submission*.

Overview

The final objective of this work is to develop an algorithm capable of generating hybrid composites hybridised within an interlayer, intralayer or an intrayarn hybrid configuration with a random distribution of fibres. Derived from this, to study whether the hybrid configuration has any significant impact on the hybrid effect and damage development using the realistic fibre packing developed.

In a hybrid material, the LE and HE fibres can be hybridised on three different scales: interlayer, intralayer or intrayarn. Currently, many studies have found higher hybrid effects with higher dispersion of the fibres [8, 31, 64]. Since an intrayarn hybrid theoretically leads to the highest dispersion, hybridisation at that level should the most efficient. In contrast with this hypothesis, Swolfs *et al.* [31] found that an interlayer hybrid of alternating single fibre layers leads to higher hybrid effects than intralayer and intrayarn hybrids. Nevertheless, Swolfs *et al.* [31] did not check the influence the hybrid configuration has on the tensile behaviour of the material. In addition, there are currently no algorithms able to generate hybrid composites hybridised within an interlayer, intralayer or an intrayarn hybrid configuration with randomly distributed fibres.

In this Chapter, an algorithm able to generate intrayarn hybrid composites with randomly distributed fibres is extended to also generate interlayer and intralayer hybrids. The influence that the hybrid configuration has on the hybrid effect, tensile behaviour and cluster development in hybrid unidirectional polymer composites is investigated using the dynamic PFM presented in Chapter 5. Results show that an intrayarn hybrid leads to higher hybrid effects, yield stresses and strength. However, an interlayer and an intralayer hybrid lead to larger failure and ductile strains. Increasing the dispersion of the fibres improves the hybrid properties. In addition, the progressive failure model is validated by comparing it against experimental results of interlayer hybrid composites showing qualitatively a good agreement.

The influence the hybrid configuration has on damage development in hybrid polymer composites under fibre tensile loading

Jose M. Guerrero[a,*], Joan A. Mayugo[a], Josep Costa[a], Albert Turon[a]

[a] *AMADE, Polytechnic School, Universitat de Girona, Campus Montilivi s/n, E-17003 Girona, Spain*

Abstract

Fibre hybrid composites, obtained by mixing two fibres with different properties in a single matrix, are able to increase the ductility of non-hybrid composites. This mixture may take place at different scales, nonetheless, the effect that mixing the fibres at different scales has on the hybrid properties is not broadly explored. In this paper, the effect of hybridising the fibres at different scales is investigated by micromechanical modelling using randomly distributed fibres. Results show that an intrayarn hybrid configuration leads to higher hybrid effects, yield stresses and strengths. In contrast, an interlayer and an intralayer hybrid lead to larger failure and ductile strains. Increasing the dispersion of the fibres considerably improves the efficiency of the hybridisation. In addition, the micromechanical model used is validated by comparing it against experimental results of interlayer hybrid composites available in the literature showing qualitatively a good agreement.

keywords: Fibre dispersion, Hybrid configuration, Computational modelling, Micro-mechanics

SUBMITTED PAPER. EMBARGO UNTIL PUBLICATION DATE

* Corresponding author

Paper *in preparation for submission*

Part III

Discussion and concluding remarks

Results and discussion

8

This chapter summarises the results obtained from each paper and discusses them as a whole in accordance with the main objectives of the present thesis.

As demonstrated in Chapter 2, fibre hybridisation is a potential solution to the quasi-brittle behaviour and low toughness of composite materials. Nonetheless, there is a lack of micromechanical models able to simulate the tensile failure and damage development in hybrid unidirectional polymer composites under longitudinal loading with a low computational effort. For this reason, a new model called Progressive Failure Model (PFM) was developed. The modelling approach was used to study the influence that different parameters have on the longitudinal failure of hybrid composites, covering the objectives of this thesis.

The PFM is able to simulate the failure and damage development in hybrid and non-hybrid UD composites under longitudinal tension, and presents many features and advantages: it is computationally efficient against other models like SEM, it can qualitatively represent the entire stress-strain curve of the material, it captures the formation of clusters of fibre breaks, it considers a different deformation along the model accordingly to the number of fibre breaks and the associated stiffness loss, and finally the *SCF* and ineffective length are decoupled and given by analytical equations. This means that the PFM can be improved by modifying the analytical equations to calculate the *SCF* and ineffective length without reformulating the entire model. The PFM also presents different assumptions and inconveniences: it assumes that fibres work in parallel while planes work in series, considers that the loss of stiffness along the ineffective length is proportional to the expected stress recovery of the fibre, assumes that all fibres in a certain plane carry the same strain, etc. Along the thesis, the PFM, which was firstly presented in Chapter 3, was continuously refined by adding different phenomena. Firstly, more accurate models for predicting the stress redistribution around fibre breaks were presented in Chapter 4 and after that, dynamic effects and thermal residual stresses were included into the PFM in Chapter 5.

In Chapter 3, the first version of the PFM was presented. To validate the model, two non-hybrid composite materials consisting of T700S-Epoxy and

M40-Epoxy were simulated and compared against the experimental results of Swolfs *et al.* [41] and Koyanagi *et al.* [153], respectively. As discussed in Chapter 2, there exist different models for predicting the *SCF*. In the validation carried out in Chapter 3, the models of Eitan and Wagner [252], Zhou and Wagner [251] and Swolfs *et al.* [41] were considered for predicting the *SCF* in non-hybrid composites. These were chosen over others due to their simplicity and analytical form. The ineffective length was predicted with Kelly-Tyson shear-lag model [149]. This means that the *SCF* and the ineffective length were computed using different physical principles: while the *SCF* models assumed an elastic matrix, the ineffective length model was considering a plastic matrix. In addition, dynamic effects and thermal residual stresses were omitted.

RVEs of a width and thickness of 50, 100, 150 and 200 times the fibre radius were simulated (see Fig. 3.5). For the T700S composite the length of the RVE corresponded to the experimental specimen (1.54 mm), whereas for the M40 composite it was significantly smaller (25 mm in the PFM, but 150 mm in the experiment). Nevertheless, a first study suggested that the length used to simulate the M40 composite was long enough to properly represent the real material (the reader is referred to Fig. 3.6). As expected due to size effects, the failure strain and strength of the composites decreased by increasing the number of fibres in the RVE (Figs. 3.7 and 3.8). With the largest RVE simulated, the PFM slightly overpredicted the failure strain and strength compared to the experimental data for both non-hybrid composites, with the different *SCF* models considered (Fig. 8.1). Therefore, simulating an RVE closer to the real specimen dimensions should lead to a closer prediction of failure strain and strength. The two composites exhibited a different failure process, with the T700S presenting a larger stiffness loss than the M40 composite. This different failure was well highlighted by the fibre break density evolution presented in Fig. 8.1. In the case of the T700S, the fibre break density was heavily overpredicted compared to the experimental, which could be the consequence of inaccuracies in the experimental data, or inaccuracies/omissions in the model such as dynamic effects, size effects, matrix cracks, debonding, etc. This overprediction of fibre break density also explains the fact that the PFM predicts a more significant non-linearity in the stress-strain curve close to final failure than the experiments. Thus, the PFM exhibits the same gaps compared with experiments that other similar state of the art models show [4, 39, 41].

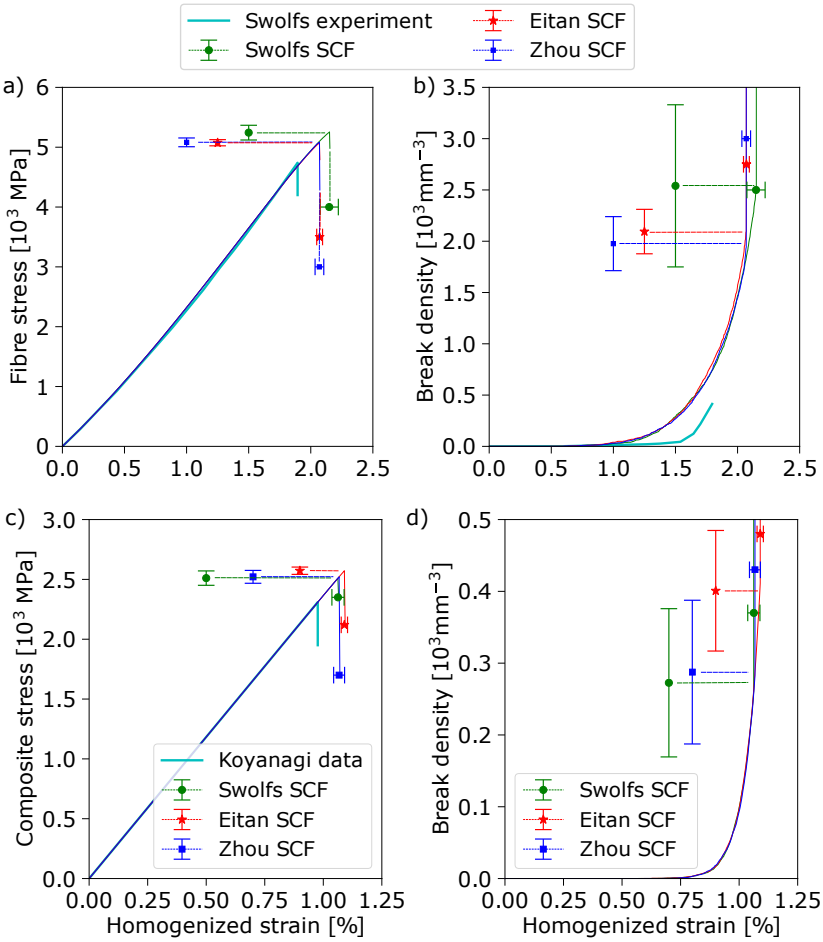

Figure 8.1: Predicted stress-strain and break density curves by the PFM compared with the experimental data. a)-b) T700S-Epoxy compared with Swolfs experimental data [41], c)-d) M40-Epoxy compared with Koyanagi data [153]. The closest curve to the average of forty runs is shown with 95% confidence intervals.

The different *SCF* models presented a distinct impact of the size effect. The Swolfs *SCF* model provoked a more localised stress redistribution, leading to a smaller size effect than the Zhou and Eitan models. In addition, the *SCF* model had a large influence on the formation of clusters (Fig. 3.10). Although with each model the clusters increased in size until failure, however, the clusters developed differently and in distinct locations along the model. Taking into account the comparison against the experimental data, it was not possible to conclude which *SCF* approach was more accurate.

Further to this, the PFM was validated by simulating an hybrid AS4-M50S

(carbon-carbon) epoxy composite and comparing it against the FEM of Tavares *et al.* [35]. Again, the first issue for performing this comparison was to define an appropriate *SCF* model, since in a hybrid material the load redistribution around fibre breaks depends on the stiffness of the fibres, the radius, and the volume fractions. To simplify the modelling, it was decided to take the results from Swolfs *et al.* [45], who provided the *SCF* for stiffness ratios of $E_j/E_q = 3.71$, $E_j/E_q = 1.85$ and $E_j/E_q = 1.0$, where E_j and E_q are the Young's modulus of the broken and intact fibre, respectively. Interpolation was then performed for obtaining the *SCF* for the ratios of $E_j/E_q = 2.05$ and $E_j/E_q = 0.49$ respectively, which corresponded to the ratios of the AS4-M50S hybrid to simulate (see Fig. 3.13). This means that the effect of the fibre radius and that of the volume fraction on the *SCF* was omitted. Moreover, these *SCF* were again considering an elastic matrix, whereas the ineffective length was plastic. Despite the different simplifications performed, the tensile stress-strain curves predicted by the PFM were qualitatively in good agreement compared with the FEM of Tavares *et al.* [35] (Fig. 8.2). However, while Tavares *et al.* FEM takes many days to be solved in a super-computer facility, the PFM only needed mere minutes. In addition, the results not only proved the capability of the PFM to capture the failure and damage development in hybrid composites, but also that fibre hybridisation can lead to a ductile failure. Pseudo-ductility was predicted for a *HVF* between 10 and 30%. The other composites either failed prematurely, or the interaction between fibres was not evident enough. These findings demonstrate that the PFM is able to capture fibre fragmentation, the formation of clusters, and the associated stiffness loss of a composite material. The discrepancies between the PFM and the FEM should be attributed to the omission of dynamic effects, as well as the simplified stress redistribution around breaks considered.

The validation performed in Chapter 3, highlighted that while the PFM compared well against literature results with hybrid and non-hybrid composites, there were some issues to be solved in the model. The ineffective length and *SCF* needed to be improved, to be consistent in between them (i.e. both considering an elastic matrix or both being plastic). Moreover, the *SCF* model had to be enhanced in order to inherently capture the geometrical and elastic properties of the fibres (instead of interpolating from a set of data), the effect of the *HVF* of the fibres, as well as the matrix behaviour. Finally, which *SCF* model was more accurate to predict failure was something to be determined. These issues were addressed

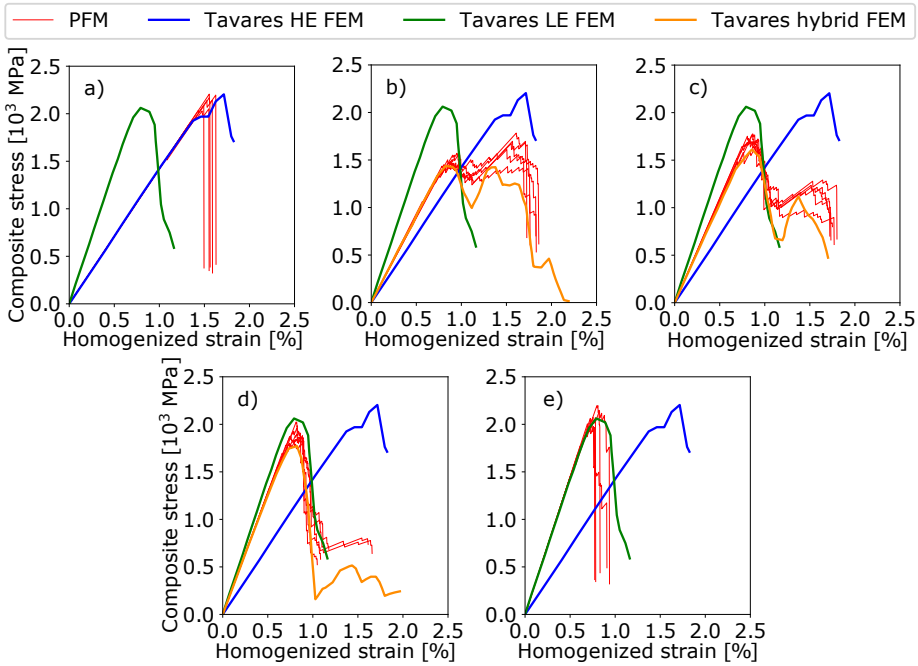

Figure 8.2: Predicted stress-strain curves by the PFM compared with the FEM of Tavares *et al.* [35]. a) *HVF*=0%, b) *HVF*=25%, c) *HVF*=50%, d) *HVF*=75% and e) *HVF*=100%. A total of five runs is shown.

in Chapter 4, as well as in a co-authored paper (not included in this thesis) with Tavares *et al.* [37], authors of the SEM.

In Tavares *et al.* [37], the PFM was improved by modifying the models to predict the *SCF* and ineffective length. Note that this did not require a reformulation of the model, since the ineffective length and *SCF* are 'interchangeable' parts in the PFM. To simulate a plastic matrix, the ineffective length and *SCF* were then calculated using the St-Pierre models [37, 198]. Instead, to simulate an elastic matrix, the ineffective length was then predicted using a modified Cox shear-lag model [37, 227], while the *SCF* was also computed using the St-Pierre model. This allowed the PFM to consider either an elastic or a plastic matrix with both ineffective length and *SCF* being consistent in between. In addition, the increase of ineffective length with cluster size [37] was also taken into account. Compared with the SEM, the enhanced PFM was in good agreement with both matrix behaviours, however, the PFM was significantly faster computationally. Moreover, the *SCF* model of Zhou and Wagner [251] was seen to be inaccurate, while the one of Swolfs *et al.* [41] was close to the results of SEM with an

elastic matrix only for certain material combinations. Overall, the St-Pierre *SCF* model [198] was in excellent agreement with the SEM [37], and thus, it is the most accurate analytical *SCF* model available.

Since the *SCF* model of St-Pierre *et al.* [198] was limited to non-hybrid composites, in Chapter 4 the model was modified for simulating hybrid composites as well. The reformulated *SCF* model is very powerful since it considers all the main effects influencing the stress redistribution around fibre breaks in hybrid composites: the cluster size, RVE size, volume fractions, fibre radius and elastic properties of each fibre population with simple analytical equations. Moreover, it can represent different matrix behaviours or effects not present into the model. The model is derived assuming that the overload carried by an intact fibre due to a break does not depend on its Young's modulus and radius. Moreover, the ineffective length used for a plastic matrix, and that for an elastic matrix, was also slightly adapted to take into account the presence of different fibres in the composite. This changes allowed the PFM to be more robust, and solve some of the modelling issues raised in Chapter 3. For more in-depth details, the reader is referred to Chapter 4. The improved PFM was used to study the load redistribution around fibre breaks, as well as the tensile behaviour, for diverse hybrid composites and as a function of the matrix behaviour. To do this, three hybrid materials were considered: AS4-Eglass, M50S-AS4 and AS4-T800G, all with epoxy matrix. To validate the model, the results were compared with Tavares *et al.*'s SEM [37, 39]. For further details of the materials and cases studied, the reader is referred to Section 4.3.

The results from Chapter 4 demonstrate that the *SCF* carried by intact fibres around broken fibres with a different stiffness is affected by the stiffness ratio of both fibres (for this the reader is referred to Figs. 4.3 and 4.4). If the HM fibre is broken, a larger ratio between the stiffness of the HM over the LM fibre increases the *SCF* on LM fibres. Oppositely, when the LM fibre is broken, a larger ratio decreases the *SCF* on HM fibres. This agrees well with Swolfs *et al.* [31, 45]. Since the HM fibres usually correspond to the LE fibres, increasing the stiffness ratio should help to increase the hybrid effect. Overall, adding LM fibres decreases the *SCF* on HM fibres. This occurs since the HM fibres are more surrounded by LM fibres, and thus, more LM fibres share the load, decreasing the *SCF* on HM fibres. This implies that a lower *HVF*

should increase the hybrid effect, as it is already well known in the literature [9, 27, 31, 34, 35, 64, 65]. Likewise, when a HM fibre is broken, the *SCF* carried by LM fibres is larger than that of the HM fibres, which should also increase the hybrid effect. These findings prove that the presence of fibres with different mechanical properties heavily influence the stress redistribution around breaks. Another remarkable fact is that the *SCFs* are smaller for both LM and HM fibres when the LM fibre fails than when the HM is broken. This occurs since the LM fibre carried a smaller stress before failure compared to the HM fibre. Overall, adding matrix yielding has a massive impact on the *SCF*, corresponding well to the literature [4, 36–39, 75–78]. Due to the limiting shear stress transfer, the *SCF* decreases, while more fibres share the load. Consequently, the effect of matrix yielding in hybrid composites is the same that occurs with non-hybrids. Results demonstrate that the model predicts well the *SCF* for different materials combinations compared with the SEM, but using simple analytical equations.

As proved in Fig. 4.5, the ineffective length of broken fibres strongly depends on the stiffness of the broken fibre: a larger stiffness provokes a larger stress to be recovered, increasing the ineffective length. Unlike the *SCF*, the ineffective length is not significantly influenced by the presence of fibres with different stiffness. Similarly, the *HVF* does not present a significant impact. These facts agree well with the results of Swolfs *et al.* [45]. Nonetheless, the matrix behaviour presents a considerable impact on the ineffective length, like with the *SCF*. When the matrix is elastic, no shear stress limit occurs. This allows the stress to be recovered quickly, leading to smaller ineffective lengths than a plastic matrix [37]. Compared to SEM, the ineffective length predicted by the PFM was always smaller, especially with the plastic matrix. This occurs because of two reasons. First of all, when the matrix is plastic, it is perfectly plastic in the PFM, but elasto-plastic in SEM. This means that the shear stress is constant along the ineffective length, causing a shorter stress recovery. Although this issue could be solved by using an elasto-plastic model in the PFM, that would also complicate further the model, and may not significantly improve the modelling predictions. Secondly, the SEM captures the local stiffness of the microstructure. This means that if the broken fibre is surrounded by more LM fibres, then the ineffective length of the broken fibre is larger. This is currently ignored by the PFM.

As evidenced in Fig. 4.6, the radial influence length is larger when the HM fibre is broken. This is because of the stiffness. When the HM fibre fails, the stiffness loss is larger, and thus, the load is spread over more fibres. Moreover, the radial influence length slightly increases by adding LM fibres, which occurs due to the decrease of overall stiffness. Like with the *SCF*, the stiffness ratio has a significant influence on the radial length. A larger stiffness ratio between HM and LM fibres increases the radial influence length when the HM fibre is broken, whereas the opposite occurs when the LM fibre is broken. Likewise, adding matrix yielding increases the radial influence length because the load transfer is limited, although the trends between elastic and plastic matrix are the same. Another remarkable fact, is that the radial influence length is heavily dependent on the microstructure, presenting a large scatter.

In general, the tensile behaviour predicted by the PFM agrees well with the SEM, both with a plastic and an elastic matrix (Figs. 4.7, 4.9 and 8.3). With a plastic matrix, the PFM overpredicted final failure compared with SEM (leading to larger cluster sizes, break density, etc.), whereas the opposite occurred with an elastic matrix. The reason for this could be related to an overprediction of *SCF* with an elastic matrix in the PFM (readers are referred to Tavares *et al.* [37]), and to an underprediction of *SCF* and ineffective length in the case of a plastic matrix. Anyway, considering that the PFM is at least 10 times faster than SEM, the small differences are well justified, and thus, the approach proposed by the PFM is accurate enough. Like in Chapter 3, the tensile behaviour of the hybrid materials varied greatly with the content of LE fibres in the hybrid. Moreover, the matrix behaviour (plastic or elastic) had a massive influence on the tensile failure process. The AS4-Eglass presented no ductility at all for the different hybrids simulated with a plastic matrix, however, some ductility appeared for an elastic matrix with an $HVF = 25\%$. The M50S-AS4 presented a large ductility of 0.5% for an $HVF = 25\%$ when matrix yielding was considered, but only a tiny ductility was predicted with an elastic matrix. Differences with the AS4-T800G composite were even more important. For this composite, the ductile strain was 0.7% with a plastic matrix, but it was 1% with an elastic matrix for an $HVF = 25\%$. Even more, for an $HVF = 50\%$ no ductility was present with matrix yielding, nonetheless, the elastic matrix exhibited a large ductility of 1.5% for SEM and 0.5% for PFM.

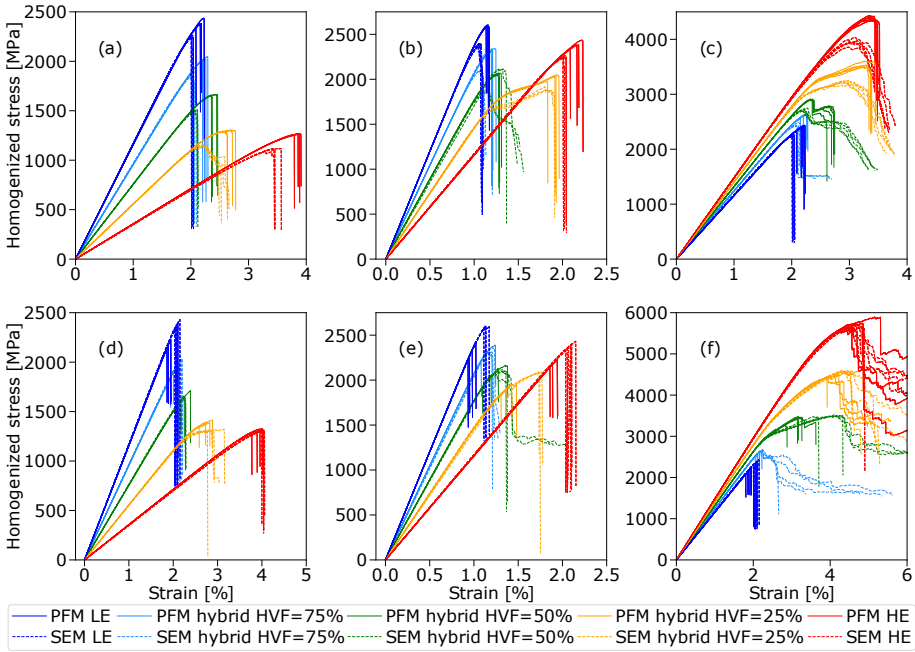

Figure 8.3: Predicted stress-strain curves by the PFM and SEM with a plastic and elastic matrix for different hybrid materials and varying the *HVF*. a) AS4-Eglass plastic, b) M50S-AS4 plastic, c) AS4-T800G plastic, d) AS4-Eglass elastic, e) M50S-AS4 elastic and f) AS4-T800G elastic. A total of five runs is shown.

By analysing the formation of clusters and the break density, the differences between elastic and plastic matrix are even more highlighted (for this the reader is referred to Figs. 4.8 and 4.10, and Tables 4.2 and 4.3). While the critical cluster size with a plastic matrix for all composites agrees relatively well with experimental data of non-hybrid composites [41], the cluster size with an elastic matrix is mostly overpredicted. In fact, with the AS4-T800G composite it is even larger than the number of fibres in the RVE. This is a consequence of the non-shear transfer limit of the elastic matrix, causing the load redistribution to be always very localised around the broken fibres. Thus, many isolated clusters form along the RVE, which need to increase very large in size to provoke final failure. With the AS4-T800G, this effect is even more exaggerated due to the small Weibull modulus of the T800G fibre. This could also explain why larger ductilities occur with some composites when the matrix is elastic. In a similar manner, the fibre break density with an elastic matrix is unrealistically large compared with a plastic matrix, albeit both PFM and SEM overpredict experimental data of non-hybrid composites in this regard [41]. This overprediction could

be attributed to errors in the Weibull distribution, dynamic effects, omission of debonding, matrix cracks, etc. An important remark is that the break density strongly depends on the ductility of the composite. A larger ductility increases the break density since the material is more damage tolerant. It is worth noting that the critical cluster size and break densities were compared with results of non-hybrid composites (since results for hybrid materials are lacking). Even if this comparison is discussable, it allows to clearly point out that an elastic matrix does not seem to be accurate. The non-hybrid composites were also in good agreement between PFM and SEM, in all cases exhibiting a brittle failure. Like with the hybrids, the plastic matrix showed better results compared to experimental data (see Table 4.4).

Overall, the results presented in Chapter 4 prove that an elastic matrix should be avoided to model hybrid materials. A plastic matrix, allows a more realistic representation of FRP composites (since it limits the shear stress transfer), leading to a more accurate load redistribution around broken fibres. The inclusion of omitted phenomena such as dynamic effects could also help to improve the models. Nevertheless, more experimental data is necessary to further validate the results, especially with hybrid composites. Another gap opened in Chapter 4 is to find a better way to determine clusters in order to avoid clusters larger than the number of fibres, and to have a more objective description of what constitutes a cluster. An attempt to solve this issue was carried out in a conference paper, where different algorithms to determine clusters were compared. Interested readers are referred to the paper in Appendix A.3.

Like it has been pointed out during previous Chapters 3 and 4, the omission of dynamic effects could explain some of the gaps compared to experiments. As proved in Chapter 2, their influence on damage development in hybrid composites has not been studied. Similarly, thermal residual stresses are usually omitted, and although their impact on the hybrid effect is secondary, their influence on cluster formation is unexplored. To answer some of these unknowns, and in an attempt to improve the model further, dynamic effects and thermal residual stresses were included into the PFM in Chapter 5. The thermal residual stresses were considered by simply adding an extra term into the main equations of the PFM, representing the thermal contribution. An analytical equation was formulated for determining the magnitude of the thermal residual stresses in

hybrid composites, see Eq. (5.3). Regarding the dynamic effects, these were added into the PFM by simply increasing the static *SCF* by a magnification factor when new breaks occur, similarly to the model of Bullegas [62]. Although simplistic, this approach allows the desired effect to be captured while still maintaining a reduced computational effort. The main disadvantage is that the entire transient effect is not considered, since only the instant of time at which the maximum dynamic effect is produced is taken into account. Nevertheless, new failures will occur when the *SCF* is maximum, and thus, that is the only time of interest. The enhanced PFM was used to study the influence dynamic effects and thermal residual stresses have on final failure and damage development in hybrid composites. Three distinct hybrid materials corresponding to X5-T300 (Carbon-Carbon), T300-Eglass (Carbon-Glass) and X5-Eglass (Carbon-Glass) were simulated, all with Epoxy matrix. For further details of the materials and cases studied, the reader is referred to Section 5.3.

The results from Chapter 5 prove that the formation of clusters is heavily influenced by the dynamic effects. As shown in Fig. 5.2, the maximum cluster size increases with the dynamic magnification factor, M_{d}. Consequently, adding dynamic effects leads to larger clusters at smaller strains and to larger critical cluster sizes compared to the static model [63]. Theoretically, this should make the model closer to the experiments. However, the formation of co-planar clusters is not clearly affected, and thus, the underprediction of co-planar clusters seen in the literature may not be related to dynamic effects.

Adding dynamic effects marginally decreases the failure strain, the strength and ductile strain, since larger stress concentrations are produced compared to the static (Figs. 5.3 and 5.4). An interesting remark is that the influence on final failure seems to be more important for the non-hybrid composites and the most brittle materials, which suggests the presence of small hybrid effects caused by the dynamic phenomenon. However, the influence is small, and thus, the dynamic effects do not significantly alter either final failure or the ductility of the hybrid composites, even for large dynamic factors. This corresponds well with the results of Tavares *et al.* [63] with non-hybrid materials. Further to this, the yield stress is totally unaffected by the dynamic effects, since it depends mainly on the initiation of damage. At that point, the number of breaks is so low that dynamic effects are negligible.

Likewise, the tensile behaviour is not significantly affected by the dynamic effects, even for large dynamic factors (see Figs. 5.5 and 8.4), although failure occurs slightly earlier for all materials. Results also prove again that hybrid composites can totally enhance the ductility of composite materials, showing ductile strains up to 1.5% for some hybrids. To obtain such ductile strain, the failure strain of the two fibres must be well apart, and the failure process must be continuous.

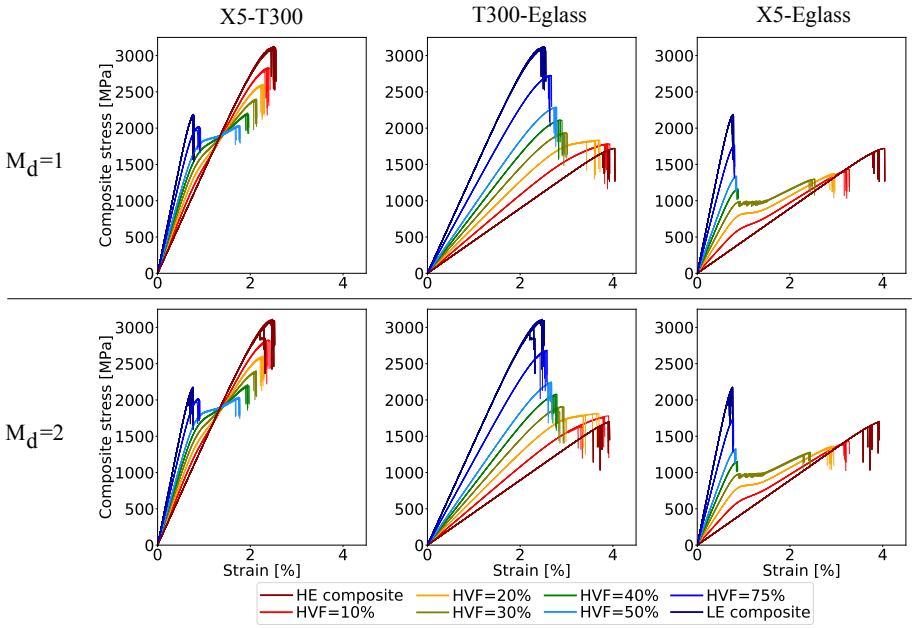

Figure 8.4: Compared stress-strain curves with each hybrid composite material between the static model ($M_d = 1$), and the dynamic model with a large dynamic factor ($M_d = 2$). The eight runs simulated are shown.

Overall, results from Chapter 5 contradict the general belief in the literature that the dynamic effects should considerably lead to an earlier final failure [5, 41]. These results were obtained by assuming a plastic matrix. Considering an elastic matrix could lead to a greater influence of the dynamic effects, as observed by Tavares *et al.* [63]. However, a plastic matrix is more realistic than an elastic matrix, as proved in Chapter 4. Even if the dynamic effects do not significantly influence final failure, their addition improves the formation of clusters compared to experiments, and thus, it should be seen as a modelling improvement. In any case, it is worth mentioning that the dynamic effects considered in the PFM are extremely simplified compared to reality, although the tendencies obtained

agree well with those seen with a more advanced dynamic SEM [63]. Currently, there is no experimental data available in the literature regarding the dynamic *SCF*, that would help to validate the results of the models and understanding their limitations. In addition, even if the SEM is more advanced than the PFM, the SEM is still a simplified FEM. Comparing the dynamic SEM (or the PFM) with a detailed 3D FEM simulation could help to establish whether the dynamic results of the PFM and SEM are valid or not, nonetheless, performing such a 3D FEM is not yet computationally feasible. Therefore, whether the dynamic results obtained in this work are really realistic or not, is yet to be seen.

Unlike the dynamic effects, the presence of thermal residual stresses shows no influence on the formation of clusters (see Fig. 5.6). However, they can have a small effect on final failure, depending on the magnitude of the thermal residual stresses (for this the reader is referred to Figs. 5.7 and 5.8). When the HE fibre residual strain is negative or tensile (but smaller than other scenarios), the initiation of damage for the HE fibre is delayed. Consequently, this allows to increase the failure and ductile strains. A similar effect is observed with the failure and yield stresses. Inducing compressive stresses into the LE fibre increases the strength and yield stress as the initiation of damage in the LE fibre is delayed. This scenario also leads to hybrid effects [7, 8, 22]. Therefore, a hybrid composite exhibiting compressive residual stresses into both LE and HE fibres should be optimum. Nevertheless, since the magnitude of the thermal residual stresses is generally small, their influence on final failure is mostly reduced. As a consequence, if the magnitude of the thermal residual stresses is known to be small, these can be omitted altogether.

With all these improvements, the new dynamic (and static) PFM was again compared against the experimental results of the T700S-Epoxy and M40-Epoxy non-hybrid composites simulated in Chapter 3, see Fig. 8.5. Overall, the static PFM is less close to the experiments than the old PFM from Chapter 3, both in terms of ultimate failure and accumulation of fibre breaks. This occurs because in Chapter 3, the *SCF* around fibre breaks was calculated using an elastic matrix, while the ineffective length was considering a plastic matrix. As proved in Chapter 4, such an approach was not an accurate way to calculate the load redistribution around fibre breaks since both the *SCF* and ineffective length were not consistent in between, which caused the *SCF* to be heavily overpredicted.

Thus, even if the new static PFM is less close to the experiments than the old model, the static PFM is clearly a more robust model. Furthermore, the dynamic PFM is closer to the experiments than the static because the dynamic effects lead to an earlier failure. In fact, some runs of the dynamic model are very close to the experimental results in the case of the T700S-Epoxy, although in broad terms, the dynamic PFM still overpredicts the ultimate failure, the accumulation of fibre breaks and the non-linearity at final failure. However, results prove that the dynamic PFM is a step forward in the modelling predictions since it is more realistic than the original PFM and closer to the experimental results than the static model.

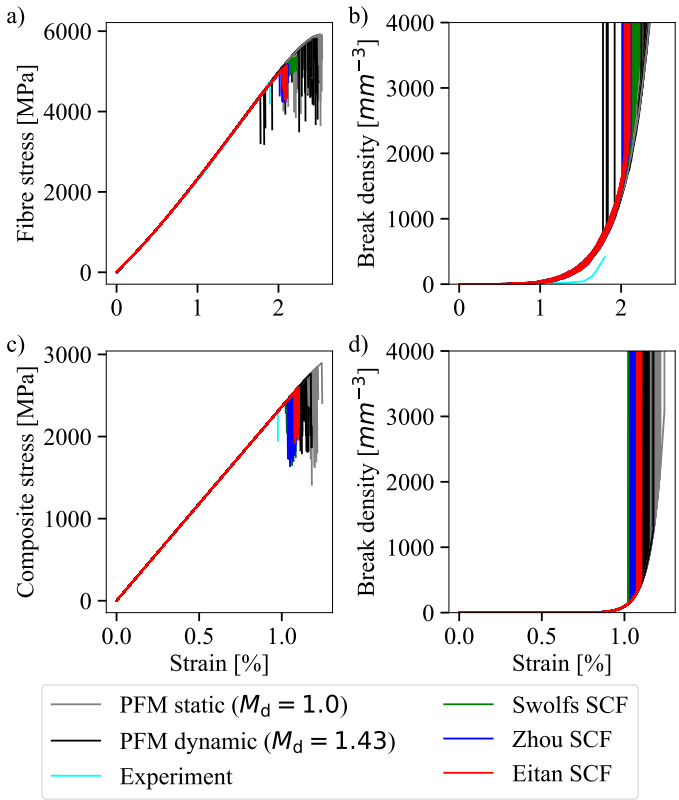

Figure 8.5: Predicted stress-strain and break density curves by the new PFM (static and dynamic) and the old PFM (as used in Chapter 3, with the Swolfs, Eitan and Zhou *SCF* models) compared with the experimental data. a)-b) T700S-Epoxy compared with Swolfs experimental data [41], c)-d) M40-Epoxy compared with Koyanagi data [153]. All forty runs simulated are shown.

Likewise, the dynamic PFM was also compared again against the FEM results of

the M50S-AS4 hybrid composite simulated in Chapter 3, see Fig. 8.6. Overall, results show that the dynamic PFM leads to similar stress-strain curves compared with the original PFM. Nonetheless, the dynamic effects lead to an earlier failure, making the model slightly closer to the FEM of Tavares *et al.* [35]. Since the dynamic PFM is clearly an improvement compared to the static and the old PFM, the dynamic model was used for the rest of this work.

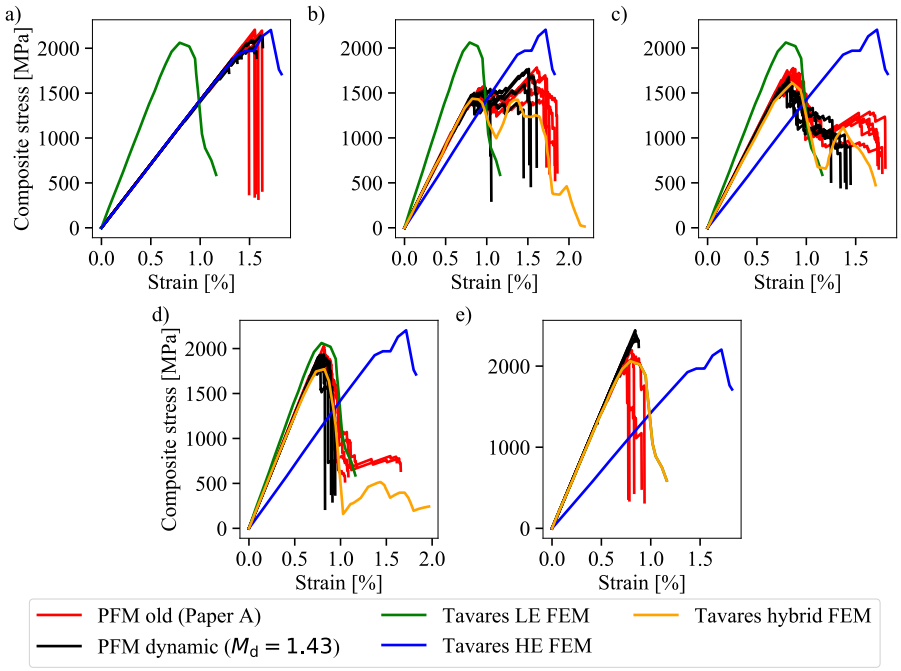

Figure 8.6: Hybrid M50S-AS4 stress-strain curves predicted by the dynamic PFM compared with the FEM of Tavares *et al.* [35], and with the results of the old PFM (as given in Chapter 3). a) $HVF = 0\%$, b) $HVF = 25\%$, c) $HVF = 50\%$, d) $HVF = 75\%$, and e) $HVF = 100\%$. For the sake of readability only five runs are shown.

As it was well pointed out in the literature review performed in Chapter 2, it is currently unclear which is the influence that the specimen size has on the hybrid effect and failure process in hybrid composites. Given that the PFM is an efficient model that can simulate composites with large volumes, this literature gap was addressed in Chapter 6. To do this, a hybrid composite consisting of X5-AS4 (Carbon-Carbon) in an Epoxy matrix was simulated for varying *HVF*s. Two different studies were performed: length scaling and cross-section scaling. In the former, an RVE with $0.303 \times 0.303\ mm^2$ cross-section was simulated for various lengths. In the latter, a 1 mm long RVE was simulated for different

cross-sections. For further details of the materials and methods, the reader is referred to Section 6.3.

Results of Chapter 6 prove that the hybrid effect considerably increases with the RVE length (Fig. 6.5a). Thus, length scaling provides a positive contribution to the hybrid effect. However, increasing the length of the RVE rapidly decreases the failure and ductile strains, and the failure and yield stresses up to a certain length (around $20-40$ mm) when a plateau starts, see Figs. 6.5b-e. This size effect agrees well with the literature [48], and may be explained as follows. When a material is longer, the number of defects increases leading to an earlier failure. However, up to a certain length the number of weak fibres becomes so large that more defects do not further lead to an earlier failure. Moreover, the presence of ductility does not seem to alter the size effect attributed to length scaling, since the decrease in strength, yield stress, failure and ductile strains is similar for all materials regardless of the presence (or not) of ductility (Fig. 6.5). In contrast, the HE non-hybrid material ($HVF = 0\%$) and the composites with a low HVF present a larger decrease in failure strain. One possible explanation for this is that these materials are dominated by the HE fibre which has a larger Weibull modulus (i.e. a narrower strength scatter) than the LE fibre. Consequently, the strength scatter governs the magnitude of the size effects.

Unlike length scaling, the hybrid effect rapidly decreases when the RVE cross-section is scaled up (Fig. 6.9a), thus, a bigger RVE cross-section provides a negative contribution to the hybrid effect. In contrast, the failure strain, ductile strain and failure stress (Figs. 6.9b-d) decrease for $HVF = 0\%$ and $HVF = 75\%$ when the cross-section is incremented, but increase for all the other HVFs, until a plateau that begins for a 1.212×1.212 mm^2 cross-section. The fact that some composites present an earlier failure by increasing the cross-section while others show a delayed failure seems contradictory and is difficult to explain. Indeed, an earlier failure has been generally reported in experimental testing with unidirectional composites [48, 49]. A possible reason for this is that each composite presents a different failure propagation because of the synergistic effects of the hybridisation, causing different size effects. Another plausible explanation is that although scaling up the RVE cross-section augments the number of weak fibres, it also increases the number of stronger fibres. For some cases one may cancel out the other, and thus, each material combination may

present a different size effect. On the other hand, the yield stress marginally decreases when increasing the RVE cross-section for all composites (Fig. 6.9e), which means that the initiation of damage occurs earlier when the scale is incremented. This is proved by the maximum cluster size (see Figs. 6.8g-i). As the cross-section is increased, larger clusters form earlier as a result of the greater number of weak fibres, consequently causing an earlier initiation of damage.

The reason why length scaling provides a positive contribution to the hybrid effect, while cross-section scaling gives a negative one is related to the size effects experienced by the all LE non-hybrid material. A hybrid composite of the same volume of the all LE non-hybrid contains less number of LE fibres. Since the failure strain of the all LE non-hybrid composite decreases by increasing the RVE length, the failure strain of the LE fibre in the hybrid is already larger than that of the baseline non-hybrid composite due to the associated size effects. This leads to a positive contribution to the hybrid effect. Contrary, since cross-section scaling increases the failure strain of the all LE non-hybrid material, the failure strain of the LE fibre in the hybrid is smaller than that of the baseline non-hybrid, providing a negative contribution to the hybrid effect. Nonetheless, it may be hypothesised that, if the failure strain of the all LE non-hybrid material decreased when scaling up the RVE cross-section rather than increased (as it occurred for instance in Chapter 3), a positive contribution to the hybrid effect would have been obtained. The fact that the size effects could play some role on the hybrid effect was already hypothesised in the literature [3], although results from Chapter 6 are the first to prove it. It is also worth mentioning that the hybrid effect generally presents a significant scatter since it strongly depends on the specific RVE and fibre strengths of each run performed (see Figs. 6.6a and 6.10a).

The maximum cluster size (Figs. 6.4g-i and 6.8g-i) always increases with either the RVE length or the RVE cross-section. This corresponds well to the literature [54, 120], and can be explained by the fact that, in a material with larger volume more clusters are formed. Eventually, two big clusters merge onto a single one, leading to larger clusters. This is well illustrated in Figs. 6.7 and 6.11.

In line with literature results [34, 35], and previous Chapters 3, 4 and 5, the hybrid composites present a ductile and progressive failure for $HVF = 10-50\%$,

proving again the efficiency of fibre hybridisation (see Fig. 8.7). A remarkable finding is that the hybrid effect with an $HVF = 75\%$ was relatively large (Figs. 6.5a and 6.9a), however, the composite is brittle. Thus, a larger hybrid effect may not correlate with ductility. An additional interesting fact is that the hybrid effect and ductile strain increase from $HVF = 0\%$ up to a certain HVF and then decrease again until $HVF = 100\%$, while the failure and yield stresses follow the opposite tendency (Figs 6.6 and 6.10). Consequently, there is a trade-off between ductility and strength, which corresponds well with the literature [14].

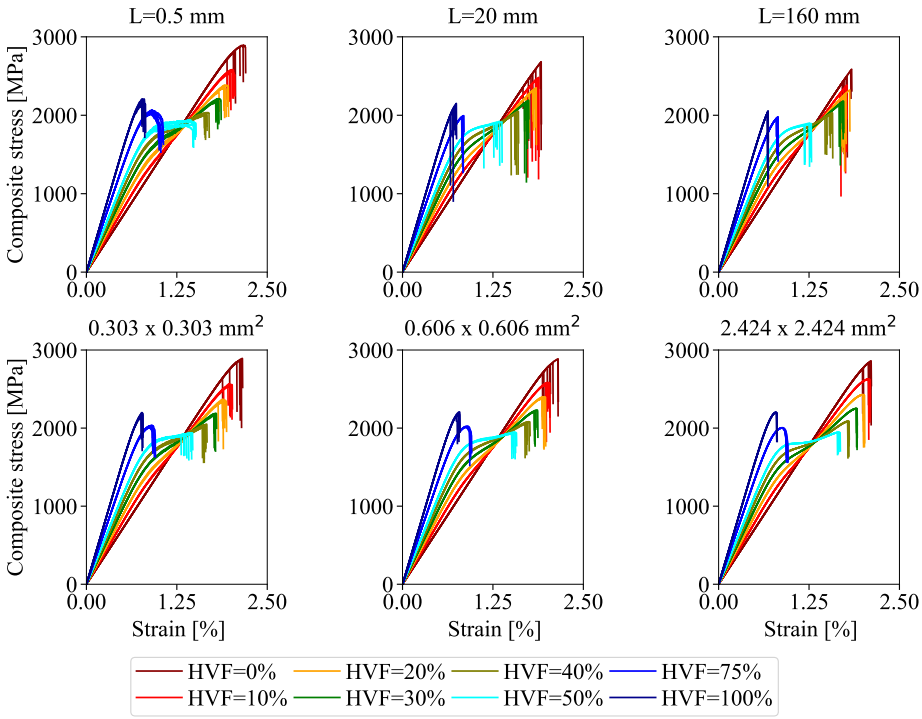

Figure 8.7: Stress-strain curves obtained for each HVF (ranging from 0% to 100%), and for different RVE lengths (0.5, 20 and 160 *mm*), and cross-sections (0.303×0.303 mm^2, 0.606×0.606 mm^2 and 2.424×2.424 mm^2). All eight runs simulated are shown.

Overall, results from Chapter 6 prove that the specimen size has a large influence on the hybrid effect and final failure. Thus, care should be taken when extrapolating the results from a small RVE or a small specimen to a bigger structure.

While in Chapters 3, 4, 5 and 6, the PFM demonstrates that a ductile failure can be achieved via fibre hybridisation, nonetheless, all work focused on intrayarn

hybrids. As it was highlighted in Chapter 2, the influence the hybrid configuration (interlayer, intralayer or intrayarn) has on the tensile behaviour and cluster development in hybrid composites is unexplored. Moreover, there is not any literature algorithm to generate intralayer and interlayer hybrid composites with randomly distributed fibres. In addition, the PFM was validated in Chapters 3 and 4 by comparing with experimental results of non-hybrid composites, and against numerical results of hybrid composites given by a FEM and a SEM. Nonetheless, the PFM has not been compared against experimental results of hybrid composites. In consequence, these literature gaps were covered in Chapter 7. To do this, firstly, a state of the art algorithm [35, 124] able to generate intrayarn hybrid composites with randomly distributed fibres, was extended to generate interlayer and intralayer hybrids as well. The algorithm only required small changes, for this the reader is referred into Section 7.2. Secondly, different real interlayer hybrid composites were simulated by the PFM, and the results were compared against the experimental data given in Czél *et al.* [16]. Finally, the model was used to study the effect of the hybrid configuration by comparing an X5-HTS (Carbon-Carbon) hybrid composite hybridised in either an interlayer, intralayer or an intrayarn configuration. Since the thickness of the plies in interlayer hybrids or that of the bundles in intralayer hybrids may have a large influence on failure, the study was performed for various thicknesses. For further details of the materials and cases studied, the reader is referred to Section 7.4.

Results from Chapter 7 prove that, in spite of the simplicity of the PFM, the model is able to capture qualitatively well the longitudinal failure of interlayer hybrid composite materials (see Fig. 7.8). Overall, the model not only captures (qualitatively) the progressive failure process of the materials but also their ultimate failure. Although for doing this comparison, the failure strain of the HE fibre was fitted to be 1.9% (the reader is referred to Section 7.4 for more details), nonetheless, the failure strain of the hybrid composites is smaller. This occurs since the accumulation of damage attributed to the failure and fragmentation of the LE plies causes a decrease of the failure strain of the HE material, and thus, the PFM accurately captures this effect. However, the PFM underpredicts the yield stress with all composites compared against the experimental data, especially for the XN80-T1000 dispersed material (see Fig. 7.8d). This issue also occurs with other similar models [100], and may be caused either by errors

in the Weibull distribution, or inaccuracies in the load redistribution around fibre breaks causing the failure initiation of the LE fibres to begin much earlier than in the experiments. Likewise, the plateau region in the stress-strain curve after failure initiation is considerably underpredicted by the PFM (particularly with the XN80-T1000 dispersed composite, see Fig. 7.8d). This could be attributed to the presence of stable and dispersed delaminations between the LE and HE plies, causing a loss of stiffness [16]. Currently, the PFM omits the presence of delaminations and thus, it cannot capture this effect. In addition to this, the model again predicts a greater non-linearity close to final failure than the experiments, like it occurred with the non-hybrids in Fig. 8.5. It is also worth mentioning that ply fragmentation is another important failure mechanism of interlayer hybrid composites [100]. Although the authors believe that the PFM is at least partially capturing this effect via the accumulation of fibre breaks, a more in-depth study of the capabilities of the model to capture this phenomenon is needed.

Despite the discrepancies with the experimental data, the PFM predicts qualitatively well the failure process of interlayer hybrid composites, although it undepredicts the yield stress and the plateau region after failure initiation of the LE fibres. Anyhow, given the simplicity of the PFM, and considering the (inevitable) inaccuracies of the modelling assumptions and input data, the results of the PFM are encouraging. At this point, more in-depth experimental data is needed regarding the formation and development of clusters to shed more light on the inaccuracies of the model and improve it further. Adding the effect of delaminations could also be a key feature for improving the models to simulate interlayer hybrids.

The tensile behaviour of the three hybrid configurations (interlayer, intralayer and intrayarn) is compared in Figs. 8.8 and 7.9 for different LE ply and bundle thicknesses. When the thickness is thin, the three hybridisations predict a similar ductile failure, with a progressive increase of fibre break density and a similar grow of the maximum cluster size. However, when the thickness is thick, the initiation of damage begins earlier for the interlayer and intralayer hybrids than for the intrayarn, leading to larger break densities and bigger maximum cluster sizes at smaller strains. Moreover, the interlayer and intralayer also present several load drops after damage initiation due to the simultaneous failure of

multiple LE fibres (see Fig. 7.9c). The reason for this is well illustrated by the hybrid effect (Fig. 7.10a). Overall, the intrayarn hybrid produces higher hybrid effects than the interlayer and intralayer. Consequently, the intrayarn configuration allows to hinder the formation of clusters of LE fibres more efficiently, leading to larger hybrid effects and a delayed damage initiation. Nonetheless, by reducing the LE ply or bundle thicknesses the results of the interlayer and intralayer composites, respectively, are improved and quite close to the intrayarn. This occurs because reducing the thickness allows to increase the dispersion of the fibres, resulting in a better hybridisation [8, 31, 64, 273]. Therefore, results prove that the dispersion of the fibres is a key parameter.

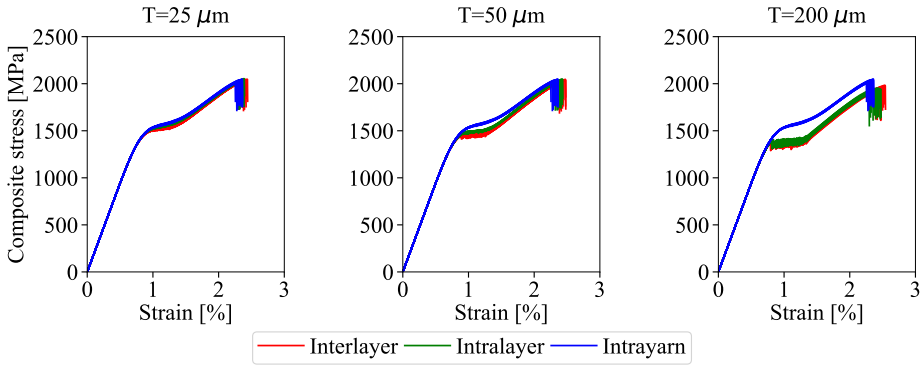

Figure 8.8: Stress-strain curves obtained for each hybrid configuration (interlayer, intralayer and intrayarn) and for different thicknesses (25, 50 and 200 μm). All twenty-four runs simulated are shown.

In line with this, the yield stress and strength are considerably larger for the intrayarn, particularly when the thickness is large (Figs. 7.10d and 7.10e). This occurs because the hybrid effect is larger for the intrayarn, causing a delayed failure of the LE fibres and a smaller stiffness loss. This in turn, results in larger failure and yield stresses. In contrast, the failure and ductile strains (Figs. 7.10b and 7.10c) are similar for the three configurations when the thickness is small, nonetheless, as the thickness is incremented the failure and ductile strains of the interlayer and intralayer increase, being then considerably larger than the intrayarn. This may be explained because as the thickness is incremented, the initiation of damage begins earlier, causing load drops and an important stiffness loss. Since these load drops are not big enough to cause final failure, the HE fibres continue to carry load. However, due to the large presence of damage, the applied strain needs to be significantly large to cause more failures, thus resulting

in larger failure and ductile strains. In any case, it is important to highlight that for even larger thicknesses, or for different material combinations, the load drops caused by the failure of the LE fibres could lead to a premature final failure. In addition, in real interlayer and intralayer hybrid composites catastrophic delaminations may appear between the plies or bundles [16, 272], which could also lead to a premature failure. Unfortunately, all current state of the art models (including the PFM) omit this mesomechanical failure mechanism, and thus it is difficult to judge its importance.

As illustrated in Fig. 7.11, the clusters form differently within each hybrid configuration, due to the different geometry and dispersion of the fibres. For the interlayer hybrids, the clusters begin to form in the LE plies and slowly propagate up to the boundaries between the layers where they are arrested by the surrounding HE fibres. Likewise, for the intralayer hybrids, these start to form in the LE bundles and afterwards spread up to the boundaries of the bundles. Eventually the HE fibres start to fail, causing the clusters to slowly propagate through the boundaries. Instead, the intrayarn hybridisation shows that clusters form randomly anywhere in the RVE because of the random dispersion of the fibres. This different formation and development of clusters is more deeply shown in Fig. 7.12. While the formation of 1-plets is significantly larger for the intrayarn hybrid, nonetheless, the formation of 3-plet and 6-plet is considerably larger for the interlayer and intralayer, than for the intrayarn. These findings mean that the intrayarn hybrid is more efficient in delaying the formation of larger clusters (thus forming more 1-plets) than the intralayer and interlayer, which in turn leads to larger hybrid effects. This is also the reason why the maximum cluster size (Figs. 7.9g-i) is smaller for the intrayarn. Furthermore, if the thickness is increased, the formation of larger clusters is increased because of the smaller dispersion of the fibres.

Overall, results from the hybrid configuration study presented in Chapter 7, are in-line with other literature work [31], although there are some discrepancies. Swolfs *et al.* [31], performed a similar study with a micromechanical model, and found that an interlayer configuration of alternating single fibre layers leads to higher hybrid effects. Contrary to that, results of Chapter 7 show that the interlayer material is the worst hybridisation in terms of hybrid effect, although within a very small ply thickness of 25 μm, (which is around 1-3

fibres thick, see Fig. 7.6), the results are close to the intrayarn. The small discrepancies between the results of this work and the ones presented in Swolfs *et al.* should be attributed to the different modelling assumptions. Swolfs *et al.* [31] assumed an hexagonal packing of fibres under a very local load sharing rule. It also considered an elastic matrix, and did not take into account dynamic effects. All these assumptions significantly change the stress redistribution around broken fibres. Instead, this work considered a more accurate random distribution of fibres, a plastic matrix and dynamic effects. In addition, Swolfs *et al.* [31] found a small difference between the maximum cluster size of the three hybrid configurations, which also does not agree with the results of this work. However, this occurs because the maximum cluster size here corresponds to the cluster at failure of the HE fibres, while it corresponds to the cluster at failure of the LE fibres in Swolfs *et al.* [31]. Anyhow, the two studies agree well that increasing the fibre dispersion augments the hybrid effect and delays break-cluster development.

Based on the results from Chapter 7 it is difficult to establish which hybrid configuration is better. On the one hand, the intrayarn leads to higher hybrid effects, a delayed damage initiation and larger yield stresses and strength. On the other hand, the interlayer hybrid leads to larger failure and ductile strains, but lesser hybrid effects and lower yield stresses and strength. The intralayer lies in-between and thus, may generally be a good compromise. Nevertheless, these findings were obtained with a specific carbon-carbon hybrid composite. Since the failure is quite dependent on the material properties (as it was for instance proved in Chapter 4), which hybrid configuration performs best may depend on each material system.

To conclude the discussion, a PFM was developed able to qualitatively predict the tensile failure and damage development in hybrid and non-hybrid unidirectional composites. The model predicts the formation of clusters of broken fibres and the stiffness loss of composite materials, taking into account matrix yielding (assuming a perfectly plastic matrix), dynamic effects and thermal residual stresses. Moreover, it presents the advantage of being computationally efficient compared to finite element models and spring elements models, but still, it is able to capture qualitatively well the failure of hybrid and non-hybrid composites. Therefore, the PFM is a suitable model for modelling composite materials.

By using the PFM, the micromechanical behaviour of hybrid composites was analysed. Results of this thesis prove that fibre hybridisation is an adequate solution to the lack of toughness of composite materials. Furthermore, it has been demonstrated that matrix yielding is necessary to predict more accurate results. Likewise, adding dynamic effects allows to predict a more realistic formation of clusters, while the thermal residual stresses are secondary and may be omitted. Additionally, it was seen that the specimen size has a significant importance on the hybrid properties. On the one hand, scaling up the composite length may enhance the hybrid effect, but on the other hand, scaling up the cross-section size of the material may reduce it. Finally, it was proved that an intrayarn hybrid configuration is more efficient than an interlayer and intralayer in terms of hybrid effect and strength, whereas an interlayer hybrid may lead to larger ductile and failure strains. At this stage, more work is needed to further improve and validate the models for blind material design. In addition, there are still several literature gaps and modelling issues that need to be addressed (for this, the reader is referred to Section 9.2).

Conclusions and future work

9

9.1 Conclusions

A Progressive Failure Model (PFM) able to qualitatively predict the failure and damage development in hybrid and non-hybrid unidirectional polymer composite materials under longitudinal loading has been developed. The model captures individual fibre breaks as well as the formation and development of clusters of broken fibres. The stress redistribution around fibre breaks takes into account matrix yielding (assuming a perfectly plastic behaviour), the cluster size, RVE size, volume fractions, fibre radius and elastic properties of each fibre population in the material with simple analytical equations. Dynamic effects caused by broken fibres and thermal residual stresses derived from the manufacturing process are also considered. Furthermore, the strain along the model is different depending on the damage state, allowing to capture larger strains at locations with more damage. Thanks to its semi-analytical framework, the PFM is computationally efficient compared to finite element models. In addition, an algorithm to generate hybrid interlayer, intralayer and intrayarn composites with a random distribution of fibres was developed.

According to the results obtained from the present thesis, several conclusions are drawn. These are classified in different blocks as follows, based on their context: Progressive Failure Model, tensile behaviour of hybrid composites, stress redistribution around fibre breaks, dynamic effects and thermal residual stresses, specimen size, and hybrid configuration.

The following conclusions are obtained regarding the Progressive Failure Model:

- The PFM captures the failure curve of hybrid and non-hybrid unidirectional composite materials containing a random distribution of fibres.
- The PFM slightly overpredicted the experimental failure strain and strength of two non-hybrid materials consisting of UD T700S-Epoxy and M40-Epoxy. Nonetheless, the fibre break density was heavily overpredicted. Increasing the dimensions of the model decreased the failure strain and strength, being coherent with size effects.

- A hybrid carbon-carbon (M50S-AS4) epoxy composite was simulated and compared with the FEM of Tavares *et al.* [35]. A good agreement was obtained, but with a much simpler and faster model than the FEM is.

- Overall the PFM is in good agreement compared with a more sophisticated SEM, but significantly faster and lighter computationally.

- The PFM predicts qualitatively well the failure process of interlayer hybrid composites, as well as their ultimate failure compared with experimental data. Notwithstanding, the model undepredicts the yield stress and the plateau region after failure initiation of the LE fibre plies.

- Additional experimental data, with hybrid composites manufactured in an intrayarn and intralayer hybrid configuration is necessary to validate and improve the models further. Likewise, the literature needs more experimental results regarding the formation and development of clusters in hybrid composites to better correlate and improve the models. Micromechanical models are not yet good enough for blind material design.

Derived from the tensile behaviour of hybrid composites, the following conclusions are obtained:

- Hybrid composites can exhibit a ductile behaviour at relatively low *HVF* (depending on the hybrid material). At large *HVF*, the failure is brittle, even though there may be important hybrid effects.

- The fibre break density is directly related to the ductility of the composite. A larger ductility increases the break density at failure, and leads to a more progressive increase of break density with the applied strain. Otherwise, a more brittle material leads to a rapid grow of break density.

- The tensile failure of hybrid composites strongly depends on the matrix behaviour. An elastic matrix leads to the formation of many isolated clusters along the model which need to significantly grow in size in order to trigger final failure. Consequently, an elastic matrix leads to unrealistically large cluster sizes and break densities. In contrast, a plastic matrix leads to a more realistic formation of clusters compared with experiments.

– A trade-off between strength and ductility may occur. For certain hybrid composites, a larger ductility may lead to a lower strength.

Regarding the stress redistribution around fibre breaks, the following findings are given:

– The *SCF* models of Swolfs *et al.* [41], Zhou and Wagner [251] and Eitan and Wagner [252] had a marginal different failure prediction. However, all three models led to the formation of clusters of broken fibres which caused final failure. The Swolfs *SCF* model generated more localised stress concentration factors. Consequently, it led to smaller size effects than the models of Zhou and Eitan.

– The *SCF* carried by an intact fibre with different stiffness than the broken fibre depends on the stiffness ratio of both fibres. A larger ratio between the HM fibre over the LM fibre increases the *SCF* when the HM fibre is broken, whereas the opposite occurs when the LM fibre is broken.

– The *SCF* on HM fibres decreases by adding LM fibres into the hybrid composite. Since the HM fibres are usually the LE fibres, this should increase the hybrid effect.

– The *SCF* carried by LM fibres is larger than that of the HM fibres when a HM fibre is broken, which should increase the hybrid effect if the HM fibre corresponds to the LE fibre. When the LM fibre fails, the *SCFs* are smaller in both populations compared with a broken HM fibre.

– The analytical model to predict the *SCF* around breaks in hybrid composites used in the PFM agrees well with the SEM for different material configurations.

– The ineffective length depends mainly on the stiffness of the broken fibre. The larger the stiffness, the larger is the ineffective length. Nonetheless, the stiffness of the other fibre in the hybrid and the *HVF* do not have any significant influence on the ineffective length.

– The radial influence length is larger when a HM fibre is broken than when the LM fibre is, and increases by adding LM fibres. Like the *SCF*, the radial influence length increases with the stiffness ratio between HM and

LM fibres when a HM fibre is broken, while the opposite occurs when the LM fibre is broken. In addition, it strongly depends on the microstructure.

- Adding matrix yielding has a significant impact on the stress redistribution around broken fibres. Since matrix plasticity limits the shear stress transfer, the *SCF* carried by intact fibres is significantly decreased compared to an elastic matrix. Contrary to this, the ineffective length is considerably longer. Likewise, the radial influence length significantly grows, and thus, the load loss is spread over more fibres.

In the case of the dynamic effects and thermal residual stresses, the following outcomes are drawn:

- The thermal residual stresses have a negligible influence on the formation of clusters and damage progression, but may have a small impact on final failure. The addition of compressive residual stresses into the LE fibre delays damage initiation, increasing the failure strength and yield stress. This may also lead to an hybrid effect. Similarly, inducing compressive stresses into the HE fibre increases the failure and ductile strains.

- Given that the magnitude of the thermal residual stresses is small, their impact on the hybrid effect and final failure is mostly secondary.

- The dynamic effects have a massive influence on the creation and development of clusters, leading to the formation of larger clusters at lower strains than the static model. However, the formation of co-planar clusters is not clearly affected.

- The dynamic effects have a minor influence on final failure, leading to a slight earlier final failure than the static. Their importance on final failure depends on each material system. In fact, some hybrid composites show a smaller influence of the dynamic effects on final failure than their baseline non-hybrid composites. Thus, there may be a small contribution to the hybrid effect given by the dynamic phenomenon for certain material combinations. In addition, the yield stress is totally unaffected by the dynamic effects. The tensile response is also not much influenced.

- Although the dynamic effects have a small impact on final failure, their addition into the modelling predictions improves the formation of clusters

and thus, closes the gap to the experiments.

In regards to the specimen size, the following conclusions are obtained:

- Increasing the RVE length strongly increases the hybrid effect, and thus, the size effects provide a positive contribution to the hybrid effect. The failure strain, ductile strain and failure strength rapidly decrease by increasing the RVE length up to a certain length when a plateau begins.
- Increasing the RVE cross-section considerably decreases the hybrid effect, thus, giving a negative contribution. Moreover, final failure is delayed for some composites whereas it leads to an earlier failure for other materials. These size effects vanish for large cross-sections.
- Increasing the RVE volume always increments the maximum cluster size, (either by scaling up the RVE length or scaling up the cross-section size), and leads to the formation of more clusters of bigger size.
- The importance of the size effects seems to be principally governed by the fibre strength scatter and it is unaffected by the presence of ductility.
- Increasing the material dimensions generally decreases the scatter of the results, except for the formation of clusters which always exhibits a large variability.

Finally, concerning the hybrid configuration, the following conclusions are found:

- The intrayarn hybrid configuration leads to higher hybrid effects, larger yield stresses and strength than interlayer and intralayer hybrids. Consequently, damage initiation begins later as well with the intrayarn. In this regard, the interlayer is the worst one whereas the intralayer is in-between. In contrast, the interlayer and intralayer lead to larger ductile and failure strains than the intrayarn, being the interlayer the best in these aspects.
- The dispersion of the fibres is a key parameter. By reducing the LE ply and the bundle thicknesses for the interlayer and intralayer hybrids, respectively, the results of these can be optimised and be close to the intrayarn.

– The maximum cluster size, as well as the number of clusters of bigger sizes, are considerably smaller with the intrayarn hybridisation. The propagation of the clusters is also different for each hybrid configuration due to the distinct geometry and dispersion of the fibres.

9.2 Future work

In this section different research lines to extend further the work carried out in this thesis are presented.

The present thesis has mainly devoted to develop a micromechanical model able to predict the failure and damage development in hybrid unidirectional FRP, and study different parameters affecting their failure. By employing the PFM proposed, the failure of composites can be simulated with a low computational effort compared to other models. Although the model has been relatively close to experimental data and includes many features and advantages compared to other state of the art models, there are still different issues to be addressed. Currently, the PFM can be improved by adding the following phenomena:

– Fibre-matrix debonding and matrix cracks around broken fibres.

– Improve the matrix further, by considering matrix viscosity and capturing the entire yielding of the matrix as well as its strain dependency. In addition, the stress redistribution around fibre breaks should be calculated accordingly.

– Scaling up the ineffective length and *SCF* also for diffuse clusters.

– Improve the RVEs entered into the PFM by including defects such as fibre waviness, voids, resin rich regions, etc.

– Possibility to simulate fatigue.

– Delamination between plies.

– Establish to which extent is the model able to capture ply fragmentation, and if needed, to include this phenomenon into the modelling predictions.

– Ability to simulate multidirectional composites.

– Possibility to simulate discontinuous fibre composites. In this way, the model with intrayarn hybrid composites could be validated by comparing against experimental results for discontinuous hybrid materials published in Yu *et al.* [17].

The addition of these phenomena in the PFM should allow to close further the gap between models and experiments, as well as to have a more robust and advanced model. To do so, not only the model needs to be improved, but also the experimental data available in the literature for hybrid composites needs to grow further. In a similar manner, there still exist multiple literature gaps. These are listed as follows:

– The proper statistical distribution (Weibull-based or not) to characterise the strength of the fibres is not clarified.

– The presence of matrix cracks around broken fibres needs to be investigated further. Determine when they occur, and investigate their influence in hybrid composites.

– Determine the importance of debonding in hybrid and non-hybrid materials.

– Study whether the viscoelastic behaviour of polymer matrices has any influence on the hybrid effect and the failure of hybrid composites.

– The stress concentration factor carried by an intact fibre varies greatly around its cross-section, being highest close to the break. Since most models use a constant stress for the entire cross-section, this effect is generally ignored. The implication of this is not clear.

– Understand why models underpredict the formation of co-planar clusters and the formation of clusters of larger size.

– Establish why models heavily overpredict the fibre break density at failure.

– Find a more objective description of what constitutes a cluster.

– Establish whether final failure occurs by the accumulation of damage or the unstable propagation of a large critical cluster.

– Obtain more experimental results with hybrid composites, especially regarding the formation of clusters. In addition, intrayarn and intralayer hybrid composites should also be manufactured.

The work proposed in the present thesis is a continuous effort in the road towards the development of accurate models which are able to predict the failure of composite materials in a blind basis. Such models would allow to design structures without the need of performing expensive and complicated experimental tests. Having accurate and reliable models could also allow to further optimise the materials, resulting in costs and weight savings. Finally, increasing the understanding in hybrid composites further can allow to produce composites with a wide margin between damage initiation and final failure resulting in better designed and optimised materials.

Bibliography

[1] A. Turon, J. Costa, P. Maimí, D. Trias, J. Mayugo, A progressive damage model for unidirectional fibre-reinforced composites based on fibre fragmentation. Part I: Formulation, Composites Science and Technology 65 (13) (2005) 2039–2048. doi:10.1016/j.compscitech.2005.04.012.

[2] P. D. Soden, M. J. Hinton, A. S. Kaddour, A comparison of the predictive capabilities of current failure theories for composite laminates, Composites Science and Technology 58 (7) (1998) 1225–1254. doi:10.1016/S0266-3538(98)00077-3.

[3] Y. Swolfs, L. Gorbatikh, I. Verpoest, Fibre hybridisation in polymer composites: A review, Composites Part A: Applied Science and Manufacturing 67 (2014) 181–200. doi:10.1016/j.compositesa.2014.08.027.

[4] A. Bunsell, L. Gorbatikh, H. Morton, S. Pimenta, I. Sinclair, M. Spearing, Y. Swolfs, A. Thionnet, Benchmarking of strength models for unidirectional composites under longitudinal tension, Composites Part A: Applied Science and Manufacturing 111 (June 2017) (2018) 138–150. doi:10.1016/j.compositesa.2018.03.016.

[5] Y. Swolfs, I. Verpoest, L. Gorbatikh, A review of input data and modelling assumptions in longitudinal strength models for unidirectional fibre-reinforced composites, Composite Structures 150 (2016) 153–172. doi:10.1016/j.compstruct.2016.05.002.

[6] Y. Swolfs, I. Verpoest, L. Gorbatikh, Tensile failure of hybrid composites: measuring, predicting and understanding, IOP Conference Series: Materials Science and Engineering 139 (2016) 012008. doi:10.1088/1757-899X/139/1/012008.

[7] A. R. Bunsell, B. Harris, Hybrid carbon and glass fibre composites, Composites 5 (4) (1974) 157–164. doi:10.1016/0010-4361(74)90107-4.

[8] P. W. Manders, M. G. Bader, The strength of hybrid glass/carbon fibre composites - Part 1 Failure strain enhancement and failure mode, Journal of Materials Science 16 (8) (1981) 2233–2245. doi:10.1007/BF00542386.

[9] K. D. Jones, A. DiBenedetto, Fiber fracture in hybrid composite systems, Composites Science and Technology 51 (1) (1994) 53–62. doi:10.1016/0266-3538(94)90156-2.

[10] M. R. Wisnom, Mechanisms to create high performance pseudo-ductile composites, IOP Conference Series: Materials Science and Engineering 139 (2016) 012010. doi:10.1088/1757-899X/139/1/012010.

[11] M. Jalalvand, G. Czel, M. R. Wisnom, Damage analysis of pseudo-ductile thin-ply UD hybrid composites - A new analytical method, Composites Part A: Applied Science and Manufacturing 69 (2015) 83–93. doi:10.1016/j.compositesa.2014.11.006.

[12] M. Fotouhi, M. Jalalvand, M. R. Wisnom, High performance quasi-isotropic thin-ply carbon/glass hybrid composites with pseudo-ductile behaviour in all fibre orientations, Composites Science and Technology 152 (2017) 101–110. doi:10.1016/j.compscitech.2017.08.024.

[13] G. Czel, T. Rev, M. Jalalvand, M. Fotouhi, M. L. Longana, O. J. Nixon-Pearson, M. R. Wisnom, Pseudo-ductility and reduced notch sensitivity in multi-directional all-carbon/epoxy thin-ply hybrid composites, Composites Part A: Applied Science and Manufacturing 104 (2018) 151–164. doi:10.1016/j.compositesa.2017.10.028.

[14] M. Jalalvand, G. Czel, M. R. Wisnom, Parametric study of failure mechanisms and optimal configurations of pseudo-ductile thin-ply UD hybrid composites, Composites Part A: Applied Science and Manufacturing 74 (2015) 123–131. doi:10.1016/j.compositesa.2015.04.001.

[15] M. R. Wisnom, G. Czel, Y. Swolfs, M. Jalalvand, L. Gorbatikh, I. Verpoest, Hybrid effects in thin ply carbon/glass unidirectional laminates: Accurate experimental determination and prediction, Composites Part A: Applied Science and Manufacturing 88 (2016) 131–139. doi:10.1016/j.compositesa.2016.04.014.

[16] G. Czel, M. Jalalvand, M. R. Wisnom, T. Czigany, Design and characterisation of high performance, pseudo-ductile all-carbon/epoxy unidirectional hybrid composites, Composites Part B: Engineering 111 (2017) 348–356. doi:10.1016/j.compositesb.2016.11.049.

[17] H. Yu, M. L. Longana, M. Jalalvand, M. R. Wisnom, K. D. Potter, Pseudo-ductility in intermingled carbon/glass hybrid composites with highly aligned discontinuous fibres, Composites Part A: Applied Science and Manufacturing 73 (2015) 35–44. doi:10.1016/j.compositesa.2015.02.014.

[18] G. Czel, M. R. Wisnom, Demonstration of pseudo-ductility in high performance glass/epoxy composites by hybridisation with thin-ply carbon prepreg, Composites Part A: Applied Science and Manufacturing 52 (2013) 23–30. doi:10.1016/j.compositesa.2013.04.006.

[19] J. Summerscales, D. Short, Carbon fibre and glass fibre hybrid reinforced plastics, Composites 9 (3) (1978) 157–166. doi:10.1016/0010-4361(78)90341-5.

[20] J. Aveston, J. M. Sillwood, Synergistic fibre strengthening in hybrid composites, Journal of Materials Science 11 (10) (1976) 1877–1883. doi:10.1007/BF00708266.

[21] M. A. Attia, M. A. Abd El-Baky, A. E. Alshorbagy, Mechanical performance of intraply and inter-intraply hybrid composites based on e-glass and polypropylene unidirectional fibers, Journal of Composite Materials 51 (3) (2017) 381–394. doi:10.1177/0021998316644972.

[22] C. Zweben, Tensile strength of hybrid composites, Journal of Materials Science 12 (7) (1977) 1325–1337. doi:10.1007/BF00540846.

[23] T. Hayashi, On the improvement of mechanical properties of composites by hybrid composition, in: Proc 8th Int Reinforced plastics Conference, 1972, pp. 149–152.

[24] H. Fukuda, T. Chou, Monte Carlo Simulation of the Strength of Hybrid Composites, Journal of Composite Materials 16 (5) (1982) 371–385. doi:10.1177/002199838201600502.

[25] H. Fukuda, An advanced theory of the strength of hybrid composites, Journal of Materials Science 19 (3) (1984) 974–982. doi:10.1007/BF00540468.

[26] J. Xing, G. Hsiao, T. Chou, A Dynamic Explanation of The Hybrid Effect, Journal of Composite Materials 15 (5) (1981) 443–461. doi:10.1177/002199838101500504.

[27] G. Kretsis, A review of the tensile, compressive, flexural and shear properties of hybrid fibre-reinforced plastics, Composites 18 (1) (1987) 13–23. doi:10.1016/0010-4361(87)90003-6.

[28] L. N. Phillips, The hybrid effect - does it exist?, Composites 7 (1) (1976) 7–8. doi:10.1016/0010-4361(76)90273-1.

[29] G. Czel, M. Jalalvand, M. R. Wisnom, Hybrid specimens eliminating stress concentrations in tensile and compressive testing of unidirectional composites, Composites Part A: Applied Science and Manufacturing 91 (2016) 436–447. doi:10.1016/j.compositesa.2016.07.021.

[30] M. J. Pitkethly, M. G. Bader, Failure modes of hybrid composites consisting of carbon fibre bundles dispersed in a glass fibre epoxy resin matrix, Journal of

Physics D: Applied Physics 20 (3) (1987) 315–322. doi:10.1088/0022-3727/20/3/013.

[31] Y. Swolfs, R. M. McMeeking, I. Verpoest, L. Gorbatikh, The effect of fibre dispersion on initial failure strain and cluster development in unidirectional carbon/glass hybrid composites, Composites Part A: Applied Science and Manufacturing 69 (2014) 279–287. doi:10.1016/j.compositesa.2014.12.001.

[32] L. Mishnaevsky, G. Dai, Hybrid carbon/glass fiber composites: Micromechanical analysis of structure-damage resistance relationships, Computational Materials Science 81 (2014) 630–640. doi:10.1016/j.commatsci.2013.08.024.

[33] Y. Swolfs, I. Verpoest, L. Gorbatikh, Maximising the hybrid effect in unidirectional hybrid composites, Materials and Design 93 (2016) 39–45. doi:10.1016/j.matdes.2015.12.137.

[34] Y. Swolfs, R. M. McMeeking, V. P. Rajan, F. W. Zok, I. Verpoest, L. Gorbatikh, Global load-sharing model for unidirectional hybrid fibre-reinforced composites, Journal of the Mechanics and Physics of Solids 84 (2015) 380–394. doi:10.1016/j.jmps.2015.08.009.

[35] R. Tavares, A. R. Melro, M. A. Bessa, A. Turon, W. K. Liu, P. Camanho, Mechanics of hybrid polymer composites: analytical and computational study, Computational Mechanics 57 (3) (2016) 405–421. doi:10.1007/s00466-015-1252-0.

[36] S. Behzadi, P. T. Curtis, F. R. Jones, Improving the prediction of tensile failure in unidirectional fibre composites by introducing matrix shear yielding, Composites Science and Technology 69 (14) (2009) 2421–2427. doi:10.1016/j.compscitech.2009.06.010.

[37] R. P. Tavares, J. M. Guerrero, F. Otero, A. Turon, J. A. Mayugo, J. Costa, P. P. Camanho, Effects of local stress fields around broken fibres on the longitudinal failure of composite materials, International Journal of Solids and Structures 156-157 (2019) 294–305. doi:10.1016/j.ijsolstr.2018.08.027.

[38] B. Fiedler, A. Klisch, K. Schulte, Stress concentrations in multiple fibre model composites, Composites Part A: Applied Science and Manufacturing 29 (9-10) (1998) 1013–1019. doi:10.1016/S1359-835X(98)00014-1.

[39] R. Tavares, F. Otero, A. Turon, P. Camanho, Effective simulation of the mechanics of longitudinal tensile failure of unidirectional polymer composites, International Journal of Fracture 208 (1-2) (2017) 269–285. doi:10.1007/s10704-017-0252-9.

[40] Y. Swolfs, R. M. McMeeking, I. Verpoest, L. Gorbatikh, Matrix cracks around fibre breaks and their effect on stress redistribution and failure development in unidirectional composites, Composites Science and Technology 108 (2015) 16–22. doi:10.1016/j.compscitech.2015.01.002.

[41] Y. Swolfs, H. Morton, A. E. Scott, L. Gorbatikh, P. A. S. Reed, I. Sinclair, S. M. Spearing, I. Verpoest, Synchrotron radiation computed tomography for experimental validation of a tensile strength model for unidirectional fibre-reinforced composites, Composites Part A: Applied Science and Manufacturing 77 (2015) 106–113. doi:10.1016/j.compositesa.2015.06.018.

[42] A. E. Scott, M. Mavrogordato, P. Wright, I. Sinclair, S. M. Spearing, In situ fibre fracture measurement in carbon-epoxy laminates using high resolution computed tomography, Composites Science and Technology 71 (12) (2011) 1471–1477. doi:10.1016/j.compscitech.2011.06.004.

[43] H. Fukuda, Micromechanical strength theory of hybrid composites, Advanced Composite Materials 1 (1) (1991) 39–53. doi:10.1163/156855191X00054.

[44] P. W. Manders, M. G. Bader, The strength of hybrid glass/carbon fibre composites - Part 2 A statistical model, Journal of Materials Science 16 (8) (1981) 2246–2256. doi:10.1007/BF00542387.

[45] Y. Swolfs, L. Gorbatikh, I. Verpoest, Stress concentrations in hybrid unidirectional fibre-reinforced composites with random fibre packings, Composites Science and Technology 85 (2013) 10–16. doi:10.1016/j.compscitech.2013.05.013.

[46] H. Fukuda, T.-W. Chou, Stress Concentrations in a Hybrid Composite Sheet, Journal of Applied Mechanics 50 (4a) (1983) 845. doi:10.1115/1.3167155.

[47] M. R. Wisnom, Relationship between strength variability and size effect in unidirectional carbon fibre/epoxy, Composites 22 (1) (1991) 47–52. doi:10.1016/0010-4361(91)90102-M.

[48] M. R. Wisnom, Size effects in the testing of fibre-composite materials, Composites Science and Technology 59 (13) (1999) 1937–1957. doi:10.1016/S0266-3538(99)00053-6.

[49] M. R. Wisnom, J. W. Atkinson, Reduction in tensile and flexural strength of unidirectional glass fibre-epoxy with increasing specimen size, Composite Structures 38 (1-4) (1997) 405–411. doi:10.1016/S0263-8223(97)00075-5.

[50] J. Hitchon, D. Phillips, The effect of specimen size on the strength of cfrp, Composites 9 (2) (1978) 119–124. doi:10.1016/0010-4361(78)90590-6.

[51] H. J. Phillips, R. A. Shenoi, S. M. Lewis, Effect of specimen size on the strength scaling of GFRP laminates, Materials Letters 21 (3-4) (1994) 229–238. doi:10.1016/0167-577X(94)90181-3.

[52] T. Okabe, N. Takeda, Size effect on tensile strength of unidirectional CFRP composites—experiment and simulation, Composites science and technology 62 (15) (2002) 2053–2064. doi:10.1016/S0266-3538(02)00146-X.

[53] M. R. Wisnom, S. R. Hallett, C. Soutis, Scaling effects in notched composites, Journal of Composite Materials 44 (2) (2010) 195–210. doi:10.1177/0021998309339865.

[54] S. Pimenta, A computationally-efficient hierarchical scaling law to predict damage accumulation in composite fibre-bundles, Composites Science and Technology 146 (2017) 210–225. doi:10.1016/j.compscitech.2017.04.018.

[55] D. Johnson, J. Morton, S. Kellas, K. Jackson, Scaling effects in sublaminate-level scaled composite laminates, AIAA Journal 36 (3) (1998) 441–447. doi:10.2514/2.384.

[56] J. Hedgepeth, Stress concentrations in filamentary structures, Tech. rep., NASA TN D-882, Nasa report (1961).

[57] J. Xing, X.-R. Liu, T.-W. Chou, Dynamic Stress Concentration Factors in Unidirectional Composites, Journal of Composite Materials 19 (3) (1985) 269–275. doi:10.1177/002199838501900305.

[58] E. N. Sakharova, A. S. Ovchinskii, Dynamics of stress redistribution in fiber fracture in composites, Mechanics of Composite Materials 16 (4) (1980) 417–422. doi:10.1007/BF00604856.

[59] E. N. Sakharova, A. S. Ovchinskii, Influence of dynamic effects accompanying rupture of fibers and separation of fibers from the matrix on interaction between failure micromechanisms of composite materials, Mechanics of Composite Materials 20 (3) (1984) 323–327.

[60] R. Ganesh, S. Sockalingam, B. Z. (Gama) Haque, J. W. Gillespie, Dynamic effects of single fiber break in unidirectional glass fiber-reinforced composites, Journal of Composite Materials 51 (9) (2017) 1307–1320. doi:10.1177/0021998316669218.

[61] R. Ganesh, S. Sockalingam, J. W. Gillespie, Dynamic effects of a single fiber break in unidirectional glass fiber-reinforced polymer composites: Effects of matrix plasticity, Journal of Composite Materials 52 (14) (2018) 1873–1886. doi:10.1177/0021998317737604.

[62] G. Bullegas, Carbon Fibre laminates with engineered fracture behaviour, Ph.D. thesis, Imperial College London (2017).

[63] R. P. Tavares, F. Otero, J. Baiges, A. Turon, P. P. Camanho, A dynamic spring element model for the prediction of longitudinal failure of polymer composites, Computational Materials Science 160 (October 2018) (2019) 42–52. doi:10.1016/J.COMMATSCI.2018.12.048.

[64] H. Fukunaga, T.-W. Chou, H. Fukuda, Strength of Intermingled Hybrid Composites, Journal of Reinforced Plastics and Composites 3 (1984) 145–160. doi:10.1177/073168448400300204.

[65] J. Aveston, A. Kelly, Tensile First Cracking Strain and Strength of Hybrid Composites and Laminates, Philosophical Transactions of the Royal Society A: Mathematical, Physical and Engineering Sciences 294 (1980) 519–534. doi:10.1098/rsta.1980.0061.

[66] D. Harlow, Statistical properties of hybrid composites. Part I: recursion analysis, Proceedings of The Royal Society of London, Series A: Mathematical and Physical Sciences 389 (1796) (1983) 67–100.

[67] H. Fukuda, Stress concentration factors in unidirectional composites with random fiber spacing, Composites Science and Technology 22 (2) (1985) 153–163. doi:10.1016/0266-3538(85)90082-X.

[68] Y. Swolfs, L. Gorbatikh, V. Romanov, S. Orlova, S. V. Lomov, I. Verpoest, Stress concentrations in an impregnated fibre bundle with random fibre packing, Composites Science and Technology 74 (2013) 113–120. doi:10.1016/j.compscitech.2012.10.013.

[69] H. Fukuda, K. Kawata, On the stress concentration factor in fibrous composites, Fibre Science and Technology 9 (3) (1976) 189–203. doi:10.1016/0015-0568(76)90003-8.

[70] H. Fukuda, K. Kawata, On the strength distribution of unidirectional fibre composites, Fibre Science and Technology 10 (1) (1977) 53–63. doi:10.1016/0015-0568(77)90028-8.

[71] Q. D. Zeng, A statistical analysis of the tensile failure and hybrid effect of an intraply hybrid composite, International Journal of Fracture 68 (4) (1994) 351–362. doi:10.1007/BF00033961.

[72] F. Conde, P. Coelho, R. Tavares, P. Camanho, J. Guedes, H. Rodrigues, Optimization of hybrid polymer composites under uniaxial traction, Engineering Computations 35 (2) (2018) 904–931. doi:10.1108/EC-11-2017-0427.

[73] P. Manders, The strength of mixed fibre composites, Ph.D. thesis, University of Surrey, UK (1979).

[74] Y. Swolfs, I. Verpoest, L. Gorbatikh, Recent advances in fibre-hybrid composites: materials selection, opportunities and applications, International Materials Reviews 64 (4) (2019) 181–215. doi:10.1080/09506608.2018.1467365.

[75] I. J. Beyerlein, S. Phoenix, Stress concentrations around multiple fiber breaks in an elastic matrix with local yielding or debonding using quadratic influence superposition, Journal of the Mechanics and Physics of Solids 44 (12) (1996) 1997–2036. doi:10.1016/S0022-5096(96)00068-3.

[76] T. Okabe, N. Takeda, Y. Kamoshida, M. Shimizu, W. A. Curtin, A 3D shear-lag model considering micro-damage and statistical strength prediction of unidirectional fiber-reinforced composites, Composites Science and Technology 61 (12) (2001) 1773–1787. doi:10.1016/S0266-3538(01)00079-3.

[77] R. Lane, S. Hayes, F. Jones, Fibre/matrix stress transfer through a discrete interphase: 2. High volume fraction systems, Composites Science and Technology 61 (4) (2002) 565–578. doi:10.1016/s0266-3538(00)00229-3.

[78] Z. H. Xia, W. A. Curtin, Multiscale modeling of damage and failure in aluminum-matrix composites, Composites Science and Technology 61 (15) (2001) 2247–2257. doi:10.1016/S0266-3538(01)00119-1.

[79] N. Pan, R. Postle, The tensile strength of hybrid fiber composites: a probabilistic analysis of the hybrid effects, Philosophical Transactions of the Royal Society A: Mathematical, Physical and Engineering Sciences 354 (1714) (1996) 1875–1897. doi:10.1098/rsta.1996.0082.

[80] F. Zhao, N. Takeda, Effect of interfacial adhesion and statistical fiber strength on tensile strength of unidirectional glass fiber/epoxy composites. Part II: Comparison with prediction, Composites Part A: Applied Science and Manufacturing 31 (11) (2000) 1215–1224. doi:10.1016/S1359-835X(00)00086-5.

[81] Z. Xia, W. A. Curtin, P. W. Peters, Multiscale modeling of failure in metal matrix composites, Acta Materialia 49 (2) (2001) 273–287. doi:10.1016/S1359-6454(00)00317-7.

[82] P. van den Heuvel, M. Wubbolts, R. Young, T. Peijs, Failure phenomena in two-dimensional multi-fibre model composites: 5. A finite element study, Composites Part A: Applied Science and Manufacturing 29 (9) (1998) 1121–1135. doi:10.1016/S1359-835X(98)00089-X.

[83] P. van den Heuvel, S. Goutianos, R. Young, T. Peijs, Failure phenomena in fibre-reinforced composites. Part 6: a finite element study of stress concentrations in unidirectional carbon fibre-reinforced epoxy composites, Composites Science and Technology 64 (5) (2004) 645–656. doi:10.1016/j.compscitech.2003.06.003.

[84] G. C. Shih, L. J. Ebert, Theoretical modelling of the effect of the interfacial shear strength on the longitudinal tensile strength of unidirectional composites, Journal of composite materials 21 (3) (1987) 207–224. doi:10.1177/002199838702100302.

[85] C. M. Landis, R. M. McMeeking, Stress concentrations in composites with interface sliding, matrix stiffness and uneven fiber spacing using shear lag theory, International Journal of Solids and Structures 36 (28) (1999) 4333–4361. doi:10.1016/S0020-7683(98)00193-0.

[86] X. Wang, J. Zhang, Z. Wang, W. Liang, L. Zhou, Finite element simulation of the failure process of single fiber composites considering interface properties, Composites Part B: Engineering 45 (1) (2013) 573–580. doi:10.1016/j.compositesb.2012.07.051.

[87] A. E. Scott, I. Sinclair, S. M. Spearing, A. Thionnet, A. R. Bunsell, Damage accumulation in a carbon/epoxy composite: Comparison between a multiscale model and computed tomography experimental results, Composites Part A: Applied Science and Manufacturing 43 (9) (2012) 1514–1522. doi:10.1016/j.compositesa.2012.03.011.

[88] Z. Z. Du, R. M. McMeeking, Creep models for metal matrix composites with long brittle fibers, Journal of the Mechanics and Physics of Solids 43 (5) (1995) 701–726. doi:10.1016/0022-5096(95)00007-6.

[89] N. Iyengar, W. A. Curtin, Time-dependent failure in fiber-reinforced composites by matrix and interface shear creep, Acta Materialia 45 (8) (1997) 3419–3429. doi:10.1016/S1359-6454(96)00412-0.

[90] D. C. Lagoudas, H. Chung-Yuen, S. Phoenix, Time evolution of overstress profiles near broken fibers in a composite with a viscoelastic matrix, International Journal of Solids and Structures 25 (1) (1989) 45–66. doi:10.1016/0020-7683(89)90103-0.

[91] D. D. Mason, C. Y. Hui, S. Phoenix, Stress profiles around a fiber break in a composite with a nonlinear, power law creeping matrix, International Journal of Solids and Structures 29 (23) (1992) 2829–2854. doi:10.1016/0020-7683(92)90143-H.

[92] S. Blassiau, A. Thionnet, A. R. Bunsell, Micromechanisms of load transfer in a unidirectional carbon fibre-reinforced epoxy composite due to fibre failures. Part 2: Influence of viscoelastic and plastic matrices on the mechanisms of load transfer, Composite Structures 74 (3) (2006) 319–331. doi:10.1016/j.compstruct.2005.04.029.

[93] B. Fabeny, W. A. Curtin, Damage-enhanced creep and rupture in fiber-reinforced composites, Acta Materialia 44 (9) (1996) 3439–3451. doi:10.1016/1359-6454(96)00027-4.

[94] I. J. Beyerlein, S. L. Phoenix, R. Raj, Time evolution of stress redistribution around multiple fiber breaks in a composite with viscous and viscoelastic matrices, International Journal of Solids and Structures 35 (24) (1998) 3177–3211. doi:10.1016/S0020-7683(98)00010-9.

[95] S. Blassiau, A. Thionnet, A. R. Bunsell, Three-dimensional analysis of load transfer micro-mechanisms in fibre/matrix composites, Composites Science and Technology 69 (1) (2009) 33–39. doi:10.1016/j.compscitech.2007.10.041.

[96] M. Jalalvand, G. Czél, M. R. Wisnom, Numerical modelling of the damage modes in UD thin carbon/glass hybrid laminates, Composites Science and Technology 94 (2014) 39–47. doi:10.1016/j.compscitech.2014.01.013.

[97] T.-W. Chou, A. Kelly, Mechanical properties of composites, Annual Review of Materials Science 10 (1980) 229–259. doi:10.1146/annurev.ms.10.080180.001305.

[98] J. D. Fuller, M. Jalalvand, M. R. Wisnom, Combining fibre rotation and fragmentation to achieve pseudo-ductile CFRP laminates, Composite Structures 142 (2016) 155–166. doi:10.1016/j.compstruct.2016.01.073.

[99] H. Diao, A. Bismarck, P. Robinson, M. R. Wisnom, Pseudo-ductile behavior of unidirectional fibre reinforced polyamide-12 composite by intra-tow hybridization, in: ECCM15 - Proceedings of the 15th European Conference on Composite Materials, 2012, pp. 1–8.

[100] F. Mesquita, Y. Swolfs, S. V. Lomov, L. Gorbatikh, Ply fragmentation in unidirectional hybrid composites linked to stochastic fibre behaviour: A dual-scale model, Composites Science and Technology 181 (March) (2019) 107702. doi:10.1016/j.compscitech.2019.107702.

[101] L. Utzig, C. Karch, J. Rehra, B. Hannemann, S. Schmeer, Modeling and simulation of the effective strength of hybrid polymer composites reinforced by carbon and steel fibers, Journal of Materials Science 53 (1) (2018) 667–677. doi:10.1007/s10853-017-1512-9.

[102] Y. Swolfs, P. De Cuyper, M. G. Callens, I. Verpoest, L. Gorbatikh, Hybridisation of two ductile materials – Steel fibre and self-reinforced polypropylene composites, Composites Part A: Applied Science and Manufacturing 100 (2017) 48–54. doi:10.1016/j.compositesa.2017.05.001.

[103] W. Weibull, A statistical distribution function of wide applicability, Journal of Applied Mechanics 18 (1951) 293–297.

[104] A. S. Watson, R. L. Smith, An examination of statistical theories for fibrous materials in the light of experimental data, Journal of Materials Science 20 (9) (1985) 3260–3270. doi:10.1007/BF00545193.

[105] I. J. Beyerlein, S. Phoenix, Statistics for the strength and size effects of microcomposites with four carbon fibers in epoxy resin, Composites Science and Technology 56 (1) (1996) 75–92. doi:10.1016/0266-3538(95)00131-X.

[106] J. Gutans, V. Tamuzs, Strength probability of unidirectional hybrid composites, Theoretical and Applied Fracture Mechanics 7 (3) (1987) 193–200. doi:10.1016/0167-8442(87)90036-X.

[107] W. A. Curtin, Tensile strength of fiber-reinforced composites: III. Beyond the traditional Weibull model for fiber strengths, Journal of Composite Materials 34 (15) (2000) 1301–1332. doi:10.1177/002199830003401503.

[108] J. Watanabe, F. Tanaka, H. Okuda, T. Okabe, Tensile strength distribution of carbon fibers at short gauge lengths, Advanced Composite Materials 23 (5-6) (2014) 535–550. doi:10.1080/09243046.2014.915120.

[109] H. Peterlik, D. Loidl, Bimodal strength distributions and flaw populations of ceramics and fibres, Engineering Fracture Mechanics 68 (3) (2000) 253–261. doi:10.1016/S0013-7944(00)00110-7.

[110] J. W. Hitchon, D. C. Phillips, The dependence of the strength of carbon fibres on length, Fibre Science and Technology 12 (3) (1979) 217–233. doi:10.1016/0015-0568(79)90032-0.

[111] K. Goda, H. Fukunaga, The evaluation of the strength distribution of silicon carbide and alumina fibres by a multi-modal Weibull distribution, Journal of Materials Science 21 (12) (1986) 4475–4480. doi:10.1007/BF01106574.

[112] D. Harlow, S. Phoenix, Probability distributions for the strength of composite materials II: A convergent sequence of tight bounds, International Journal of Fracture 17 (6) (1981) 601–630. doi:10.1007/BF00681559.

[113] C. M. Landis, I. J. Beyerlein, R. M. McMeeking, Micromechanical simulation of the failure of fiber reinforced composites, Journal of the Mechanics and Physics of Solids 48 (3) (2000) 621–648. doi:10.1016/S0022-5096(99)00051-4.

[114] J. Zhang, F. Wang, Modeling of Progressive Failure in Ductile Matrix Composites Including Local Matrix Yielding, Mechanics of Advanced Materials and Structures 16 (7) (2009) 522–535. doi:10.1080/15376490903133384.

[115] F. Wang, Z. Q. Chen, Y. Q. Wei, X. G. Zeng, Numerical Modeling of Tensile Behavior of Fiber-reinforced Polymer Composites, Journal of Composite Materials 44 (19) (2010) 2325–2340. doi:10.1177/0021998310369595.

[116] M. R'Mili, N. Godin, J. Lamon, Flaw strength distributions and statistical parameters for ceramic fibers: The normal distribution, Physical Review E - Statistical, Nonlinear, and Soft Matter Physics 85 (5) (2012) 1–6. doi:10.1103/PhysRevE.85.051106.

[117] M. Ibnabdeljalil, S. L. Phoenix, Scalings in the statistical failure of brittle matrix composites with discontinuous fibers-I. Analysis and Monte Carlo simulations, Acta Metallurgica Et Materialia 43 (8) (1995) 2975–2983. doi:10.1016/0956-7151(95)00017-P.

[118] M. R. Gurvich, A. DiBenedetto, S. V. Ranade, A new statistical distribution for characterizing the random strength of brittle materials, Journal of Materials Science 32 (10) (1997) 2559–2564. doi:10.1023/A:1018594215963.

[119] K. K. Phani, Strength distribution and gauge length extrapolations in glass fibre, Journal of Materials Science 23 (4) (1988) 1189–1194. doi:10.1007/BF01154577.

[120] Y. Swolfs, I. Verpoest, L. Gorbatikh, Issues in strength models for unidirectional fibre-reinforced composites related to Weibull distributions, fibre packings and boundary effects, Composites Science and Technology 114 (2015) 42–49. doi:10.1016/j.compscitech.2015.04.002.

[121] J.-M. Berthelot, Classical laminate theory, Springer New York, 1999.

[122] D. Trias, J. Costa, A. Turon, J. E. Hurtado, Determination of the critical size of a statistical representative volume element (SRVE) for carbon reinforced polymers, Acta Materialia 54 (13) (2006) 3471–3484. doi:10.1016/j.actamat.2006.03.042.

[123] J. Zangenberg, P. Brøndsted, Determination of the minimum size of a statistical representative volume element from a fibre-reinforced composite based on point pattern statistics, Scripta Materialia 68 (7) (2013) 503–505. doi:10.1016/j.scriptamat.2012.11.032.

[124] A. R. Melro, P. Camanho, S. T. Pinho, Generation of random distribution of fibres in long-fibre reinforced composites, Composites Science and Technology 68 (9) (2008) 2092–2102. doi:10.1016/j.compscitech.2008.03.013.

[125] D. Trias, J. Costa, J. Mayugo, J. E. Hurtado, Random models versus periodic models for fibre reinforced composites, Computational Materials Science 38 (2) (2006) 316–324. doi:10.1016/j.commatsci.2006.03.005.

[126] V. Romanov, S. V. Lomov, Y. Swolfs, S. Orlova, L. Gorbatikh, I. Verpoest, Statistical analysis of real and simulated fibre arrangements in unidirectional composites, Composites Science and Technology 87 (2013) 126–134. doi:10.1016/j.compscitech.2013.07.030.

[127] T. J. Vaughan, C. T. McCarthy, A combined experimental-numerical approach for generating statistically equivalent fibre distributions for high strength laminated composite materials, Composites Science and Technology 70 (2) (2010) 291–297. doi:10.1016/j.compscitech.2009.10.020.

[128] L. Yang, Y. Yan, Z. Ran, Y. Liu, A new method for generating random fibre distributions for fibre reinforced composites, Composites Science and Technology 76 (2013) 14–20. doi:10.1016/j.compscitech.2012.12.001.

[129] Z. Shan, A. M. Gokhale, Representative volume element for non-uniform microstructure, Computational Materials Science 24 (3) (2002) 361–379. doi:10.1016/S0927-0256(01)00257-9.

[130] R. M. Sencu, Z. Yang, Y. C. Wang, P. J. Withers, C. Rau, A. Parson, C. Soutis, Generation of micro-scale finite element models from synchrotron X-ray CT images for multidirectional carbon fibre reinforced composites, Composites Part A: Applied Science and Manufacturing 91 (2016) 85–95. doi:10.1016/j.compositesa.2016.09.010.

[131] R. Pyrz, Quantitative description of the microstructure of composites. Part I: Morphology of unidirectional composite systems, Composites Science and Technology 50 (2) (1994) 197–208. doi:10.1016/0266-3538(94)90141-4.

[132] V. A. Buryachenko, R. Y. Kim, N. J. Pagano, J. E. Spowart, Quantitative description and numerical simulation of random microstructures of composites and their effective elastic moduli, International Journal of Solids and Structures 40 (1) (2003) 47–72. doi:10.1016/S0020-7683(02)00462-6.

[133] J. H. Oh, K. K. Jin, S. K. Ha, Interfacial strain distribution of a unidirectional composite with randomly distributed fibers under transverse loading, Journal of Composite Materials 40 (9) (2006) 759–778. doi:10.1177/0021998305055546.

[134] T. Zhang, Y. Yan, A comparison between random model and periodic model for fiber-reinforced composites based on a new method for generating fiber distributions, Polymer Composites 38 (1) (2017) 77–86. doi:10.1002/pc.23562.

[135] Y. Ismail, D. Yang, J. Ye, Discrete element method for generating random fibre distributions in micromechanical models of fibre reinforced composite laminates, Composites Part B: Engineering 90 (2016) 485–492. doi:10.1016/j.compositesb.2016.01.037.

[136] Y. Ismail, Y. Sheng, D. Yang, J. Ye, Discrete element modelling of unidirectional fibre-reinforced polymers under transverse tension, Composites Part B: Engineering 73 (2015) 118–125. doi:10.1016/j.compositesb.2014.12.024.

[137] A. Wongsto, S. Li, Micromechanical FE analysis of UD fibre-reinforced composites with fibres distributed at random over the transverse cross-section, Composites Part A: Applied Science and Manufacturing 36 (9) (2005) 1246–1266. doi:10.1016/j.compositesa.2005.01.010.

[138] S. A. Elnekhaily, R. Talreja, Damage initiation in unidirectional fiber composites with different degrees of nonuniform fiber distribution, Composites Science and Technology 155 (2018) 22–32. doi:10.1016/j.compscitech.2017.11.017.

[139] H. Qing, L. Mishnaevsky, Unidirectional high fiber content composites: Automatic 3D FE model generation and damage simulation, Computational Materials Science 47 (2) (2009) 548–555. doi:10.1016/j.commatsci.2009.09.023.

[140] H. E. Daniels, The Statistical Theory of the Strength of Bundles of Threads. I, Proceedings of the Royal Society A: Mathematical, Physical and Engineering Sciences 183 (995) (1945) 405–435. doi:10.1098/rspa.1945.0011.

[141] B. W. Rosen, Tensile failure of fibrous composites, AIAA Journal 2 (11) (1964) 1985–1991. doi:10.2514/3.2699.

[142] W. A. Curtin, Exact theory of fibre fragmentation in a single-filament composite, Journal of Materials Science 26 (19) (1991) 5239–5253. doi:10.1007/BF01143218.

[143] W. A. Curtin, Stochastic damage evolution and failure in fiber-reinforced composites, Advances in Applied Mechanics 36 (C) (1998) 163–253. doi:10.1016/S0065-2156(08)70186-8.

[144] W. A. Curtin, N. Takeda, Tensile strength of fiber-reinforced composites: I. Model and effects of local fiber geometry, Journal of Composite Materials 32 (22) (1998) 2042–2059. doi:10.1177/002199839803202203.

[145] W. A. Curtin, B. Ahn, N. Takeda, Modeling brittle and tough stress–strain behavior in unidirectional ceramic matrix composites, Acta Materialia 46 (10) (1998) 3409–3420. doi:10.1016/S1359-6454(98)00041-X.

[146] W. A. Curtin, N. Takeda, Tensile strength of fiber-reinforced composites: II. Application to polymer matrix composites, Journal of Composite Materials 32 (22) (1998) 2060–2081. doi:10.1177/002199839803202204.

[147] W. A. Curtin, The "tough" to brittle transition in brittle matrix composites, Journal of the Mechanics and Physics of Solids 41 (2) (1993) 217–245. doi:10.1016/0022-5096(93)90007-3.

[148] W. A. Curtin, Theory of Mechanical Properties of Ceramic-Matrix Composites, Journal of the American Ceramic Society 74 (11) (1991) 2837–2845. doi:10.1111/j.1151-2916.1991.tb06852.x.

[149] A. Kelly, W. Tyson, Tensile properties of fibre-reinforced and metals: copper/tungsten and copper/molybdenum, Journal of the mechanics and physics of solids 13 (6) (1965) 329–350. doi:10.1016/0022-5096(65)90035-9.

[150] C. Y. Hui, S. Phoenix, M. Ibnabdeljalil, R. L. Smith, An exact closed form solution for fragmentation of Weibull fibers in a single filament composite with applications to fiber-reinforced ceramics, Journal of the Mechanics and Physics of Solids 43 (10) (1995) 1551–1585. doi:10.1016/0022-5096(95)00045-K.

[151] J. M. Neumeister, A constitutive law for continuous fiber reinforced brittle matrix composites with fiber fragmentation and stress recovery, Journal of the Mechanics and Physics of Solids 41 (8) (1993) 1383–1404. doi:10.1016/0022-5096(93)90085-T.

[152] A. B. de Morais, Prediction of the longitudinal tensile strength of polymer matrix composites, Composites Science and Technology 66 (15) (2006) 2990–2996. doi:10.1016/j.compscitech.2006.02.005.

[153] J. Koyanagi, H. Hatta, M. Kotani, H. Kawada, A Comprehensive Model for Determining Tensile Strengths of Various Unidirectional Composites, Journal of Composite Materials 43 (18) (2009) 1901–1914. doi:10.1177/0021998309341847.

[154] V. Calard, J. Lamon, Failure of fiber bundles, Composites Science and Technology 64 (5) (2004) 701–710. doi:10.1016/j.compscitech.2003.07.003.

[155] J. Vanegas, A. Turon, J. Costa, L. Cruz, J. Mayugo, Analytical model for predicting the tensile strength of unidirectional composites based on the density of fiber breaks, Composites Part B: Engineering 141 (February 2017) (2018) 84–91. doi:10.1016/j.compositesb.2017.12.012.

[156] R. B. Henstenburg, S. L. Phoenix, Interfacial shear strength studies using the single-filament-composite test. Part II: A probability model and Monte Carlo simulation, Polymer Composites 10 (6) (1989) 389–408. doi:10.1002/pc.750100603.

[157] S. Phoenix, Statistical Issues in the Fracture of Brittle Matrix Fibrous Composites, Composites Science and Technology 48 (1-4) (1993) 65–80. doi:10.1016/0266-3538(93)90121-V.

[158] S. Jansson, K. Kedward, Ultimate tensile strength of composites exhibiting fiber fragmentation, Composites Science and Technology 56 (1) (1996) 31–35. doi:10.1016/0266-3538(95)00133-6.

[159] S. Pimenta, S. T. Pinho, Hierarchical scaling law for the strength of composite fibre bundles, Journal of the Mechanics and Physics of Solids 61 (6) (2013) 1337–1356. doi:10.1016/j.jmps.2013.02.004.

[160] J. Hedgepeth, P. Van Dyke, Local stress concentrations in imperfect filamentary composite materials, Journal of Composite Materials 1 (3) (1967) 294–309. doi:10.1177/002199836700100305.

[161] L. Mishnaevsky, P. Brøndsted, Statistical modelling of compression and fatigue damage of unidirectional fiber reinforced composites, Composites Science and Technology 69 (3-4) (2009) 477–484. doi:10.1016/j.compscitech.2008.11.024.

[162] J. Lamon, Stochastic models of fragmentation of brittle fibers or matrix in composites, Composites Science and Technology 70 (5) (2010) 743–751. doi:10.1016/j.compscitech.2010.01.005.

[163] A. DiBenedetto, N. Gurvich, Statistical simulation of fiber fragmentation in a single-fiber composite, Composites Science and Technology 57 (5) (1997) 543–555. doi:10.1016/S0266-3538(97)00008-0.

[164] K. Goda, S. Phoenix, Reliability approach to the tensile strength of unidirectional CFRP composites by Monte-Carlo simulation in a shear-lag model, Composites Science and Technology 50 (1994) 457–468. doi:10.1016/0266-3538(94)90054-X.

[165] M. Ibnabdeljalil, W. A. Curtin, Strength and reliability of fiber-reinforced composites: localized load sharing and associated size-effects, International Journal of Solids and Structures 34 (21) (1997) 2649–2668. doi:10.1016/S0020-7683(96)00179-5.

[166] P. Laumakis, P. Bonacuse, Monte-Carlo simulation and the chain-of-bundles model for titanium-matrix composite materials, Journal of Composite Materials 35 (20) (2001) 1975–20. doi:10.1106/TVCD-WLK9-0KCN-KMXE.

[167] M. Lienkamp, P. Schwartz, A Monte Carlo simulation of the failure of a seven fiber microcomposite, Composites Science and Technology 46 (2) (1993) 139–146. doi:10.1016/0266-3538(93)90169-H.

[168] M. Lienkamp, H. E. Exner, Prediction of the strength distribution for unidirectional fibre reinforced composites, Acta Materialia 44 (11) (1996) 4433–4446. doi:10.1016/1359-6454(96)00067-5.

[169] J. C. McNulty, F. W. Zok, Application of Weakest-Link Fracture Statistics to Fiber-Reinforced Ceramic Matrix Composites, Journal of the American Ceramic Society 80 (6) (1997) 1535–1543.

[170] S. Ochiai, T. Sawada, M. Hojo, Application of Monte Carlo simulation method to tensile behavior of FRM., Science and Engineering of Composite Materials 6 (2) (1997) 63–76.

[171] H. Stumpf, P. Schwartz, A Monte Carlo simulation of the stress-rupture of seven-fiber microcomposites, Composites Science and Technology 49 (3) (1993) 251–263. doi:10.1016/0266-3538(93)90107-R.

[172] M. Tanaka, M. Hojo, T. Hobbiebrunken, S. Ochiai, Y. Hirosawa, K. Fujita, Y. Sawada, Influence of non-uniform fiber arrangement on tensile fracture behavior of unidirectional fiber/epoxy model composites, Composite Interfaces 12 (3-4) (2005) 365–378. doi:10.1163/1568554053971542.

[173] M. Tunák, A. Linka, P. Volf, Load-sharing and Monte Carlo models of defects in a bundle of fibres, Composites Science and Technology 69 (9) (2009) 1417–1421. doi:10.1016/j.compscitech.2008.09.004.

[174] A. Wada, H. Fukuda, Approximate upper and lower bounds for the strength of unidirectional composites, Composites Science and Technology 59 (1) (1999) 89–95. doi:10.1016/S0266-3538(98)00052-9.

[175] W. Fang, W. Yuqing, C. Zhiqian, Micromechanical modeling of the effect of progressive damage on the tensile behavior in fiber-reinforced polymer composites, Advanced Materials Research 79-82 (2009) 1347–1350. doi:10.4028/www.scientific.net/AMR.79-82.1347.

[176] J. Yuan, Y. Xia, B. Yang, A note on the Monte Carlo simulation of the tensile deformation and failure process of unidirectional composites, Composites Science and Technology 52 (2) (1994) 197–204. doi:10.1016/0266-3538(94)90205-4.

[177] W. Yufen, Z. Weifang, W. Shuang, Z. Boming, Prediction method of longitudinal tensile strength for unidirectional composites with interphase, Journal of Reinforced Plastics and Composites 32 (8) (2013) 540–546. doi:10.1177/0731684412473358.

[178] Y. Zhou, W. Huang, Y. Xia, A microscopic dynamic Monte Carlo simulation for unidirectional fiber reinforced metal matrix composites, Composites Science and Technology 62 (15) (2002) 1935–1946. doi:10.1016/S0266-3538(02)00111-2.

[179] M. A. Khiat, Z. Sereir, A. Chateauneuf, Uncertainties of unidirectional composite strength under tensile loading and variation of environmental condi-

tion, Theoretical and Applied Fracture Mechanics 56 (3) (2011) 169–179. doi:10.1016/j.tafmec.2011.11.005.

[180] J.-K. Kim, C.-S. Kim, D.-Y. Song, Strength evaluation and failure analysis of unidirectional composites using Monte-Carlo simulation, Materials Science and Engineering: A 340 (1-2) (2003) 33–40. doi:10.1016/S0921-5093(02)00159-4.

[181] K. Liao, K. L. Reifsnider, Tensile strength model for unidirectional fiber-reinforced brittle matrix composite, International Journal of Fracture 106 (2) (2000) 95–115. doi:10.1023/A:1007645817753.

[182] R. L. Smith, S. Phoenix, M. R. Greenfield, R. B. Henstenburg, R. E. Pitt, Lower-Tail Approximations for the Probability of Failure of Three- Dimensional Fibrous Composites with Hexagonal Geometry, Proceedings of the Royal Society of London. Series A, Mathematical and Physical Sciences. 1795 (1983) 353–391. doi:10.1098/rspa.1983.0087.

[183] F. Wang, X. Zhang, Z. Chen, L. Li, J. Shao, Stress profiles around broken fibers in unidirectional composites using influence superimposition technique, Polymer Composites 34 (3) (2013) 313–319. doi:10.1002/pc.22411.

[184] D. Harlow, S. Phoenix, Probability distributions for the strength of composite materials I: two-level bounds, International Journal of Fracture 17 (4) (1981) 347–372. doi:10.1007/BF00036188.

[185] R. L. Smith, Limit theorems and approximations for the reliability of load-sharing systems, Advances in Applied Probability 15 (2) (1983) 304–330. doi:10.2307/1426438.

[186] S. Phoenix, R. L. Smith, A comparison of probabilistic techniques for the strength of fibrous materials under local load-sharing among fibers, International Journal of Solids and Structures 19 (6) (1983) 479–496. doi:10.1016/0020-7683(83)90086-0.

[187] M. Ibnabdeljalil, W. A. Curtin, Strength and reliability of fiber- reinforced composites: localized load- sharing and associated size effects, International Journal of Solids and Structures 34 (21) (1997) 2649–2668. doi:10.1016/S0020-7683(96)00179-5.

[188] M. Y. M. Chiang, X. Wang, C. R. Schultheisz, J. He, Prediction and three-dimensional Monte-Carlo simulation for tensile properties of unidirectional hybrid composites, Composites Science and Technology 65 (11-12) (2005) 1719–1727. doi:10.1016/j.compscitech.2005.02.012.

[189] S. J. Zhou, W. A. Curtin, Failure of fiber composites: A lattice green function model, Acta Metallurgica Et Materialia 43 (8) (1995) 3093–3104. doi:10.1016/0956-7151(95)00003-E.

[190] Z. Xia, W. A. Curtin, T. Okabe, Green's function vs. shear-lag models of damage and failure in fiber composites, Composites Science and Technology 62 (10-11) (2002) 1279–1288. doi:10.1016/S0266-3538(02)00073-8.

[191] I. J. Beyerlein, C. M. Landis, Shear-lag model for failure simulations of unidirectional fiber composites including matrix stiffness, Mechanics of Materials 31 (5) (1999) 331–350. doi:10.1016/S0167-6636(98)00075-1.

[192] I. J. Beyerlein, S. Phoenix, A. M. Sastry, Comparison of shear-lag theory and continuum fracture mechanics for modeling fiber and matrix stresses in an elastic cracked composite lamina, International Journal of Solids and Structures 33 (18) (1996) 2543–2574. doi:10.1016/0020-7683(95)00172-7.

[193] A. M. Sastry, S. Phoenix, Load redistribution near non-aligned fibre breaks in a two-dimensional unidirectional composite using break-influence superposition, Journal of Materials Science Letters 12 (20) (1993) 1596–1599. doi:10.1007/BF00627024.

[194] T. Okabe, H. Sekine, K. Ishii, M. Nishikawa, N. Takeda, Numerical method for failure simulation of unidirectional fiber-reinforced composites with spring element model, Composites Science and Technology 65 (6) (2005) 921–933. doi:10.1016/j.compscitech.2004.10.030.

[195] T. Okabe, K. Ishii, M. Nishikawa, N. Takeda, Prediction of Tensile Strength of Unidirectional CFRP Composites, Advanced Composite Materials 19 (3) (2010) 229–241. doi:10.6089/jscm.33.205.

[196] B. Delaunay, Sur la sphere vide, Izv. Akad. Nauk SSSR, Otdelenie Matematicheskii i Estestvennyka Nauk 7 (793-800) (1934) 1–2.

[197] M. J. DeJong, M. A. Hendriks, J. G. Rots, Sequentially linear analysis of fracture under non-proportional loading, Engineering Fracture Mechanics 75 (18) (2008) 5042–5056. doi:10.1016/j.engfracmech.2008.07.003.

[198] L. St-Pierre, N. J. Martorell, S. T. Pinho, Stress redistribution around clusters of broken fibres in a composite, Composite Structures 168 (2017) 226–233. doi:10.1016/j.compstruct.2017.01.084.

[199] E. Casoni, A. Jérusalem, C. Samaniego, B. Eguzkitza, P. Lafortune, D. D. Tjahjanto, X. Sáez, G. Houzeaux, M. Vázquez, Alya: Computational Solid Mechanics

for Supercomputers, Archives of Computational Methods in Engineering 22 (4) (2015) 557–576. doi:10.1007/s11831-014-9126-8.

[200] S. Banerjee, B. V. Sankar, Mechanical properties of hybrid composites using finite element method based micromechanics, Composites Part B: Engineering 58 (2014) 318–327. doi:10.1016/j.compositesb.2013.10.065.

[201] A. R. Melro, P. Camanho, S. T. Pinho, Influence of geometrical parameters on the elastic response of unidirectional composite materials, Composite Structures 94 (11) (2012) 3223–3231. doi:10.1016/j.compstruct.2012.05.004.

[202] C. T. Sun, R. S. Vaidya, Prediction of composite properties from a representative volume element, Composites Science and Technology 56 (2) (1996) 171–179. doi:10.1016/0266-3538(95)00141-7.

[203] C. Döbert, R. Mahnken, E. Stein, Numerical simulation of interface debonding with a combined damage/friction constitutive model, Computational Mechanics 25 (5) (2000) 456–467. doi:10.1007/s004660050493.

[204] V. I. Kushch, S. V. Shmegera, L. Mishnaevsky, Explicit modeling the progressive interface damage in fibrous composite: Analytical vs. numerical approach, Composites Science and Technology 71 (7) (2011) 989–997. doi:10.1016/j.compscitech.2011.03.005.

[205] T. J. Vaughan, C. T. McCarthy, Micromechanical modelling of the transverse damage behaviour in fibre reinforced composites, Composites Science and Technology 71 (3) (2011) 388–396. doi:10.1016/j.compscitech.2010.12.006.

[206] A. R. Melro, P. Camanho, F. M. Andrade Pires, S. T. Pinho, Micromechanical analysis of polymer composites reinforced by unidirectional fibres: Part I-Constitutive modelling, International Journal of Solids and Structures 50 (11-12) (2013) 1897–1905. doi:10.1016/j.ijsolstr.2013.02.009.

[207] A. R. Melro, P. Camanho, F. M. Andrade Pires, S. T. Pinho, Micromechanical analysis of polymer composites reinforced by unidirectional fibres: Part II-Micromechanical analyses, International Journal of Solids and Structures 50 (11-12) (2013) 1906–1915. doi:10.1016/j.ijsolstr.2013.02.007.

[208] C. Gonzalez, J. LLorca, Mechanical behavior of unidirectional fiber-reinforced polymers under transverse compression: Microscopic mechanisms and modeling, Composites Science and Technology 67 (13) (2007) 2795–2806. doi:10.1016/j.compscitech.2007.02.001.

[209] E. Totry, C. Gonzalez, J. LLorca, Failure locus of fiber-reinforced composites under transverse compression and out-of-plane shear, Composites Science and Technology 68 (3-4) (2008) 829–839. doi:10.1016/j.compscitech.2007.08.023.

[210] L. P. Canal, J. Segurado, J. LLorca, Failure surface of epoxy-modified fiber-reinforced composites under transverse tension and out-of-plane shear, International Journal of Solids and Structures 46 (11-12) (2009) 2265–2274. doi:10.1016/j.ijsolstr.2009.01.014.

[211] E. J. Pineda, B. A. Bednarcyk, A. M. Waas, S. M. Arnold, Progressive failure of a unidirectional fiber-reinforced composite using the method of cells: Discretization objective computational results, International Journal of Solids and Structures 50 (9) (2013) 1203–1216. doi:10.1016/j.ijsolstr.2012.12.003.

[212] A. Arteiro, G. Catalanotti, A. R. Melro, P. Linde, P. Camanho, Micro-mechanical analysis of the effect of ply thickness on the transverse compressive strength of polymer composites, Composites Part A: Applied Science and Manufacturing 79 (2015) 127–137. doi:10.1016/j.compositesa.2015.09.015.

[213] X. Chen, T. D. Papathanasiou, Interface stress distributions in transversely loaded continuous fiber composites: Parallel computation in multi-fiber RVEs using the boundary element method, Composites Science and Technology 64 (9) (2004) 1101–1114. doi:10.1016/j.compscitech.2003.07.006.

[214] L. Mishnaevsky, P. Brøndsted, Micromechanisms of damage in unidirectional fiber reinforced composites: 3D computational analysis, Composites Science and Technology 69 (7-8) (2009) 1036–1044. doi:10.1016/j.compscitech.2009.01.022.

[215] L. Mishnaevsky, P. Brøndsted, Three-dimensional numerical modelling of damage initiation in unidirectional fiber-reinforced composites with ductile matrix, Materials Science and Engineering A 498 (1-2) (2008) 81–86. doi:10.1016/j.msea.2007.09.105.

[216] L. Mishnaevsky, Three-dimensional numerical testing of microstructures of particle reinforced composites, Acta Materialia 52 (14) (2004) 4177–4188. doi:10.1016/j.actamat.2004.05.032.

[217] L. Mishnaevsky, Automatic voxel-based generation of 3D microstructural FE models and its application to the damage analysis of composites, Materials Science and Engineering A 407 (1-2) (2005) 11–23. doi:10.1016/j.msea.2005.06.047.

[218] L. Mishnaevsky, Functionally gradient metal matrix composites: Numerical analysis of the microstructure-strength relationships, Composites Science and Technology 66 (11-12) (2006) 1873–1887. doi:10.1016/j.compscitech.2005.09.003.

[219] K. Derrien, D. Baptiste, D. Guedra-Degeorges, J. Foulquier, Multiscale modeling of the damaged plastic behavior and failure of Al/SiCp composites, International journal of plasticity 15 (6) (1999) 667–685. doi:10.1016/S0749-6419(99)00009-1.

[220] L. Mishnaevsky Jr., N. Lippmann, S. Schmauder, Computational modeling of crack propagation in real microstructures of steels and virtual testing of artificially designed materials, International Journal of Fracture 120 (4) (2003) 581–600. doi:10.1023/A:1025524214322.

[221] G. Dai, L. Mishnaevsky, Damage evolution in nanoclay-reinforced polymers: A three-dimensional computational study, Composites Science and Technology 74 (2013) 67–77. doi:10.1016/j.compscitech.2012.10.003.

[222] A. Thionnet, H. Y. Chou, A. Bunsell, Fibre break processes in unidirectional composites, Composites Part A: Applied Science and Manufacturing 65 (2014) 148–160. doi:10.1016/j.compositesa.2014.06.009.

[223] H. W. Wang, H. W. Zhou, L. Mishnaevsky, P. Brøndsted, L. N. Wang, Single fibre and multifibre unit cell analysis of strength and cracking of unidirectional composites, Computational Materials Science 46 (4) (2009) 810–820. doi:10.1016/j.commatsci.2009.04.024.

[224] N. K. Parambil, S. Gururaja, Micromechanical damage analysis in laminated composites with randomly distributed fibers, Journal of Composite Materials 50 (21) (2016) 2911–2924. doi:10.1177/0021998315614992.

[225] C. Gonzalez, J. LLorca, Multiscale Modeling of Fracture in Fiber-Reinforced Composites, Acta Materialia 54 (16) (2006) 4171–4181. doi:10.1016/j.actamat.2006.05.007.

[226] F. Wang, Z. Q. Chen, Q. F. Meng, Multiscale Modelling of Progressive Damage in Fiber-Reinforced Composites, Advanced Materials Research 250-253 (2011) 213–217. doi:10.4028/www.scientific.net/AMR.250-253.213.

[227] H. Cox, The elasticity and strength of paper and other fibrous materials, British Journal of Applied Physics 3 (3) (1952) 72–79. doi:10.1088/0508-3443/3/3/302.

[228] M. R. Piggott, Expressions governing stress-strain curves in short fibre reinforced polymers, Journal of Materials Science 13 (8) (1978) 1709–1716. doi:10.1007/BF00548734.

[229] J. Ivens, M. Wevers, I. Verpoest, Influence of carbon fibre surface treatment on composite UD strength, Composites 25 (7) (1994) 722–728. doi:10.1016/0010-4361(94)90207-0.

[230] T. Lacroix, B. Tilmans, R. Keunings, M. Desaeger, I. Verpoest, Modelling of critical fibre length and interfacial debonding in the fragmentation testing of polymer composites, Composites Science and Technology 43 (4) (1992) 379–387. doi:10.1016/0266-3538(92)90061-7.

[231] J. Favre, P. Sigety, D. Jacques, Stress transfer by shear in carbon fibre model composites - Part 2 computer simulation of the fragmentation test, Journal of Materials Science 26 (1) (1991) 189–195. doi:10.1007/BF00576050.

[232] P. Feillard, G. Desarmot, J. P. Favre, Theoretical aspects of the fragmentation test, Composites Science and Technology 50 (2) (1994) 265–279. doi:10.1016/0266-3538(94)90148-1.

[233] J. A. Nairn, A variational mechanics analysis of the stresses around breaks in embedded fibers, Mechanics of Materials 13 (2) (1992) 131–154. doi:10.1016/0167-6636(92)90042-C.

[234] D. Tripathi, F. Chen, F. Jones, A comprehensive model to predict the stress fields in a single fibre composite, Journal of Composite Materials 30 (14) (1996) 1514–1538. doi:10.1177/002199839603001401.

[235] C. M. Landis, R. M. McMeeking, A shear-lag model for a broken fiber embedded in a composite with a ductile matrix, Composites Science and Technology 59 (3) (1999) 447–457. doi:10.1016/S0266-3538(98)00091-8.

[236] A. Balacó De Morais, Stress distribution along broken fibres in polymer-matrix composites, Composites Science and Technology 61 (11) (2001) 1571–1580. doi:10.1016/S0266-3538(01)00058-6.

[237] Z. Xia, T. Okabe, W. A. Curtin, Shear-lag versus finite element models for stress transfer in fiber-reinforced composites, Composites Science and Technology 62 (9) (2002) 1141–1149. doi:10.1016/S0266-3538(02)00072-6.

[238] T. Lacroix, R. Keunings, M. Desaeger, I. Verpoest, A new data reduction scheme for the fragmentation testing of polymer composites, Journal of Materials Science 30 (1995) 683–692. doi:10.1007/BF00356328.

[239] P. Zhao, S. Ji, Refinements of shear-lag model and its applications, Tectonophysics 279 (1-4) (1997) 37–53. doi:10.1016/S0040-1951(97)00129-7.

[240] B. Fiedler, K. Schulte, Stress distribution in single-fibre model composites with perfect bonding, Composites Science and Technology 57 (9-10) (1997) 1331–1339. doi:10.1016/S0266-3538(97)00064-X.

[241] S. Khosoussi, M. Mondali, A. Abedian, A new approach to the elastic–plastic stress transfer analysis of metal matrix composites, Archive of Applied Mechanics 85 (2015) 1701–1717. doi:10.1007/s00419-015-1013-8.

[242] Z. Chen, W. Yan, A shear-lag model with a cohesive fibre-matrix interface for analysis of fibre pull-out, Mechanics of Materials 91 (2015) 119–135. doi:10.1016/j.mechmat.2015.07.007.

[243] D. Harlow, S. Phoenix, The Chain-of-Bundles Probability Model for the Strength of Fibrous Materials II : A Numerical Study of Convergence, Journal of Composite Materials 12 (3) (1978) 314–334.

[244] H. D. Wagner, A. Eitan, Stress concentration factors in two-dimensional composites: effects of material and geometrical parameters, Composites Science and Technology 46 (4) (1993) 353–362. doi:10.1016/0266-3538(93)90181-F.

[245] M. R. Nedele, M. R. Wisnom, Stress concentration factors around a broken fibre in a unidirectional carbon fibre-reinforced epoxy, Composites 25 (7) (1994) 549–557. doi:10.1016/0010-4361(94)90183-X.

[246] D. T. Grubb, Z. F. Li, S. Phoenix, Measurement of stress concentration in a fiber adjacent to a fiber break in a model composite, Composites Science and Technology 54 (3) (1995) 237–249. doi:10.1016/0266-3538(95)00055-0.

[247] P. van den Heuvel, T. Peijs, R. Young, P. Heuvel, Analysis of stress concentrations in multi-fibre microcomposites by means of Raman spectroscopy, Journal of materials science letters 15 (21) (1996) 1908–1911. doi:10.1007/BF00264093.

[248] P. van den Heuvel, T. Peijs, R. Young, Failure phenomena in two-dimensional multi-fibre microcomposites - 3. A Raman spectroscopy study of the influence of interfacial debonding on stress concentrations, Composites Science and Technology 58 (6) (1998) 933–944. doi:10.1016/S0266-3538(97)00004-3.

[249] P. van den Heuvel, T. Peijs, R. Young, Failure phenomena in two-dimensional multifibre microcomposites: 2. A Raman spectroscopic study of the influence of inter-fibre spacing on stress concentrations, Composites Science and Technology 57 (8) (1997) 899–911. doi:10.1016/S0266-3538(97)00004-3.

[250] P. van den Heuvel, T. Peijs, R. Young, Failure phenomena in two-dimensional multi-fibre microcomposites. Part 4: a Raman spectroscopic study on the influence of the matrix yield stress on stress concentrations, Composites Part A: Applied Science and Manufacturing 31 (2) (2000) 165–171. doi:10.1016/S1359-835X(99)00059-7.

[251] X. F. Zhou, H. D. Wagner, Stress concentrations caused by fiber failure in two-dimensional composites, Composites Science and Technology 59 (7) (1999) 1063–1071. doi:10.1016/S0266-3538(98)00145-6.

[252] A. Eitan, H. D. Wagner, Fiber interactions in two-dimensional composites, Applied Physics Letters 58 (10) (1991) 1033–1035. doi:10.1063/1.105209.

[253] A. H. Nayfeh, Thermomechanically induced interfacial stresses in fibrous composites, Fibre Science and Technology 10 (3) (1977) 195–209. doi:10.1016/0015-0568(77)90020-3.

[254] X. F. Zhou, H. D. Wagner, Fragmentation of two-fiber hybrid microcomposites: Stress concentration factors and interfacial adhesion, Composites Science and Technology 60 (3) (2000) 367–377. doi:10.1016/S0266-3538(99)00135-9.

[255] N. Ohno, S. Okabe, T. Okabe, Stress concentrations near a fiber break in unidirectional composites with interfacial slip and matrix yielding, International Journal of Solids and Structures 41 (16-17) (2004) 4263–4277. doi:10.1016/j.ijsolstr.2004.03.018.

[256] Y. Yu, B. Zhang, Z. Tang, G. Qi, Stress transfer analysis of unidirectional composites with randomly distributed fibers using finite element method, Composites Part B: Engineering 69 (2014) 278–285. doi:10.1016/j.compositesb.2014.09.035.

[257] U. S. The MathWorks, Inc., Natick, Massachusetts, MATLAB and Statistics Toolbox Release 2013a.

[258] J. Ahrens, B. Geveci, C. Law, ParaView: An End-User Tool for Large Data Visualization, in: Visualization Handbook, Visualization Handbook, Elsevier, 2005, pp. 717–731. doi:10.1016/B978-012387582-2/50038-1.

[259] N. Toyama, J. Takatsubo, An investigation of non-linear elastic behavior of CFRP laminates and strain measurement using Lamb waves, Composites Science and Technology 64 (16) (2004) 2509–2516. doi:10.1016/j.compscitech.2004.05.007.

[260] J. M. Guerrero, J. A. Mayugo, J. Costa, A. Turon, A 3D Progressive Failure Model for predicting pseudo-ductility in hybrid unidirectional composite materials under fibre tensile loading, Composites Part A: Applied Science and Manufacturing 107 (February) (2018) 579–591. doi:10.1016/j.compositesa.2018.02.005.

[261] J. M. Guerrero, R. P. Tavares, F. Otero, J. A. Mayugo, J. Costa, A. Turon, P. P. Camanho, An analytical model to predict stress fields around broken fibres and their effect on the longitudinal failure of hybrid composites, Composite Structures 211 (December 2018) (2019) 564–576. doi:10.1016/j.compstruct.2018.12.044.

[262] R. Prussak, D. Stefaniak, C. Hühne, M. Sinapius, Residual Stresses in Intrinsic UD-CFRP-Steel-Laminates - Experimental Determination, Identification of Sources, Effects and Modification Approaches, Materials Science Forum 825-826 (2015) 369–376. doi:10.4028/www.scientific.net/MSF.825-826.369.

[263] H. D. Wagner, Residual Stresses in Microcomposites and Macrocomposites, The Journal of Adhesion 52 (1) (1995) 131–148. doi:10.1080/00218469508015190.

[264] S. Tsai, H. Hahn, Introduction to Composite Materials, Technomic Publishing Co, Inc., 1980.

[265] A. Arteiro, G. Catalanotti, A. R. Melro, P. Linde, P. P. Camanho, Micromechanical analysis of the in situ effect in polymer composite laminates, Composite Structures 116 (1) (2014) 827–840. doi:10.1016/j.compstruct.2014.06.014.

[266] X. Xu, M. R. Wisnom, Y. Mahadik, S. R. Hallett, An experimental investigation into size effects in quasi-isotropic carbon/epoxy laminates with sharp and blunt notches, Composites Science and Technology 100 (2014) 220–227. doi:10.1016/j.compscitech.2014.06.002.

[267] M. R. Wisnom, B. Khan, S. R. Hallett, Size effects in unnotched tensile strength of unidirectional and quasi-isotropic carbon/epoxy composites, Composite Structures 84 (1) (2008) 21–28. doi:10.1016/j.compstruct.2007.06.002.

[268] J. D. Fuller, M. R. Wisnom, Exploration of the potential for pseudo-ductility in thin ply CFRP angle-ply laminates via an analytical method, Composites Science and Technology 112 (2015) 8–15. doi:10.1016/j.compscitech.2015.02.019.

[269] J. M. Guerrero, J. A. Mayugo, J. Costa, A. Turon, Failure of hybrid composites under longitudinal tension: influence of dynamic effects and thermal residual stresses, Submitted to Composite Structures.

[270] J. A. Lavoie, C. Soutis, J. Morton, Apparent strength in continuous fiber composite laminates, Composites Science and Technology 60 (2000) 283–299. doi:10.1016/S0266-3538(99)00124-4.

[271] P. P. Camanho, P. Maimí, C. G. Dávila, Prediction of size effects in notched laminates using continuum damage mechanics, Composites Science and Technology 67 (13) (2007) 2715–2727. doi:10.1016/j.compscitech.2007.02.005.

[272] G. Czel, M. Jalalvand, M. R. Wisnom, Design and characterisation of advanced pseudo-ductile unidirectional thin-ply carbon/epoxy-glass/epoxy hybrid composites, Composite Structures 143 (2016) 362–370. doi:10.1016/j.compstruct.2016.02.010.

[273] J. M. Finley, H. Yu, M. L. Longana, S. Pimenta, M. S. Shaffer, K. D. Potter, Exploring the pseudo-ductility of aligned hybrid discontinuous composites using controlled fibre-type arrangements, Composites Part A: Applied Science and Manufacturing 107 (2018) 592–606. doi:10.1016/j.compositesa.2017.11.028.

[274] K. Naito, J. M. Yang, Y. Kagawa, Tensile properties of high strength polyacrylonitrile (PAN)-based and high modulus pitch-based hybrid carbon fibers-reinforced epoxy matrix composite, Journal of Materials Science 47 (6) (2012) 2743–2751. doi:10.1007/s10853-011-6101-8.

Part IV

Appendices

Papers in their journal form

A.1 Paper A – A 3D Progressive Failure Model for predicting pseudo-ductility in hybrid unidirectional composite materials under fibre tensile loading

The paper has been published in *Composites Part A: Applied Science and Manufacturing* 107 (2018) 579-591.

Composites Part A 107 (2018) 579–591

Contents lists available at ScienceDirect

Composites Part A

journal homepage: www.elsevier.com/locate/compositesa

A 3D Progressive Failure Model for predicting pseudo-ductility in hybrid unidirectional composite materials under fibre tensile loading

J.M. Guerrero*, J.A. Mayugo, J. Costa, A. Turon

AMADE, Polytechnic School, Universitat de Girona, Campus Montilivi s/n, E-17003 Girona, Spain

ARTICLE INFO

Keywords:
A. Hybrid
A. Polymer-matrix composites (PMCs)
C. Computational modelling
C. Micro-mechanics

ABSTRACT

This paper presents a three-dimensional Progressive Failure Model based on the chain of bundles able to represent the stiffness loss in unidirectional composite materials loaded in the fibre direction. A representative volume element with a random distribution of fibres with their own radius is considered. Complete stress distributions around fibre breaks are obtained by associating a damage variable to the loss of stress transfer capability along the ineffective length and applying local stress concentrations. The model has been validated by comparing it against the literature results and exhibits good agreement with hybrids and non-hybrid composites. The aim of this model is to simulate the tensile response of unidirectional composite systems dominated by fibre fragmentation mechanisms using a very reduced computational effort, even for larger representative volume elements, compared to micro-mechanical finite element models.

1. Introduction

Fibre reinforced polymers (FRP) are widely used in lightweight structures mainly thanks to their high specific strength and stiffness. However, their quasi-brittle behaviour and low toughness leads to fibre tensile failure with hardly any prior damage symptoms, thus limiting their use and applicability [1]. One potential way to solve this problem is with fibre hybridization [2]. In a hybrid composite, two kinds of fibres with different longitudinal failure strains are mixed. The mixture can be arranged on three different scales [2], which are also able to be combined into: (i) interlayer or layer-by-layer i.e. by mixing layers of different fibres, (ii) intralayer or yarn-by-yarn i.e. by mixing the fibres within the layers but not within the separate yarns, and (iii) intrayarn or fibre-by-fibre i.e. by mixing the fibres completely at the yarn/tow.

A low elongation fibre (LE) has a low failure strain and a high elongation fibre (HE) has a high failure strain. Thanks to this combination, the LE failure strain in a hybrid can be larger than that in a non-hybrid composite. This phenomenon is known as the hybrid effect [3]. Moreover, with the appropriate hybridization design, a progressive failure of fibres under tensile load can be induced leading to pseudo-ductile behaviour [4]. Currently [2], to explain the hybrid effect the scientific community outlines three main reasons: (i) changes in the development of the failure, (ii) thermal residual stresses and (iii) dynamic effects.

Nowadays, changes in the failure propagation are assumed to be the main reason for the hybrid effect. Because of the presence of flaws, the strength of brittle fibres is not deterministic and follows a statistical distribution. When a fibre breaks, shear stresses are transferred from the fibre to the matrix. As a consequence, the broken fibre recovers its stress in a distance called the ineffective length, whereas the surrounding fibres withstand stress concentration. Eventually, the neighbouring fibres of each broken fibre fail, thus initiating several clusters of broken fibres which grow further upon loading. When one of these clusters reaches a certain size, it propagates unstably and leads to the final failure. Other phenomena, such as debonding, matrix cracking or yielding and fibre pullout, may also contribute. Notwithstanding, in a hybrid composite the differences between the elastic and geometrical properties and the failure strains can alter and delay the formation of clusters. Moreover, by reducing the quantity of LE fibres in the hybrid, LE failure strain can also be increased because of the size effects [5].

An additional and secondary cause of the hybrid effect is related to the residual stresses generated during the manufacturing process [2]. Residual stresses appear when mixing different populations of fibres with dissimilar thermal expansion coefficients, which leads to different residual stresses in each fibre population.

The third reason given for the hybrid effect is the dynamic effect in the process of tensile failure. When a fibre breaks, the elastic energy that was sustained by that fibre is released and becomes kinetic energy which dampens after some time. During this period, dynamic loads propagate through the composite and increase the probability of failure. However, in the case of a hybrid composite, the dynamic phenomena can be altered. Xing et al. [6] demonstrated that in a hybrid

* Corresponding author.
E-mail address: josemanuel.guerrero@udg.edu (J.M. Guerrero).

https://doi.org/10.1016/j.compositesa.2018.02.005
Received 20 July 2017; Received in revised form 25 January 2018; Accepted 3 February 2018
Available online 05 February 2018
1359-835X/

composite two out-of-phase stress waves, one for each fibre population, propagate after an LE fibre break. If both waves compensate each other, lower dynamic loads are produced, leading to larger failure strains. However, this topic has not been studied in depth and its importance remains unclear [2,7].

In addition, the hybrid effect is also influenced somewhat by different parameters which include the relative volume fraction between both fibres, strength distribution, fibre dispersion, fibre stiffness ratios and the failure strain ratio. Other parameters, such as the matrix stiffness or debonding, have no clear influence [3]. Moreover, the specimen size effect on the hybrid effect is also unknown [8].

Over the past decades different authors have attempted to study hybrid composites under fibre tensile loading. Hayashi [9] was the first author who observed the hybrid effect in a carbon-glass layer-by-layer hybrid in an experimental test. Later, Zweben [10] extended a shear-lag model to hybrid composites to obtain the hybrid effect analytically. While Fukuda [11] improved the model further, it still has major limitations. According to Swolfs et al. [3], Fukuda's and Zweben's models can be used as the upper and lower bounds for predicting the hybrid effect.

Recently, Tavares et al. [12] presented a fibre-by-fibre micro-mechanical finite element model (FEM) simulating fibre, matrix and fibre-matrix interphase damage [13]. The results demonstrated the importance of the failure strain ratio of both fibres, the statistical strength distribution and a progressive failure between both HE and LE fibres in obtaining pseudo-ductility. However, the model requires high computational resources and is limited to simulating a small number of fibres.

Okabe et al. [14,15] presented an advanced shear-lag model able to represent the fibre failure process of composite materials. The model represents the fibres through tensile springs and the matrix through shear springs. The advantage of these types of models is that they are simpler, faster and cheaper in computational cost than FEM models are. Furthermore, they are still able to simulate the key physics involved, without being limited to only a few fibres as in the FEM approach. However, Okabe et al.'s model is limited to hexagonal or square packings, which do not allow hybrid composites with fibres of different radii to be studied.

Swolfs et al. [3,5,16–18] presented a strength model under the assumption of a local load sharing rule, based on the chain of bundles approach from Rosen [19], Okabe et al. [14,15] and others [20,21]. Unlike the model of Okabe et al., a random fibre packing with each fibre with its own radius was considered. With their model, Swolfs et al. demonstrated that larger LE strength dispersions, lower number of LE fibres, higher HE fibre stiffness or larger failure strain ratios all ultimately lead to greater hybrid effects. Fibre dispersion also showed an evident impact. However, Swolfs' model [3,5,16–18] attempts to predict the behaviour only up to the onset of LE fibre fragmentation, because it does not capture a non-linear response attributable to fragmentation mechanisms. Thus, it is unable to predict pseudo-ductility.

In recent years, an increase in the amount of experimental work conducted concerning fibre hybridization has also been seen. Czél and Wisnom [22] hybridized thin carbon fibre prepreg plies with standard thick plies of glass fibres. They found pseudo-ductility with specimens of one and two plies of thin carbon. However, specimens with three and four plies failed with unstable delamination. Later, Wisnom et al. [8] obtained similar findings. Moreover, they compared their results with a simplified version of Swolfs et al. [5] strength model and obtained good agreement. Yu et al. [23] also manufactured intermingled hybrid composites using aligned discontinuous fibres. By combining high-modulus carbon and E-glass in the hybrid, good pseudo-ductile responses were also obtained as a result of the carbon fibres fragmentation. Further to this, Jalalvand et al. [24] developed a new simple analytical method to predict all possible damage mode maps in unidirectional hybrid composites. By using the method as a design guideline, new hybrid specimens of a standard-thickness glass/thin-ply carbon hybrid were manufactured and tested, leading to a good pseudo-ductile response. Quite recently, Fotouhi et al. [25] tested quasi-isotropic high performance thin-ply carbon/glass hybrid laminates. Pseudo-ductility was also obtained in all fibre orientations under tensile loading. Last but no least, Czél et al. [26] hybridized thin-ply unidirectional interlayer all carbon-epoxy composites comprising high modulus and high strength. Again, large pseudo-ductile responses were obtained.

Despite advances in the modelling and understanding of hybrid composites, there is no local load sharing model for these materials that is capable of representing the pseudo-ductile behaviour within a random distribution of fibres. At the moment, the exception to this are the micro-mechanics FEM models which require huge computational resources and so are unsuitable as a design tool or to perform parametric studies.

In the present work, the authors propose a new three-dimensional Progressive Failure Model, (called here PFM) based on the chain of bundles which is able to accurately represent both progressive damage and pseudo-ductile behaviour in unidirectional composites. The proposed model implicitly allows fibre fragmentation mechanisms to be captured, thus estimating multiple breaks along the length of the fibre. A random distribution of fibres of a given radius is considered. The methodology leads to different deformations along the model, using the hypothesis that fibres work in parallel but taking into account the local stress fields around each fibre break. The complete stress distribution around the fibre breaks is obtained through two dependent approaches. Firstly, a damage variable related to fibre breaks and to a shear-lag model is computed. Secondly, local stress concentrations are applied through all stress recoveries. Thermal residual stresses and dynamic loads are omitted but the model framework allows for its future implementation. The remainder of this paper is as follows: firstly, we present the model, which we then validate by comparing it with the literature results, and finally some conclusions are drawn.

2. Chain of bundles Progressive Failure Model

2.1. Definition of the fibre random distributed RVE

A representative volume element (RVE) with a random distribution of fibres is generated to capture the interaction between the fibres and the matrix. The RVE represents, on a micro-mechanical scale, a portion of a real material model containing the matrix and a sufficient number of fibres. According to Trias et al. [27] and Zangernberg et al. [28], the minimum transversal size of the RVE in an elastic model should be 50 times the fibre radius ($50 \times R$). However, in a model with damage, the minimum size of the RVE could be even larger to capture the fibre effects. Similarly, the RVE length in the fibre longitudinal direction should be long enough to ensure that the ineffective length will be well captured. Some studies employed RVEs with a length of between $15 \times R$ and $40 \times R$ [12,29]. However, an RVE using these length values does not ensure a good prediction of the fibre fragmentation. A congruent RVE length depends on the fibre and matrix elastic properties as well the ineffective and debonding lengths. Thus, RVEs length with an order of magnitude equal to several times the ineffective length should be used [5,18]. Furthermore, size effects may occur. Therefore, the RVE must be big enough to capture the micro-mechanisms of the damage, the stress redistribution around the broken fibres during the failure process, and the clusters of fibre breaks on the different planes.

The model proposed considers an RVE that contains a certain number of parallel fibres randomly allocated, with a total length L, height a, and width b. All the fibres are divided into elements of constant length l. This leads to a domain consisting of a number of *fibres* working in parallel and divided into different *planes* working in series, also known as chain of bundles [19]. The RVE may represent a hybrid, where each fibre has its own radius and properties, or a non-hybrid composite. Each fibre element is noted by the sub-indices (p,q), where p is the plane identity ranging from 1 to N_p, with N_p being the total

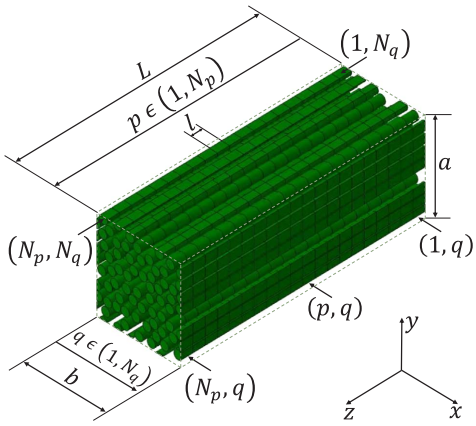

Fig. 1. Schema of the RVE for the Progressive Failure Model. The enumeration of the planes is sorted from 1 to N_p, with plane 1 always being the plane to the extreme right and plane N_p to the extreme left. Fibre numeration is random from 1 to N_q. (For interpretation of the references to colour in this figure legend, the reader is referred to the web version of this article.)

number of planes, and q is the fibre identity ranging from 1 to N_q, with N_q being the total number of fibres. The matrix is not really represented, but it is accounted for by means of its stiffness and a shear-lag model. Fibres at the outskirts of the RVE are cut and symmetric so that the geometry obtained is completely periodic. This schema is illustrated in Fig. 1. The random distribution of fibres is generated using the formulation of Melro et al. [30], and extended to hybrid composites by Tavares et al. [12].

Because of the strength scatter of the fibres, each fibre element has a different tensile strength, $\sigma^{u}_{p,q}$. To do this, a random number between 0 and 1 is applied to all elements, $P_{p,q}$. Then, the strength $\sigma^{u}_{p,q}$ of each element is obtained according to a statistical distribution, the element length l and $P_{p,q}$. Any statistical distribution could be adopted and implemented in the proposed model. In the literature, the Weibull distribution [31] is most commonly used to represent fibre strength, although other variants such as the bimodal and the power-law accelerated Weibull distribution are also employed [32,33].

2.2. Constitutive equation

The model assumes the complete stress distribution on the RVE in two dependent ways. On the one hand, when a fibre breaks, shear-lag stresses are transferred between the fibre and the matrix, which can lead to debonding, matrix cracking, yielding, or a combination of these [14,34,35]. Consequently, an ineffective length appears so that the stress in the fibre is recovered. A shear-lag model is used to obtain the ineffective length of a broken fibre element. According to Xia et al. [36], shear-lag models are accurate in polymer matrix composites if the fibre stiffness is much larger than the matrix, the matrix yields and the fibre volume fraction is relatively high. Assuming that the loss of stress transfer capability produces a reduction in local effective stiffness, the shear-lag model is implemented by simply updating the damage variable of all the elements inside the ineffective length of the broken fibre. On the other hand, local stress concentration factors (*SCF*) are applied through all stress recoveries, so that the neighbouring fibres to a break are locally overloaded, increasing their failure probability. Therefore, the (*SCF*) is assumed as a dimensionless parameter equal to 1 if the fibre element is not affected by any break, or higher than 1 if it is affected by breaks. In the literature, the $SCF_{p,q}$ is measured as the ratio between the real local fibre stress, $\sigma_{p,q}$, and the fibre far field stress, $\sigma^{\infty}_{p,q}$, where the stress is not influenced by the damage, fibre breaks or stress concentration

$$\sigma_{p,q} = SCF_{p,q}\sigma^{\infty}_{p,q} \tag{1}$$

In this work, the main hypothesis is that all fibre elements in each plane work in parallel, while all planes work in series. This means that all fibre elements in the plane undergo the same deformation, ε_p, (evaluated in Section 2.4). As damage is different on each plane, a different deformation is obtained along the model. Therefore, the effective stress is given by relating the effective Young's modulus and the deformation of the plane

$$\tilde{\sigma}_{p,q} = E_q(1-D_{p,q})\varepsilon_p \tag{2}$$

where E_q is the Young's modulus of fibre q and $D_{p,q}$ is the state damage variable on element p,q. Therefore, the effective stress, $\tilde{\sigma}_{p,q}$, depends on the stiffness and damage distribution: the plane stiffness -by ε_p-, and the element stiffness -directly by $D_{p,q}$-, but it does not take into account the stress concentration.

To obtain the real fibre stress, $\sigma_{p,q}$, it is necessary to relate the effective stress $\tilde{\sigma}_{p,q}$, and the far-field stress, $\sigma^{\infty}_{p,q}$, that appear in the definition of $SCF_{p,q}$. To do that, a stress ratio, Ω_p, is defined

$$\Omega_p = \frac{\tilde{\sigma}_{p,q}}{\sigma^{\infty}_{p,q}} \tag{3}$$

The stress ratio associated to each plane p is evaluated according to the plane level equilibrium condition explained in Section 2.4. By putting together Eqs. (1)–(3), the constitutive equation of a fibre element relates the real local longitudinal fibre stress with the longitudinal plane strain

$$\sigma_{p,q} = \frac{SCF_{p,q}}{\Omega_p}E_q(1-D_{p,q})\varepsilon_p \tag{4}$$

When the element's tensile stress $\sigma_{p,q}$ exceeds its strength $\sigma^{u}_{p,q}$, the element fails and its damage variable $D_{p,q}$ is set equal to 1. This causes an ineffective length in the broken fibre which is represented as damage in all the elements inside the ineffective length. Therefore, damage is equal to 0 for a pristine fibre element, equal to 1 for a broken fibre element, or between 0 and 1 for a fibre element that is influenced by the ineffective length predicted by a shear-lag model. In the following, how to evaluate $D_{p,q}$ and $SCF_{p,q}$ is explained.

The PFM is able to use any model to predict the ineffective length. In this work, the widely used Kelly-Tyson [35] shear-lag model is adopted, which assumes a perfectly plastic matrix leading to a linear stress recovery. Therefore, the ineffective length $L^{in}_{p,q}$ of a broken fibre is given by

$$L^{in}_{p,q} = \frac{E_q r_q}{2\tau_q}\varepsilon_p \tag{5}$$

where τ_q is the shear yield strength of the matrix for fibre q and r_q is the radius of fibre q. Note that both can be different for each fibre population in the case of a hybrid composite. The Kelly-Tyson model leads to different ineffective lengths depending on the elastic and geometrical properties and increases with the strain as the load is incremented.

As previously outlined, the damage variable, (calculated assuming the loss of stress transfer capability in the ineffective length), produces a reduction of local effective stiffness. Thus, a gradual decrease of damage from 1 at the position of the break, to 0 at both ends of the ineffective length (see Fig. 2a and b) is applied. As fibres may fail many times along their length, different ineffective lengths may overlap. Then, the highest damage always prevails for each element inside overlapping stress recoveries. Another potential case is an element failure located close to the boundaries of the model. In that case, the ineffective length is not fully recovered, (see Fig. 2 c). According to these hypotheses, an element p,q is affected by each break in the fibre q

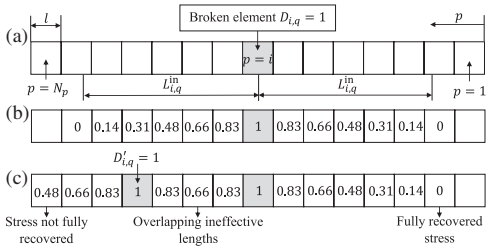

Fig. 2. (a) Schema of the ineffective length around a broken element, (b) resultant damage distribution, (c) overlapping ineffective lengths and not fully-recovered stresses in a fibre with two breaks.

at each plane i with

$$D_{p,q} = \begin{cases} \max\left(\frac{L^{in}_{i,q} - |i-p| + l}{L^{in}_{i,q}}\right) & \forall\ i\text{: } (D_{i,q} = 1) \cup (|i-p|\ l < L^{in}_{i,q}) \\ 0 & \text{otherwise.} \end{cases} \quad (6)$$

In general, according to the literature [29,37,38], the *SCF* of an affected fibre element (p,q) around a broken element (i,j) can be predicted with two interacting functions: one which depends on the radial distance between both fibres, $\delta_{(q-j)}$, and the other which depends on the plane position along the ineffective length, $\lambda_{(p-i)}$. A schematic example of the *SCF* for a fibre around a broken one is shown in Fig. 3. The interaction functions $\delta_{(q-j)}$ and $\lambda_{(p-i)}$ can be parametrized with computational micro-mechanics studies (for example the work of Swolfs et al. [16,18,29,39]), or can be formulated with analytical approaches (such as the Zhou and Wagner [37], and Eitan and Wagner [38] models). The corresponding functions are shown in Table 1.

It should be highlighted that in order to simplify the model, the widely used Kelly-Tyson shear-lag model was adopted to predict the ineffective length. Nonetheless, the *SCF* models of Eitan and Wagner and Zhou and Wagner are based on Cox's shear-lag model [34,38] and Nayfeh's shear-lag model [37] respectively. This means that the *SCFs* are calculated using a different physical principle than the ineffective length. Nevertheless, we assume it is a reasonable approach considering the complexity involved in the process of fibre breakage. In any case, the functions to predict the *SCF* and the ineffective length are an 'exchangeable part' in the proposed Progressive Failure Model. Thus, any another model to predict the *SCF* or the ineffective length could be used instead.

Whenever different broken fibres are present, the *SCF* of an affected fibre (p,q) is obtained by assuming a linear superposition of the contribution given by all the breaks on the fibres. However, the *SCF* is bounded by the limitation of transfering load to the fibre by shear-lag. On the one hand, the elements inside any ineffective length (elements where $0 < D_{p,q} < 1$) have their stress limited by the shear-lag model.

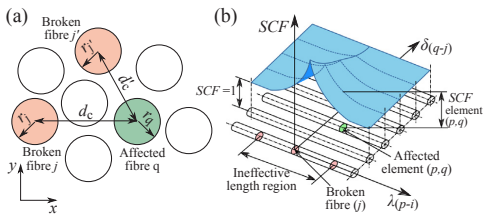

Fig. 3. (a) In-plane separation between broken and affected fibre, (b) stress concentration schema for intact fibres around a broken fibre depending on the in-plane distance and the position along the ineffective length. (For interpretation of the references to colour in this figure legend, the reader is referred to the web version of this article.)

Table 1
Functions to obtain the stress concentration factor according to three different models. (∗) Swolfs et al. [18] function along the ineffective length has been assumed. (∗∗) Zhou and Wagner [37] provided equations for debonding and non-debonding regions. Here, only non-debonding regions are considered.

SCF model	Functions: radial distance $\delta_{(q-j)}$ and ineffective length $\lambda_{(p-i)}$
Swolfs et al. [18] (∗)	$\delta_{(q-j)} = -P_1 \ln\left(\frac{d^c_{q-j} - (r_j + r_q)}{r_j}\right) + P_2$ where P_1 and P_2 are two constants from a micro-mechanic model and d^c_{q-j} is the centre-to-centre distance between fibres q and j $\lambda_{(p-i)} = \frac{L^{in}_{i,j} - l\ \|i-p\|}{L^{in}_{i,j}} \quad \forall\ (i,j)\text{: } l\ \|i-p\| < L^{in}_{i,j}$
Eitan and Wagner [38]	$\delta_{(q-j)} = \frac{\varphi_j}{\pi}$ where $\varphi_j = \arcsin(r_j/d^c_{q-j})$ $\lambda_{(p-i)} = \frac{\sinh\beta^c_{(q-j)}(L^{in}_{i,j} - l\ \|i-p\|)}{\sinh\beta^c_{(q-j)} L^{in}_{i,j}} \quad \forall\ (i,j)\text{: } l\ \|i-p\| < L^{in}_{i,j}$ where $\beta^c_{(q-j)}$ is Cox's [34] shear-lag parameter: $\beta^c_{(q-j)} = \frac{1}{r_j}\sqrt{\frac{2G_m}{E_j \ln\frac{0.5d^c_{q-j}}{r_j}}}$ where G_m is the matrix shear modulus.
Zhou and Wagner [37] (∗∗)	$\delta_{(q-j)} = \left(1 - \frac{\psi l}{r_j}\right)\frac{2\varphi_j}{\pi}$ where ψ is a friction coefficient $\lambda_{(p-i)} = \frac{\sinh\beta_j(L^{in}_{i,j} + 0.5l - l\ \|i-p\|)}{\sinh\beta_j L^{in}_{i,j}} \quad \forall\ (i,j)\text{: } l\ \|i-p\| < L^{in}_{i,j}$ where β_j is Nayfeh's shear-lag parameter, as given in [37]: $\beta_j^2 = \frac{2}{r_f^2 E_j E_m}\left(\frac{\frac{r_f^2}{E_j}\frac{r_f^2}{r_m^2} + E_m\left(1 - \frac{r_f^2}{r_m^2}\right)}{\frac{1}{4G_j}\left(1 - \frac{r_f^2}{r_m^2}\right) + \frac{1}{2G_m}\left(\frac{r_m^2}{r_m^2 - r_f^2}\ln\left(\frac{r_m^2}{r_f^2}\right) - \frac{1}{2}\left(3 - \frac{r_f^2}{r_m^2}\right)\right)}\right)$ where G_j and r_m are the broken fibre shear modulus and the radius of the shear-carrying matrix cylinder

Therefore, only intact fibre elements ($D_{p,q} = 0$) can be over loaded by the *SCF*. On the other hand, another important related fact is to secure the stress continuity at the end of an ineffective length of a broken fibre. In the last element in the ineffective length region, no *SCF* is applied, but the subsequent elements can cover part of the *SCF*. To achieve this continuity, *SCF* is limited in the elements close to ineffective length regions also in accordance with the shear-lag limitation over load transfer to the fibre. Thus, the $SCF_{p,q}$ expressed in a general form is

$$SCF_{p,q} = \begin{cases} \min(SCF^0_{p,q}, SCF^L_{p,q}) & \forall\ p,q\text{: } D_{p,q} = 0 \\ 1 & \text{otherwise,} \end{cases} \quad (7)$$

where $SCF^0_{p,q}$ is the *SCF* predicted by the linear superposition of the contribution of all the fibre breaks using the interacting functions as

$$SCF^0_{p,q} = 1 + \sum_{i=1}^{N_p}\sum_{j=1}^{N_q} \delta_{(q-j)}\lambda_{(p-i)}[D_{i,j} = 1] \quad (8)$$

where here $[\bullet]$ are the Iverson brackets and define 1 if $\bullet$ is true, and 0 if it is false. $SCF^L_{p,q}$ is the *SCF* limit according to the shear-lag capacity to transfer load to the fibre, and is calculated as the slope defined by the stress gradient of the nearest ineffective length:

$$SCF^L_{p,q} = \min\left(\frac{1}{L^{in}_{i,q}}\ |i-p|\ l\right) \quad \forall\ i\text{: } D_{i,q} = 1 \quad (9)$$

The constitutive equation presented here allows the fibre

fragmentation mechanism to be captured by means of the fibre breaks and its associated damage variable. The redistribution of stress using the shear-lag model permits several breaks along the length of any fibre. However, other mechanisms, such as delamination, are ignored by the model. Nonetheless, neglecting delamination is an acceptable assumption in the failure prediction of non-hybrids and of an intrayarn hybrid, where the different fibre populations are mixed at the fibre level. In other hybrid configurations, such as an interlayer hybrid where the different fibres are located in different layers, delamination should be considered.

2.3. Element stiffness, plane stiffness and global RVE stiffness

As previously mentioned, the proposed methodology leads to different elongations through the domain, causing a dissimilar strain for each plane ε_p. The approach proposed is to compute the strains of each plane according to the element's stiffness and the initial hypothesis that fibres work in parallel and planes in series.

The progressive failure is formulated using the stiffness damage of each fibre element, $D_{p,q}$. To do so, Hooke's law of an element under tensile stress defines the longitudinal stiffness of a single fibre element, $k_{p,q}$, with

$$k_{p,q} = E_q(1-D_{p,q})\frac{A_q}{l} \tag{10}$$

where A_q is the cross-sectional area of fibre q given by $A_q = s_q\,\pi r_q^2$, and where s_q is a factor which guarantees the appropriate area of not entire fibres on the domain will be considered ($s_q = 1$ for entire fibres and $s_q < 1$ for fibres located at the corners, or the outskirts of the RVE).

The total stiffness of each plane can be obtained by assuming that all fibre elements in the plane and the matrix stiffness work in parallel

$$k_p = \sum_{q=1}^{N_q} k_{p,q} + E_\mathrm{m}\frac{A_\mathrm{m}}{l} \tag{11}$$

where the matrix behaviour is assumed to be linear elastic, with E_m being the matrix Young's modulus, and A_m the matrix cross-sectional area of the RVE, $A_\mathrm{m} = a\,b - \sum_{q=1}^{N_q} A_q$.

Similarly, the total stiffness is calculated by assuming that all planes work in series

$$K = \left(\sum_{p=1}^{N_p}\frac{1}{k_p}\right)^{-1} \tag{12}$$

2.4. External and internal equilibrium

Because of mechanical equilibrium, the internal force of each plane, F_p, must be equal to the total external force, F, sustained by the system so that $F = F_p$. The total external force can be found by relating the current total stiffness, K, and the global longitudinal homogenized strain, ε^0, given in Section 2.6. Similarly, the force of each plane can also be obtained by relating the plane stiffness and the strain of the plane leading to

$$F = F_p \quad K\,\varepsilon^0\,L = k_p\,\varepsilon_p\,l \tag{13}$$

Therefore, ε_p is obtained as a function of ε^0 with

$$\varepsilon_p = \frac{K\,L}{k_p\,l}\varepsilon^0 \tag{14}$$

To maintain local load equilibrium, the aggregation of the loads of the fibres and the matrix, must be equal to the load of the plane, therefore

$$F_p = k_p\,\varepsilon_p\,l = \sum_{q=1}^{N_q}\sigma_{p,q}A_q + \varepsilon_p E_\mathrm{m}A_\mathrm{m} \tag{15}$$

By substituting Eq. (4) in (15), and re-organizing, Ω_p can be found as

$$\Omega_p = \frac{\sum_{q=1}^{N_q} SCF_{p,q}E_q(1-D_{p,q})A_q}{k_p\,l - E_\mathrm{m}A_\mathrm{m}} \tag{16}$$

where Ω_p as result of a plane level equilibrium becomes constant to all fibre elements in plane p. An additional formulation of Ω_p is obtained by substituting (11) in (16) leading to

$$\Omega_p = \frac{\sum_{q=1}^{N_q} SCF_{p,q}E_q(1-D_{p,q})A_q}{\sum_{q=1}^{N_q} E_q(1-D_{p,q})A_q} \tag{17}$$

Once Ω_p has been evaluated, all $\sigma_{p,q}$ can be calculated from Eq. (4) and compared with their strength $\sigma_{p,q}^u$. It is worth mentioning that small deformations are assumed. Thus, the element length l, total RVE length L and cross-sectional areas A_q, A_m remain constant.

2.5. Composite homogenized stress and break density

The homogenized composite stress is obtained as an average of both element stresses and matrix stress, weighed by their volume fraction. For a non-hybrid, this leads to

$$\sigma^0 = \frac{v_\mathrm{f}}{N_p N_q}\sum_{p=1}^{N_p}\sum_{q=1}^{N_q}\sigma_{p,q} + \frac{1-v_\mathrm{f}}{N_p}\sum_{p=1}^{N_p}E_\mathrm{m}\varepsilon_p \tag{18}$$

where v_f is the total fibre volume fraction.

For a hybrid composite, the average of the fibre stress must be calculated independently for each fibre type to capture the differences in the cross-sectional area

$$\sigma^0 = \frac{v_{\mathrm{f}1}}{N_p N_1}\sum_{p=1}^{N_p}\sum_{q\in\mathrm{f}1}\sigma_{p,q} + \frac{v_{\mathrm{f}2}}{N_p N_2}\sum_{p=1}^{N_p}\sum_{q\in\mathrm{f}2}\sigma_{p,q} + \\ + \frac{1-v_{\mathrm{f}1}-v_{\mathrm{f}2}}{N_p}\sum_{p=1}^{N_p}E_\mathrm{m}\varepsilon_p \tag{19}$$

where $v_{\mathrm{f}1}$ and $v_{\mathrm{f}2}$ are the relative fibre volume fractions of each fibre population in the case of a hybrid, and N_1 and N_2 are the number of fibres in populations f1 and f2, respectively.

The break density is calculated by dividing the number of broken elements into the total RVE volume as

$$\rho_\mathrm{b} = \frac{1}{a\,b\,L}\sum_{p=1}^{N_p}\sum_{q=1}^{N_q}[D_{p,q} = 1] \tag{20}$$

where $[\bullet]$is the Iverson bracket. In the case of a hybrid composite, the break density of each population can also be calculated with the respective number of broken elements.

2.6. Algorithm procedure

A controlled monotonic increment of longitudinal displacement is performed along z direction to guarantee a stable tensile damage process. Hence, each new loading step t starts by increasing the current longitudinal displacement applied, $(u)_t$, with

$$(u)_t = (u)_{t-1} + (\Delta u)_t \tag{21}$$

where $(u)_{t-1}$ is the displacement from the previous step, and $(\Delta u)_t$ is the displacement increment. In each load step, the longitudinal displacement and the global longitudinal homogenized strain, ε^0, assuming a uni-axial behaviour, are both related by the total length of the model with

$$(\varepsilon^0)_t = \frac{(u)_t}{L} \tag{22}$$

Following this, the stiffness, forces, strains and Ω_p are first estimated with the damage variable and the *SCF* from the previous step with Eqs.

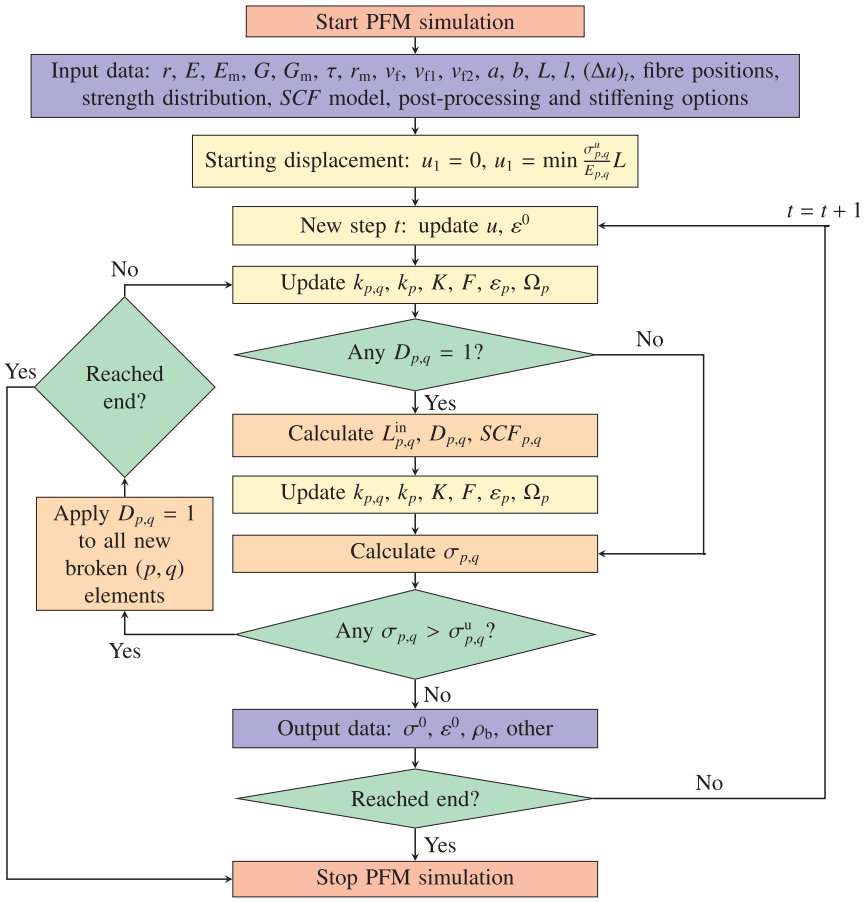

Fig. 4. Progressive Failure Model flowchart. (For interpretation of the references to colour in this figure legend, the reader is referred to the web version of this article.)

(10)–(12), (14) and (17). Note that, in the first step $t = 1$, all damage variables $D_{p,q}$ are equal to zero, and all $SCF_{p,q}$ are equal to one. If there are broken elements, then the ineffective length, damage variable and the *SCF* are calculated with the estimated stiffness, forces, strains and Ω_p using Eqs. (5)–(7). As the damage has changed, the stiffness, forces, strains and Ω_p are re-calculated to obtain the true actual current magnitudes. Next, the element stresses are computed with Eq. (4). If no elements break, the composite stress and break densities are evaluated with Eqs. (18)–(20). If new elements fail, the damage $D_{p,q}$ of all new broken elements is set equal to 1 and the same procedure is repeated without increasing the applied displacement and with the current damage and latest calculated *SCF*, until no more failures happen in the current step. When no new elements fail, a new step is started by updating $(u)_t$ and $(\varepsilon^0)_t$ with equations (21) and (22). This procedure is shown in the flowchart in Fig. 4. The model stops when either all elements in a plane are damaged, or the composite stress has decreased by a pre-defined percentage of maximum load value. For non-hybrid composites, where a brittle failure is expected, the simulation is stopped when the stress decreases 10% from the maximum reached. In a hybrid composite, LE fibre population could fail originating a large load drop. To avoid an early end of the simulation before HE fibre failure, the calculation is stopped when the stress decreases more than 80%. The model was implemented in MatLab (The MathWorks Inc., USA) [40] and Python programming language (Python Software Foundation, https://www.python.org/). The results can be exported into ParaView (Kitware Inc., USA) [41] for visual post-processing.

3. Results and discussion

3.1. Non-hybrid UD T700S and M40 carbon fibre epoxy

Two different non-hybrid UD composites consisting of T700S-Epoxy and M40-Epoxy were simulated using the proposed PFM. The results were compared with the reported experimental data in Swolfs et al. [18] and Koyanagi et al. [42] respectively, in an attempt to validate the model. All model properties shown in Table 2, except the estimated matrix and *SCF* related properties, were also taken from [18,42]. The tensile behaviour of each composite system was performed with all three models shown in Table 1 to observe their impact on the final

Table 2
UD composites and model properties.

Composite	Fibre properties			Weibull properties			Matrix properties			*SCF* properties		RVE data	
	E, E_0 [GPa]	G [GPa]	r [mm]	m [–]	σ_0 [MPa]	L_0 [mm]	E_m [GPa]	G_m [GPa]	τ [MPa]	r_m [mm]	ψ [–]	L [mm]	v_f [%]
T700S-Epoxy	197.9	78.53	3.5×10^{-3}	$m_1 = 4.8$ $m_2 = 12$	$\sigma_{01} = 5200$ $\sigma_{02} = 6100$	10	3.0	1.11	40	42×10^{-3}	0.5	1.54	55
M40-Epoxy	392.0	155.55	3.0×10^{-3}	16	4500	25	3.5	1.29	50	36×10^{-3}	0.18	25	60
AS4 -Epoxy	234.0	92.85	3.5×10^{-3}	10.7	4275	12.7	3.76	1.39	50	–	–	$15 \times R$	60
M50S	480.0	190.48	2.65×10^{-3}	9	4600	10				–	–		

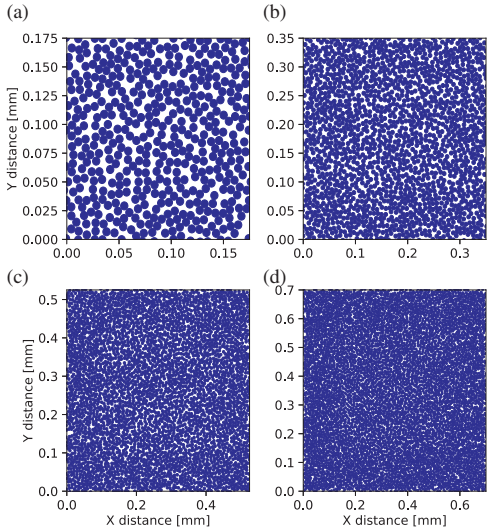

Fig. 5. Cross-section view examples of RVEs with T700S fibre (a) $50 \times R$, (b) $100 \times R$, (c) $150 \times R$, (d) $200 \times R$. (For interpretation of the references to colour in this figure legend, the reader is referred to the web version of this article.)

failure. The parameters P_1 and P_2 were taken to be $P_1 = 6.12$ and $P_2 = 7.74$, as in [18].

Like [18], a bimodal Weibull distribution was applied to assign the strength, $\sigma^u_{p,q}$, to each fibre element of the T700S composite with

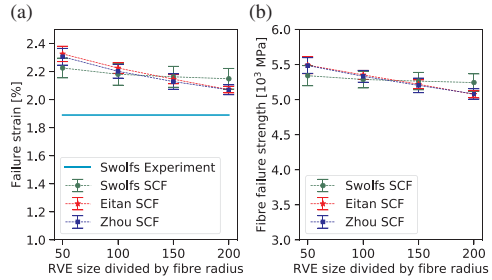

Fig. 7. T700S error bars for 40 simulations at each simulated RVE size for each *SCF* model compared with Swolfs et al. [18] experimental results, (a) failure strain, (b) fibre failure stress. (For interpretation of the references to colour in this figure legend, the reader is referred to the web version of this article.)

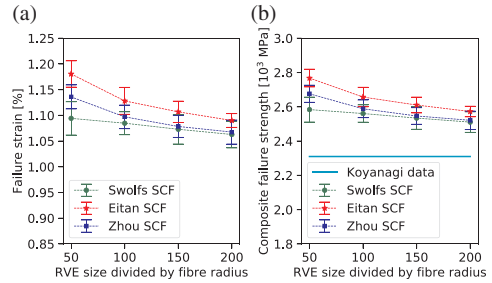

Fig. 8. M40 error bars for 40 simulations for each simulated RVE size for each *SCF* model compared with Koyanagi et al. [42] experimental results, (a) failure strain, (b) composite failure stress. (For interpretation of the references to colour in this figure legend, the reader is referred to the web version of this article.)

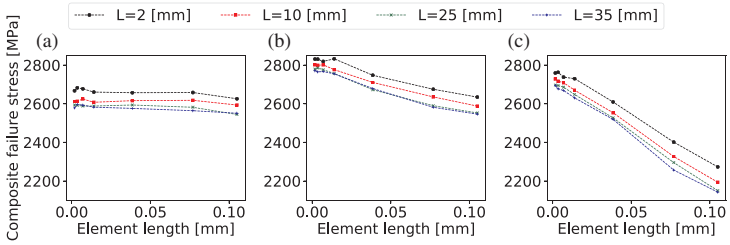

Fig. 6. Influence of the total RVE length (L) and element length (l) on the failure strength for the M40 composite. The mean result for 20 simulations is shown. The RVE width and thickness were $50 \times R$. (a) Using the Swolfs et al. *SCF* model, (b) using the Eitan and Wagner *SCF* model, and (c) using the Zhou and Wagner *SCF* model. (For interpretation of the references to colour in this figure legend, the reader is referred to the web version of this article.)

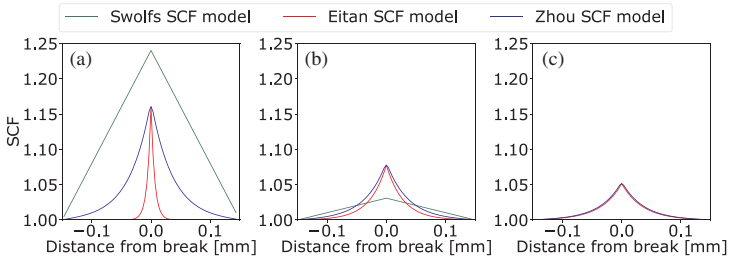

Fig. 9. Predicted *SCF* to an intact fibre at different centre-to-centre distances, d^c_{q-j}, according to the Zhou and Wagner, Eitan and Wagner and Swolfs et al. models. (a) $d^c_{q-j} = 2.07r$, (b) $d^c_{q-j} = 4.14r$, (c) $d^c_{q-j} = 6.21r$. The *SCF* is shown along the ineffective length of a 0.15 mm broken fibre, with all material data corresponding to the T700S fibre in Table 2. (For interpretation of the references to colour in this figure legend, the reader is referred to the web version of this article.)

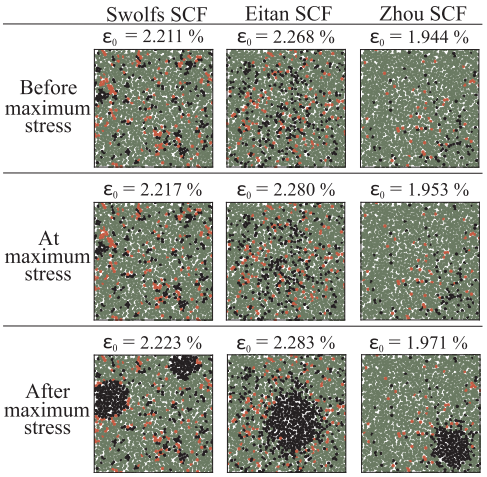

Fig. 10. Cluster evolution at different stages during final failure within 16% of total length in each direction of the section with largest break density for the T700S composite. Broken fibres in black, damaged fibres in red and intact fibres in green. RVE size corresponds to 100 × *R*. (For interpretation of the references to colour in this figure legend, the reader is referred to the web version of this article.)

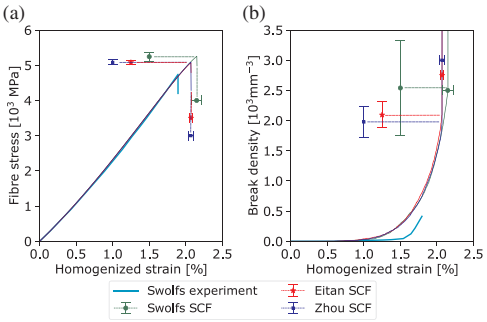

Fig. 11. T700S closest curve to the mean from all 40 simulations with a size of 200 × *R* for each *SCF* model compared against the experimental results from Swolfs et al. [18], (a) mean stress-strain curve, (b) mean break density curve. (For interpretation of the references to colour in this figure legend, the reader is referred to the web version of this article.)

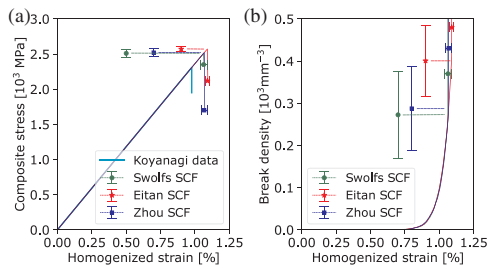

Fig. 12. M40 closest curve to the mean from all 40 simulations of size 200 × *R* for each *SCF* model compared against the experimental results from Koyanagi et al. [42], (a) mean stress-strain curve, (b) mean break density curve. The experimental stress-strain curve was assumed to be linear from the experimental strength with Young's modulus given by the rule of mixtures. (For interpretation of the references to colour in this figure legend, the reader is referred to the web version of this article.)

$$P_{p,q} = 1 - \exp\left(-\left(\frac{l}{L_0}\right)\left(\frac{\sigma^u_{p,q}}{\sigma_{01}}\right)^{m_1} - \left(\frac{l}{L_0}\right)\left(\frac{\sigma^u_{p,q}}{\sigma_{02}}\right)^{m_2}\right) \quad (23)$$

Whereas, according to [42], a traditional Weibull distribution was applied for the M40 composite using

$$P_{p,q} = 1 - \exp\left(-\frac{l}{L_0}\left(\frac{\sigma^u_{p,q}}{\sigma_0}\right)^{m}\right) \quad (24)$$

where $P_{p,q}$ is a random number between 0 and 1, L_0, m, σ_0, σ_{01}, m_1, σ_{02} and m_2 are Weibull parameters and $\sigma^u_{p,q}$ is the corresponding strength of the fibre element.

A stiffening effect was assumed for the T700S composite only, to be consistent with [18]. Hence, the Young's modulus of the fibres at a step t was given as described in Toyama and Takatsubo [43]

$$(E_q)_t = E_0 + 1000(4133.6(\varepsilon^0)_t - 70331(\varepsilon^0)_t^2) \quad (25)$$

The initial Young's modulus, E_0, was chosen to be consistent with [18].

The main issue in defining the model was to decide on the appropriate width, thickness and length of the RVE. These dimensions had to be as close as possible to the real specimen but still ensure that the model would be workable. To observe the influence the RVE size has on the results, RVEs of a width and thickness of 50 × *R*, 100 × *R*, 150 × *R* and 200 × *R* —where *R* is the fibre radius— were generated. Fig. 5 shows a cross-section view of an example of the fibre distributions obtained.

The RVE length of the T700S was 1.54 mm for all cases, which

Table 3
Obtained failure strains and stress with 95% normal distribution confidence intervals for 40 realizations of each RVE size and *SCF* model. T700S failure stress corresponds to the fibre failure stress, whereas M40 corresponds to the composite failure stress. The CPU times are the mean values for each realization (simulation). Simulations were run on an Intel i7-5820 K 3.3 GHz processor. (*) Estimated values.

Composite	Experimental test	*SCF* model	Variable	RVE width and thickness size (R is the fibre radius)			
				$50 \times R$	$100 \times R$	$150 \times R$	$200 \times R$
T700S-Epoxy	1.89 % [18]	Swolfs et al.	Failure strain [%]	2.23 ± 0.07	2.18 ± 0.08	2.16 ± 0.07	2.15 ± 0.07
			Failure stress [MPa]	5341 ± 143	5287 ± 121	5264 ± 124	5243 ± 123
			CPU time [h:mm:ss]	0:01:28	0:06:00	0:15:10	0:34:50
		Eitan and Wagner	Failure strain [%]	2.33 ± 0.05	2.22 ± 0.04	2.15 ± 0.03	2.07 ± 0.02
	4740 MPa (*)		Failure stress [MPa]	5491 ± 121	5352 ± 64	5219 ± 62	5075 ± 52
			CPU time [h:mm:ss]	0:03:20	0:28:12	1:49:47	4:37:00
		Zhou and Wagner	Failure strain [%]	2.31 ± 0.06	2.20 ± 0.05	2.13 ± 0.05	2.07 ± 0.04
			Failure stress [MPa]	5486 ± 112	5332 ± 84	5203 ± 104	5081 ± 73
			CPU time [h:mm:ss]	0:03:14	0:25:59	1:40:16	4:59:00
M40-Epoxy	0.976 % (*)	Swolfs et al.	Failure strain [%]	1.09 ± 0.03	1.08 ± 0.02	1.07 ± 0.03	1.06 ± 0.03
			Failure stress [MPa]	2584 ± 73	2561 ± 51	2534 ± 66	2511 ± 60
			CPU time [h:mm:ss]	0:02:08	0:13:36	0:45:41	1:09:00
		Eitan and Wagner	Failure strain [%]	1.18 ± 0.03	1.13 ± 0.03	1.11 ± 0.02	1.09 ± 0.01
	2310 MPa [42]		Failure stress [MPa]	2768 ± 52	2657 ± 57	2610 ± 46	2572 ± 31
			CPU time [h:mm:ss]	0:03:42	0:22:43	0:42:28	2:53:00
		Zhou and Wagner	Failure strain [%]	1.14 ± 0.02	1.10 ± 0.02	1.08 ± 0.02	1.07 ± 0.02
			Failure stress [MPa]	2676 ± 50	2589 ± 51	2546 ± 49	2521 ± 54
			CPU time [h:mm:ss]	0:02:51	0:27:26	0:24:22	2:30:00

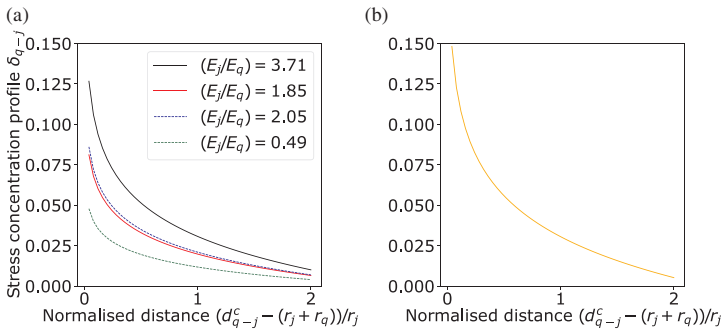

Fig. 13. Hybrid stress concentration profiles. (a) for different ratios E_j/E_q between broken and intact fibres when both fibres belong to different fibre populations, (b) for the same fibre population. (For interpretation of the references to colour in this figure legend, the reader is referred to the web version of this article.)

corresponded to the length of the testing coupon [18]. However, for the M40, the experimental length was 150 mm [42], which is too long to be simulated while maintaining an appropriate small element length. Thus, a first previous study was performed with the M40 composite to determine the sensitivity of the results for both the RVE length L and the element length l. The results obtained from this analysis (Fig. 6) suggested that an element length below $3 \times R$ is small enough, while an RVE length of 25 mm is acceptably long enough. Hence, the RVE length L of the M40 composite was set to 25 mm. Consequently, an element length l of 3.5×10^{-3} and 8.3×10^{-3} mm for the T700S and M40 composites, respectively, was applied. These values were taken as a compromise between accuracy and computational time.

In addition, the variability in the results caused by the randomness of fibre position and fibre strengths had to be considered. Thus, all simulations of each size and *SCF* model were solved 40 times with different fibre distributions, leading to a total of 480 simulations for each composite.

Considering all the inevitable inaccuracies in the modelling assumptions and in the input data, the predicted ultimate strain and strength presented remarkable agreement with the given experimental data for both the T700S and M40 composites, especially for the largest RVE sizes. For the T700S composite, the proposed PFM predicted in the largest RVE, a mean failure strain of 2.14% with the Swolfs *SCF* model, and of 2.07%, using the Eitan *SCF* and the Zhou *SCF* models which over-predict the experimental result of 1.89%, but are close to the 2.17% prediction of Swolfs' strength model [18]. Similarly, for the M40 composite the models predicted a mean failure strength between 2511 MPa and 2572 MPa, albeit with a small over-prediction of 2310 MPa for the experimental one as well.

The obtained failure strain and stress decreased as the RVE cross-sectional size increased; which is coherent with the size effect. These findings suggest that an RVE with a width and thickness size of $50 \times R$ (adequate for elastic predictions according to [27,28]) is not enough to predict unidirectional composite failure mechanisms. The error bars within the 95% confidence intervals in Figs. 7 and 8, decrease with larger RVE sizes.

The size effect was remarkably less pronounced in the Swolfs et al. [18] *SCF* model. To better understand the differences between the *SCF* models implemented, a plot example of the predicted *SCF* with all models is shown in Fig. 9. As can be seen, the Swolfs *SCF* model predicts a much larger *SCF* at a smaller centre-to-centre distance, d^c_{q-j}, to the broken fibre. However, the *SCF* decreases much faster by increasing, d^c_{q-j}, in comparison to the other models. Therefore, the Swolfs *SCF* model is more localized than the others. This should explain why

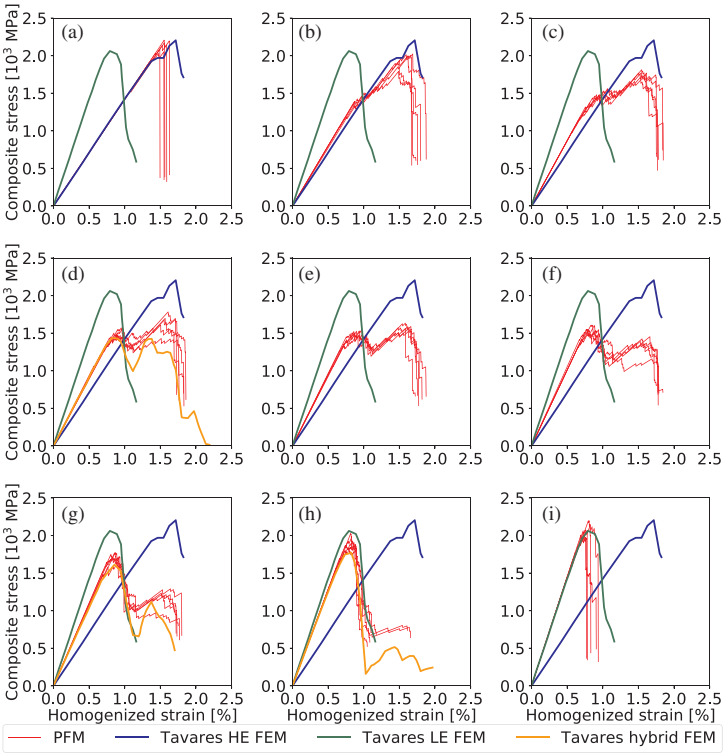

Fig. 14. Stress-strain curves obtained for hybrid M50S-AS4 fibre compared with Tavares et al. [12] FEM when varying the relative LE hybrid fibre volume fraction. (a) 0%LE, (b) 10%LE, (c) 20%LE, (d) 25%LE, (e) 30%LE, (f) 40%LE, (g) 50%LE, (h) 75%LE, (i) 100%LE. For the sake of readability only 5 realisations are shown. (For interpretation of the references to colour in this figure legend, the reader is referred to the web version of this article.)

the size effect is smaller with the Swolfs model: causing *SCF* in a smaller centre-to-centre distance means that fewer fibres are needed to accurately represent stress re-distribution around fibre breaks. The Zhou and Wagner and Eitan and Wagner *SCF* models both estimate the same stress peak, but the *SCF* along the ineffective length is different. For the Eitan and Wagner model, the *SCF* distribution along the ineffective length is narrower and affects only a small region of the intact fibres close to the broken fibre. By increasing d^c_{q-j}, the *SCF* distribution along the ineffective length tends to coincide with the Zhou and Wagner model.

The cluster evolutions, with the T700S composite for each *SCF* model, are shown at different instants close to final failure in Fig. 10. It can be observed that groups of clusters formed with all models. These clusters increased in size as the load was incremented until a critical cluster propagated and led to final failure. Even though the same fibre strengths were used with all three *SCF* models, the failure procedure was clearly different. Not only was the failure strain different, but so too were the clusters formed at the different places in the model. Moreover, final failure, due to unstable cluster propagation, also happened at a different location.

By observing the results obtained, it is not possible to conclude if an *SCF* approach is more accurate than the others. Indeed, the results show that the *SCF* model has only a relative influence on the predicted failure. The significant difference between the *SCF* models analysed is the formulation basics and the nature of the identification parameters. The Zhou and Wagner model and the Eitan and Wagner model are formulations totally based on theoretical shear-lag assumptions. These models need a major number of parameters, which are not always simple to estimate, such as ψ or r_m. However, the Swolfs *SCF* model proposes a completely different approach, by where the *SCF* is obtained by fitting results from a micro-mechanic finite element analysis using a relatively large RVE with hundreds of fibres and a long length.

Both composites presented a different failure. The T700S composite experimented some stiffness loss before final failure, whereas the M40 composite exhibited a very brittle failure, as seen in Figs. 11a and 12a. This effect is highlighted by the evolution of the break densities in Figs. 11b and 12b, as the curve of the M40 presents a more sudden degradation than that of T700S. The break density of T700S was over-predicted by the model compared to the experimental results, as in Swolfs et al. [18], which could be the consequence of inaccuracies in the model or in the experimental data. A summary of the results obtained is presented in Table 3. The total computational time is also shown for each set of simulations and presented a strong exponential increase by increasing the width/thickness of the RVE. The simulations using the Swolfs *SCF* model needed smaller computational time in the PFM. However, it must be remarked that the two constants (P_1 and P_2) used by this *SCF* model are obtained from micromechanical finite element analyses which represent a considerable effort.

3.2. Hybrid UD AS4-M50S carbon fibres/epoxy

A UD intrayarn hybridization within M50S carbon (LE fibre) and

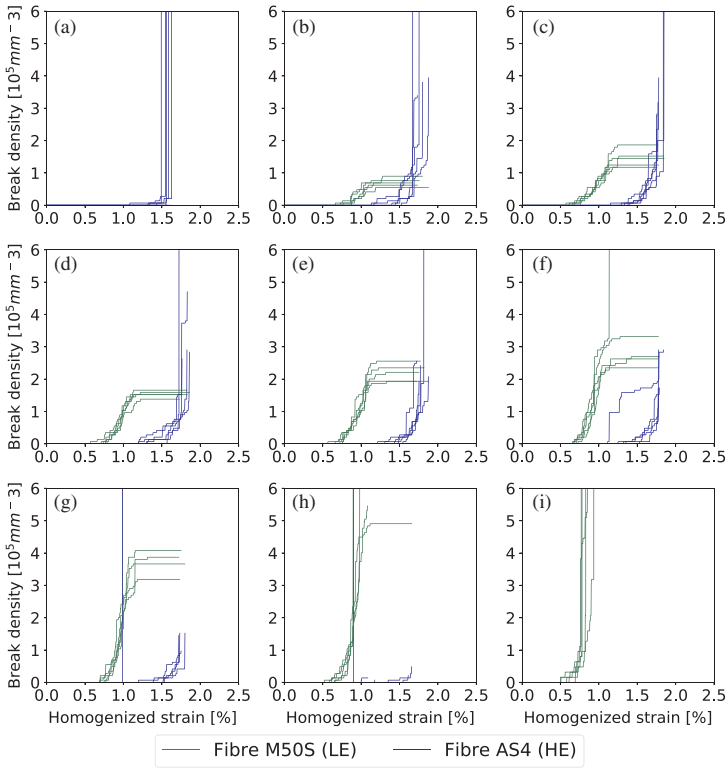

Fig. 15. Break density-strain curves obtained for hybrid M50S-AS4 fibre composite when varying the relative hybrid fibre volume fraction. (a) 0%LE, (b) 10%LE, (c) 20%LE, (d) 25%LE, (e) 30%LE, (f) 40%LE, (g) 50%LE, (h) 75%LE, (i) 100%LE. For the sake of readability only 5 realisations are shown. (For interpretation of the references to colour in this figure legend, the reader is referred to the web version of this article.)

AS4 Carbon (HE fibre) with epoxy matrix was simulated at different LE relative hybrid volume fractions. All data, shown in Table 2, was taken from Tavares et al. [12]. In order to carry out a clean comparison with [12] FEM results, the simulations were performed using the same RVE dimensions. Thus, RVEs with width, thickness and length of $15 \times R$ were generated, with R being the largest fibre radius in the RVE. It is important to remark that while such a small RVE is not big enough to properly represent the failure process accurately, it is the appropriate configuration to compare the PFM simulation with the micro-mechanical FEM results. A Weibull distribution extrapolated to the total gauge length (instead of the element length) was also used:

$$P_{p,q} = 1 - \exp\left(-\frac{L}{L_0}\left(\frac{\sigma^u_{p,q}}{\sigma_0}\right)^m\right) \tag{26}$$

where the element length L was set to 0.35×10^{-3} mm.

The *SCF* model used was from Swolfs et al. [18]. In a hybrid composite the appropriate *SCFs* profiles depend on the stiffness ratio between the broken and the intact fibre (E_j/E_q). Three combination cases are then possible: (i) a broken LE fibre causing *SCF* to an HE fibre ($E_j/E_q = 2.05$), (ii) a broken HE fibre causing *SCF* to an LE fibre ($E_j/E_q = 0.49$), and (iii) a broken fibre (LE or HE) causing *SCF* to a fibre of the same population ($E_j/E_q = 1$). Swolfs et al. [39] provided the *SCF* for $E_j/E_q = 3.71$ and $E_j/E_q = 1.85$. Thus, interpolation and extrapolation was performed in between to obtain the *SCF* for $E_j/E_q = 2.05$ and $E_j/E_q = 0.49$, respectively. These profiles are shown in Fig. 13a. When either a broken LE fibre causes *SCF* to an intact LE, or a broken HE fibre causes *SCF* to an intact HE fibre, the profile shown in Fig. 13b was assumed, which was also taken from [39]. Thus, the corresponding parameters P_1 and P_2 from Table 1 are $P_1 = 2.982$, $P_2 = 3.068$ for $E_j/E_q = 3.71$, $P_1 = 1.908$, $P_2 = 1.975$ for $E_j/E_q = 1.85$, and $P_1 = 3.656$, $P_2 = 3.053$ for the *SCF* profile between fibres of the same population. Note that for the two non-hybrid cases (a 100% HE composite and a 100% LE composite), the same Swolfs et al. [18] *SCF* model used in Section 3.1 was applied. Moreover, it is worth mentioning that the stress re-distribution between fibres of the same type (Fig. 13b), which share the same stiffness and radius, differs from the one obtained between fibres of different type (Fig. 13a), with distinct stiffness and fibre radii. Therefore, the *SCF* for $E_j/E_q = 1$ does not fit in between the curves of $E_j/E_q = 0.49$ and $E_j/E_q = 1.85$.

Within each hybrid relative volume fraction modelled (see Fig. 14), 40 simulations were solved leading to a total of 360 simulations, with each set of 40 simulations taking approximately 9 min to be completed. The tensile stress-strain curves obtained are shown and compared with the [12] FEM results in Fig. 14 at LE hybrid volume fractions of 0, 25, 50, 75 and 100%. A good agreement was obtained, which led to similar failure responses.

Pseudo-ductility was predicted at LE relative volume fractions between 10 and 30%. The other composites either failed prematurely, or the interaction between fibres was not evident enough. This failure process is highlighted in Fig. 15. For nearly all the hybrid

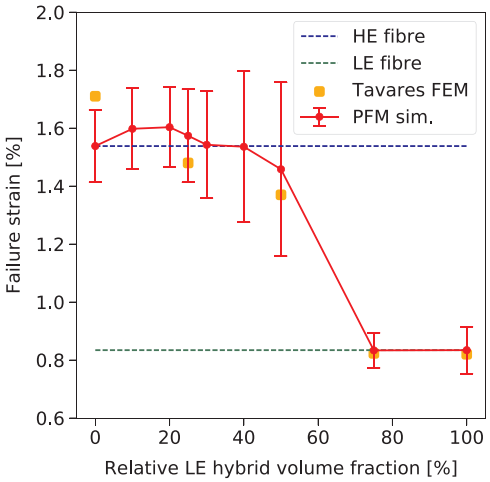

Fig. 16. Hybrid failure strain obtained for different LE and HE relative volume fractions. The results of the simulations are compared with [12] FEM results. The error bars are shown within the 95% confidence intervals for 40 realizations. (For interpretation of the references to colour in this figure legend, the reader is referred to the web version of this article.)

configurations it is possible to observe that the LE fibre break density does not increase once a certain point is reached. That means that the LE fibre is fully fragmented and is incapable of breaking further, even when the applied load is incremented. At low LE volume fractions between 10 and 30%, the breaks of the LE fibre saturated while the HE fibre was failing, which led to pseudo-ductility until the final failure. However, at higher LE volume fractions the failure was sudden and brittle. These results demonstrate that the proposed model is able to capture fibre fragmentation, which is one of the most relevant mechanisms associated to pseudo-ductility.

The hybrid failure strain is also presented in Fig. 16. For LE volume fractions lower than 70%, the hybrid failure strain was considered as the corresponding strain at the second maximum in the stress-strain curve, which corresponded to the failure of the HE fibre in the hybrid. However, for larger LE volume fractions, the first maximum was considered as failure strain instead, because the drop in stress afterwards did not show any evidence of a second maximum. These failure strain values correspond to the failure of the LE fibres.

The small discrepancies between PFM and FEM are attributed to the shear-lag model, the prediction of *SCF* and, in particular, the omission of dynamic phenomena. Nonetheless, the proposed model predicted similar results using a very simple model that can be run on a regular computer in a short time, whereas Tavares et al.'s [12] model requires an enormous computational effort in a high power computational facility.

Future work should try to address the problems omitted here such as matrix damage, thermal residual stresses and dynamic effects. Further parametric studies to design hybrid configurations to maximise pseudo-ductility and the effect of unknown parameters such as the effect of debonding or the effect of the size in the hybrid effect should also be included.

4. Conclusions

A 3D Progressive Failure Model based on the chain of bundles approach [19], was developed and validated. The model accurately represents the failure curve of unidirectional composite materials with a random distribution of fibres. A complete stress distribution is obtained by associating a damage variable to the loss of stress transfer capability along the ineffective length, which produces a reduction of local effective stiffness. Consequently, local stress concentrations are applied through all stress recoveries, so that the neighbouring fibres are locally overloaded. The method, formulated in an explicit form, leads to different deformations along the length of the model.

The model has been validated with results available in the literature. Each simulation, with different random distribution of fibres, has been repeated multiple times to evaluate the uncertainly of the results. For non-hybrids, T700S-Epoxy and M40-Epoxy UD composites were simulated and compared to results from Swolfs et al. [18] and Koyanagi et al. [42], respectively. Moreover, an RVE size with transversal dimensions larger than $200 \times R$ is needed to capture the size effect inherent to the failure process, which is more exigent than the required $50 \times R$ for elastic RVE predictions according to [27,28]. Three *SCF* models corresponding to the models of Swolfs et al. [18], Zhou and Wagner [37] and Eitan and Wagner [38] were compared and found to have a slightly different failure prediction. A significant difference between these formulations is the parameters identification method. The Zhou and Wagner model and the Eitan and Wagner model are entirely based on theoretical assumptions. They need a significant number of parameters and some of them are not easy to calculate or estimate. Meanwhile, the Swolfs *SCF* model is parametrized with a simpler set of values. The exact identification of these must be performed by a micromechanical finite element approach. However, all three models led to a similar failure procedure which showed a tendency to form clusters of broken fibres and which led to final failure. In any case, the Swolfs *SCF* model generates more localized stress concentration factors, leading to predictions significantly less sensitive to the size effect when compared to the other models. Finally, a hybrid carbon-carbon (M50S-AS4) epoxy composite was simulated and pseudo-ductility was obtained at LE volume fractions between 10 and 30%. The results were compared with those of Tavares et al. [12] micro-mechanical FEM and also obtained good agreement, but with a much faster and simpler model than the FEM is.

Acknowledgments

The authors would like to acknowledge P.P. Camanho, A.R. Melro and R.P. Tavares for their permission to use their random fibre generator. The authors acknowledge the financial support from the Spanish 'Ministerio de Ciencia e Innovación' (MINECO) under the projects MAT2015-69491-C3-1-R and TRA2015-71491-R co-financed by the European Regional Development Fund (ERDF). The first author would like to acknowledge the predoctoral Grant BES-2016-078270 from the 'Subprograma Estatal de Formación del MICINN' co-financed by the European Social Fund.

References

[1] Turon A, Costa J, Maimí P, Trias D, Mayugo JA. A progressive damage model for unidirectional fibre-reinforced composites based on fibre fragmentation. Part I: Formulation. Compos Sci Technol 2005;65(13):2039–48. http://dx.doi.org/10.1016/j.compscitech.2005.04.012.

[2] Swolfs Y, Gorbatikh L, Verpoest I. Fibre hybridisation in polymer composites: a review. Compos Part A: Appl Sci Manuf 2014;67:181–200. http://dx.doi.org/10.1016/j.compositesa.2014.08.027.

[3] Swolfs Y, Verpoest I, Gorbatikh L. Maximising the hybrid effect in unidirectional hybrid composites. Mater Des 2016;93:39–45. http://dx.doi.org/10.1016/j.matdes.2015.12.137.

[4] Czél G, Jalalvand M, Wisnom MR. Design and characterisation of advanced pseudo-ductile unidirectional thin-ply carbon/epoxy-glass/epoxy hybrid composites. Compos Struct 2016;143:362–70. http://dx.doi.org/10.1016/j.compstruct.2016.02.010.

[5] Swolfs Y, McMeeking RM, Verpoest I, Gorbatikh L. The effect of fibre dispersion on initial failure strain and cluster development in unidirectional carbon/glass hybrid composites. Compos Part A: Appl Sci Manuf 2014;69:279–87. http://dx.doi.org/10.1016/j.compositesa.2014.12.001.

[6] Xing J, Hsiao G, Chou T-W. A dynamic explanation of the hybrid effect. J Compos

Mater 1981;15(5):443–61. http://dx.doi.org/10.1177/002199838101500504.
[7] Swolfs Y, Verpoest I, Gorbatikh L. A review of input data and modelling assumptions in longitudinal strength models for unidirectional fibre-reinforced composites. Compos Struct 2016;150:153–72. http://dx.doi.org/10.1016/j.compstruct.2016.05.002.
[8] Wisnom MR, Czel G, Swolfs Y, Jalalvand M, Gorbatikh L, Verpoest I. Hybrid effects in thin ply carbon/glass unidirectional laminates: Accurate experimental determination and prediction. Compos Part A: Appl Sci Manuf 2016;88:131–9. http://dx.doi.org/10.1016/j.compositesa.2016.04.014.
[9] Hayashi T. On the improvement of mechanical properties of composites by hybrid composition. In: Proc 8th int reinforced plastics conference; 1972. p. 149–52.
[10] Zweben C. Tensile strength of hybrid composites. J Mater Sci 1977;12(7):1325–37. http://dx.doi.org/10.1007/BF00540846.
[11] Fukuda H. An advanced theory of the strength of hybrid composites. J Mater Sci 1984;19(3):974–82. http://dx.doi.org/10.1007/BF00540468.
[12] Tavares RP, Melro AR, Bessa MA, Turon A, Liu WK, Camanho PP. Mechanics of hybrid polymer composites: analytical and computational study. Comput Mech 2016;57(3):405–21. http://dx.doi.org/10.1007/s00466-015-1252-0.
[13] Melro AR, Camanho PP, Andrade Pires FM, Pinho ST. Micromechanical analysis of polymer composites reinforced by unidirectional fibres: Part I-Constitutive modelling. Int J Solids Struct 2013;50(11–12):1897–905. http://dx.doi.org/10.1016/j.ijsolstr.2013.02.009.
[14] Okabe T, Takeda N, Kamoshida Y, Shimizu M, Curtin WA. A 3D shear-lag model considering micro-damage and statistical strength prediction of unidirectional fiber-reinforced composites. Compos Sci Technol 2001;61(12):1773–87. http://dx.doi.org/10.1016/S0266-3538(01)00079-3.
[15] Okabe T, Sekine H, Ishii K, Nishikawa M, Takeda N. Numerical method for failure simulation of unidirectional fiber-reinforced composites with spring element model. Compos Sci Technol 2005;65(6):921–33. http://dx.doi.org/10.1016/j.compscitech.2004.10.030.
[16] Swolfs Y, McMeeking RM, Verpoest I, Gorbatikh L. Matrix cracks around fibre breaks and their effect on stress redistribution and failure development in unidirectional composites. Compos Sci Technol 2015;108:16–22. http://dx.doi.org/10.1016/j.compscitech.2015.01.002.
[17] Swolfs Y, Verpoest I, Gorbatikh L. Issues in strength models for unidirectional fibre-reinforced composites related to Weibull distributions, fibre packings and boundary effects. Compos Sci Technol 2015;114:42–9. http://dx.doi.org/10.1016/j.compscitech.2015.04.002.
[18] Swolfs Y, Morton H, Scott AE, Gorbatikh L, Reed PAS, Sinclair I, Spearing SM, Verpoest I, et al. Synchrotron radiation computed tomography for experimental validation of a tensile strength model for unidirectional fibre-reinforced composites. Compos Part A: Appl Sci Manuf 2015;77:106–13. http://dx.doi.org/10.1016/j.compositesa.2015.06.018.
[19] Rosen BW. Tensile failure of fibrous composites. AIAA J 1964;2(11):1985–91. http://dx.doi.org/10.2514/3.2699.
[20] Fukuda H. Micromechanical strength theory of hybrid composites. Adv Compos Mater 1991;1(1):39–53. http://dx.doi.org/10.1163/156855191X00054.
[21] Fang W, Yuqing W, Zhiqian C. Micromechanical modeling of the effect of progressive damage on the tensile behavior in fiber-reinforced polymer composites. Adv Mater Res 2009;79–82:1347–50. http://dx.doi.org/10.4028/www.scientific.net/AMR.79-82.1347.
[22] Czél G, Wisnom MR. Demonstration of pseudo-ductility in high performance glass/epoxy composites by hybridisation with thin-ply carbon prepreg. Compos Part A: Appl Sci Manuf 2013;52:23–30. http://dx.doi.org/10.1016/j.compositesa.2013.04.006.
[23] Yu H, Longana ML, Jalalvand M, Wisnom MR, Potter KD. Pseudo-ductility in intermingled carbon/glass hybrid composites with highly aligned discontinuous fibres. Compos Part A: Appl Sci Manuf 2015;73:35–44. http://dx.doi.org/10.1016/j.compositesa.2015.02.014.
[24] Jalalvand M, Czel G, Wisnom MR. Damage analysis of pseudo-ductile thin-ply UD hybrid composites – a new analytical method. Compos Part A: Appl Sci Manuf 2015;69:83–93. http://dx.doi.org/10.1016/j.compositesa.2014.11.006.
[25] Fotouhi M, Jalalvand M, Wisnom MR. High performance quasi-isotropic thin-ply carbon/glass hybrid composites with pseudo-ductile behaviour in all fibre orientations. Compos Sci Technol 2017;152:101–10. http://dx.doi.org/10.1016/j.compscitech.2017.08.024.
[26] Czél G, Jalalvand M, Wisnom MR. Design and characterisation of advanced pseudo-ductile unidirectional thin-ply carbon/epoxy-glass/epoxy hybrid composites. Compos Struct 2016;143:362–70. http://dx.doi.org/10.1016/j.compstruct.2016.02.010.
[27] Trias D, Costa J, Turon A, Hurtado JE. Determination of the critical size of a statistical representative volume element (SRVE) for carbon reinforced polymers. Acta Mater 2006;54(13):3471–84. http://dx.doi.org/10.1016/j.actamat.2006.03.042.
[28] Zangenberg J, Brøndsted P. Determination of the minimum size of a statistical representative volume element from a fibre-reinforced composite based on point pattern statistics. Scripta Mater 2013;68(7):503–5. http://dx.doi.org/10.1016/j.scriptamat.2012.11.032.
[29] Swolfs Y, Gorbatikh L, Romanov V, Orlova S, Lomov SV, Verpoest I. Stress concentrations in an impregnated fibre bundle with random fibre packing. Compos Sci Technol 2013;74:113–20. http://dx.doi.org/10.1016/j.compscitech.2012.10.013.
[30] Melro AR, Camanho PP, Pinho ST. Generation of random distribution of fibres in long-fibre reinforced composites. Compos Sci Technol 2008;68(9):2092–102. http://dx.doi.org/10.1016/j.compscitech.2008.03.013.
[31] Weibull W. A statistical distribution function of wide applicability. ASME J 1952:293–7.
[32] Harlow DG, Phoenix SL. Probability distributions for the strength of composite materials II: a convergent sequence of tight bounds. Int J Fract 1981;17(6):601–30. http://dx.doi.org/10.1007/BF00681559.
[33] Watson AS, Smith RL. An examination of statistical theories for fibrous materials in the light of experimental data. J Mater Sci 1985;20(9):3260–70. http://dx.doi.org/10.1007/BF00545193.
[34] Cox H. The elasticity and strength of paper and other fibrous materials. Br J Appl Phys 1952;3(3):72–9. http://dx.doi.org/10.1088/0508-3443/3/3/302.
[35] Kelly A, Tyson W. Tensile properties of fibre-reinforced and metals: copper/tungsten and copper/molybdenum. J Mech Phys Solids 1965;13(6):329–50. http://dx.doi.org/10.1016/0022-5096(65)90035-9.
[36] Xia Z, Okabe T, Curtin WA. Shear-lag versus finite element models for stress transfer in fiber-reinforced composites. Compos Sci Technol 2002;62(9):1141–9. http://dx.doi.org/10.1016/S0266-3538(02)00072-6.
[37] Zhou XF, Wagner HD. Stress concentrations caused by fiber failure in two-dimensional composites. Compos Sci Technol 1999;59(7):1063–71. http://dx.doi.org/10.1016/S0266-3538(98)00145-6.
[38] Eitan A, Wagner HD. Fiber interactions in two-dimensional composites. Appl Phys Lett 1991;58(10):1033–5. http://dx.doi.org/10.1063/1.105209.
[39] Swolfs Y, Gorbatikh L, Verpoest I. Stress concentrations in hybrid unidirectional fibre-reinforced composites with random fibre packings. Compos Sci Technol 2013;85:10–6. http://dx.doi.org/10.1016/j.compscitech.2013.05.013.
[40] U.S. The MathWorks, Inc., Natick, Massachusetts, MATLAB and Statistics Toolbox Release; 2013.
[41] Ahrens J, Geveci B, Law C. ParaView: an end-user tool for large data visualization. Visualization handbook, visualization handbook Elsevier; 2005. p. 717–31. http://dx.doi.org/10.1016/B978-012387582-2/50038-1.
[42] Koyanagi J, Hatta H, Kotani M, Kawada H. A comprehensive model for determining tensile strengths of various unidirectional composites. J Compos Mater 2009;43(18):1901–14. http://dx.doi.org/10.1177/0021998309341847.
[43] Toyama N, Takatsubo J. An investigation of non-linear elastic behavior of CFRP laminates and strain measurement using Lamb waves. Compos Sci Technol 2004;64(16):2509–16. http://dx.doi.org/10.1016/j.compscitech.2004.05.007.

A.2 Paper B – An analytical model to predict stress fields around broken fibres and their effect on the longitudinal failure of hybrid composites

The paper has been published in *Composite Structures* 211 (2019) 564–576.

Composite Structures 211 (2019) 564–576

Contents lists available at ScienceDirect

Composite Structures

journal homepage: www.elsevier.com/locate/compstruct

An analytical model to predict stress fields around broken fibres and their effect on the longitudinal failure of hybrid composites

Jose M. Guerrero[a,*], Rodrigo P. Tavares[a,b,c], Fermin Otero[c,d], Joan A. Mayugo[a], Josep Costa[a], Albert Turon[a], Pedro P. Camanho[b,c]

[a] AMADE, Polytechnic School, Universitat de Girona, Campus Montilivi s/n, E-17003 Girona, Spain
[b] DEMec Faculdade de Engenharia, Universidade do Porto, Rua Dr. Roberto Frias, 4200-465 Porto, Portugal
[c] INEGI, Rua Dr. Roberto Frias, 400, 4200-465 Porto, Portugal
[d] Centre Internacional de Mètodes Numèrics a l'Enginyeria (CIMNE), Edifici C1, Campus Nord UPC C/ Gran Capità S/N, 08034 Barcelona, Spain

ARTICLE INFO

Keywords:
Stress concentration
Hybrid composites
Modelling
Micro-mechanics

ABSTRACT

This paper presents an analytical model to predict the stress redistribution around broken fibres in hybrid polymer composites. The model is used under the framework of a progressive failure approach to study the load redistribution around breaks in hybrid composites. The outcomes of the model are validated by comparing it with a spring element model. Moreover, the approach is further used to study the tensile behaviour of different hybrid composites. The results obtained show that the load redistribution around breaks depends on the stiffness ratio between both fibres as well as the matrix behaviour considered and the hybrid volume fraction. Furthermore, the different material parameters have a large effect on the tensile behaviour, with an increase of ductility achieved if the failure process of the two fibres is gradual.

1. Introduction

Fibre hybridization is a potential solution to the quasi-brittle behaviour of fibre reinforced polymers (FRP), resulting in fibre tensile failure with hardly any previous damage symptoms [1–5]. In a hybrid composite, a Low Elongation (LE) fibre is combined with a High Elongation (HE) fibre. This combination may lead to a larger failure strain of baseline composites based on LE fibres, resulting in a hybrid effect. Moreover, the failure process of the material can become gradual leading to an increase of ductility [6,7]. It is currently accepted that progressive failure, dynamic effects, and thermal residual stresses are the main reasons to explain the hybrid effect [4,8,9].

The strength of the fibres is not deterministic and follows a statistical distribution. When a fibre fails, the fibre locally loses its loading capability, which is recovered by shear transfer in the matrix over a distance called ineffective length. In this region the neighbour intact fibres are subjected to stress concentrations. As the load is incremented, clusters of broken fibres are created increasing the stress concentration in intact fibres even further. In a non-hybrid composite this process quickly leads to final failure, whilst in a hybrid composite the stress redistribution around broken fibres is altered due to the presence of fibres with different mechanical and geometrical properties [10]. These differences may alter and delay the formation of clusters leading to hybrid effects [11–13]. However, it remains to be understood if final failure happens either by the accumulation of damage and clusters or by the unstable propagation of a large critical cluster [4].

Different models that attempt to represent the failure process of composite materials and the stress redistribution around breaks are available in the literature. These models can be classified as Global Load Sharing (GLS) and Local Load Sharing (LLS). In GLS models, the stress loss by a broken fibre is redistributed equally among all intact fibres [1,14–17]. As a consequence, such models cannot predict the formation of clusters, which in general leads to a large overprediction of the failure strength. Nonetheless, GLS models can capture some trends affecting the failure process such as fibre fragmentation or the effect of the fibre strength variation [18,19].

In the LLS models, the load of broken fibres is redistributed into the closest intact fibres allowing to capture the formation of clusters. In these models, different modelling approaches exist [20]: analytical models [21–23], spring element models [24–26], fibre bundle models [2,11] and micromechanical finite element models [18,27,28]. Though all methods, in general, predict the failure strength accurately, all predict different cluster formation and evolution due to the different modelling strategies. Moreover, all models omit the dynamic effects and overpredict the fibre break density compared with experiments [3,4].

Currently there is not any analytical model that can predict

* Corresponding author.
E-mail address: josemanuel.guerrero@udg.edu (J.M. Guerrero).

https://doi.org/10.1016/j.compstruct.2018.12.044
Received 3 August 2018; Received in revised form 17 December 2018; Accepted 19 December 2018
Available online 21 December 2018

accurately the Stress Concentration Factor (*SCF*) around clusters of broken fibres in hybrid composites taking into account the differences in elastic and geometrical properties of the two fibres in the hybrid [10]. Moreover, in depth parametric analysis of the load redistribution around breaks in hybrid composites, and their effect on the tensile response still remain scarce [2,11,12,18,24]. Furthermore, recent simulations showed that the load redistribution around breaks in non-hybrid composites is heavily influenced by the matrix behaviour [20]. However, such effects have not been studied with hybrid composites. It is, therefore, vital to further understand the load redistribution and to improve the available tools to predict this load redistribution as this is believed to be the main mechanism that triggers final failure of composites.

In this work, a new analytical model to compute the load redistribution around a cluster of broken fibres in a hybrid composite is presented. The model is an extension of the non-hybrid model presented in St-Pierre et al. [22]. The analytical model is used within the framework of a progressive failure model approach [2] to study the load redistribution around broken fibres in different hybrid composites using both a plastic and an elastic matrix. The model is validated by comparing with the extension of the Spring Element Model (SEM) to hybrid composites proposed by Tavares et al. [24]. Furthermore, the tensile failure of different hybrid composites is simulated using the same approach with the objective of understanding the influence of the modelling parameters on the macroscopic response. These simulations are also validated and compared with the SEM.

2. Modelling strategy

In this work, a new analytical model to predict the *SCF* around broken fibres in hybrid composites is presented. The analytical model is used within the framework of a Progressive Failure Model (PFM) [2]. In the PFM, a three dimensional Representative Volume Element (RVE) containing a random distribution of fibres is used. By applying known functions to predict the load redistribution around broken fibres, the PFM can simulate the tensile failure process of composite materials, capturing fibre clustering, fibre fragmentation and stiffness loss. This model is reviewed in the next sections where also the new analytical model to predict the *SCF* around breaks is presented.

To validate the new proposed model used in PFM, the obtained results are compared with the SEM. The SEM was firstly developed by Okabe et al. [26,25,29] and was recently extended to hybrid composites, damageable interfaces, and random fibre microstructures by Tavares et al. [24]. The SEM consists of a more complex three dimensional RVE where the fibres are longitudinal tensile springs connected by transverse springs representing the matrix. Unlike the PFM, the SEM can predict the load redistribution around breaks inherently from the equilibrium equations, being a finite element model. However, SEM is computationally more expensive than PFM. Further details of the SEM can be seen in Tavares et al. [24].

2.1. Progressive failure model

The PFM consists of a RVE of width a, height b and length L containing a random distribution of fibres of a given radius. The fibres are divided into elements of length l along their longitudinal direction, leading to a succession of planes. Each fibre is denoted with the sub-index $q \in [1,..., N_q]$, while each plane is denoted with the sub-index $p \in [1,..., N_p]$, where N_q and N_p are the number of fibres and planes respectively, see Fig. 1. Each element has a different strength according to a statistical distribution. Once an element fails, a damage distribution is applied over the ineffective length of the broken fibre, whereas stress concentration is applied into the neighbouring intact fibre elements.

2.1.1. Constitutive equation

The constitutive equation relating the stress of each element, $\sigma_{p,q}$, and the strain ε_p is

$$\sigma_{p,q} = \frac{SCF_{p,q}}{\Omega_p} E_q (1 - D_{p,q}) \varepsilon_p \tag{1}$$

where $SCF_{p,q}$ is the stress concentration factor of element p, q, E_q is the Young's modulus of fibre q, $D_{p,q}$ is the state damage variable, which is equal to 1 for broken elements, equal to 0 for intact elements and in between for elements in any stress recovery, ε_p is the strain of the plane (which is considered to be the same for all elements of plane p) and Ω_p is a stress ratio which enforces load equilibrium by modifying the stress concentration according to the strain level. Readers are referred to Guerrero et al. [2] for an in-depth description of the model.

The evolution of $D_{p,q}$ and $SCF_{p,q}$, depends on the model used to predict the ineffective length and the *SCF* around breaks, respectively. Even though any model may be applied to predict both, it is important to use models that are consistent for both parameters. In the following section, the model to predict damage is explained, whereas the new model for predicting the *SCF* is explained in Section 2.1.3.

2.1.2. Functions for ineffective length

In this work two different behaviours to simulate damage are considered, i.e. the matrix is plastic or the matrix is elastic.

When the matrix is plastic, a modified version of Kelly-Tyson shear-lag model [30] is adapted as given in St-Pierre et al. [22]. This approach adds a factor, H, which scales the ineffective length with cluster size. Here, two broken fibre elements belong to the same cluster (c), if the distance between the centres of both fibres is below four times the fibre radius and both elements are in the same plane p. Each cluster is represented with the sub-index p, c, with $c \in [1,..., N_p^c]$ where N_p^c is the number of clusters at plane p. This means that the scaling effects depend on the element length, l. Nonetheless, it was verified that varying the element length does not significantly change neither the macroscopic response of the composite nor the damage development. The ineffective length of a broken fibre in cluster p, c is then

$$L_{p,q}^{\text{in}} = \frac{R_q E_q}{2\tau_q} H_{p,c} \varepsilon_p = \frac{n_{p,c} \pi R_q^2 E_q}{C_{p,c} \tau_q} \varepsilon_p \tag{2}$$

where τ_q is the matrix shear yield stress, R_q is the fibre radius, $C_{p,c} = 4s\sqrt{n_{p,c}}$, where $n_{p,c}$ is the number of broken fibres on cluster p, c and s is the mean centre-to-centre distance between each fibre and its closest neighbour. Here, it is estimated with $s = ((R_{f1} V_{f1} + R_{f2} V_{f2})/V_f)\sqrt{\pi/V_f}$, where R_{f1} and R_{f2} are the fibre radius of fibre populations 1 and 2 respectively, V_f is the overall fibre volume fraction and V_{f1} and V_{f2} are the fibre volume fraction of each population respectively ($V_f = V_{f1} + V_{f2}$). It is worth mentioning that here, s, is not the average inter-fibre spacing of the cluster, but the average inter-fibre spacing of the overall RVE. That is, because the ineffective length should depend not only on the fibres in the broken cluster but also on the fibres that surround it.

The damage of element p, q according to each break in the fibre q at each plane i follows a linear recovery with

$$D_{p,q} = \begin{cases} \max\left(\frac{L_{i,q}^{\text{in}} - |i-p|\, l}{L_{i,q}^{\text{in}}}\right) & \forall\, i\text{: } (D_{i,q} = 1) \cup (|i-p|\, l < L_{i,q}^{\text{in}}) \\ 0 & \text{otherwise.} \end{cases} \tag{3}$$

If the matrix behaves elastically, the Cox's shear-lag model [31,32] is adapted as in [20]. Then the ineffective length is

$$L_{p,q}^{\text{in}} = \frac{H_{p,c} E_q}{2G_m} \left(s - 2\frac{R_{f1} V_{f1} + R_{f2} V_{f2}}{V_f}\right) (-\ln 0.001) \sqrt{\frac{2G_m R_q}{E_q \left(s - 2\frac{R_{f1} V_{f1} + R_{f2} V_{f2}}{V_f}\right)}} \tag{4}$$

where G_m is the matrix shear modulus. It should be noted that this length corresponds to a recovery of 99.9% of the fibre stress [20]. The damage is then computed with

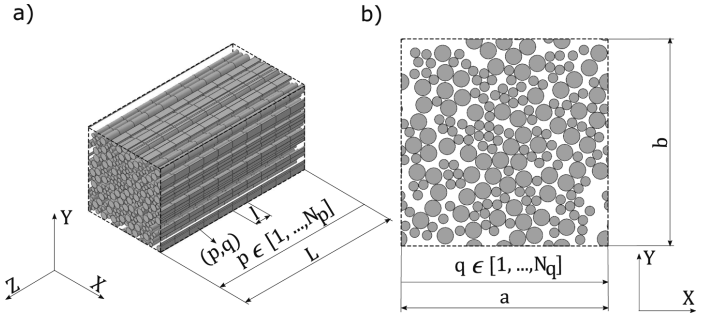

Fig. 1. Schema of the RVE used in the PFM: a) 3D view, b) plane view.

$$D_{p,q}=\begin{cases}\max\left(\exp\left(-\frac{|i-p|\,l}{H_{p,c}R_q}\sqrt{\frac{2G_mR_q}{E_q\left(s-2\frac{R_{f1}V_{f1}+R_{f2}V_{f2}}{V_f}\right)}}\right)\right) & \forall\, i\text{: } (D_{i,q}=1)\cup(|i-p|\,l<L^{in}_{i,q})\\ 0 & \text{otherwise.}\end{cases} \tag{5}$$

2.1.3. Stress concentration factor model

Different approaches have been used to predict the *SCF* around breaks [3,22,33,34]. Recently, St-Pierre et al. [22] presented a model capable of predicting the *SCF* around co-planar clusters of broken fibres in non-hybrid composites. St-Pierre's et al. [22] approach is adapted and extended here to work with hybrid composite materials. The reason why this model was chosen over others is related to the fact that the model predicts the *SCF* around clusters instead of isolated fibre breaks, and it is built on a simple but solid physical background. The model assumes that the *SCF* around a cluster of broken fibres takes a power-law shape.

$$\lambda_{1_{(p-i)}}=\begin{cases}\frac{L^{in}_{1i,c}-l\,|\,i-p|}{L^{in}_{1i,c}} & \forall\,(i,c)\text{: } l\,|i-p|<L^{in}_{1i,c} \quad \text{Plastic matrix}\\ \exp\left(-\frac{|i-p\,|\,lC_{i,c}}{2\pi n_{i,c}R^2_{f1}}\sqrt{\frac{2G_mR_{f1}}{E_{f1}\left(s-2\frac{R_{f1}V_{f1}+R_{f2}V_{f2}}{V_f}\right)}}\right) & \forall\,(i,c)\text{: } l\,|i-p|<L^{in}_{1i,c} \quad \text{Elastic matrix}\end{cases}$$

$$\lambda_{2_{(p-i)}}=\begin{cases}\frac{L^{in}_{2i,c}-l\,|\,i-p|}{L^{in}_{1i,c}} & \forall\,(i,c)\text{: } l\,|i-p|<L^{in}_{2i,c} \quad \text{Plastic matrix}\\ \exp\left(-\frac{|i-p\,|\,lC_{i,c}}{2\pi n_{i,c}R^2_{f2}}\sqrt{\frac{2G_mR_{f2}}{E_{f2}\left(s-2\frac{R_{f1}V_{f1}+R_{f2}V_{f2}}{V_f}\right)}}\right) & \forall\,(i,c)\text{: } l\,|i-p|<L^{in}_{2i,c} \quad \text{Elastic matrix}\end{cases} \tag{7}$$

In this work, the increment of *SCF* for an intact element p, q due to cluster i, c is represented with two functions, δ and λ, so that $\Delta SCF=\delta\cdot\lambda$. The function δ depends on the in-plane distance (r_{q-c}) between the geometrical centre of coordinates of cluster i, c and intact element p, q, while λ depends on the plane position along the in-effective length. As each cluster may contain broken fibres of each type, an intact element may receive *SCF* from broken fibres of the same population or the other, leading to four combinations of δ

$$\delta_{11_{(q-c)}}=I_{11i,c}\left(\frac{R_{i,c}}{r_{q-c}}\right)^{\alpha}\qquad \delta_{22_{(q-c)}}=I_{22i,c}\left(\frac{R_{i,c}}{r_{q-c}}\right)^{\alpha}$$
$$\delta_{12_{(q-c)}}=I_{12i,c}\left(\frac{R_{i,c}}{r_{q-c}}\right)^{\alpha}\qquad \delta_{21_{(q-c)}}=I_{21i,c}\left(\frac{R_{i,c}}{r_{q-c}}\right)^{\alpha} \tag{6}$$

where $\delta_{11_{(q-c)}}$ and $\delta_{22_{(q-c)}}$ represent the increment of *SCF* that an intact element of fibre population 1 and 2 respectively receives due to broken fibres of its own type in cluster i, c, while $\delta_{12_{(q-c)}}$ and $\delta_{21_{(q-c)}}$ are the increment of *SCF* that an element of fibre population 1 and 2 respectively receives due to broken fibres of different type in cluster i, c. $R_{i,c}$ is the equivalent radius of the cluster, estimated with $\pi R^2_{i,c}=n_{i,c}S^2_{i,c}$, where $S_{i,c}$ is the average fibre spacing of the cluster, $S_{i,c}=((n_{1i,c}R_{f1}+n_{2i,c}R_{f2})/n_{i,c})\sqrt{\pi/V_f}$, where $n_{1i,c}$ and $n_{2i,c}$ are the number of broken fibres of population 1 and 2 respectively in cluster i, c and $n_{i,c}=n_{1i,c}+n_{2i,c}$. The exponent α is an input parameter which controls the maximum value of *SCF* and the shape of the curve. According to the literature, this value can be adopted as $\alpha=2$ for a plastic matrix and $\alpha=3.8$ for elastic matrix [20,22]. The terms I are constants, which are determined later in this section, see Eq. (10).

Similarly, as there are two fibre populations, each cluster i, c has two ineffective lengths, the ineffective length of broken elements of type 1, $L^{in}_{1i,c}$, and that of broken elements of type 2, $L^{in}_{2i,c}$. Therefore, two functions appear for λ as

where $\lambda_{1_{(p-i)}}$ represents the evolution of $\delta_{11_{(q-c)}}$ and $\delta_{21_{(q-c)}}$ along $L^{in}_{1i,c}$, while $\lambda_{2_{(p-i)}}$ represents the evolution of $\delta_{22_{(q-c)}}$ and $\delta_{12_{(q-c)}}$ along $L^{in}_{2i,c}$. E_{f1} and E_{f2} are the Young's modulus of fibre type 1 and 2 respectively.

Because of load equilibrium, the load loss of each fibre population in the cluster, must be redistributed into the remaining intact fibres at same plane. Thus, the following equilibrium equations arise

$$\pi R^2_{f1}n_{1i,c}\sigma_1^{\infty}=\int_{R_{i,c}}^{R_t}I_{11i,c}\left(\frac{R_{i,c}}{r_{q-c}}\right)^{\alpha}\sigma_1^{\infty}V_{f1}2\pi r_{q-c}\,dr_{q-c}+\int_{R_{i,c}}^{R_t}I_{21i,c}\left(\frac{R_{i,c}}{r_{q-c}}\right)^{\alpha}\sigma_2^{\infty}V_{f2}2\pi r_{q-c}\,dr_{q-c}$$
$$\pi R^2_{f2}n_{2i,c}\sigma_2^{\infty}=\int_{R_{i,c}}^{R_t}I_{22i,c}\left(\frac{R_{i,c}}{r_{q-c}}\right)^{\alpha}\sigma_2^{\infty}V_{f2}2\pi r_{q-c}\,dr_{q-c}+\int_{R_{i,c}}^{R_t}I_{12i,c}\left(\frac{R_{i,c}}{r_{q-c}}\right)^{\alpha}\sigma_1^{\infty}V_{f1}2\pi r_{q-c}\,dr_{q-c} \tag{8}$$

where R_t is the RVE equivalent radius, $R_t=\sqrt{(a\cdot b)/\pi}$, while σ_1^{∞} and σ_2^{∞} are the stress at infinite for each fibre population respectively. Assuming that the strain is the same for both fibre populations, $\sigma_1^{\infty}/E_{f1}=\sigma_2^{\infty}/E_{f2}$. In addition, it is assumed that two intact fibre elements of different type located at the exact same distance to the same

break, receive the same increment of force due to the break. This assumption means that the overload transferred from a break to an intact fibre is independent of both the Young's modulus and the fibre radius of the intact fibre. This fact is supported by the results presented in Swolfs et al. [10]. As isostrain conditions are considered, force equality implies that the increment of stress concentration solely depends on the stiffness and cross-sectional area of both fibres leading to

$$I_{21_{i,c}} = \frac{E_{f1}R_{f1}^2}{E_{f2}R_{f2}^2} I_{11_{i,c}} \qquad I_{12_{i,c}} = \frac{E_{f2}R_{f2}^2}{E_{f1}R_{f1}^2} I_{22_{i,c}} \tag{9}$$

These conditions imply that a fibre with lower stiffness located at the same distance to the break is subjected to a higher *SCF* than a fibre with a higher stiffness, which is consistent to the general observations seen in the literature [10,12]. By substituting the relation between σ_1^{∞} and σ_2^{∞} and Eq. (9) into Eq. (8), the constants $I_{11_{i,c}}$, $I_{22_{i,c}}$, $I_{12_{i,c}}$ and $I_{21_{i,c}}$ are obtained as functions of α:

$$I_{11_{i,c}} = \begin{cases} \dfrac{n_{1_{i,c}} R_{f1}^2 R_{f2}^2}{2R_{i,c}^2 \ln(R_t / R_{i,c})(R_{f1}^2 V_{f2} + R_{f2}^2 V_{f1})} & \text{for } \alpha = 2 \\ \dfrac{n_{1_{i,c}} R_{f1}^2 R_{f2}^2 R_{i,c}^{-\alpha}(\alpha - 2)}{2(R_{f1}^2 V_{f2} + R_{f2}^2 V_{f1})(R_{i,c}^2 (1 / R_{i,c})^{\alpha} - R_t^2 (1 / R_t)^{\alpha})} & \text{otherwise.} \end{cases}$$

$$I_{21_{i,c}} = \begin{cases} \dfrac{E_{f1} n_{1_{i,c}} R_{f1}^4}{2E_{f2} R_{i,c}^2 \ln(R_t / R_{i,c})(R_{f1}^2 V_{f2} + R_{f2}^2 V_{f1})} & \text{for } \alpha = 2 \\ \dfrac{E_{f1} n_{1_{i,c}} R_{f1}^4 R_{i,c}^{-\alpha}(\alpha - 2)}{2E_{f2}((R_{f1}^2 V_{f2} + R_{f2}^2 V_{f1})(R_{i,c}^2 (1 / R_{i,c})^{\alpha} - R_t^2 (1 / R_t)^{\alpha}))} & \text{otherwise.} \end{cases}$$

$$I_{22_{i,c}} = \begin{cases} \dfrac{n_{2_{i,c}} R_{f1}^2 R_{f2}^2}{2R_{i,c}^2 \ln(R_t / R_{i,c})(R_{f1}^2 V_{f2} + R_{f2}^2 V_{f1})} & \text{for } \alpha = 2 \\ \dfrac{n_{2_{i,c}} R_{f1}^2 R_{f2}^2 R_{i,c}^{-\alpha}(\alpha - 2)}{2(R_{f1}^2 V_{f2} + R_{f2}^2 V_{f1})(R_{i,c}^2 (1 / R_{i,c})^{\alpha} - R_t^2 (1 / R_t)^{\alpha})} & \text{otherwise.} \end{cases}$$

$$I_{12_{i,c}} = \begin{cases} \dfrac{E_{f2} n_{2_{i,c}} R_{f2}^4}{2E_{f1} R_{i,c}^2 \ln(R_t / R_{i,c})(R_{f1}^2 V_{f2} + R_{f2}^2 V_{f1})} & \text{for } \alpha = 2 \\ \dfrac{E_{f2} n_{2_{i,c}} R_{f2}^4 R_{i,c}^{-\alpha}(\alpha - 2)}{2E_{f1}((R_{f1}^2 V_{f2} + R_{f2}^2 V_{f1})(R_{i,c}^2 (1 / R_{i,c})^{\alpha} - R_t^2 (1 / R_t)^{\alpha}))} & \text{otherwise.} \end{cases} \tag{10}$$

The model is very powerful as it takes into account the cluster size, RVE size, volume fractions, fibre radius and elastic properties of each fibre population with simple analytical equations. Moreover, it can represent different matrix behaviours or effects not present into the model by adjusting the value of α.

As there can be multiple clusters along the RVE, a superposition rule is considered. Therefore, the total *SCF* for an intact fibre element is obtained by linear superposition of the *SCF* of all clusters. Nonetheless, the *SCF* of a given element is bounded according to shear-lag transfer. This limitation ensures that there is a stress continuity between elements inside any ineffective length (elements where $0 < D_{p,q} < 1$) that are not affected by *SCF*, and subsequent intact elements ($D_{p,q} = 0$), which can be affected by the *SCF*. Thus, the total *SCF* of an intact element p, q is given by

$$SCF_{p,q} = \begin{cases} \min(SCF_{p,q}^0, SCF_{p,q}^L) & \forall\ p, q\colon D_{p,q} = 0 \\ 1 & \text{otherwise,} \end{cases} \tag{11}$$

where $SCF_{p,q}^0$ is the *SCF* predicted by the linear superposition of the contribution of all clusters using the previous δ and λ functions given by

$$SCF_{p,q}^0 = 1 + \sum_{i=1}^{N_p} \sum_{c=1}^{N_i^c} \delta_{11_{(q-c)}} \lambda_{1_{(p-i)}} + \delta_{12_{(q-c)}} \lambda_{2_{(p-i)}} \quad \forall\ i, c\colon n_{i,c} > 0 \quad \& \quad q \in f1$$

$$SCF_{p,q}^0 = 1 + \sum_{i=1}^{N_p} \sum_{c=1}^{N_i^c} \delta_{22_{(q-c)}} \lambda_{2_{(p-i)}} + \delta_{21_{(q-c)}} \lambda_{1_{(p-i)}} \quad \forall\ i, c\colon n_{i,c} > 0 \quad \& \quad q \in f2 \tag{12}$$

where f_1 and f_2 are fibre populations 1 and 2 respectively. $SCF_{p,q}^L$ is the *SCF* limitation for broken fibre q to achieve stress continuity. This limit for intact element p, q is calculated according to the slope of the stress gradient of the nearest ineffective length, $1/L_{i,q}^{\text{in}}$, in the fibre q, multiplied by the distance between planes i and p:

$$SCF_{p,q}^L = \min\left(\frac{1}{L_{i,q}^{\text{in}}} |i - p|\ l\right) \quad \forall\ i\colon D_{i,q} = 1 \tag{13}$$

It should be noted that the broken and damaged fibre elements are not excluded from Eq. (8). Therefore, the *SCF* of each intact element is computed independently of the percentage of broken and damaged elements. However, the percentage of broken and damaged elements is taken into account to compute the strain of each plane, ε_p, and the stress ratio, Ω_p, which affect the final stress of the elements, $\sigma_{p,q}$. This is explained in detail in Guerrero et al. [2].

3. Methodology

In a hybrid composite the stress redistribution around broken fibres depends mainly on the elastic and geometrical properties of both fibres, the matrix behaviour (plastic or elastic), the hybrid volume fraction as well as the local fibre arrangement [10,11]. All these properties will affect the creation and propagation of clusters that lead to final failure. In this work, the effects of the Young's modulus of the fibres, matrix shear strength (plastic or elastic) and hybrid volume fraction on the stress redistribution around a broken fibre are investigated in detail. Later, their effect on the tensile failure behaviour are also evaluated. The simulations are performed with the PFM using the new *SCF* model presented in previous Section 2.1.3. All simulations are compared with the SEM [24] to validate the results.

A modified version of Melro's et al. [35] random fibre generator is used to create a RVE of width, thickness and length of 75 × 75 × 300 times the fibre radius. The element length is always 2 times the fibre radius, with both fibres in the RVE having the same radius. The same RVE is used for both PFM and SEM when studying the same problem. Note however that a new RVE is generated for each case in study. To observe the differences in load redistribution and failure process with different properties, three hybrid composites are considered by combining different fibres. These hybrids correspond to AS4-Eglass, M50S-AS4 and AS4-T800G, whose properties are shown in Table 1. In all cases, the matrix corresponds to epoxy with elastic properties $E_m = 1260$ MPa and $G_m = 450$ MPa. To understand the impact of the matrix behaviour, all cases are simulated with plastic ($\tau_q = 50$ MPa) and elastic matrix ($\tau_q \to \infty$). In addition, each hybrid is simulated with a hybrid volume fraction of 25%, 50% and 75%. Here, the Hybrid Volume Fraction (*HVF*) is referred to be as the percentage of HE fibre volume fraction, V_{HE}, over the total fibre volume fraction, $HVF = (V_{HE}/V_f)\cdot 100$.

In the case of SEM, the model calculates all unknown variables directly from the equilibrium equations, as a function of the material properties and RVE geometry, being a very robust tool. However, it is less efficient computationally than the PFM. For the PFM instead, the ineffective length and *SCF* need to be applied according to the matrix behaviour. In all cases where the matrix is plastic ($\tau_q \neq \infty$), the ineffective length and damage are simulated within Eqs. (2) and (3). In these cases, the *SCF* is calculated using $\alpha = 2$. However, when the matrix is elastic ($\tau_q = \infty$), then the ineffective length and damage are simulated with Eqs. (4) and (5) and $\alpha = 3.8$. It is worth mentioning that, when the matrix is plastic, its behaviour is considered to be perfectly plastic in the PFM, whilst it is elastic–plastic in the SEM.

Table 1
Fibre properties.

Fibre type	Fibre properties		Weibull properties		
	E_f [GPa]	R_f [mm]	m [–]	σ_0 [MPa]	L_0 [mm]
AS4	230	$3.5{\cdot}10^{-3}$	10.7	4275	12.7
M50S	480		9	4600	10
T800G	295		4.8	6800	10
E-glass	70		6.34	1550	24

To investigate the stress redistribution around breaks, a broken fibre is arbitrarily placed around the middle of the RVE for each hybrid composite. This broken fibre is either the fibre with lower Young's modulus (LM) or the fibre with higher Young's modulus (HM). Usually, the LM fibre corresponds to the fibre with larger failure strain, i.e. the HE fibre, whereas the HM fibre corresponds to the fibre with smaller failure strain, i.e. the LE fibre. Even tough the LE fibres will break before the HE fibres, it is important to study the HE fibre load redistribution as well as towards final failure the HE fibre also fails. A remote tensile strain, ε, of 2% is applied and the consequent obtained load redistribution around the broken fibre is characterized with three different metrics. The first one is the maximum *SCF* obtained on intact LM and HM fibres. The *SCF* is calculated as the ratio between the actual stress on the fibre over the stress if there were no breaks, i.e. $E_f\varepsilon$. The second metric is the ineffective length of the broken fibre, which is defined as the distance where the broken fibre recovers 90% of the nominal load, whereas the last metric is the radial influence length. This is defined as the maximum distance in the break plane in which the *SCF* is higher than 1%. The results shown for both the ineffective length and radial length are normalised by the fibre radius. Ten realisations are performed for each case, leading to a total of 360 simulations.

To understand the influence of the modelling parameters on the tensile failure process, the same hybrid composites are simulated under fibre tensile loading. Moreover, non-hybrid composites of each fibre type are also simulated. To do so, a random strength, $\sigma^{ult}_{p,q}$, is generated for each element in the RVE according to the Weibull distribution [36] with $P_{p,q} = 1 - \exp(-(l/L_0)(\sigma^{ult}_{p,q}/\sigma_0)^m)$, where $P_{p,q}$ is a random number between 0 and 1, while σ_0, L_0 and m are the corresponding Weibull parameters of the fibre element shown in Table 1. To compare the results between simulations, different metrics are proposed based on literature [37]. The first metric is the yield stress, σ^y, which is understood as the knee point where the stress–strain curve deviates from the initial linear elastic regime at a strain of 0.1%. The second metric is the ductile strain, ε^d, defined as the strain difference between the strain at peak stress, and the initial slope line at the failure stress level ($\varepsilon^d = \varepsilon^{ult} - \sigma^{ult}/E_0$), where E_0 is the initial Young's modulus of the composite given by the rule of mixtures. The third metric is the peak stress, σ^{ult}, whereas the fourth metric is the strain at peak stress, ε^{ult}. These metrics are summarized in Fig. 2. The fifth metric is the cluster size at peak stress, N^c. Here, two broken fibres belong to the same cluster if the distance between centres is smaller than 4 times the fibre radius and the axial distance between break planes is smaller than 10 times the fibre radius [3,24,20]. It should be noted that the definition of clusters used to assess the damage evolution explained in this section, is different than the one used for calculating the *SCF* and ineffective length shown in previous Section 2.1.2. This is done to allow a fair comparison between the analytical and numerical model, and other models in the literature. The sixth and final metric is the fibre break density at peak stress, δ^{ult}_f. Five realisations are performed for each case in study, leading to 110 simulations in total.

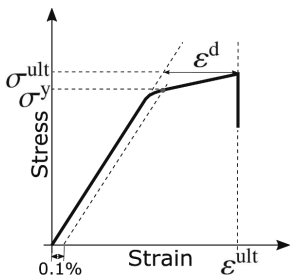

Fig. 2. Main metrics used to characterize the tensile behaviour of hybrid composites.

4. Stress redistribution around breaks

In this section the stress redistribution around a broken fibre is analysed. A comparison of the results between the SEM and the analytical *SCF* model used in the framework of the PFM is performed to asses the validity of the analytical model. The overall volume fraction considered was 60% for all cases studied. It should be noted that in this section, because the fibres have no strength, the *HVF* is referred to be as the percentage of LM fibre volume fraction over the total fibre volume fraction.

4.1. Stress concentration factor

The trends predicted by both PFM and SEM are the same for all hybrid materials and matrix behaviour, even though the absolute values are not the same. However, their relative difference is remarkably small considering the simplicity of the analytical model. These results justify the assumption done in Eq. 9.

In Fig. 3, the *SCF* around a broken HM fibre is shown with a plastic matrix and an elastic matrix as a function of the *HVF* for the different hybrids in study. The *SCF* calculated is larger for the LM fibres when compared with the HM fibres. As the LM fibres have a lower stiffness, their stress before the break was lower compared with the HM fibre. Hence, the relative increase of stress is larger on the LM fibre causing a larger *SCF* [10].

Interestingly, the *SCF* on HM fibres decreases when adding LM fibres, while the opposite happens for the *SCF* on LM fibres. That should be related to the fact that by increasing the LM fibre content, the distance of the HM fibre to the break increases, and the load to redistribute is mainly taken by the LM fibres. This will cause larger hybrid effects at smaller HM volume fractions as has already been reported in literature [2,18,12,11]. Moreover, the *SCF* on HM fibres is not strongly affected by the LM stiffness, whereas the opposite happens with the *SCF* on LM fibres. The larger the ratio between the stiffness of the HM and LM fibre is, the larger is the *SCF* obtained on the LM fibres. This fact agrees well with the findings of Swolfs et al. [10].

The matrix behaviour i.e. plastic or elastic changes the maximum value of *SCF*, being larger with elastic matrix, however, the trends are the same. The reason for this difference is the fact that, in an elastic matrix, there is no upper limit for shear stress transfer between fibre and matrix, hence causing a more localised effect and larger *SCF*.

In Fig. 4 the *SCF* around a broken LM fibre is shown with both plastic and elastic matrix for different *HVF* and materials. The *SCF* on HM fibres again decreases by increasing the content of LM fibres, whilst the opposite happens with the LM fibres. Interestingly, the *SCF* on both HM and LM fibres are smaller than in the previous case. That is related to the fact that the LM fibre carried less load than the HM fibre before failure, hence resulting in smaller *SCF*. It should be noted however, that in reality the LM fibres usually fail after the failure of multiple HM fibres. Thus, the *SCF* obtained will be much larger than the ones predicted here, as the HM fibres no longer support load. The *SCF* on the LM fibre is not strongly affected by the stiffness of the HM fibre. Nonetheless, the *SCF* on the HM fibre is highly influenced by the stiffness of the LM fibre. A smaller stiffness ratio between HM and LM fibre leads to a larger *SCF* on the HM fibres, which is the opposite as observed in the previous case.

Although the models are able to take into account fibres with different radii [24,2], in this study the fibres were considered to always have the same radii. Otherwise, it would add another layer of complexity due to higher differences in the microstructures of the composites analysed.

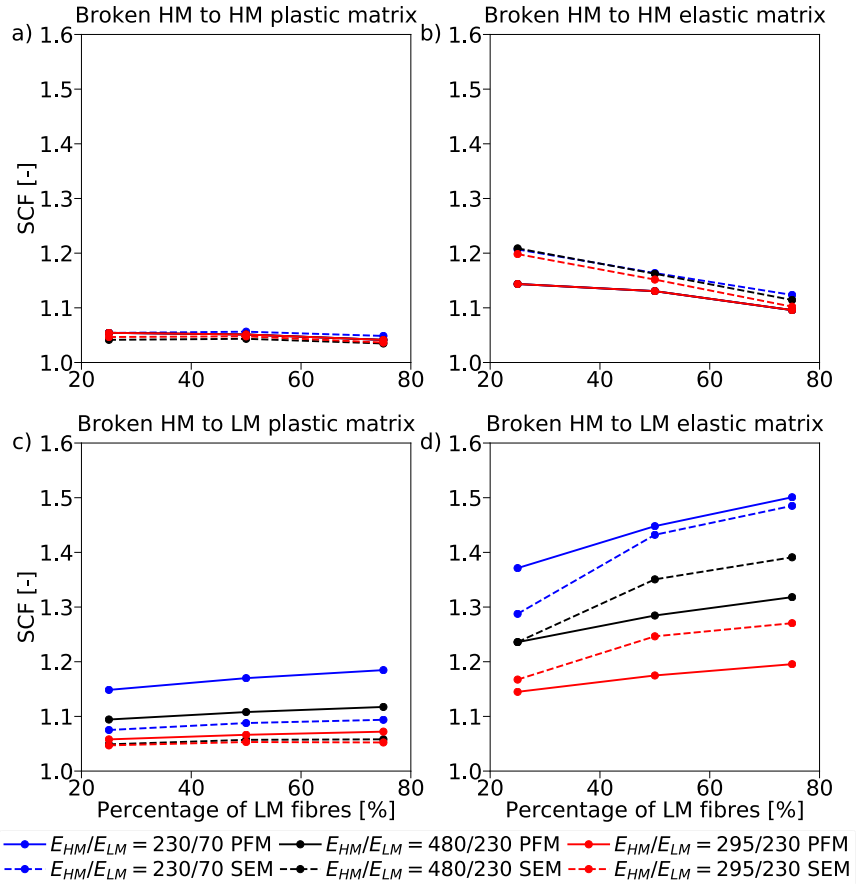

Fig. 3. Maximum stress concentration factors around a broken HM fibre as a function of the hybrid volume fraction for different hybridizations: a) on HM fibres with plastic matrix, b) on HM fibres with elastic matrix, c) on LM fibres with plastic matrix, d) on LM fibres with elastic matrix. The average of 10 realisations are shown (τ_q = 50 MPa for plastic matrix). Note that in a) and b), all PFM results are the same.

4.2. Ineffective length

In Fig. 5 the ineffective length is shown for a broken HM fibre and a broken LM fibre with both plastic and elastic matrix as a function of the *HVF* for each material system.

The ineffective length is larger for the HM fibre than for the LM fibre. That is due to its stiffness: a larger stiffness means that a larger load needs to be recovered, hence causing a larger ineffective length. Interestingly, the ineffective length is not significantly affected by the stiffness of the other fibre in the hybrid, which corresponds well to the findings of Swolfs et al. [10]. Similarly, the *HVF* has a small effect on the ineffective length. In Fig. 5d), a minimum can be observed for the SEM at *HVF* = 50%, however, the difference is small compared to other volume fractions. In the same way, in Fig. 5 b) and c) a small increase of ineffective length is observed in the SEM for *HVF* = 75%. In any of these cases, the small difference in ineffective length due to the *HVF* should be related to the changes in the microstructure, as the ratio between HM and LM fibres is different.

The ineffective length exhibits a large change between plastic and elastic matrix, the same trend that was observed for the *SCF*. The ineffective length is smaller for an elastic matrix, as there is no limit in shear stress transfer, making it possible for the stress to be recovered in the broken fibre in a shorter region. With the plastic matrix the shear transfer is limited by the matrix shear strength resulting in a larger ineffective length. In any case the trends remain the same for both matrix behaviours.

In general, the results predicted between the SEM and the analytical models in PFM follow similar trends, although some differences are observed. In the PFM the ineffective length is always smaller than in SEM. This is specially evident for the plastic matrix cases. There are two main reasons which can explain this difference. Firstly, with a plastic matrix, the behaviour of the matrix is elastic-plastic in the SEM, whilst it is perfectly plastic in PFM. Because of this, the shear stress is constant along the ineffective length, causing an underprediction of the ineffective length. This issue could in principle be improved by using an elastic–plastic model in PFM instead of a perfectly plastic. The second reason could be related to the microstructure. In the SEM, the ineffective length of each broken fibre depends on the local stiffness

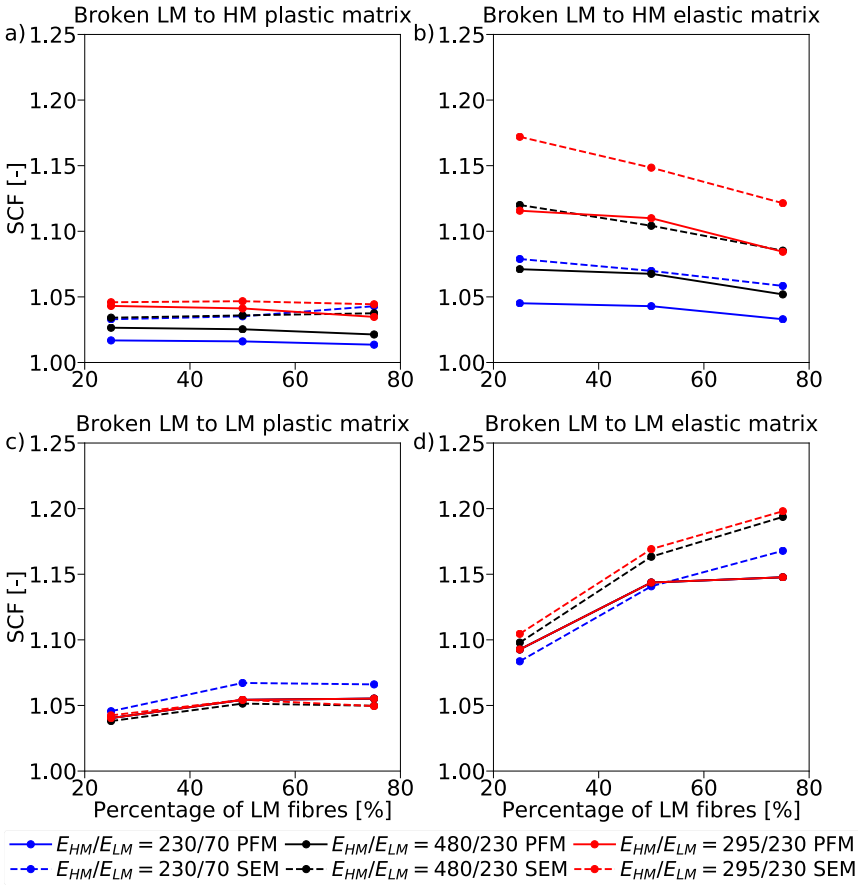

Fig. 4. Maximum stress concentration factors around a broken LM fibre as a function of the hybrid volume fraction for different hybridizations: a) on HM fibres with plastic matrix, b) on HM fibres with elastic matrix, c) on LM fibres with plastic matrix, d) on LM fibres with elastic matrix. The average of 10 realisations are shown (τ_y = 50 MPa for plastic matrix). Note that in c) and d), all PFM results are the same.

around the broken fibre. This means that if the broken fibre is surrounded by more LM fibres (with lower stiffness), then the ineffective length of the broken fibre is higher. This explains why the SEM predicts an increase in ineffective length at larger *HVF*. However, this effect is unlikely to be captured by a simple analytical model.

4.3. Radial influence length

The radial influence length for each material system, as a function of the *HVF* is shown in Fig. 6.

As it can be observed, the radial influence length is larger when a HM fibre is broken than when a LM fibre is. That is because the HM fibre has a larger stiffness, causing a larger load to be redistributed over intact fibres leading to a larger radial length. In most cases a small increase of the radial length can be observed by increasing the *HVF*. This increase is larger for the SEM than for the PFM, although overall the trends are similar. In general, the radial influence length is slightly larger for the PFM than for SEM.

Overall the radial length is affected by the stiffness of the fibres. A larger ratio of stiffness between HM and LM fibres causes a larger radial influence length when the HM fibre is broken. The opposite trend is observed when the LM fibre is broken. This observation corresponds well to what was observed with the *SCF*.

Changing the matrix from elastic to plastic maintains the same trends as it was seen with the *SCF* and ineffective length. As expected, the radial length is smaller with an elastic matrix, which is again caused by the no upper limit in shear transfer between fibre and matrix. In any case, the radial influence length is heavily dependent on the microstructure and its average value for each realization performed presents an error of approximately ± 1 mm/mm.

5. Tensile behaviour

In this section the tensile failure of the hybrid materials cases used in Section 4 is simulated under strain controlled conditions. A comparison of results is performed between SEM and PFM. In this section, the total fibre volume fraction considered is 50%.

A summary of all the results obtained for the hybrid materials with

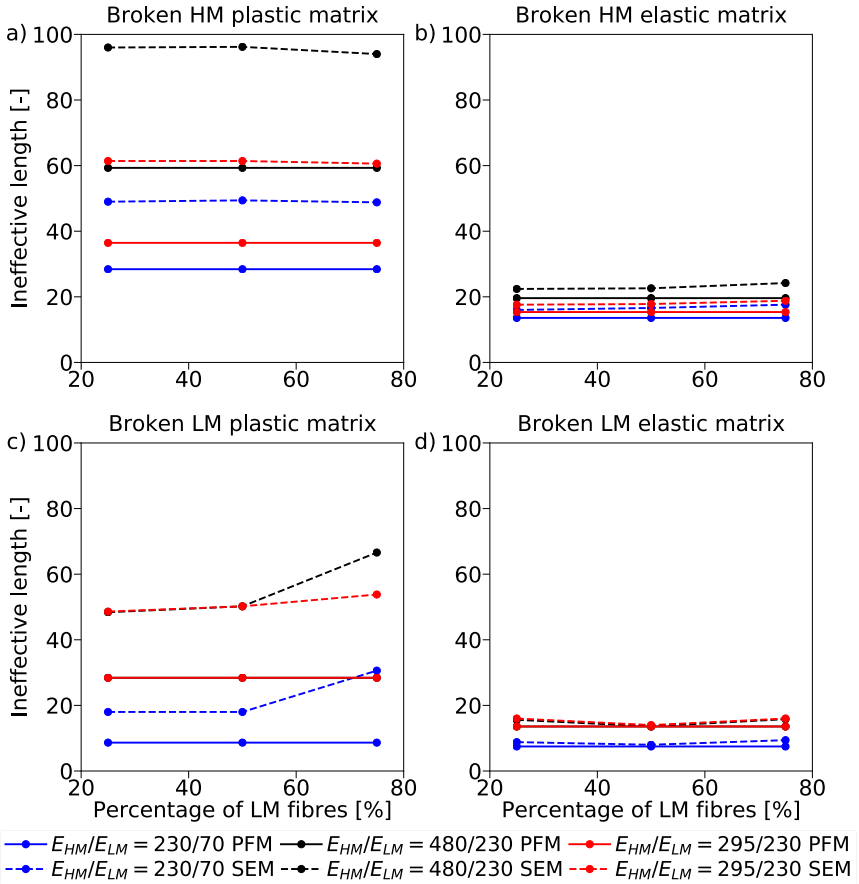

Fig. 5. Normalised ineffective length at 90% of load recovery: a) broken HM fibre and plastic matrix, b) broken HM fibre and elastic matrix, c) broken LM fibre and plastic matrix, d) broken LM fibre and elastic matrix. The average of 10 realisations are shown (τ_y = 50 MPa for plastic matrix). Note that in c) and d), the results for $E_{HM}/E_{LM} = 480/230\,PFM$ and $E_{HM}/E_{LM} = 295/230\,PFM$ are the same.

plastic matrix is presented in Table 2, while the results with elastic matrix are shown in Table 3. The results for the non–hybrid cases are summarized in Table 4. The presented results, correspond to the average of 5 realisations for each case. The average computational time for performing one run of the cases studied was 1314 s for the SEM, whereas it was 114 s for the PFM. Therefore, the simplified model is approximately 10 times faster.

The stress-strain curves obtained for all materials with a plastic matrix are shown in Fig. 7. The tensile behaviour predicted by the two modelling approaches is in good agreement for all cases despite of the differences in the modelling assumptions. In general, the PFM over-predicts the final failure of the composite, leading to larger peak stresses, yield stresses, strain and break densities, when compared with the SEM.

The failure process is seen to be very different for each hybrid configuration and varies greatly with the *HVF*. For the AS4-Eglass hybrid, no ductility is observed at the different *HVF* simulated. However, at a *HVF* = 75%, there is a larger stiffness loss when compared with *HVF* = 50% and *HVF* = 25% before the final load drop, which suggests that ductility could be present for *HVF* > 75%. This is also indicated by the fibre break density evolution presented in Fig. 8. As it can be seen, the fibre break density increases exponentially for all hybrid volume fractions leading to a brittle failure, nonetheless, this increase is less abrupt for *HVF* = 75%.

For the M50S-AS4 hybrid, brittle failures are also obtained at *HVF* of 25% and 50%. Nonetheless, a rather large ductility of around 0.5% is predicted by the models for *HVF* = 75%, meaning that for this composite material the failure process is gradual. This is clearly demonstrated by the evolution of fibre break density, which increases linearly but not exponentially, until final failure.

Similarly, a ductility of around 0.7% is observed within the AS4-T800G hybridization at a *HVF* = 75%. However, by decreasing the *HVF* brittle failures are obtained. In the case of *HVF* = 25%, the failure is completely brittle whereas for the *HVF* = 50% two load drops can be observed. The first load drop corresponds to the failure of the LE fibres, whilst the second one corresponds to the failure of the HE fibres. Nevertheless this case cannot be considered as ductile because the failure is not really continuous.

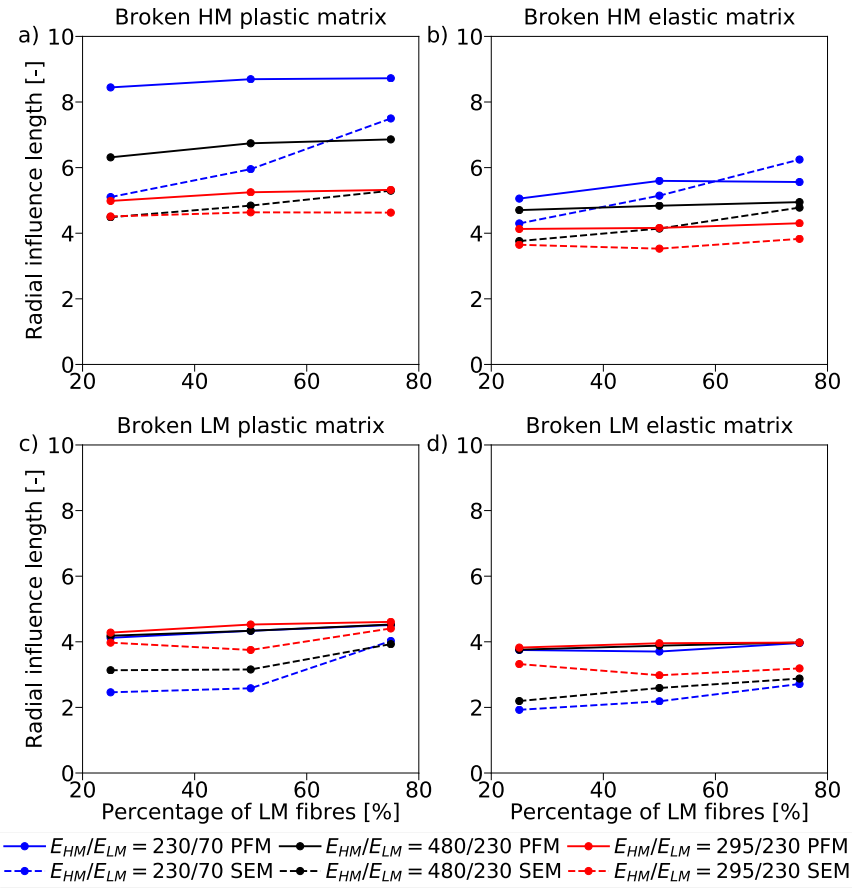

Fig. 6. Normalised radial influence length: a) broken HM fibre and plastic matrix, b) broken HM fibre and elastic matrix, c) broken LM fibre and plastic matrix, d) broken LM fibre and elastic matrix. The average of 10 realisations are shown (τ_q = 50 MPa for plastic matrix).

Table 2
Obtained results for all hybrid materials with plastic matrix.

Material		SEM						PFM					
	HVF [%]	σ^{y} [MPa]	σ^{ult} [MPa]	ε^{d} [%]	ε^{ult} [%]	N^{c} [–]	δ_f^{ult} [1/mm^3]	σ^{y} [MPa]	σ^{ult} [MPa]	ε^{d} [%]	ε^{ult} [%]	N^{c} [–]	δ_f^{ult} [1/mm^3]
Hybrid AS4-Eglass	25	1844	1858	0.101	2.026	5.2	2880	2009	2025	0.134	2.251	10.4	6195
	50	1481	1494	0.101	2.067	4.4	2380	1624	1660	0.192	2.388	9.4	6712
	75	1144	1153	0.124	2.201	4.0	2480	1239	1299	0.316	2.653	14.2	8141
Hybrid M50S-AS4	25	2163	2163	0.065	1.098	10.6	4235	2310	2321	0.091	1.199	8.6	7063
	50	1955	1966	0.109	1.210	14.8	6435	2052	2060	0.119	1.275	7.0	6922
	75	1680	1897	0.525	1.808	14.4	9692	1817	2020	0.517	1.893	60.2	16229
Hybrid AS4-T800G	25	2432	2444	0.115	2.076	7.2	3831	2604	2614	0.112	2.223	33.8	6397
	50	2687	2720	0.157	2.213	7.0	4719	2880	2908	0.141	2.345	11.6	7439
	75	2978	3222	0.646	2.949	8.8	10670	3213	3533	0.760	3.282	31.0	21340

Table 3
Obtained results for all hybrid materials with elastic matrix.

Material		SEM						PFM					
	HVF [%]	σ^y [MPa]	σ^{ult} [MPa]	ε^d [%]	ε^{ult} [%]	N^c [–]	δ_f^{ult} [1/mm^3]	σ^y [MPa]	σ^{ult} [MPa]	ε^d [%]	ε^{ult} [%]	N^c [–]	δ_f^{ult} [1/mm^3]
Hybrid AS4-Eglass	25	2001	2002	0.070	2.144	16.2	5661	1927	1927	0.022	2.038	9.4	2471
	50	1627	1635	0.102	2.253	18.6	6585	1648	1652	0.061	2.246	77.2	5739
	75	1247	1315	0.531	2.900	135.2	22360	1290	1349	0.221	2.648	132.6	17150
Hybrid M50S-AS4	25	2278	2313	0.074	1.180	30.8	7958	2237	2237	0.039	1.107	33.2	5979
	50	2069	2090	0.157	1.327	34.8	13141	2060	2075	0.064	1.229	116.0	8625
	75	1923	2078	0.299	1.706	42.8	19782	1876	1893	0.069	1.358	80.0	6977
Hybrid AS4-T800G	25	2602	2656	0.063	2.194	49.3	9242	2583	2585	0.042	2.130	115.2	6073
	50	2969	3495	1.557	4.199	4745.0	92451	3006	3414	0.539	3.127	1136.0	56394
	75	3447	4576	1.054	4.326	159.0	63661	3525	4484	0.991	4.192	3909.8	78179

Table 4
Obtained results for all non-hybrid materials with plastic ($\tau_q = 50$) and elastic matrix ($\tau_q = \infty$).

Material		SEM						PFM					
	τ_q [MPa]	σ^y [MPa]	σ^{ult} [MPa]	ε^d [%]	ε^{ult} [%]	N^c [–]	δ_f^{ult} [1/mm^3]	σ^y [MPa]	σ^{ult} [MPa]	ε^d [%]	ε^{ult} [%]	N^c [–]	δ_f^{ult} [1/mm^3]
AS4	50	2252	2252	0.094	2.018	4.2	3265	2383	2391	0.105	2.172	14.2	5927
	∞	2397	2397	0.065	2.114	14.0	6482	2173	2173	0.009	1.887	8.2	1413
T800G	50	3605	3950	0.377	3.055	3.4	4940	3873	4388	0.416	3.376	6.0	7864
	∞	4615	5613	0.671	4.476	75.5	31195	4725	5708	0.935	4.785	1035.8	45807
M50S	50	2388	2388	0.059	1.054	5.2	3477	2590	2592	0.074	1.150	8.0	7187
	∞	2599	2599	0.058	1.141	17.4	7900	2385	2385	0.015	1.005	5.2	2604
E-glass	50	1043	1111	0.251	3.426	10.6	9479	1168	1263	0.316	3.859	22.0	18335
	∞	1222	1301	0.246	3.964	47.8	26062	1244	1311	0.217	3.895	177.0	25973

In general, the predicted cluster size is larger for the PFM than for SEM. The reason for this is likely to be related to the fact that final failure occurs later in PFM. In any case, the cluster size predicted are in general in good agreement with results of non-hybrid composites [3]. Similarly, the fibre break density is in general larger for the PFM for the same reason, although in this case both models predict larger values than seen in the literature [3]. The fibre break density seems to increase with ductility. The larger is the ductile strain, the larger is the break density. This is caused by the fact that final failure is being delayed, leading to larger break densities. For the M50S-AS4 hybrid, the fibre break density at maximum stress for $HVF = 75\%$ is more than 2 times larger compared to $HVF = 25\%$, being this increase from 4235 to 9692 mm^{-3} for SEM and from 7063 to 16229 mm^{-3} for PFM. Similarly, for the AS4-T800G hybrid, the fibre break density at $HVF = 75\%$ is approximately 3 times larger than at $HVF = 25\%$, with an increase from 3831 to 10670 mm^{-3} and 6397 to 21340 mm^{-3} for SEM and PFM

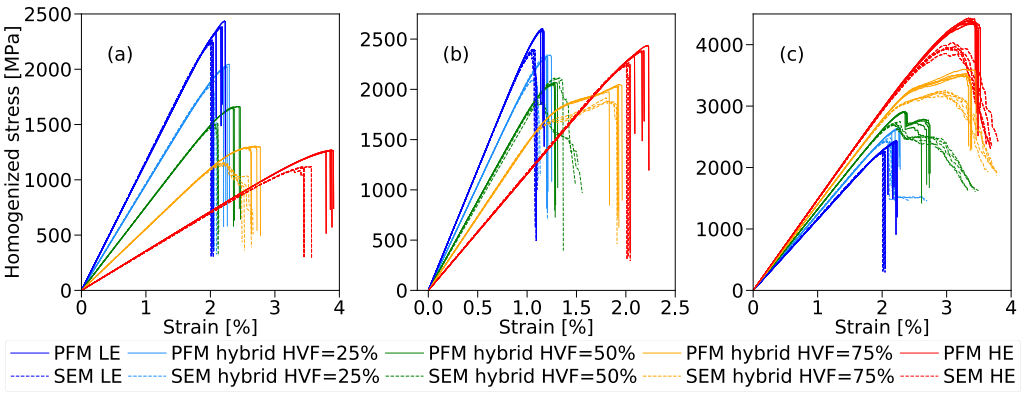

Fig. 7. Simulated stress-strain curves for different hybrid materials at different hybrid volume fractions (HVF) using a plastic matrix. (a) hybrid AS4-Eglass, (b) hybrid M50S-AS4, and (c) hybrid AS4-T800G. The non–hybrid composites are also shown.

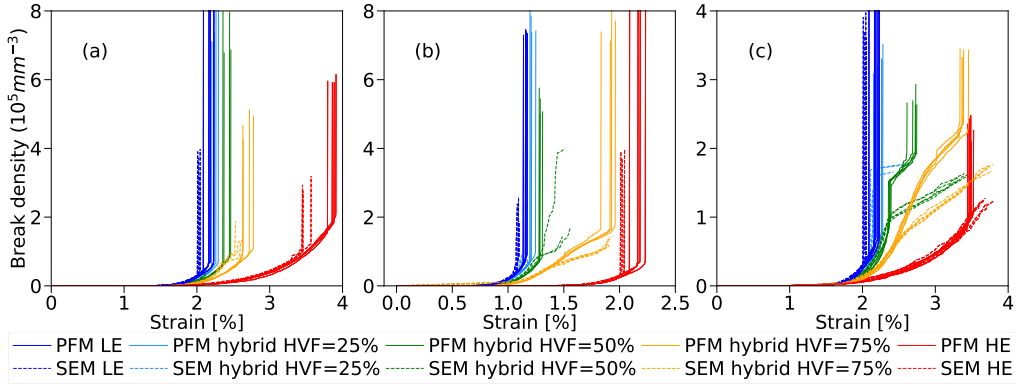

Fig. 8. Simulated break-density curves for different hybrid materials at different hybrid volume fractions (*HVF*) using a plastic matrix. (a) hybrid AS4-Eglass, (b) hybrid M50S-AS4, and (c) hybrid AS4-T800G. The non-hybrid composites are also shown.

respectively. It is worth mentioning that both the cluster size and fibre break density are here being compared with results of non-hybrid composites, which are brittle and less damage tolerant than the analysed hybrids. Therefore, this comparison should be taken with care. Nonetheless, although there is no certainty in the results for hybrid composites, the models seem to partially capture the results in non hybrid composites and their application to hybrid composites, although debatable, can lead to important insights.

The predicted stress-strain curves using an elastic matrix are shown in Fig. 9, while the fibre break density can be seen in Fig. 10. Both models are again in good agreement for most material configurations, although now the PFM is in general underpredicting final failure compared to SEM. Nonetheless, the obtained stress–strain curves and failure process differ greatly from the ones observed by using a plastic matrix. Unlike the plastic matrix case, some ductility appears within the AS4-Eglass hybrid at a $HVF = 75\%$. However, a very small ductility is predicted for the M50S-AS4 hybrid at a $HVF = 75\%$ compared to the plastic matrix case. The differences between plastic and elastic matrix are even larger for the AS4-T800G hybrid. With this material, the ductile strain at a $HVF = 75\%$ is of 1%, which is much larger than the 0.7% predicted for plastic matrix. Similarly, at a $HVF = 50\%$ a large ductility of 1.5% for SEM and 0.5% for PFM is predicted whilst no ductility was present with a plastic matrix.

By further analysing the cluster evolution and break density with an elastic matrix, larger differences appear in comparison with the plastic matrix. For the ductile cases, the models with an elastic matrix predict a much larger break density than with a plastic matrix. The cluster size is also unrealistically large compared with experimental data [3]. This is especially evident for the AS4-T800G hybrid, in which the cluster size predicted by the models exceeds the number of fibres in the RVE for $HVF = 75\%$ and $HVF = 50\%$. This means that in some cases, some fibres were broken more than once over the 10 axial element lengths considered, corresponding to 20 times the fibre radius. Therefore, the same fibre was broken multiple times in the same cluster. This effect is even more exaggerated due to the small Weibull modulus, m, of the T800G fibre which causes a large strength variation for that fibre. However, it should be highlighted again that both the cluster size and fibre-break density are being compared with results of non-hybrid composites which are brittle and less damage tolerant than the simulated hybrids.

For the cases of the non-hybrid composites the models are again in good agreement. For these materials the final failure is brittle for all cases, being similar between elastic and plastic matrix. However, the fibre break density and cluster size are again very large for some cases with elastic matrix and do not correspond well to data available in the

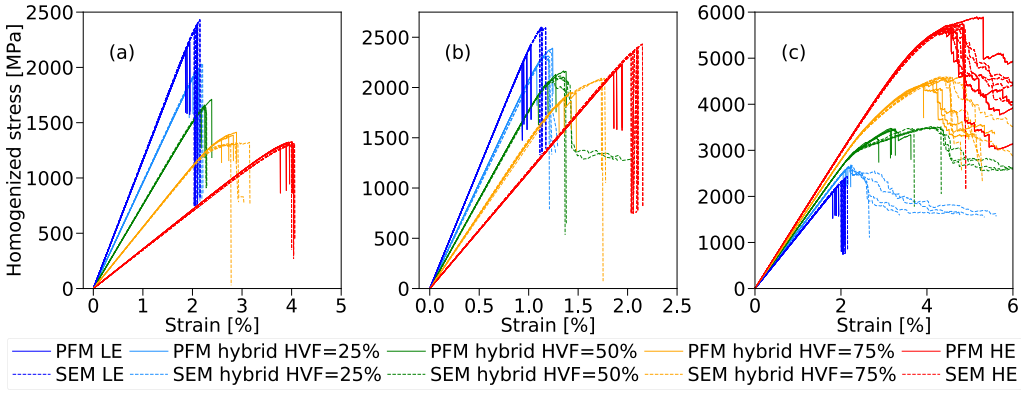

Fig. 9. Simulated stress-strain curves for different hybrid materials at different hybrid volume fractions (*HVF*) using an elastic matrix. (a) hybrid AS4-Eglass, (b) hybrid M50S-AS4, and (c) hybrid AS4-T800G. The non-hybrid composites are also shown.

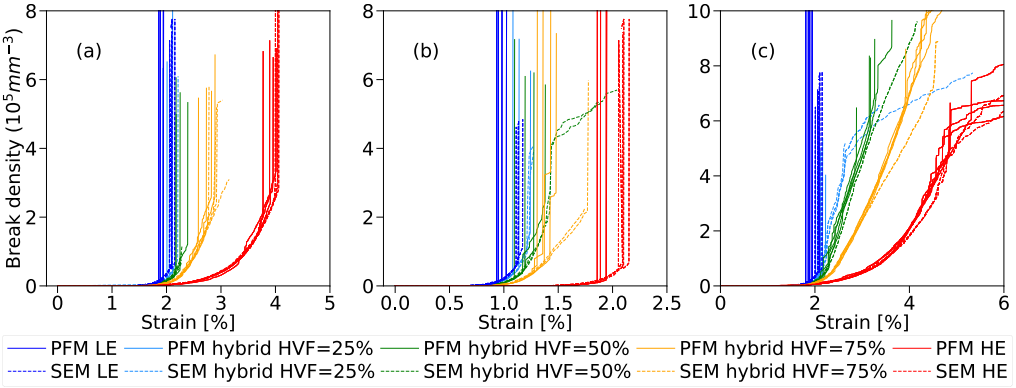

Fig. 10. Simulated break-density curves for different hybrid materials at different hybrid volume fractions (*HVF*) using an elastic matrix. (a) hybrid AS4-Eglass, (b) hybrid M50S-AS4, and (c) hybrid AS4-T800G. The non-hybrid composites are also shown.

literature [3].

The large differences of results between plastic and elastic matrix highlight that the differences in load redistribution, seen in previous Section 4, lead to very different failure progression. In an elastic matrix, the shear stress transfer between fibre and matrix is not limited which causes the stress redistribution to be always very localized around the break. As a consequence, many isolated clusters along the model appear which need to grow very large in size to propagate unstably. This is the reason why the cluster size is usually larger for the elastic matrix cases. Similarly, it should also explain why larger ductilities are observed with an elastic matrix. In a real composite however, the shear stresses are limited by the matrix strength, like it is the case with a plastic matrix approach. Results of this work suggest that, while an elastic matrix may lead to similar failure prediction in non-hybrid composites compared to a plastic matrix, the use of an elastic matrix can lead to inaccurate results when modelling hybrid composites. Nonetheless, it is impossible to further validate the results due to the lack of experimental data. Furthermore, a better definition of cluster size is needed to avoid clusters larger than the number of fibres.

6. Conclusions

In this work, a new analytical model for predicting the *SCF* around clusters of broken fibres in hybrid unidirectional composites was presented. The model was used within the framework of a PFM [2] to study the stress redistribution around breaks in different hybrid composites and their effect on the tensile response and failure process. The results were validated by comparing with the SEM [24].

The predicted stress redistribution around broken fibres in hybrid composites was seen to vary with the stiffness ratio of the fibres on the hybrid, the matrix behaviour being plastic or elastic, the broken fibre stiffness as well as the hybrid volume fraction. Three different metrics were used to quantify this load redistribution: maximum *SCF* on HM and LM fibres, ineffective length and radial length.

The *SCF* on an intact fibre with different stiffness than the broken fibre is affected by the stiffness ratio of both fibres. The larger the ratio, the larger the *SCF* when the HM fibre is broken, whereas the opposite happens when the LM fibre is broken. Adding LM fibres into the hybrid composite decreases the *SCF* on HM fibres, which should lead to larger hybrid effects. When a HM fibre is broken, the *SCF* is larger on the LM fibres than on the HM fibres. However, the *SCFs* are smaller in both populations when the LM fibre is broken. Changing the matrix from plastic to elastic has an important impact on the *SCF*. With an elastic matrix, the *SCF* is larger due to the fact that there is no limit in shear stress transfer. The new proposed analytical model predicted well the trends and stress redistribution in all cases and is in good agreement with the SEM. Moreover, assuming that the overload carried by an intact fibre due to a break does not depend on its Young's modulus and radius, provides a good correlation between the analytical model and the SEM.

The ineffective length was found to depend mainly on the stiffness of the broken fibre. The larger the stiffness, the larger the ineffective length. As a difference from the *SCF*, the stiffness of the hybridization fibre and the *HVF* has no significant impact on the ineffective length. However, the matrix behaviour has a strong effect, being the ineffective length smaller with an elastic matrix. Finally, the radial influence length follows the same trends as the *SCF* and is smaller with an elastic matrix.

In addition, a simulation of the fibre tensile failure of different hybrid materials was performed under strain controlled conditions. Different ductile responses were predicted for some composites at low *HVF*, whereas in other cases brittle and sudden failures were obtained. The ductile composites presented a gradual and progressive increase of fibre break density, whereas an exponential increase was obtained for the brittle materials.

Large differences were again found between plastic and elastic matrix, meaning that the differences in load redistribution lead to different failure progression. When the matrix was considered elastic, many isolated clusters appeared along the model. These clusters needed to grow very large in size before unstable propagation. As a consequence, unrealistically large cluster size and break densities were predicted for some simulations. This wasn't the case with a plastic matrix, which presented more realistic results compared to experiments [3]. Therefore, results suggest that using an elastic matrix may lead to erroneous predictions when modelling hybrid composites. Additional experimental data is required to further validate and improve the different models for hybrid composites.

Data availability

The raw/processed data required to reproduce these findings cannot be shared at this time due to legal or ethical reasons.

Acknowledgments

The authors of Universitat de Girona acknowledge the financial support from the Spanish Ministerio de Economía, Industria y Competitividad (MINECO) under the projects MAT2015-69491-C3-1-R

and TRA2015-71491-R co-financed by the European Regional Development Fund (ERDF). Jose M. Guerrero acknowledges the pre-doctoral Grant BES-2016-078270 from the Subprograma Estatal de Formación del MICINN cofinanced by the European Social Fund. Rodrigo P. Tavares acknowledges the support of the Portuguese Government's Fundação para a Ciência e Tecnologia, under the Grant SFRH/BD/115872/2016. Fermin Otero acknowledges the funding of Project NORTE-01-0145-FEDER-000022 SciTech Science and Technology for Competitive and Sustainable Industries, cofinanced by Programa Operacional Regional do Norte (NORTE2020), through ERDF. Pedro P. Camanho acknowledges the funding of Project PTDC/EMS-PRO/4732/2014, cofinanced by Programa Operacional Competitividade e Internacionalização and Programa Operacional Regional de Lisboa, through ERDF and by National Funds through FCT – Fundação para a Ciência e Tecnologia.

References

[1] Turon A, Costa J, Maimí P, Trias D, Mayugo JA. A progressive damage model for unidirectional fibre-reinforced composites based on fibre fragmentation. Part I: Formulation. Compos Sci Technol 2005;65(13):2039–48. https://doi.org/10.1016/j.compscitech.2005.04.012.

[2] Guerrero J, Mayugo J, Costa J, Turon A. A 3D Progressive Failure Model for predicting pseudo-ductility in hybrid unidirectional composite materials under fibre tensile loading. Compos Part A: Appl Sci Manuf 2018;107:579–91. https://doi.org/10.1016/j.compositesa.2018.02.005.

[3] Swolfs Y, Morton H, Scott AE, Gorbatikh L, Reed PAS, Sinclair I, Spearing SM, Verpoest I. Synchrotron radiation computed tomography for experimental validation of a tensile strength model for unidirectional fibre-reinforced composites. Compos Part A: Appl Sci Manuf 2015;77:106–13. https://doi.org/10.1016/j.compositesa.2015.06.018.

[4] Bunsell A, Gorbatikh L, Morton H, Pimenta S, Sinclair I, Spearing M, Swolfs Y, Thionnet A, et al. Benchmarking of strength models for unidirectional composites under longitudinal tension. Compos Part A: Appl Sci Manuf 2018;111(June 2017):138–50. https://doi.org/10.1016/j.compositesa.2018.03.016.

[5] Scott AE, Mavrogordato M, Wright P, Sinclair I, Spearing SM. In situ fibre fracture measurement in carbon-epoxy laminates using high resolution computed tomography. Compos Sci Technol 2011;71(12):1471–7. https://doi.org/10.1016/j.compscitech.2011.06.004.

[6] Czél G, Wisnom MR. Demonstration of pseudo-ductility in high performance glass/epoxy composites by hybridisation with thin-ply carbon prepreg. Compos Part A: Appl Sci Manuf 2013;52:23–30. https://doi.org/10.1016/j.compositesa.2013.04.006.

[7] Czél G, Jalalvand M, Wisnom MR. Design and characterisation of advanced pseudo-ductile unidirectional thin-ply carbon/epoxy-glass/epoxy hybrid composites. Compos Struct 2016;143:362–70. https://doi.org/10.1016/j.compstruct.2016.02.010.

[8] Swolfs Y, Gorbatikh L, Verpoest I. Fibre hybridisation in polymer composites: a review. Compos Part A: Appl Sci Manuf 2014;67:181–200. https://doi.org/10.1016/j.compositesa.2014.08.027.

[9] Xing J, Hsiao G, Chou T-W. A dynamic explanation of the hybrid effect. J Compos Mater 1981;15(5):443–61. https://doi.org/10.1177/002199838101500504.

[10] Swolfs Y, Gorbatikh L, Verpoest I. Stress concentrations in hybrid unidirectional fibre-reinforced composites with random fibre packings. Compos Sci Technol 2013;85:10–6. https://doi.org/10.1016/j.compscitech.2013.05.013.

[11] Swolfs Y, Verpoest I, Gorbatikh L. Maximising the hybrid effect in unidirectional hybrid composites. Mater Des 2016;93:39–45. https://doi.org/10.1016/j.matdes.2015.12.137.

[12] Swolfs Y, McMeeking RM, Verpoest I, Gorbatikh L. The effect of fibre dispersion on initial failure strain and cluster development in unidirectional carbon/glass hybrid composites. Compos Part A: Appl Sci Manuf 2014;69:279–87. https://doi.org/10.1016/j.compositesa.2014.12.001.

[13] Wisnom MR, Czel G, Swolfs Y, Jalalvand M, Gorbatikh L, Verpoest I. Hybrid effects in thin ply carbon/glass unidirectional laminates: accurate experimental determination and prediction. Compos Part A: Appl Sci Manuf 2016;88:131–9. https://doi.org/10.1016/j.compositesa.2016.04.014.

[14] Vanegas-Jaramillo JD, Turon A, Costa J, Cruz LJ, Mayugo JA. Analytical model for predicting the tensile strength of unidirectional composites based on the density of fiber breaks. Compos Part B: Eng 2018;141(February 2017):84–91. https://doi.org/10.1016/j.compositesb.2017.12.012.

[15] Hui CY, Phoenix SL, Ibnabdeljalil M, Smith RL. An exact closed form solution for fragmentation of Weibull fibers in a single filament composite with applications to fiber-reinforced ceramics. J Mech Phys Solids 1995;43(10):1551–85. https://doi.org/10.1016/0022-5096(95)00045-K.

[16] Curtin WA. Exact theory of fibre fragmentation in a single-filament composite. J Mater Sci 1991;26(19):5239–53. https://doi.org/10.1007/BF01143218.

[17] Neumeister JM. A constitutive law for continuous fiber reinforced brittle matrix composites with fiber fragmentation and stress recovery. J Mech Phys Solids 1993;41(8):1383–404. https://doi.org/10.1016/0022-5096(93)90085-T.

[18] Tavares RP, Melro AR, Bessa MA, Turon A, Liu WK, Camanho PP. Mechanics of hybrid polymer composites: analytical and computational study. Comput Mech 2016;57(3):405–21. https://doi.org/10.1007/s00466-015-1252-0.

[19] Swolfs Y, McMeeking RM, Rajan VP, Zok FW, Verpoest I, Gorbatikh L. Global load-sharing model for unidirectional hybrid fibre-reinforced composites. J Mech Phys Solids 2015;84:380–94. https://doi.org/10.1016/j.jmps.2015.08.009.

[20] Tavares RP, Guerrero JM, Otero F, Turon A, Mayugo JA, Costa J, Camanho PP. Effects of local stress fields around broken fibres on the longitudinal failure of composite materials. Int J Solids Struct. 2019;156–157:294–305.

[21] Pimenta S. A computationally-efficient hierarchical scaling law to predict damage accumulation in composite fibre-bundles. Compos Sci Technol 2017;146:210–25. https://doi.org/10.1016/j.compscitech.2017.04.018.

[22] St-Pierre L, Martorell NJ, Pinho ST. Stress redistribution around clusters of broken fibres in a composite. Compos Struct 2017;168:226–33. https://doi.org/10.1016/j.compstruct.2017.01.084.

[23] Pimenta S, Pinho ST. Hierarchical scaling law for the strength of composite fibre bundles. J Mech Phys Solids 2013;61(6):1337–56. https://doi.org/10.1016/j.jmps.2013.02.004.

[24] Tavares RP, Otero F, Turon A, Camanho PP. Effective simulation of the mechanics of longitudinal tensile failure of unidirectional polymer composites. Int J Fract 2017;208(1–2):269–85. https://doi.org/10.1007/s10704-017-0252-9.

[25] Okabe T, Sekine H, Ishii K, Nishikawa M, Takeda N. Numerical method for failure simulation of unidirectional fiber-reinforced composites with spring element model. Compos Sci Technol 2005;65(6):921–33. https://doi.org/10.1016/j.compscitech.2004.10.030.

[26] Okabe T, Takeda N, Kamoshida Y, Shimizu M, Curtin WA. A 3D shear-lag model considering micro-damage and statistical strength prediction of unidirectional fiber-reinforced composites. Compos Sci Technol 2001;61(12):1773–87. https://doi.org/10.1016/S0266-3538(01)00079-3.

[27] Mishnaevsky L, Brøndsted P. Micromechanisms of damage in unidirectional fiber reinforced composites: 3D computational analysis. Compos Sci Technol 2009;69(7–8):1036–44. https://doi.org/10.1016/j.compscitech.2009.01.022.

[28] Thionnet A, Chou HY, Bunsell A. Fibre break processes in unidirectional composites. Compos Part A: Appl Sci Manuf 2014;65:148–60. https://doi.org/10.1016/j.compositesa.2014.06.009.

[29] Okabe T, Ishii K, Nishikawa M, Takeda N. Prediction of tensile strength of unidirectional CFRP composites. Adv Compos Mater 2010;19(3):229–41. https://doi.org/10.6089/jscm.33.205.

[30] Kelly A, Tyson W. Tensile properties of fibre-reinforced and metals: copper/tungsten and copper/molybdenum. J Mech Phys Solids 1965;13(6):329–50. https://doi.org/10.1016/0022-5096(65)90035-9.

[31] Cox H. The elasticity and strength of paper and other fibrous materials. Br J Appl Phys 1952;3(3):72–9. https://doi.org/10.1088/0508-3443/3/3/302.

[32] Landis CM, McMeeking RM. A shear-lag model for a broken fiber embedded in a composite with a ductile matrix. Compos Sci Technol 1999;59(3):447–57. https://doi.org/10.1016/S0266-3538(98)00091-8.

[33] Eitan A, Wagner HD. Fiber interactions in two-dimensional composites. Appl Phys Lett 1991;58(10):1033–5. https://doi.org/10.1063/1.105209.

[34] Zhou XF, Wagner HD. Stress concentrations caused by fiber failure in two-dimensional composites. Compos Sci Technol 1999;59(7):1063–71. https://doi.org/10.1016/S0266-3538(98)00145-6.

[35] Melro AR, Camanho PP, Pinho ST. Generation of random distribution of fibres in long-fibre reinforced composites. Compos Sci Technol 2008;68(9):2092–102. https://doi.org/10.1016/j.compscitech.2008.03.013.

[36] Weibull W. A statistical distribution function of wide applicability. ASME J 1952:293–7.

[37] Jalalvand M, Czél G, Wisnom MR. Parametric study of failure mechanisms and optimal configurations of pseudo-ductile thin-ply UD hybrid composites. Compos Part A: Appl Sci Manuf 2015;74:123–31. https://doi.org/10.1016/j.compositesa.2015.04.001.

A.3 Conference paper – A comparison of algorithms for determining the cluster development in unidirectional composite materials under fibre tensile loading

The paper has been presented in *7th ECCOMAS Thematic Conference on the Mechanical Response of Composites (COMPOSITES 2019)*. Girona (Spain), 18-20th September 2019.

7th ECCOMAS Thematic Conference on the Mechanical Response of Composites
COMPOSITES 2019
A. Turon, P. Maimí & M. Fagerström (Editors)

A COMPARISON OF ALGORITHMS FOR DETERMINING THE CLUSTER DEVELOPMENT IN UNIDIRECTIONAL COMPOSITE MATERIALS UNDER FIBRE TENSILE LOADING

Jose M. Guerrero[1,*], **Joan A. Mayugo**[1], **Josep Costa**[1], **Albert Turon**[1]

[1] AMADE, Polytechnic School, Universitat de Girona, Campus Montilivi s/n, E-17003 Girona, Spain
[*] josemanuel.guerrero@udg.edu

Keywords: Micromechanics, Clustering, Failure.

Summary: *In this paper the failure development of different hybrid and non-hybrid unidirectional composite materials is simulated under fibre tensile loading using a progressive failure model. Different hierarchical clustering analysis algorithms as well as the OPTICS method are used to predict the formation of clusters of broken fibres in the simulated materials, and the outcomes of these algorithms are compared. Results show that the diverse hierarchical algorithms may lead to similar formation of clusters, but different critical cluster sizes depending on the algorithm, whereas the OPTICS method predicts considerable different formation of clusters, leading to more clusters of large size. However, the formation of co-planar clusters is similar between all algorithms.*

1. INTRODUCTION

The fibre tensile failure of unidirectional composite materials is mainly dominated by the formation of clusters of broken fibres. The strength of brittle fibres is not deterministic, and follows a statistical distribution. Consequently, the formation of clusters is governed by the stochastic strength of the fibres as well as the stress redistribution around broken fibres. When a fibre fails, the fibre locally loses its load carrying capability, but it is then recovered due to shear transfer in the matrix over a distance known as ineffective length. Along this region, the surrounding intact fibres are subjected into stress concentrations. As the load is increased, clusters of broken fibres start to form. Eventually, final failure is triggered either due to the unstable propagation of a large critical cluster or due to the accumulation of damage [1, 2].

There are two main modelling approaches to simulate the failure of composite materials: Global Load Sharing models (GLS) and Local Load Sharing models (LLS). While GLS models cannot capture the formation of clusters, LLS models are able to do so. Many different LLS with diverse modelling assumptions and backgrounds are available: analytical models [3, 4], fibre bundle models [5, 6], spring element models [7, 8] and micromechanical finite element models [9, 10]. Currently, one of the main difficulties in LLS models is to determine the formation of clusters of broken fibres. At present, the literature has considered metrics based on the distance between broken fibres to establish whether they form a cluster or not. Overall, it has been considered that two broken fibres belong to the same cluster if their centre-to-centre distance is

smaller than four times the fibre radius and their axial distance between break planes is smaller than ten times the fibre radius [1, 6, 11]. Although this approach is valid, there exit different clustering algorithms that, alternatively, may also be employed to determine the formation of clusters with distinct considerations [12–15]. However, to the authors' best knowledge, the use of alternative methods has not been explored.

In this work, the failure development of hybrid and non-hybrid unidirectional composite materials is simulated under fibre tensile loading using a progressive failure model [1, 5, 11, 16]. The formation of clusters is determined using various hierarchical clustering analysis algorithms as well as OPTICS, and results with all methods are compared. The remainder of this article is as follows. Firstly, the progressive failure model is briefly summarised. Secondly, different algorithms to determine clusters are outlined, and some of them are used to predict the formation of clusters of broken fibres. Finally, some conclusions are obtained.

2. PROGRESSIVE FAILURE MODEL

The Progressive Failure Model (PFM) [1, 5, 11, 16] is a micromechanical model consisting of a Representative Volume Element (RVE) of width a, height b and length L. The RVE contains a random distribution of fibres, each with its own radius. Each fibre is divided into elements of length l along its longitudinal direction, thus leading to a domain of parallel tensile springs divided into planes in series. The RVE may consist of fibres all of the same type, being a non-hybrid composite, or can contain fibres of different types, leading to a hybrid composite. Fibres are labelled with subindices $q \in [1, ..., N_q]$, while planes are referred with $p \in [1, ..., N_p]$ where N_q and N_p are the number of fibres and planes respectively. This scheme is shown in Figure 1.

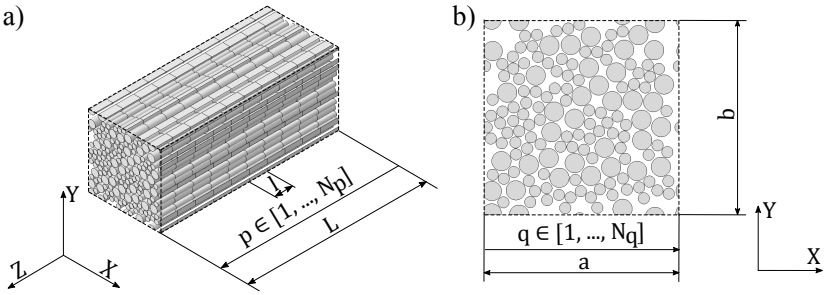

Figure 1. Schema of the Progressive Failure Model, a) 3D view, b) cross-section.

A stochastic strength is assigned to each element in the RVE according to an appropriate statistical distribution representing the strength of the fibres. An unixial strain controlled simulation is then performed, by slowly increasing the applied strain. At each loading step, the stress of each element, $\sigma_{p,q}$, is calculated with

$$\sigma_{p,q} = \frac{SCF_{p,q}}{\Omega_p} E_q \left(1 - D_{p,q}\right) \left(\varepsilon_p + \varepsilon_q^{\mathrm{r}}\right) \tag{1}$$

where $SCF_{p,q}$ is the Stress Concentration Factor (SCF) of element p, q, E_q is the Young's modulus of fibre q, $D_{p,q}$ is the damage factor which is equal to 1 for broken elements, equal to 0 for intact elements and in between for elements in any stress recovery, ε_p is the mechanical strain of the plane, $\varepsilon_q^{\mathrm{r}}$ is the fibre's thermal residual strain and Ω_p is a stress ratio which enforces load equilibrium at each plane [5, 11, 16].

When the stress of an element exceeds its strength, the element fails. A damage factor is then applied along the ineffective length of the broken fibre whereas stress concentration is applied onto the intact fibre elements surrounding the broken fibre. Therefore, $D_{p,q}$ and $SCF_{p,q}$ are computed by an analytical model that is entered into the PFM. This model takes into account the matrix behaviour, which can be considered as elastic or perfectly plastic, since debonding is omitted. When new elements fail, dynamic effects are also considered by increasing the SCF with a magnification factor [16]. Additionally, a load equilibrium condition is employed for computing Ω_p and ε_p, taking into account the damage along the RVE. Further details of the model can be seen in Guerrero *et al.* [5, 11, 16].

The PFM explicitly captures individual fibre breaks and the formation of clusters of multiple broken fibres. Since damage is considered, the stiffness loss of composite materials is captured, allowing to model pseudo-ductility in fibre hybrid composites [5, 11, 16]. Unlike other models, the PFM scales up the ineffective length of the broken fibres when the number of breaks increases, and considers dynamic effects. Given the semi-analytical framework considered, the PFM is computationally more efficient than other similar models [11].

3. COMMON DEFINITION OF CLUSTERS

One of the key problems in the literature is to determine the formation of clusters, i.e., to establish which broken fibres in a given domain should be considered as a *cluster of broken fibres*. Ideally, two different broken fibres should form a cluster as long as these are 'sufficiently close', which implies that one of the fibres failed under stress concentration caused by the other one.

Currently, the literature in composite materials has used a criterion based on the stress redistribution around broken fibres to determine the formation of clusters. Consequently, two broken fibres are considered to belong to the same cluster if the radial distance between the two broken fibres, d_{r}, is equal or smaller than Δ_{r}, and the longitudinal distance between break planes, d_{l}, is smaller or equal than Δ_{l} (see Figure 2a). By default, most authors have used $\Delta_{\mathrm{r}} = 4R_{\mathrm{f}}$ and $\Delta_{\mathrm{l}} = 10R_{\mathrm{f}}$ respectively (where R_{f} is the fibre radius) [1, 6, 7, 11, 17], since these are reasonable values for carbon reinforced polymer composites (although this should ideally be calculated for each material system). Once many broken fibres are present, it may occur that a new broken fibre links two different clusters. When this occurs, the two clusters and the new broken fibre are merged into a sole single cluster (see Figure 2b). Consequently, Δ_{r} and Δ_{l}, are not upper distances.

Although this approach has been satisfactorily used in many recent works [6, 7, 11], there exist different algorithms able to link or cluster a set of data (in this case broken fibre elements), based on their similarity (or dissimilarity), which in this work corresponds to how close or far

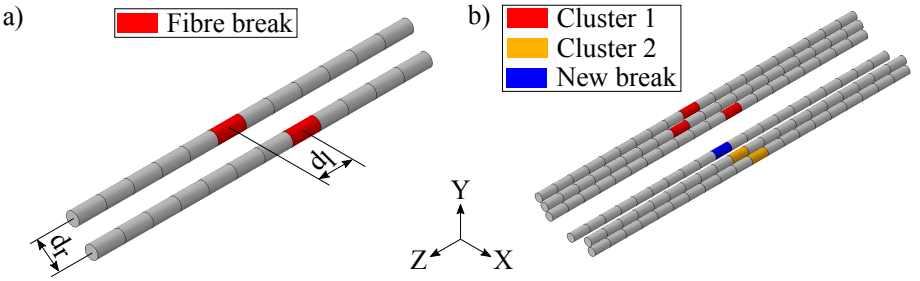

Figure 2. Criterion to determine clusters. a) Two fibre breaks form a cluster if the radial distance between the two breaks, d_r, is equal or smaller than Δ_r, and the longitudinal distance, d_l, is smaller or equal than Δ_l. b) A new fibre break (in blue colour) complies the conditions Δ_r and Δ_l with one fibre in 'cluster 2' (coloured orange), and also with one fibre in 'cluster 1' (coloured red), thus, the two clusters (and the new break) are merged into a single cluster.

these breaks are placed in the material. Although similar in some form, these methods could allow to determine clusters by considering different linkage criteria. Moreover, these methods are available in different programming languages (such as Python [18]) which may facilitate the determination of clusters. In the next section, different clustering algorithms are explained.

4. ALGORITHMS FOR DETERMINING CLUSTERS

There exist many algorithms able to cluster a set of data. The most common ones in unsupervised machine learning are centroid-based clustering, hierarchical clustering, distribution based clustering and density-based clustering [12–15, 19]. In the following, these methods are broadly summarised.

4.1 CENTROID-BASED: K-MEANS

Centroid-based methods divide a given set of data points into different groups, and each sample is assigned to the closest one. The most common centroid-based algorithm is k-means, which clusters data by separating it into k groups of equal variance [12]. This is done by minimizing either a criterion called the *inertia* or a *sum-of-squares* [18]. These criteria can be seen as a measure of how similar or dissimilar the clusters are.

The procedure is composed of three basic steps. Firstly, the algorithm starts by choosing the initial centroid of each cluster. After that, each sample is assigned to its nearest centroid. In the third step, the centroid of each cluster is recomputed by averaging all data points in it. Steps 2 and 3 are then repeated until convergence is reached.

Although this method is broadly used, it has some drawbacks [18]. Firstly, it needs the number of clusters, k, to be known a priori. Secondly, it assumes that clusters are convex and isotropic (thus not capturing irregular shapes). In addition, it generates clusters of even sizes.

4.2 HIERARCHICAL CLUSTERING

Hierarchical Clustering Analysis (HCA) algorithms build a hierarchy of clusters by merging or splitting data successively [19]. Two main approaches are possible: Agglomerative or Divisive. In Agglomerative clustering each sample in the data starts being a cluster on its own. These clusters are then successively merged together step by step (based on their distance and a linkage criteria), until the entire data forms a single cluster. Instead, divisive clustering starts with all samples in a single cluster, and these are successively split step by step until each sample is a cluster. This hierarchy can be represented by a tree or dendrogram. By cutting the dendrogram at a given certain height (which represents the distance at which clusters are merged or split), the clusters are directly determined, see Figure 3a.

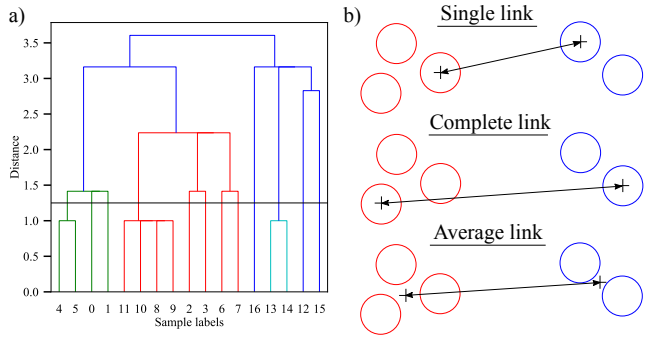

Figure 3. a) Example of a dendrogram. The x axis represents the different samples while the y axis shows the distance at which the samples are merged into clusters. By cutting at a distance of 1.25, twelve clusters are obtained. b) distances used to merge two different clusters into one according to the linkage criteria.

HCA may calculate the distance between points using different metrics such as Euclidean, Manhattan or Cosine [18], or alternatively, a distance/dissimilarity matrix may be considered. The distance matrix is a 2-dimensional matrix where the value in the i-th row j-th column, is the distance between the i-th and j-th elements. To merge or split the clusters, different linkage criteria exist, being the most common single, complete or maximum, average and ward [18, 19]. Single takes the minimum distance between all samples in different clusters to link them. Instead, complete takes the maximum, average takes the average, whereas ward considers the sum of squared differences (thus this is similar to k-means method), see Figure 3b.

Unlike k-means, in hierarchical clustering the number of clusters does not need to be known, instead, a distance threshold is needed for cutting the dendrogram. In addition, hierarchical clustering may capture clusters of uneven sizes (in this sense single linkage leads to more uneven clusters, ward would lead to more regular sizes, while the other methods would be in-between). HCA can also capture clusters of irregular shapes.

4.3 DISTRIBUTION BASED

Distribution based clustering models are more related to statistics. One of the most well knowns algorithms is the Gaussian Mixture Model (GMM) [14]. With this algorithm, the data points are assumed to be Gaussian distributed. Hence, two parameters describe the shape of the clusters: the mean and the standard deviation. These are usually calculated with an Expectation Maximization (EM) algorithm [14].

Like k-means, the procedure follows three steps. First, GMM starts by initiating the Gaussian parameters of each cluster, according to the given number of clusters. In step 2, the probability of a point to belong into a cluster is computed, and the point is assigned to the cluster it most likely belongs to. In step 3, the Gaussian distribution parameters are recalculated to maximize the probability that each data point belongs to the cluster. Finally, Steps 2 and 3 are repeated until convergence.

GMM captures clusters of elliptical shape, and thus, it is less restrictive than k-means in that sense. However, like k-means, GMM also fails to capture clusters of largely irregular shapes (and assuming that clusters are Gaussian distributed is a strong assumption) [18]. In addition, the number of clusters needs to be known a priori.

4.4 DENSITY BASED

Density based algorithms cluster the data by separating areas of high density from areas of lower density [15, 20, 21]. The most common density-based algorithm is DBSCAN (Density-Based Spatial Clustering of Applications with Noise) [15]. This algorithm requires two input parameters: eps and $min\_samples$, which determine what is considered to be 'dense'.

Given a dataset of n-dimensional data points, the algorithm proceeds as follows. Firstly, a point is taken, and an n-dimensional sphere of radius eps around the point is created. If the number of points in the sphere (including the sample on its own) is equal or larger than $min\_samples$, then all points in it belong to the same cluster. The point in the centre is known as a *core* sample, and it is considered to be in a dense region. The cluster is then recursively expanded by creating another sphere at each of these points. However, any of these points that have less than $min\_samples$ inside their own sphere are omitted. Intuitively, these points define the border of the cluster. In addition, any point that has less than $min\_samples$ inside its own sphere and that it is not inside the sphere of a core sample, is labelled as 'noise' and does not belong to any cluster. Essentially, this means that the value of $min\_samples$ determines which is the minimum cluster size. In this way, DBSCAN captures clusters of any shape and of uneven sizes.

Therefore, DBSCAN is similar to single link HCA, but including the concept of dense regions. In fact, when $min\_samples = 2$, DBSCAN is equivalent to single link hierarchical clustering, with eps being the same value that is used to cut the dendrogram. An alternative version of DBSCAN is OPTICS [21], which takes eps as a range instead of a single value. Thus, OPTICS eliminates the need of determining a proper value for eps, since this is established by the algorithm, albeit a maximum value for eps can be given to reduce CPU time.

5. METHODOLOGY AND MATERIALS

To compare the formation of clusters between algorithms, different hybrid and non-hybrid unidirectional composite materials are simulated using the PFM. A perfectly plastic matrix is used, because it should be more realistic than an elastic matrix [11]. Consequently, a magnification factor for dynamic effects of 1.43 is considered, since this should be accurate for a plastic matrix [22]. In addition, thermal residual stresses due to the manufacturing process are omitted. A RVE of width, a, height, b, and length L of $0.2625 \times 0.2625 \times 1.05$ mm is created, containing around 1100-1800 fibres. Hybrid composites are preferably to be simulated for the porpoise of this work, since these are more damage tolerant and will contain more clusters than non-hybrid composites, allowing to better highlight the difference between clustering methods. In a fibre hybrid composite, a Low Elongation (LE) fibre, is combined with a High Elongation (HE) fibre in a single matrix. Thanks to this combination, synergistic effects may occur allowing to increase the composite ductility compared to non-hybrid composites [5, 6, 9, 11].

The RVEs contain a random distribution of fibres each with its own radius, and are generated using a state of the art algorithm [9, 23]. The material comprising the RVEs consists of an intrayarn hybrid M40S-T700 (Carbon-Carbon) fibres in an Epoxy matrix with Young's modulus, $E_{\mathrm{m}} = 3760$ MPa, and shear yield stress, $\tau_q = 50$ MPa. The properties of the fibres can be seen in Table 1. The overall fibre volume fraction (V_{f}) is always 60%, whereas the HVF is varied between 0, 20, 40, 60, 80 and 100% as it significantly influences the tensile response of hybrid composites [9, 11]. Here, the HVF is considered as the percentage of LE fibre volume fraction (V_{LE}) over the total volume fraction (V_{f}), with $HVF = V_{\mathrm{LE}}/V_{\mathrm{f}}$ [16]. Note that, $HVF = 0\%$ and $HVF = 100\%$ correspond to the base-line non-hybrid materials, T700-Epoxy and M40S-Epoxy, so that the M40S is the LE fibre and the T700 is the HE fibre respectively.

Table 1. Fibre properties.

Fibre type	Fibre properties		Weibull parameters		
	E_{f} [GPa]	R_{f} [μm]	σ_0 [MPa]	L_0 [mm]	m [-]
M40S	380	2.7	4900	10	5.2
T700	220	3.5	5470	20	5.6

The strength of each element in the RVE, $\sigma^{\mathrm{u}}_{p,q}$, is computed by a Weibull distribution [1, 5–7, 11, 16, 17], with $P_{p,q} = 1 - \exp\left(-\left(l/L_0\right)\left(\sigma^{\mathrm{u}}_{p,q}/\sigma_0\right)^m\right)$ where $P_{p,q}$ is a random number between 0 and 1, and σ_0, m and L_0 are the Weibull parameters given in Table 1. To take into consideration both the random nature of the position of the fibres and the stochastic fibre strength 8 runs are performed within each RVE considered. For each run, a different RVE with new element strengths is generated. In Figure 4, a cross-section example of the materials simulated is shown.

For each material considered, the formation of clusters during the simulation (i.e., at each loading step) is determined in different ways. Firstly, with the HCA algorithm, using the single,

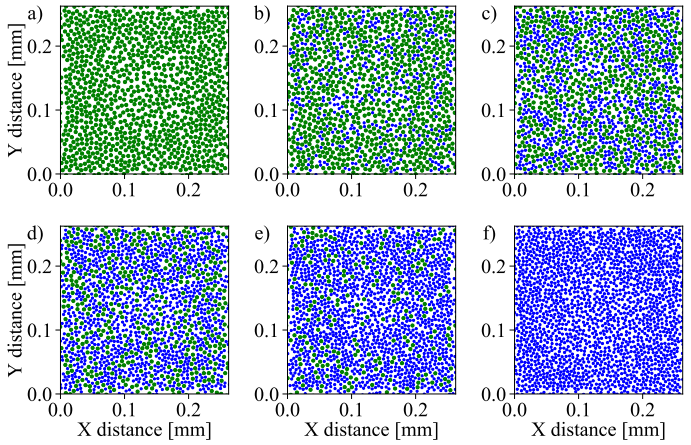

Figure 4. Cross-section examples of the RVEs generated, a) $HVF = 0\%$, b) $HVF = 20\%$, c) $HVF = 40\%$, d) $HVF = 60\%$, e) $HVF = 80\%$ and f) $HVF = 100\%$. The LE fibres are coloured blue, while HE fibres are coloured green.

average, and complete linkage criteria. Ward will not be used since it should be similar to complete and average [18]. For HCA, a distance criterion is needed to establish when two broken fibres form a cluster. To do this, a distance matrix is computed where the value in the i-th row j-th column, is considered to be 0 if the radial distance between the i-th and j-th elements is smaller or equal than $\Delta_r = 4R_f$, and if their axial distance is smaller or equal than $\Delta_l = 10R_f$. Otherwise, a value of 1 is assigned. The dendrogram is then cut at a distance of 0.5. With this consideration, two broken fibres form a cluster or not according to their radial and longitudinal distance. Consequently, the single link algorithm is exactly equivalent to the method explained in section 3. (although the two algorithms are different). Secondly, the OPTICS method is also employed. Here, a maximum eps of $10R_f$ is considered (larger values do not really make sense). The algorithm will determine by itself the proper value of eps, but will be equal to or smaller than the given maximum. Unlike HCA, OPTICS will establish by itself if two breaks form a cluster, according to the value of eps it determines. Consequently no distance matrix is needed either, only the coordinates of the broken fibres. In addition, $min\_samples = 2$, since the minimum cluster size in a composite should contain at least two broken fibres. Finally, k-means and GMM algorithms will not be used, since these cannot capture clusters of irregular shapes and need the number of clusters to be known a priori. Consequently, these methods are not feasible for this study. For all cases considered, the implementation provided in Python language is used to get the clusters [18].

Derived from this, the maximum cluster size along the simulation, the number of i-plets (clusters of size 'i'), and the percentage of co-planar clusters are compared between the different

algorithms. A cluster is co-planar if the longitudinal distance between break planes, d_l, is smaller or equal than the element length (which corresponds to 5.4 μm) otherwise it is diffuse. Note that, all this data is solely output information by the PFM. Hence, the different algorithms do not change the modelling predictions, but only this output information.

6. RESULTS AND DISCUSSION

In Figure 5 the maximum cluster size and the formation of co-planar clusters along the simulations is compared between the different algorithms for all materials. Overall, the single HCA algorithm leads to significant larger cluster sizes than the complete and average HCA. The complete HCA leads to the smallest cluster sizes, which occurs since it considers the maximum distance between samples to merge the clusters, and thus clusters are less likely to be linked. The average is in between the single and complete methods. The OPTICS algorithm leads to similar cluster sizes compared to the single HCA, but slightly smaller. An important remark is that, all algorithms predict a constant increase in cluster size with the applied strain except OPTICS, which in some instants predicts a decrease. Hence, OPTICS may have considered different values for eps at different loading steps, causing a change in the maximum cluster size. This is an inconsistent behaviour, since a continuous grow of the cluster size with the applied strain is expected due to the increased number of fibre breaks. In addition, all tendencies are generally the same regardless of the HVF, and therefore, the materials do not change the differences between the algorithms.

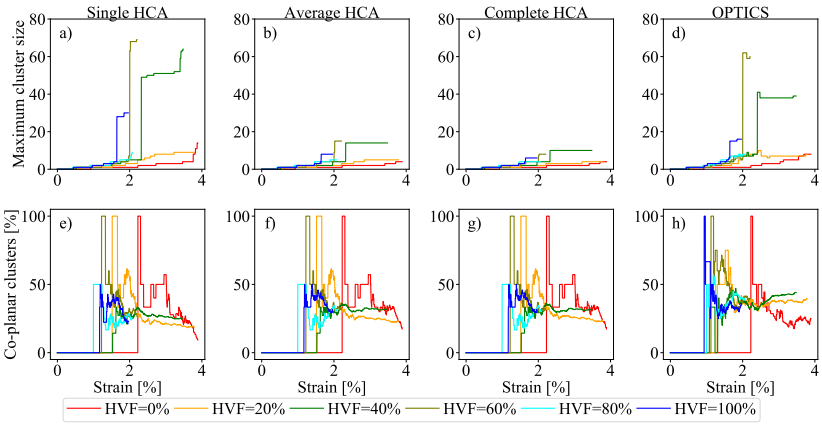

Figure 5. Maximum cluster size and percentage of co-planar clusters predicted by each algorithm along the simulation. a)-d) maximum cluster size for each algorithm, e)-h) percentage of co-planar clusters for each algorithm. The average of 8 runs is shown.

In terms of co-planarity, the difference between algorithms seems to be smaller, especially

between the single, average and complete HCA. The OPTICS method shows larger differences, particularly for $HVF = 20\%$ and $HVF = 60\%$ which lead to more co-planar clusters than the HCA cases. This should be attributed to the different way OPTICS creates the clusters. Generally, the single HCA leads to smaller number of co-planar clusters than the rest. This may be explained because it leads to larger cluster sizes, and thus, larger cluster sizes are more likely to be more spread in a larger volume, leading to more diffuse clusters instead of co-planar.

In Figure 6 the number of 'i-plets' (clusters of size 'i') along the simulation is shown for the different algorithms. The formation of 1-plets is considerably smaller for the OPTICS algorithm than for the other ones. The HCA algorithms are all similar, with the average and complete leading to slightly larger number of 1-plets, compared to the single HCA. However, the formation of 3-plets and 6-plets shows the opposite trend. The OPTICS algorithm predicts a considerable larger number of 3-plets and 6-plets. Thus, OPTICS generates a bigger number of large clusters (hence forming less 1-plets) than the other algorithms. The opposite occurs with the average and complete HCA which lead to the smallest 3-plets and 6-plets, since these consider bigger distances to merge clusters. Thus, these algorithms lead to a lesser number of big clusters (and consequently to smaller cluster sizes and larger number of 1-plets). The single HCA forms more 3-plets and 6-plets than the average and complete, but less than OPTICS.

To better illustrate the differences obtained by the algorithms, a 2D representation of the formation of clusters at failure is presented in Figure 7. The single, average and complete HCA algorithms may lead to the formation of clusters in similar locations (although the clusters do not have the same size, and the critical cluster may be in a different place). However, the OPTICS algorithm predicts a very distinct formation of clusters. In addition, clusters generally span over a bigger area with the OPTICS algorithm, and more clusters of a big size are formed. This is probably related to the fact that OPTICS is using the same value of eps for all dimensions, whereas in HCA, a different distance was considered for the radial and longitudinal directions. Hence, although the data is the same, the algorithms are finding distinct clusters, especially the OPTICS method.

The results suggest that all algorithms may be used to determine the formation of clusters. The single, complete and average HCA may form clusters in similar locations, albeit the single method leads to larger cluster sizes. The OPTICS method may lead to the formation of more clusters of large size, and these may also form in different places than the other algorithms. OPTICS is the only method which calculates the clusters entirely by itself, without having to consider a certain distance threshold to establish what constitutes a cluster. Instead, this is estimated by the algorithm, facilitating the process. Currently, choosing a proper distance criterion to predict the clusters is an open issue in the literature [2], and thus OPTICS may overcome this issue, allowing a more objective formation of clusters. Nonetheless, OPTICS is computationally expensive compared to HCA, and may lead to 'inconsistent' results (such as a decrease in cluster size by increasing the number of breaks) depending on what the algorithm ends up considering to be a cluster.

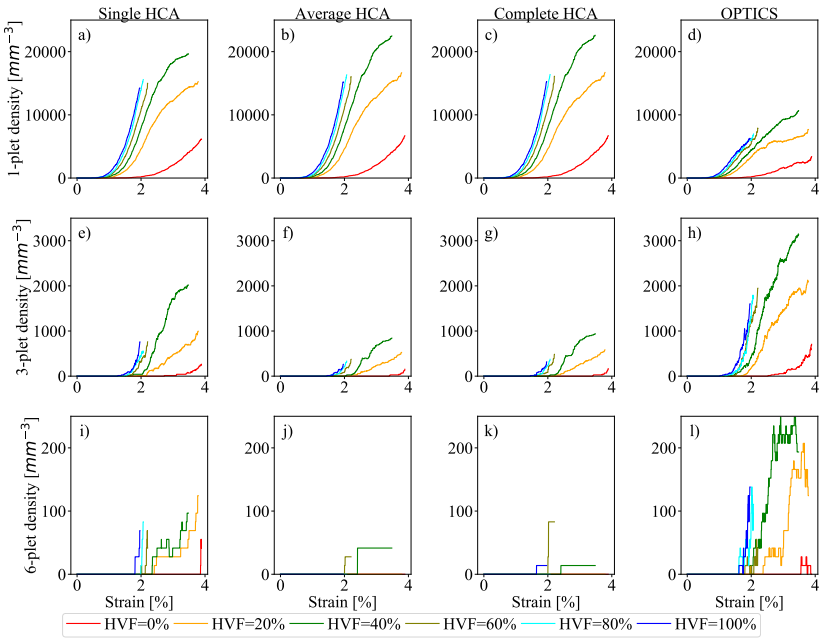

Figure 6. Formation of 'i-plets' (clusters of size 'i') predicted by each algorithm along the simulation. The number of i-plets is normalized by the RVE volume. a)-d) 1-plets for each algorithm, e)-h) 3-plets for each algorithm and i)-l) 6-plets for each method respectively. The average of 8 runs is shown.

7. CONCLUSIONS

In this work, HCA and OPTICS algorithms were employed to determine the formation of clusters of broken fibres in hybrid and non-hybrid unidirectional composite materials under longitudinal loading. The outcomes of these methods were compared between them.

The results obtained show that HCA and OPTICS are alternative algorithms to determine the formation of clusters of broken fibres in composite materials. The single link HCA is equivalent to the distance based method that has been broadly used in the literature [6, 7, 11] and leads to the formation of larger clusters than the average and complete HCA algorithms. The OPTICS model leads to smaller critical clusters than the single link HCA. Nevertheless, it tends to predict a larger number of big clusters compared to the other methods. Moreover, these may form in different locations. Overall, the formation of co-planar clusters is similar between algorithms, being partially smaller for the single link HCA.

Results suggest that all algorithms can be used to predict the formation of clusters. However,

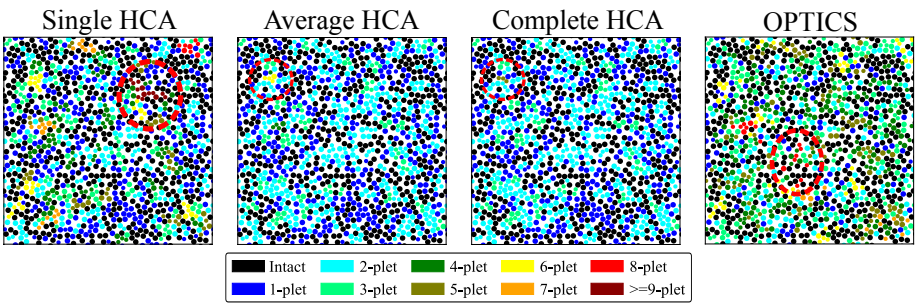

Figure 7. 2D representation of the formation of clusters at failure for one run with $HVF = 20\%$. The largest cluster at which each fibre belongs to is indicated with the corresponding fibre colour. Fibres in black have no breaks along their length. An 'i-plet' refers to a cluster of size 'i'. The larger clusters are indicated with a red dashed circle.

care must be taken to properly predict the clusters. The HCA algorithms depend on a given distance criterion to constitute what is a cluster, and thus results will depend on the chosen distance. Oppositely, OPTICS has the advantage that it determines the distance to merge the clusters by itself. However, OPTICS may lead to 'inconsistent' results depending on what the algorithm considers to be a cluster.

ACKNOWLEDGMENTS

The authors acknowledge the financial support from the Spanish Ministerio de Economía, Industria y Competitividad (MINECO) under the project TRA2015-71491-R co-financed by the European Regional Development Fund (ERDF). In addition, the authors thank the financial support of the grant RTI2018-097880-B-I00 from the Spanish Ministerio de Ciencia, Innovación y Universidades. The first author also acknowledges the predoctoral Grant BES-2016-078270 from the 'Subprograma Estatal de Formación del MICINN' co-financed by the European Social Fund.

References

[1] Rodrigo P. Tavares, Jose M. Guerrero, Fermin Otero, Albert Turon, Joan A. Mayugo, Josep Costa, and Pedro P. Camanho. Effects of local stress fields around broken fibres on the longitudinal failure of composite materials. *International Journal of Solids and Structures*, 156-157:294–305, 2019.

[2] Anthony Bunsell, L. Gorbatikh, H. Morton, S. Pimenta, I. Sinclair, Mark Spearing, Y. Swolfs, and A. Thionnet. Benchmarking of strength models for unidirectional composites under longitudinal tension. *Composites Part A: Applied Science and Manufacturing*, 111(June 2017):138–150, 2018.

[3] S. Pimenta. A computationally-efficient hierarchical scaling law to predict damage accumulation in composite fibre-bundles. *Composites Science and Technology*, 146:210–225, 2017.

[4] S. Pimenta and S. T. Pinho. Hierarchical scaling law for the strength of composite fibre bundles. *Journal of the Mechanics and Physics of Solids*, 61(6):1337–1356, 2013.

[5] J. M. Guerrero, J. A. Mayugo, J. Costa, and A. Turon. A 3D Progressive Failure Model for predicting pseudo-ductility in hybrid unidirectional composite materials under fibre tensile loading. *Composites Part A: Applied Science and Manufacturing*, 107(February):579–591, 2018.

[6] Y. Swolfs, I. Verpoest, and L. Gorbatikh. Maximising the hybrid effect in unidirectional hybrid composites. *Materials and Design*, 93:39–45, 2016.

[7] R.P. Tavares, Fermin Otero, A. Turon, and P.P. Camanho. Effective simulation of the mechanics of longitudinal tensile failure of unidirectional polymer composites. *International Journal of Fracture*, 208(1-2):269–285, 2017.

[8] T Okabe, H. Sekine, K. Ishii, M. Nishikawa, and N. Takeda. Numerical method for failure simulation of unidirectional fiber-reinforced composites with spring element model. *Composites Science and Technology*, 65(6):921–933, 2005.

[9] R.P. Tavares, A. R. Melro, Miguel A. Bessa, A. Turon, Wing K. Liu, and P.P. Camanho. Mechanics of hybrid polymer composites: analytical and computational study. *Computational Mechanics*, 57(3):405–421, 2016.

[10] A. Thionnet, H. Y. Chou, and A. Bunsell. Fibre break processes in unidirectional composites. *Composites Part A: Applied Science and Manufacturing*, 65:148–160, 2014.

[11] Jose M. Guerrero, Rodrigo P. Tavares, Fermin Otero, Joan A. Mayugo, Josep Costa, Albert Turon, and Pedro P. Camanho. An analytical model to predict stress fields around broken fibres and their effect on the longitudinal failure of hybrid composites. *Composite Structures*, 211(December 2018):564–576, 2019.

[12] J. MacQueen. Some methods for classification and analysis of multivariate observations. *Proceedings of 5th Berkeley Symposium on Mathematical Statistics and Probability.*, 1:281–297, 1967.

[13] R. Sibson. SLINK: An optimally efficient algorithm for the single-link cluster method. *The Computer Journal. British Computer Society.*, 16(1):30–34, 1973.

[14] A. P. Dempster, N. M. Laird, and D. B. Rubin. Maximum likelihood from incomplete data via the EM algorithm. *Journal of the Royal Statistical Society. Series B. Methodological*, 39(1):1–38, 1977.

[15] Martin Ester, Hans-Peter Kriegel, Jorg Sander, and Xiaowei Xu. A Density-Based Algorithm for Discovering Clusters in Large Spatial Databases with Noise. *Proceedings of the Second International Conference on Knowledge Discovery and Data Mining (KDD-96). AAAI Press.*, pages 226–231, 1996.

[16] Jose M. Guerrero, Joan A. Mayugo, J. Costa, and A. Turon. The influence dynamic effects and thermal residual stresses have on damage development in hybrid composite materials under longitudinal tensile loading. *Submitted to Composite Structures*, 2019.

[17] Y. Swolfs, H. Morton, A. E. Scott, L. Gorbatikh, P. A S Reed, I. Sinclair, S. M. Spearing, and I. Verpoest. Synchrotron radiation computed tomography for experimental validation of a tensile strength model for unidirectional fibre-reinforced composites. *Composites Part A: Applied Science and Manufacturing*, 77:106–113, 2015.

[18] F. Pedregosa, G. Varoquaux, A. Gramfort, V. Michel, B. Thirion, O. Grisel, M. Blondel, P. Prettenhofer, R. Weiss, V. Dubourg, J. Vanderplas, A. Passos, D. Cournapeau, M. Brucher, M. Perrot, and E. Duchesnay. Scikit-learn: Machine learning in Python. *Journal of Machine Learning Research*, 12:2825–2830, 2011.

[19] Fionn Murtagh and Pedro Contreras. Algorithms for hierarchical clustering: An overview. *Wiley Interdisciplinary Reviews: Data Mining and Knowledge Discovery*, 2(1):86–97, 2012.

[20] K. Fukunaga and L. D. Hostetler. The Estimation of the Gradient of a Density Function, with Applications in Pattern Recognition. *IEEE Transactions on Information Theory*, 21(1):32–40, 1975.

[21] Mihael Ankerst, Markus M. Breunig, Hans-Peter Kriegel, and Jorg Sander. OPTICS: Ordering Points To Identify the Clustering Structure. *ACM SIGMOD international conference on Management of data. ACM Press*, pages 49–60, 1999.

[22] Rodrigo P. Tavares, Fermin Otero, Joan Baiges, Albert Turon, and Pedro P. Camanho. A dynamic spring element model for the prediction of longitudinal failure of polymer composites. *Computational Materials Science*, 160(October 2018):42–52, 2019.

[23] A. R. Melro, P.P. Camanho, and S. T. Pinho. Generation of random distribution of fibres in long-fibre reinforced composites. *Composites Science and Technology*, 68(9):2092–2102, 2008.


AMADE
Universitat de Girona